6 Methods of Evaluation

Geodetic evaluation methods may be separated into positioning and gravity field determination. This separation is possible because positioning only requires an approximate knowledge of the gravity field, and gravity field modeling needs only approximate positions. The linearization of the gravity field is essential in both cases, and it permits a statistical description [6.1]. Nowadays, positioning is based on three-dimensional models [6.2], while classical strategies distinguished between horizontal positioning [6.3] and height determination [6.4]. Gravity field modeling utilizes some basic observables and can be formulated as a boundary-value problem of potential theory [6.5]. Global models are derived mainly from the results of space geodesy [6.6], whereas local gravity field estimation is primarily based on terrestrial data [6.7]. Special methods have been developed for combining positioning and gravity field determination [6.8].

Geodetic evaluation methods are described in textbooks on geodesy, e.g., LEDERSTEGER (1956/1969), HEISKANEN and MORITZ (1967), GROTEN (1979), MORITZ (1980), VANIČEK and KRAKIWSKY (1986), HECK (1995).

6.1 Residual Gravity Field

The actual gravity field can be sufficiently well approximated by the normal gravity field of the level ellipsoid, cf. [4.2.2], which results in linear relations between the observations and the unknown parameters. The fundamental quantity of the residual gravity field is the disturbing potential. It is closely related to the height anomaly and the geoid height [6.1.1]. The residual gravity vector generally is expressed by the gravity anomaly and the deflection of the vertical [6.1.2]. The residual gravity field may be treated by statistical methods, which is of interest in gravity field interpolation and modeling [6.1.3].

6.1.1 Disturbing Potential, Height Anomaly, Geoid Height

Approximation of the actual gravity potential W (3.42) by the normal gravity potential U (4.37) leads to the *disturbing potential* (also anomalous potential) T defined at the point P:

$$T_P = W_P - U_P . \tag{6.1}$$

W and U contain a gravitational and a centrifugal part. As the centrifugal acceleration of the earth is known with high accuracy, cf. [3.1.4], we may

assume that the centrifugal parts of W and U are identical. The disturbing potential then is formed by the difference of the gravitation of the earth and of the level ellipsoid, and thus is a harmonic function outside the earth's masses. Hence, it obeys *Laplace's* differential equation (3.29)

$$\Delta T = 0, \tag{6.2}$$

where Δ = Laplace operator. T can be expanded into spherical harmonics, in analogy to the corresponding developments for the gravitational potentials (3.89) and (4.45). Expressed in spherical coordinates r, ϑ, λ, the disturbing potential as a spatial function reads, in abreviated form, see (3.88):

$$T = T(r,\vartheta,\lambda) = \sum_{l=2}^{\infty}\left(\frac{a}{r}\right)^{l+1} T_l(\vartheta,\lambda). \tag{6.3}$$

In its full form the disturbing potential is given by

$$T = \frac{GM}{r}\sum_{l=2}^{\infty}\left(\frac{a}{r}\right)^{l}\sum_{m=0}^{l}\left(\Delta C_{lm}\cos m\lambda + \Delta S_{lm}\sin m\lambda\right)P_{lm}(\cos\vartheta). \tag{6.4}$$

Comparing (6.3) and (6.4) yields the surface spherical harmonics

$$T_l = \frac{GM}{a}\sum_{m=0}^{l}\left(\Delta C_{lm}\cos m\lambda + \Delta S_{lm}\sin m\lambda\right)P_{lm}(\cos\vartheta). \tag{6.5}$$

Due to the properties of U, only the even zonal harmonic coefficients ΔC_l differ from C_l, while all the other coefficients are identical with the coefficients of the actual gravity field, cf. [4.2.2]. The development of (6.3) and (6.4) starts at $l = 2$ since equality of the masses of the earth and the ellipsoid is assumed, as is coincidence of the center of the earth's masses with the center of the ellipsoid, cf. [3.3.4].

The disturbing potential is closely related to the vertical distance between P and the point Q located on the spheroidal surface $U = U_Q$, cf. [6.5.1]. Q is associated with P by the condition

$$U_Q = W_P, \tag{6.6}$$

cf. [4.2.3], Fig. 6.1. This distance is called *height anomaly* ζ. Geometrically, it is the difference between the ellipsoidal height h and the normal height H^N (3.107), (4.66):

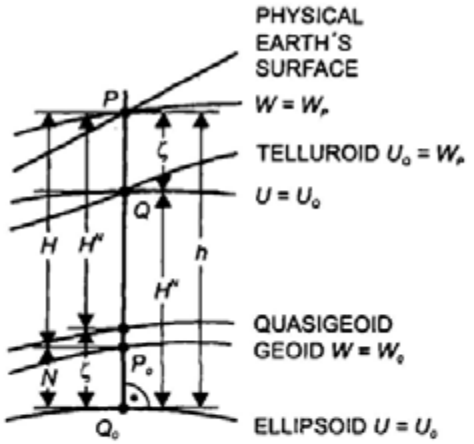

Fig. 6.1. Ellipsoidal, normal and orthometric height

$$\zeta = h - H^N , \tag{6.7}$$

where we have neglected the slight curvature of the normal plumb line. The surface for which (6.6) holds at every point is called the *telluroid* (HIRVONEN 1960). A corresponding relation holds at any point in the exterior space.

The telluroid represents an approximation to the physical surface of the earth. By extending H^N downward from P we obtain the *quasigeoid,* and ζ becomes the distance between the level ellipsoid $U = U_0$ and the quasigeoid, which is often used as a zero height surface, cf. [3.4.3]. ζ is also called quasigeoid height.

If P is located on the geoid, we obtain the *geoid height* N (also called geoid undulation) as the vertical distance between the ellipsoid and the geoid. A geometric definition follows by differencing the ellipsoidal height h and the orthometric height H (3.106):

$$N = h - H , \tag{6.8}$$

where the effect of the plumb line curvature has been neglected.

The difference between the geoid height and the height anomaly is equal to the difference between the normal height and the orthometric height and follows from (3.106) and (3.107):

$$N - \zeta = H^N - H = \frac{\overline{g} - \overline{\gamma}}{\overline{\gamma}} H = \frac{\Delta g_B}{\overline{\gamma}} H . \tag{6.9}$$

The difference depends on the height and thus is zero on the oceans. It also depends on the "mean" gravity anomaly $\overline{g} - \overline{\gamma}$, which corresponds to the Bouger anomaly Δg_B, cf. [6.5.3].

6.1.2 Gravity Disturbance, Gravity Anomaly, Deflection of the Vertical

The gravity vector $\boldsymbol{g}$ at P can be approximated by the vector of normal gravity γ, which leads to the *gravity disturbance*

$$\delta \mathbf{g}_P = \mathbf{g}_P - \boldsymbol{\gamma}_P, \tag{6.10}$$

Fig. 6.2. Neglecting the small angle between the directions of $\boldsymbol{g}$ and γ (deflection of the vertical), we obtain the magnitude

$$\delta g_P = g_P - \gamma_P. \tag{6.11}$$

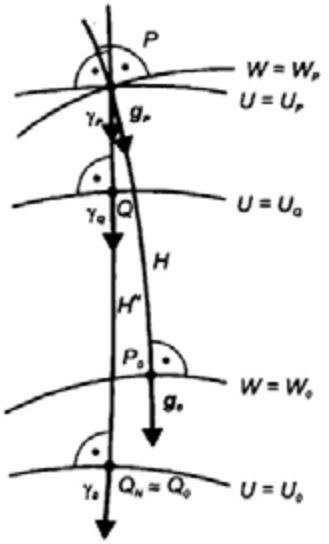

Fig. 6.2. Actual and normal gravity

g can be measured on the earth's surface and in the exterior space. The calculation of γ_P, on the other hand, presupposes the knowledge of the geodetic coordinates of P, which is not assumed in the classical geodetic boundary value problem, cf. [6.5.1]. Consequently, gravity field modeling generally employs the *gravity anomaly*

$$\Delta \mathbf{g}_P = \mathbf{g}_P - \boldsymbol{\gamma}_Q, \tag{6.12}$$

with the magnitude

$$\Delta g_P = g_P - \gamma_Q . \tag{6.13}$$

Again, Q is related to P by the condition (6.6). γ_Q can be calculated by (4.63), starting from normal gravity γ_0 on the ellipsoid (4.41) and replacing h by H^N (3.107) as determined by leveling, cf. [3.4.3]. This free-air reduction is given by (4.61):

$$\delta g_F^N = -\frac{\partial \gamma}{\partial H^N} H^N . \tag{6.14}$$

The *free-air gravity anomaly*, defined on and outside the earth's surface according to *Molodenski*, reads

$$\Delta g_F^N = g + \delta g_F^N - \gamma_0 . \tag{6.15}$$

In many applications, $\partial\gamma/\partial H^N$ is approximated by $-3.086\ \mu\text{ms}^{-2}/\text{m}$.

The determination of the *geoid* requires that the gravity anomalies are given everywhere on that level surface. In order to apply the Laplace equation, the masses outside the geoid have to be removed. Several types of gravity reductions are available for this purpose. The methods differ by the manner in which the topographical masses are displaced, cf. [6.5.3]. The gravity anomaly on the geoid is defined as the difference between the gravity on the geoid g_0, and the normal gravity γ_0 on the ellipsoid (Fig. 6.2):

$$\Delta g = g_0 - \gamma_0 . \tag{6.16}$$

The difference (vector quantity) between the directions of the actual plumb line and a reference direction in the normal gravity field is called *deflection of the vertical* (Fig. 6.3). With respect to the reference direction, we distinguish between (JEKELI 1999):

- The deflection of the vertical θ^N defined on the surface or the exterior of the earth, with the direction of the normal plumb line at Q as a reference (*Molodenski* definition). The reference direction practically coincides with the surface normal to $U = U_P$ at P,
- The deflection of the vertical θ at the earth's surface, referring to the ellipsoidal normal at P (*Helmert* definition). It differs from θ^N only by the slight curvature (effect of a few $0.1''$) of the normal plumb line, cf. [4.2.3]. This definition is preferred generally, as the ellipsoidal normal is provided by the geodetic coordinates,

- The deflection of the vertical θ_0 defined on the geoid (*Pizetti* definition). It is given by the difference between the actual plumb line on the geoid and the ellipsoidal normal. It differs from the previous definitions by the curvature of the actual plumb line and is of importance for the determination of the geoid.

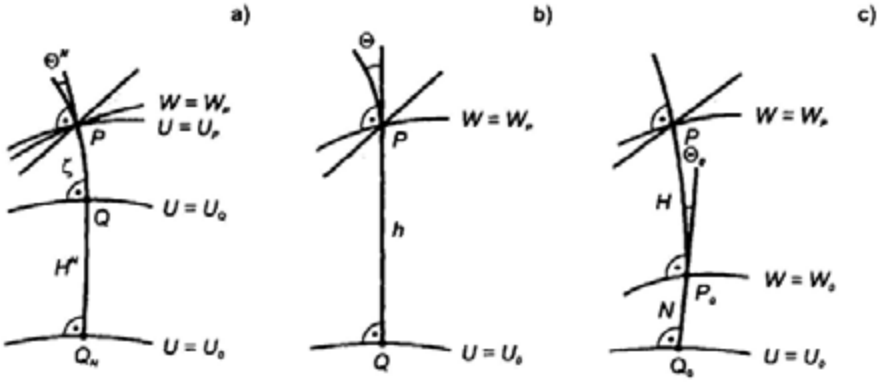

Fig. 6.3. Deflection of the vertical according to a) Molodenski, b) Helmert, c) Pizetti

The deflection of the vertical is expressed either by its magnitude θ and its azimuth α_θ or, more generally, by its components in the north-south and east-west directions. A geometric derivation follows from spherical trigonometry on the unit sphere around the definition point P (Fig. 6.4). Here, we assume that the minor axis of the reference ellipsoid is parallel to the Z-axis of the global reference system and that the ellipsoidal initial meridian is parallel to the X-axis. These conditions are practically fulfilled with modern reference systems and well approximated by classical geodetic systems, cf. [6.2.2]. After parallel displacement, we identify N as the point of intersection of the Z-axis with the unit sphere and Z_a and Z_g as the directions to the astronomic and the geodetic zenith respectively. The deflection of the vertical represents the spherical distance between Z_a and Z_g; its azimuth is denoted by α_θ. The deflection is decomposed into the meridional component ξ (positive when Z_a is north of Z_g) and the component in the prime vertical η (positive when Z_a is east of Z_g). Along the azimuth α to a target point P_i, we have the vertical deflection component ε.

From spherical trigonometry we get

$$\sin\varphi = \cos\eta \sin(\Phi - \xi), \quad \sin\eta = \cos\varphi \sin(\Lambda - \lambda),$$

and with

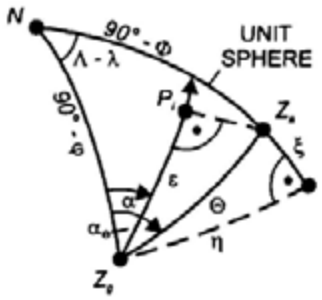

Fig. 6.4. Vertical deflection components

$$\cos\eta \approx 1, \quad \sin\eta \approx \eta, \quad \sin(\Lambda - \lambda) \approx \Lambda - \lambda,$$

the components are given by (linear approximation)

$$\xi = \Phi - \varphi, \quad \eta = (\Lambda - \lambda)\cos\varphi. \tag{6.17}$$

According to Fig. 6.4, the component ε in the azimuth α is composed by two parts:

$$\varepsilon = \xi\cos\alpha + \eta\sin\alpha. \tag{6.18}$$

These relations can also be derived by differencing (3.45) and (4.36), after linearization, cf. [6.2.2].

Equations (6.17) and (6.18) are valid for all definitions of the deflection of the vertical.

The residual gravity field quantities depend on the geodetic earth model used for approximating the gravity field and on its orientation with respect to the earth, cf. [6.2.2]. If referred to a geocentric mean earth ellipsoid, they are designated as absolute quantities, otherwise they are relative only. The r.m.s. scatter of absolute height anomalies and geoid heights is ±30 m (maximum values about 100 m). The free-air gravity anomalies vary by about ±400 μms^{-2} (maximum values of a few 1000 μms^{-2}) and the deflections of the vertical by ±7″ (maximum 30″ to 1′ in the high mountains).

6.1.3 Statistical Description of the Gravity Field, Interpolation

The residual gravity field can be viewed as a realization of a stochastic process and treated by statistical methods (MORITZ 1962, 1970). The gravity anomaly is used as a fundamental gravity-field parameter in this aspect, as gravity data are available with high resolution on the continents and on the oceans.

We assume that the *mean value* of the gravity anomalies Δg over the earth is zero, cf. [6.5.4]:

$$M\{\Delta g\} = \frac{1}{4\pi}\iint_{\sigma} \Delta g \, d\sigma = 0, \tag{6.19}$$

where M{ } is the mean value operator and σ represents the unit sphere. The surface element can be expressed in spherical coordinates ϑ, λ by

$$d\sigma = \sin\vartheta \, d\vartheta \, d\lambda . \tag{6.20}$$

The statistical behavior of Δg is described by the *covariance function*

$$C(\psi) = \operatorname{cov}(\Delta g, \Delta g', \psi) = M\{\Delta g \cdot \Delta g'\}_{\psi} = \frac{1}{4\pi}\iint_{\sigma} \Delta g \Delta g' \, d\sigma . \tag{6.21}$$

It is calculated as the mean value of all products of gravity anomalies at the points P and P', having constant spherical distance ψ on the unit sphere. $C(\psi)$ shall only depend on ψ and not depend on the position (homogeneity of the anomalous gravity field) and the azimuth (isotropy), GRAFAREND (1976). $C(\psi)$ describes the mutual correlation of the gravity anomalies, which decreases with increasing distance. For $\psi = 0$, we have $\Delta g = \Delta g'$, and the covariance transforms into the *variance*

$$\sigma^2(\Delta g) = M\{\Delta g^2\} = \frac{1}{4\pi}\iint_{\sigma} \Delta g^2 \, d\sigma . \tag{6.22}$$

From the theory of stochastic processes, the statistical properties should be derived from an infinite number of process realizations. As only one realization of the gravity field is available, the hypothesis of ergodicity is necessary, which states that the statistical quantities may also be calculated from mean values over one realization (MORITZ 1980, p.269).

As shown in [6.6.1], Δg as a functional of T can be expanded into spherical harmonics. On the earth's surface ($r = R$) the abbreviated form of this expansion reads

$$\Delta g(\vartheta, \lambda) = \sum_{l=2}^{\infty} \Delta g_l(\vartheta, \lambda), \tag{6.23}$$

with Δg_l = Laplace's surface harmonics, cf. [3.3.2]. Again the terms of degree 0 and 1 are missing. As a consequence of (6.23), $C(\psi)$ also can be expanded into spherical harmonics in the definition range $0 \le \psi \le \pi$:

$$C(\psi)=\sum_{l=2}^{\infty} c_l P_l(\cos\psi), \tag{6.24}$$

with $P_l(\cos\psi)$ = Legendre polynomials. Because of isotropy, only zonal terms exist in (6.24). The harmonic coefficients c_l are derived by inversion

$$c_l=\frac{2l+1}{2}\int_0^{\pi} C(\psi)P_l(\cos\psi)\sin\psi\, d\psi, \tag{6.25}$$

according to potential theory. Equation (6.25) can be solved for a known covariance function by numerical integration. By inserting (6.21) into (6.25), and taking (6.23) into account, we obtain

$$c_l = M\{\Delta g_l^2\}=\sigma_l^2(\Delta g). \tag{6.26}$$

Hence, the coefficients are given by the *anomaly degree variances* defined as mean values over the squares of Δg_l.

Based on a global set of point free-air anomalies, KAULA (1959) first gave an estimate for the covariance function. TSCHERNING and RAPP (1974) derived a covariance function and a degree variance model that are often applied. The model is based on satellite-derived harmonic coefficients for the degrees 2 to 10 and a set of 1° equal area anomalies (approximately quadratic compartments with constant area 110km×110km). The variance of the point anomalies is

$$\sigma^2(\Delta g)=\left(424\,\mu\mathrm{ms}^{-2}\right)^2$$

and that of the mean anomalies

$$\sigma^2\left(\overline{\Delta g}\right)_{1^\circ}=\left(303\,\mu\mathrm{ms}^{-2}\right)^2.$$

The correlation of the anomalies approaches zero at a spherical distance of about 30° to 40° (Fig. 6.5). The anomaly degree variance model reads

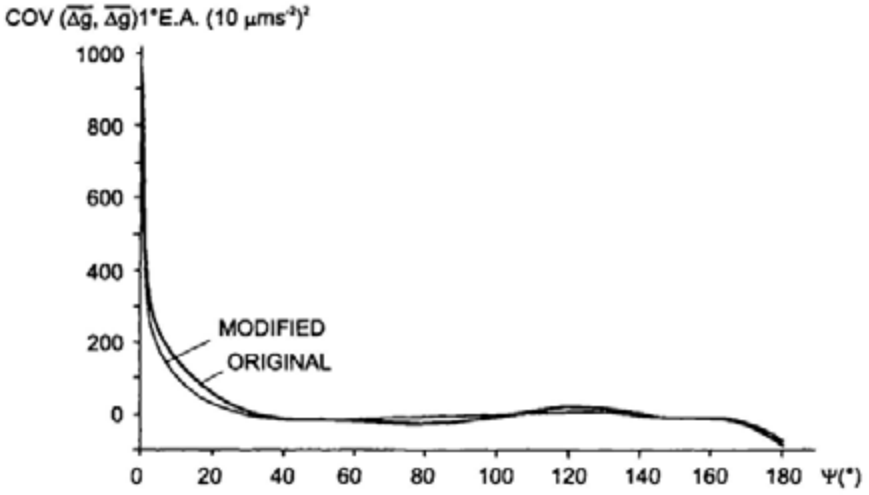

Fig. 6.5. Global covariance function of gravity anomalies, model TSCHERNING and RAPP (1974)

$$\sigma_l^2(\Delta g) = \begin{cases} 0 & \text{for } l = 0,1 \\ 754 & \text{for } l = 2 \quad \left(\mu\text{ms}^{-2}\right)^2, \\ \dfrac{A(l-1)}{(l-2)(l+B)}\sigma_0^{l+2} & \text{for } l \geq 3 \end{cases} \tag{6.27}$$

with $A = 42\,528$ and $B = 24$. $\sigma_0 = \left(R_B/R\right)^2 = 0.999\,617$ is the ratio between the radii of the Bjerhammar sphere, cf. [3.3.2], and the earth, Fig. 6.6.

For regional applications, a covariance function may be derived by subtracting the long-wave part of the gravity field, which results in a decrease in the variance and in the correlation length. Local interpolation is even possible by a plane covariance function, e.g., the Gauss function

$$C(\psi) = C_0 \exp\left(-A^2\psi^2\right), \tag{6.28}$$

Fig. 6.7, TORGE et al. (1984).

It should be noted that covariance functions have to be positive definite. This condition is fulfilled for (6.24), as all coefficients according to (6.26) are non-negative.

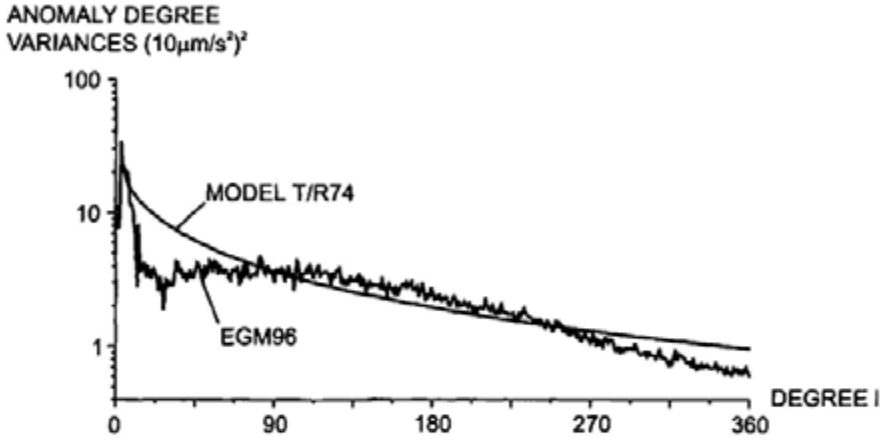

Fig. 6.6. Anomaly degree variances, model TSCHERNING and RAPP (1974) and geopotential model EGM96 (LEMOINE et al. 1998)

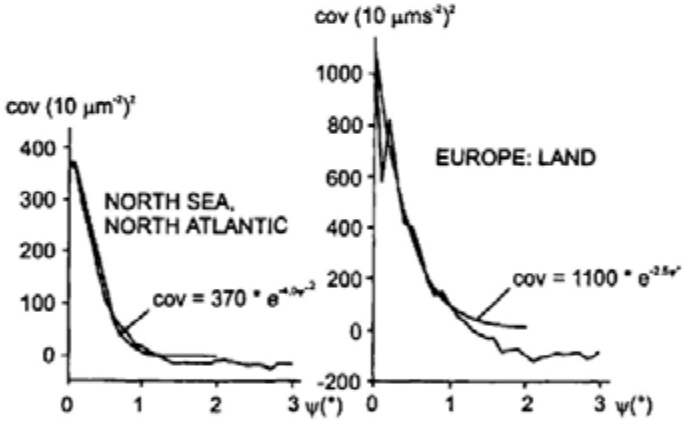

Fig. 6.7. Local covariance functions of trend-removed 6'x10' mean free air anomalies (TORGE et al. 1984)

An important application of the anomaly covariance function is the *interpolation* of gravity anomalies at points not surveyed. Simple interpolation methods such as the manual construction of isoanomaly maps or the geometric interpolation using adjacent data are not ideal and do not deliver optimum results. *Least squares prediction* utilizes the statistical information inherent in the covariance function and takes the errors of the observations into account.

In the usual *linear* prediction, the gravity anomaly at the point P is estimated by a linear function of the anomalies observed at the points $P_i \ (i=1,\ldots,n)$. We assume that, in addition to the covariance function of the anomalies, an *error covariance function* is also available. Such a function can be derived from a priori error and error correlation estimates, although generally only error variances are known. The following covariances, for any distance ψ, can be calculated:

$C_{P_i} = M\{\Delta g_P \cdot \Delta g_i\}$: crosscovariance of Δg_P with the observation Δg_i,

$C_{ij} = M\{\Delta g_i \cdot \Delta g_j\}$: autocovariance of the observations,

$D_{ij} = M\{n_i \cdot n_j\}$: autocovariance of the observational errors (noise n),

and combined into

$$\left.\begin{aligned} \mathbf{c}_P^{\mathrm{T}} &= \left(C_{P_1},\ldots,C_{P_i},\ldots,C_{P_n}\right) \\ \mathbf{C} &= \begin{pmatrix} C_{11} & \cdots & \cdots & \cdots & C_{1n} \\ \vdots & \ddots & & & \vdots \\ \vdots & & C_{ij} & & \vdots \\ \vdots & & & \ddots & \vdots \\ C_{n1} & \cdots & \cdots & \cdots & C_{nn} \end{pmatrix}, \quad \mathbf{D} = \begin{pmatrix} D_{11} & \cdots & \cdots & \cdots & D_{1n} \\ \vdots & \ddots & & & \vdots \\ \vdots & & D_{ij} & & \vdots \\ \vdots & & & \ddots & \vdots \\ D_{n1} & \cdots & \cdots & \cdots & D_{nn} \end{pmatrix} \end{aligned}\right\}. \quad (6.29)$$

Now, the prediction error is introduced, being the difference between the true gravity anomaly and the predicted value $\Delta\hat{g}$. The requirement of a minimum prediction error variance, in analogy to least squares adjustment, leads to the result of least squares prediction

$$\Delta\hat{g}_P = \mathbf{C}_P^{\mathrm{T}}\bar{\mathbf{C}}^{-1}\Delta g\,, \quad (6.30)$$

where the observed anomalies have been collected in the vector

$$\Delta\mathbf{g}^{\mathrm{T}} = \left(\Delta g_1, \ \ldots \ \Delta g_i, \ \ldots \ \Delta g_n\right). \quad (6.31)$$

Under the assumption that the gravity anomalies and their errors are not correlated, the corresponding matrices $\boldsymbol{C}$ and $\boldsymbol{D}$ can be added element by element, leading to

$$\bar{\mathbf{C}} = \mathbf{C} + \mathbf{D} . \tag{6.32}$$

The prediction of point free-air anomalies is successful only for very densely surveyed areas, as these anomalies strongly depend on height. A smoother gravity anomaly field is obtained by averaging over larger surface elements (e.g., 5′×5′, 30′×30′) or reduction of the effect of the topographic masses, where the Bouguer anomalies are especially well suited for interpolation, cf. [6.5.3]. As well known from least-squares adjustment theory, the predicted values of the gravity anomalies are relatively independent from the choice of the covariance function, while the error estimates strongly depend on it. Realistic prediction results can be expected only within the correlation length defined by a covariance of $1/2\sigma^2(\Delta g)$.

6.2 Three-dimensional Positioning

Three-dimensional positioning is generally carried out in a Cartesian coordinate system; the use of ellipsoidal coordinates results in more complicated models [6.2.1]. The Geodetic Datum provides the orientation of a three-dimensional model with respect to the global geocentric system [6.2.2]. Three-dimensional modeling has been investigated by WOLF (1963a, b), GRAFAREND (1978), and TORGE (1980a) among others.

The *observation equations* relate the observed quantities to the unknown station coordinates and other parameters (functional model). By "observations," we mean geometric quantities that result from preprocessing of the original measurements, such as signal travel time, phase and frequency, and readings on graduated circles or staffs. We also assume that instrumental corrections have been applied (e.g., calibration) and that influences from the atmosphere (refraction) and the gravity field (earth tides) have been taken into account. The observations equations are mostly non-linear. They have to be linearized for the subsequent least squares adjustment, which also includes the errors of the observations (stochastic model). The theory of errors and adjustment methods are discussed in textbooks by GRAFAREND and SCHAFFRIN (1993), WOLF (1997), and KOCH (1999).

6.2.1 Observation Equations

The observations used for three-dimensional positioning may be divided into satellite and terrestrial measurements.

Satellite observations include

- Spatial directions, cf. [5.2.4],
- Ranges derived from GPS and laser distance measurements, cf. [5.2.5], [5.2.6],

- Range rates from Doppler measurements, cf. [5.2.4].

We add

- Baseline vectors obtained from VLBI, cf. [5.3.4].

Satellite and VLBI networks generally are adjusted separately. The resulting

- Cartesian coordinates and
- Cartesian coordinate differences

can then be introduced as "observed" parameters into subsequent combined adjustments, together with other satellite networks or with terrestrial data.

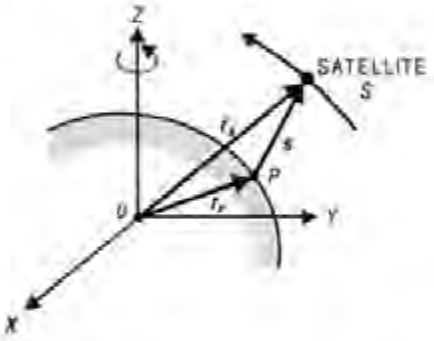

Fig. 6.8. Satellite tracking principle

Satellite observations provide the components of the *topocentric observation vector* **s** directed from the station P to the satellite S (Fig. 6.8). The vector **s** is related to the geocentric station vector $\mathbf{r}_P$ and the radius vector $\mathbf{r}_S$ of the satellite by

$$\mathbf{r}_P + \mathbf{s} - \mathbf{r}_S = \mathbf{0}\,, \tag{6.33a}$$

with

$$\mathbf{r}_P = \begin{pmatrix} X_P \\ Y_P \\ Z_P \end{pmatrix}, \quad \mathbf{r}_S = \begin{pmatrix} X \\ Y \\ Z \end{pmatrix}, \quad \mathbf{r}_S - \mathbf{r}_P = \begin{pmatrix} \Delta X_P^S \\ \Delta Y_P^S \\ \Delta Z_P^S \end{pmatrix}. \tag{6.33b}$$

The observation vector is formed by the distance and the spatial direction to the satellite given in the hour angle system:

$$\mathbf{s} = s \begin{pmatrix} \cos h_{Gr} \cos\delta \\ \sin h_{Gr} \cos\delta \\ \sin\delta \end{pmatrix}, \tag{6.34}$$

where δ is the declination and

$$h_{Gr} = \mathrm{GAST} - \alpha \tag{6.35}$$

is the Greenwich hour angle, cf. [2.4.1].

Inserting (6.34) into (6.33) and solving for the components of **s** yields the observation equations

$$\left.\begin{aligned} h_{Gr} &= \arctan \frac{\Delta Y_P^s}{\Delta X_P^s} \\ \delta &= \arctan \frac{\Delta Z_P^s}{\sqrt{\Delta X_P^{s\,2} + \Delta Y_P^{s\,2}}} \\ s &= \sqrt{\Delta X_P^{s\,2} + \Delta Y_P^{s\,2} + \Delta Z_P^{s\,2}} \end{aligned}\right\}. \tag{6.36}$$

Range rates to the satellite positions (i, j) are given by

$$s_j - s_i = \sqrt{\Delta X_P^{j\,2} + \Delta Y_P^{j\,2} + \Delta Z_P^{j\,2}} - \sqrt{\Delta X_P^{i\,2} + \Delta Y_P^{i\,2} + \Delta Z_P^{i\,2}}\,, \tag{6.37a}$$

with

$$\Delta X_P^j = X_j - X_P \text{ etc.}, \quad \Delta X_P^i = X_i - X_P\,, \text{ etc.} \tag{6.37b}$$

If the directions to the quasars are known, VLBI observations deliver the *baseline vector* between two terrestrial stations P_1 and P_2 (5.65):

$$\mathbf{b}_{1,2} = \mathbf{r}_2 - \mathbf{r}_1 = \begin{pmatrix} X_2 - X_1 \\ Y_2 - Y_1 \\ Z_2 - Z_1 \end{pmatrix}. \tag{6.38}$$

The relations of the original measurements to the geometrical quantities introduced in (6.36) to (6.38) are given by (5.42) for Doppler counts, (5.43) and (5.45) for GPS, (5.48) for satellite laser ranging, and (5.65) for VLBI.

The observation equations contain a large number of parameters in addition to the station coordinates. Among them are the earth orientation parameters, parameters describing earth tide effects and crustal deformation, as well as the satellite coordinates and the coefficients of the gravitational field and other "disturbing" forces. There are two strategies to handle the large amount of data and unknown parameters.

The first one consists in estimating most of the unknowns in *one* adjustment and to adopt only a few parameters (e.g., the earth orientation parameters) from other sources. This leads to "satellite-only" earth models, which provide a global set of station coordinates and the harmonic coefficients of the gravitational field, cf. [6.6.2].

In positioning, only a limited number of parameters, mainly the station coordinates, are introduced as unknowns, while numerical values for the other parameters are taken from models. Highly accurate orbital parameters are available for GPS and laser satellites and are disseminated by operational services. Parameter corrections taken from models are small and can easily be introduced into the adjustment. Examples include the orbital improvement for short arcs (less than one revolution) through corrections to the six Keplerian elements, the introduction of a local tropospheric "scale factor," and the determination of clock biases.

Several error influences are eliminated or greatly reduced when *simultaneous* measurements are carried out from two or more ground stations to the same satellites (relative positioning). This is due to the high error correlation between neighboring stations. By differencing the measurements, a large part of the errors cancel. Since the absolute orientation is lost with this strategy, the absolute coordinates of at least one station have to be provided.

Exact simultaneous measurements lead to a purely *geometric method* of evaluation. The satellite is regarded as a high-altitude target, and short-arc orbital fitting can improve the results (WOLF 1967, SCHWARZ 1969). Geometric satellite networks were established by stellar triangulation and by trilateration from the 1960's to the 1970's. The global network of the U.S. National Geodetic Survey (1966-1970, 45 stations) was determined by direction measurements with Wild BC4 cameras to the Pageos satellite, cf. [5.2.4]. The scale of this network was derived from long traverses measured with electronic distance meters; an accuracy of ±4 to 5 m was achieved (SCHMID 1974).

Different methods have been developed for the evaluation of *simultaneously* observed *GPS networks* by forming linear combinations of the observations (WELLS et al. 1987, TEUNISSEN and KLEUSBERG 1998b). As a standard, *"single differences"* $s_1^A - s_2^A$ between the distances measured simultaneously from two receivers P_1, P_2 to the satellite A at epoch t_i are formed (Fig. 6.9). Thereby, the satellite clock errors are eliminated and refraction and orbital errors are reduced.

"Double differences" are formed by differencing two single differences taken to different satellites A, B at the same epoch t_i: $\left(s_1^A - s_2^A\right) - \left(s_1^B - s_2^B\right)$. With double difference, the receiver clock errors vanish and refraction and orbital errors are further reduced. *"Triple differences"* are constructed by differencing two double differences taken at the epochs t_i and t_j. The ambiguity which enters into carrier phase measurements cancels in the observation equation. Due to the loss of information, triple differences allow reduced-accuracy positioning only but are useful for the removal of cycle slips, cf. [5.2.5].

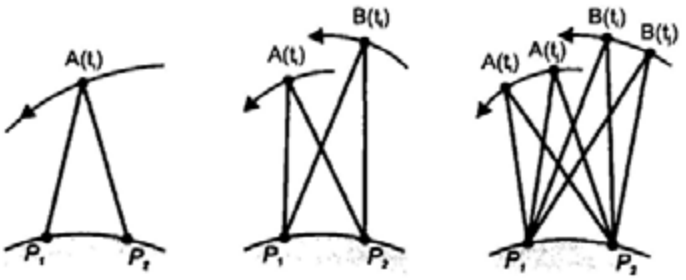

Fig. 6.9. GPS single, double and triple differences

Sophisticated software packages are available for the *adjustment* of satellite networks; for GPS networks we mention WÜBBENA (1989), BEUTLER et al. (1996a), WEBB and ZUMBERGE (1997). The adjustment delivers the Cartesian coordinates or coordinate differences of the ground stations and their full variance-covariance matrix, which has to be taken into account for further processing, e.g., for the combination with terrestrial data. If the orientation of the networks to be combined is not identical, a corresponding transformation (datum shift) has to be included in the adjustment, cf. [6.2.3].

Terrestrial measurements include

- Astronomic azimuths, latitudes, and longitudes, cf. [5.3.2],
- Horizontal directions (azimuths without orientation) and horizontal angles (differences of azimuths), cf. [5.5.1],
- Zenith angles, cf. [5.5.1],
- Distances, cf. [5.5.2],
- Leveled height differences, cf. [5.5.3].

By substituting (2.20) into (2.29) and taking (2.30) into account, we obtain the *observation equations* for azimuths A, zenith angles z, and distances s:

$$\left.\begin{aligned} A &= \arctan\frac{-\sin\Lambda\,\Delta X + \cos\Lambda\,\Delta Y}{-\sin\Phi\cos\Lambda\,\Delta X - \sin\Phi\sin\Lambda\,\Delta Y + \cos\Phi\,\Delta Z} \\ z &= \arccos\frac{\cos\Phi\cos\Lambda\,\Delta X + \cos\Phi\sin\Lambda\,\Delta Y + \sin\Phi\Delta Z}{\left(\Delta X^2 + \Delta Y^2 + \Delta Z^2\right)^{1/2}} \\ s &= \left(\Delta X^2 + \Delta Y^2 + \Delta Z^2\right)^{1/2} \end{aligned}\right\}, \qquad (6.39)$$

with

$$\Delta X = X_2 - X_1, \quad \Delta Y = Y_2 - Y_1, \quad \Delta Z = Z_2 - Z_1 .$$

Astronomic latitude Φ and astronomic longitude Λ enter as orientation parameters in (6.39). They relate the local astronomic to the global geocentric system and are treated as additional unknown parameters. If observed latitudes and longitudes are available, they are introduced as observed parameters in the adjustment.

Least squares adjustment requires linear relations between the observations and the unknowns. Corresponding *differential relations* are derived by numerical or analytical differentiation of (6.39). Analytical expressions for the partial derivatives $\partial A/\partial X$, etc. are found in WOLF (1963b) and HEISKANEN and MORITZ (1967, p.217).

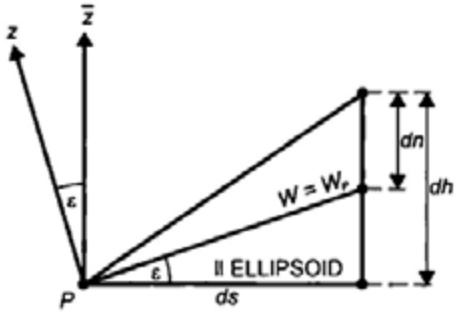

Fig. 6.10. Geometric-astronomic leveling

Geometric leveling can be incorporated into three-dimensional computations after transformation of the leveled height difference $\delta n \approx dn$ (5.111) into the geocentric coordinate system. An ellipsoidal height difference dh is obtained by reducing dn for the effect of the (surface) deflection of the vertical (Fig. 6.10). In the azimuth of the leveling line, the component ε (6.18) is effective, which gives

$$dh = dn - \varepsilon\, ds\,. \tag{6.40}$$

The negative sign prefixing $\varepsilon\, ds$ is based on the sign definitions inherent in (6.17) and (6.7) resp. (6.8). A differential relationship between the ellipsoidal height and X,Y,Z is provided by (4.26a) and (4.27). With

$$d\bar{\mathbf{r}}_Q = \mathbf{0}\,,$$

and replacing φ,λ with Φ,Λ, we obtain

$$dh = \bar{\mathbf{n}}^{\mathrm{T}} \cdot d\mathbf{r} = \cos\Phi\cos\Lambda\, dX + \cos\Phi\sin\Lambda\, dY + \sin\Phi\, dZ\,. \tag{6.41}$$

Again, we have assumed that the axes of the ellipsoidal and the geocentric system are parallel:

$$d\bar{X} = dX, \quad d\bar{Y} = dY, \quad d\bar{Z} = dZ\,.$$

Integration of (6.40) yields the ellipsoidal height difference

$$\Delta h_{1,2} = h_2 - h_1 = \int_1^2 dn - \int_1^2 \varepsilon\, ds\,, \tag{6.42}$$

which can be included as an "observation" in spatial computations: *Geometric-astronomic leveling* (HEITZ 1973). It is noted that both integrals in (6.42) have to be formed over the same path. The differential relation for (6.42) follows from differencing (6.41) for the points P_1 and P_2:

$$d\left(\Delta h_{1,2}\right) = dh_2 - dh_1\,. \tag{6.43}$$

The first integral in (6.42) can be easily computed by summing the leveled height differences. The evaluation of the second integral poses difficulties, as vertical deflections are generally only available at larger station distances (several 10 km in classical networks). This introduces the problem of the interpolation of deflections of the vertical, cf. [6.7.4]. In flat and hilly areas, with an average distance of the vertical deflection stations of 25 km, an accuracy of ±0.1 m/100km can be achieved for the ellipsoidal height differences (BÄUMKER 1984), while "cm" accuracy requires station distances of 5 to 10 km and sophisticated interpolation methods (TORGE 1977).

The three-dimensional concept was already introduced by VILLARCEAU (1868) and BRUNS (1878). Bruns suggested a pointwise determination of the earth's surface by a spatial polyhedron constructed from terrestrial measurements and orientated by astronomical observations. The

feasibility of this concept was demonstrated in some test networks (TORGE and WENZEL 1978, HRADILEK 1984), but large-scale application was prevented due to the uncertainties of trigonometrical height transfer over larger distances and the problems with reducing geometric leveling.

Ellipsoidal coordinates φ,λ, and sometimes h, cf. [4.1.3], are used for many applications in geodesy, cartography, and navigation. They can be easily derived from the Cartesian coordinates by the transformation (4.28). Network adjustments in the φ,λ,h-system are more complicated and restricted to special cases. Nevertheless, differential relations between the observations and the ellipsoidal coordinates are useful for certain problems, e.g., deriving reductions onto the ellipsoid and for two-dimensional ellipsoidal calculations, cf. [6.3.2], [6.3.3].

Equations (4.27) provide the fundamental relations between the φ,λ,h and the X,Y,Z-systems. Differentiation yields

$$\begin{pmatrix} d\bar{X} \\ d\bar{Y} \\ d\bar{Z} \end{pmatrix} = \bar{\mathbf{A}} \begin{pmatrix} (M+h)d\varphi \\ (N+h)\cos\varphi\, d\lambda \\ dh \end{pmatrix}, \tag{6.44}$$

where $\bar{\mathbf{A}}$ is given by (4.32). Again we assume parallelism of the ellipsoidal and the Cartesian coordinate systems. Equation (6.44) can be immediately used if satellite derived coordinates or coordinate differences are to be adjusted in the φ,λ,h-system. Differential formulas for the terrestrial observations A, z, s are obtained by inserting (6.44) into the differential relations for Cartesian coordinates and reordering (WOLF 1963b, HEISKANEN and MORITZ 1967), cf. [6.3.2].

We finally mention the straightforward transformation from the "natural" coordinates Φ,Λ,H (orthometric height) or H^N (normal height) to ellipsoidal coordinates φ,λ,h, where H and H^N are derived from the gravity potential W by (3.106) resp. (3.107). According to (6.17), the deflection of the vertical (ξ,η) transforms from the plumb line direction to the ellipsoidal normal:

$$\varphi = \Phi - \xi, \quad \lambda = \Lambda - \frac{\eta}{\cos\varphi}. \tag{6.45a}$$

If *normal* geodetic coordinates φ^N,λ^N (4.73) are required, the curvature of the normal plumb line has to be taken into account by $\delta\varphi^N$ (4.74):

$$\varphi^N = \Phi - \left(\xi + \delta\varphi^N\right) = \Phi - \xi^N, \quad \lambda^N = \lambda = \Lambda - \frac{\eta}{\cos\varphi}. \tag{6.45b}$$

The relation between h and H resp. H^N is given by, see Fig. 6.2:

$$h = H + N = H^N + \zeta, \tag{6.46}$$

where we have neglected the small (sub mm-order of magnitude) effect of the plumb line curvature. Gravimetric evaluation techniques allow calculation of the deflection of the vertical and the geoid height or the height anomaly from gravity data, cf. [6.7]. Equations (6.45) and (6.46) thus would allow us to establish a geocentric system of ellipsoidal coordinates (HEISKANEN 1951).

Since Φ and Λ can be determined only with an accuracy of $\pm 0.1''$ (corresponding to 3 m in horizontal position) or less, this method is no longer of interest for horizontal positioning. The height transformation (6.46), on the other hand, is most useful, as it permits connection of GPS-derived ellipsoidal heights with heights determined by geometric leveling, cf. [6.4.3].

6.2.2 Geodetic Datum

The *geodetic datum* describes the orientation of any geodetic system with respect to the global geocentric system, cf. [2.5.1]. Nowadays, networks established by satellite methods are tied to the ITRF, cf. [2.5.3], and hence geocentric. Larger deviations occur with classical geodetic networks, which were orientated by astronomical observations, cf. [6.3.3].

In the most general case, a non-geocentric $\bar{X},\bar{Y},\bar{Z}$ -system is transformed to the X,Y,Z-system by a *similarity transformation* in space, i.e., by three translations, three rotations, and a change in scale (Fig. 6.11):

$$\mathbf{r} = \mathbf{r}_0 + (1+m)\mathbf{R}\left(\varepsilon_{\bar{X}}, \varepsilon_{\bar{Y}}, \varepsilon_{\bar{Z}}\right)\bar{\mathbf{r}}. \tag{6.47}$$

Here, $\mathbf{r}^\mathsf{T} = (X,Y,Z)$ and $\bar{\mathbf{r}}^\mathsf{T} = (\bar{X},\bar{Y},\bar{Z})$ are the position vectors in the two systems, and $\mathbf{r}_0^\mathsf{T} = (X_0,Y_0,Z_0)$ contains the coordinates of the origin $\bar{O}$ of the $\bar{X},\bar{Y},\bar{Z}$ -system with respect to the geocenter O. We assume that the scale of the $\bar{X},\bar{Y},\bar{Z}$ -system differs only slightly from the scale of the global reference frame and that the axes of the two systems are approximately parallel. Consequently, m is a small scale correction, and the rotation matrix is composed of three small Eulerian angles; it takes the form

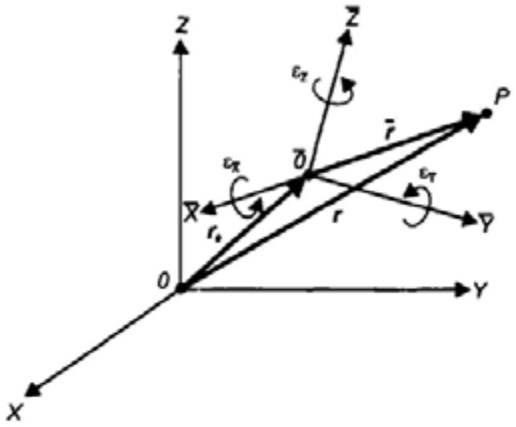

Fig. 6.11. Transformation between 3D-Cartesian coordinate systems

$$\mathbf{R}\left(\varepsilon_{\bar{X}},\varepsilon_{\bar{Y}},\varepsilon_{\bar{Z}}\right)=\begin{pmatrix}1 & \varepsilon_{\bar{Z}} & -\varepsilon_{\bar{Y}}\\ -\varepsilon_{\bar{Z}} & 1 & \varepsilon_{\bar{X}}\\ \varepsilon_{\bar{Y}} & -\varepsilon_{\bar{X}} & 1\end{pmatrix}. \tag{6.48}$$

In order to determine the seven parameters of the transformation (6.47), at least three points with coordinates given in both systems are required.

After converting the Cartesian coordinates into ellipsoidal ones, (6.47) can be expressed in ellipsoidal coordinates φ,λ,h. The datum parameters in that case also have to include the geometric parameters of the ellipsoid, i.e., the semimajor axis a and the flattening f. Of practical interest are the *changes* of the *ellipsoidal coordinates* that result from translation, rotation, change in scale, and change of the parameters of the ellipsoid. We insert (4.27) into (6.47) and take the total differential. As the real position of P does not change, we have $d\mathbf{r}=\mathbf{0}$. Neglecting the linear scale factor and substituting the differentials by (small) differences, a spherical approximation ($M+h=N+h=a, f=0$) yields (MERRY and VANIČEK 1974, Torge 1980b):

$$\begin{pmatrix}a\,\delta\varphi\\ a\cos\varphi\,\delta\lambda\\ \delta h\end{pmatrix}=-\bar{\mathbf{A}}^{-1}\delta\mathbf{r}_0+\mathbf{C}\begin{pmatrix}\delta\varepsilon_{\bar{X}}\\ \delta\varepsilon_{\bar{Y}}\\ \delta\varepsilon_{\bar{Z}}\end{pmatrix}+\mathbf{F}\begin{pmatrix}\delta a\\ a\,\delta f\end{pmatrix}, \tag{6.49a}$$

where $\bar{\mathbf{A}}^{-1}$ is given by (4.34) and

$$\mathbf{C} = a\begin{pmatrix} \sin\lambda & -\cos\lambda & 0 \\ -\sin\varphi\cos\lambda & -\sin\varphi\sin\lambda & \cos\varphi \\ 0 & 0 & 0 \end{pmatrix}, \quad \mathbf{F} = \begin{pmatrix} 0 & \sin 2\varphi \\ 0 & 0 \\ -1 & \sin^2\varphi \end{pmatrix}. \quad (6.49b)$$

Equation (6.49) can be used for estimating the changes of the coordinates if the changes of the parameters of the geodetic datum are known. All differences are formed in the sense geocentric – non-geocentric, e.g., δa = a(geocentric) – a(non-geocentric). Formulas which take the flattening into account are given by EHLERT (1991), and ABD-ELMOTAAL and EL-TOKHEY (1995).

Classical geodetic networks have been orientated by the ellipsoidal coordinates of an *initial (fundamental) point* P_F and by condition equations for the parallelism of the axes with respect to the geocentric system. If we apply (6.49) at a running point P and at the fundamental point P_F, the translation can be expressed in changes $\delta\varphi_F, \delta\lambda_F, \delta h_F$ of the fundamental point (TORGE 1980b). By differentiating (6.45) and (6.46), and considering that $d\Phi = d\Lambda = dH = 0$, we obtain

$$\delta\xi = -\delta\varphi, \quad \delta\eta = -\cos\varphi\,\delta\lambda, \quad dN = dh\,. \quad (6.50)$$

Corresponding equations hold for the "normal" geodetic coordinates, cf. [4.2.3]. Hence, the coordinate changes at any point also can be expressed as *changes* of the *deflection of the vertical* and the *geoid height* (or height anomaly), in dependence on the corresponding changes in the fundamental point (VENING-MEINESZ 1950). Spherical approximation yields (HEISKANEN and MORITZ 1967, p.208)

$$\begin{aligned} d\xi = {} & \left(\cos\varphi_F\cos\varphi + \sin\varphi_F\sin\varphi\cos(\lambda-\lambda_F)\right)d\xi_F \\ & -\sin\varphi\sin(\lambda-\lambda_F)\,d\eta_F \\ & -\left(\sin\varphi_F\cos\varphi - \cos\varphi_F\sin\varphi\cos(\lambda-\lambda_F)\right) \\ & \times\left(\frac{dN_F}{a} + \frac{da}{a} + \sin^2\varphi_F\,df\right) - 2\cos\varphi(\sin\varphi - \sin\varphi_F)\,df \quad (6.51) \\ d\eta = {} & \sin\varphi_F\sin(\lambda-\lambda_F)\,d\xi_F + \cos(\lambda-\lambda_F)\,d\eta_F \\ & +\cos\varphi_F\sin(\lambda-\lambda_F)\left(\frac{dN_F}{a} + \frac{da}{a} + \sin^2\varphi_F\,df\right) \end{aligned}$$

$$
\begin{aligned}
dN = &-a\left(\cos\varphi_F \sin\varphi - \sin\varphi_F \cos\varphi \cos\left(\lambda - \lambda_F\right)\right) d\xi_F \\
&- a\cos\varphi \sin\left(\lambda - \lambda_F\right) d\eta_F \\
&+ \left(\sin\varphi_F \sin\varphi + \cos\varphi_F \cos\varphi \cos\left(\lambda - \lambda_F\right)\right) \quad \text{.(6.51 continued)} \\
&\times \left(dN_F + da + a\sin^2\varphi_F \, df\right) - da \\
&+ \left(\sin^2\varphi - 2\sin\varphi_F \sin\varphi\right) a \, df
\end{aligned}
$$

These relations have played a role in the optimum fitting of horizontal control networks to the geoid, cf. [7.1.2].

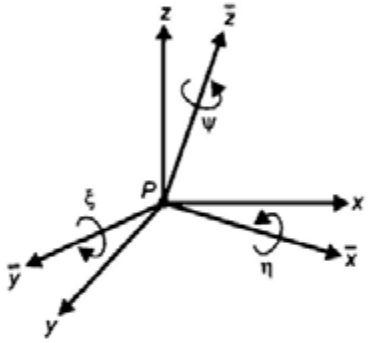

Fig. 6.12. Rotations between the local ellipsoidal and the local astronomic system

We now investigate how the (approximate) *parallelism of the axes* of classical geodetic networks with respect to the geocentric system has been achieved.

We describe the deviation between the local astronomic x,y,z-system (2.20) and the local ellipsoidal $\bar{x},\bar{y},\bar{z}$-system (4.29) by three Eulerian angles, after reflection of the y and $\bar{y}$-axes (producing right-handed systems), Fig. 6.12:

$$
\mathbf{x} = \mathbf{R}\left(\xi,\eta,\psi\right)\bar{\mathbf{x}}\,, \tag{6.52a}
$$

with the rotation matrix

$$
\mathbf{R}\left(\xi,\eta,\psi\right) = \begin{pmatrix} 1 & \psi & -\xi \\ -\psi & 1 & \eta \\ \xi & -\eta & 1 \end{pmatrix}. \tag{6.52b}
$$

The Eulerian angles are the components of the *deflection of the vertical* , cf. [6.1.2], in the meridian (ξ), in the prime vertical (η), and in the horizontal plane

(ψ). If the axes of the global X,Y,Z and $\bar{X},\bar{Y},\bar{Z}$ -systems are not parallel, the following relations hold, according to (2.26), (4.20), (6.47), and (6.52):

$$\Delta\mathbf{X} = \mathbf{A}\mathbf{x} = \mathbf{A}\mathbf{R}(\xi,\eta,\psi)\bar{\mathbf{x}} = \mathbf{R}(\varepsilon_{\bar{X}},\varepsilon_{\bar{Y}},\varepsilon_{\bar{Z}})\bar{\mathbf{A}}\bar{\mathbf{x}} \tag{6.53}$$

or

$$\mathbf{R}(\varepsilon_{\bar{X}},\varepsilon_{\bar{Y}},\varepsilon_{\bar{Z}})\bar{\mathbf{A}} = \mathbf{A}\mathbf{R}(\xi,\eta,\psi). \tag{6.54}$$

After inserting $\bar{\mathbf{A}}$ (4.32) and $\mathbf{A}$ (2.28), the evaluation of (6.54) results in nine equations. Three of the nine equations are independent from each other (orthogonality relations). After Taylor expansion of the trigonometrical functions (Φ,Λ) inherent in (2.28) at the point (φ,λ), we obtain the components (linear approximation) of the *deflection of the vertical* if the axes of the global systems are not parallel:

$$\left.\begin{aligned}
\xi &= \Phi - \varphi + \sin\lambda\,\varepsilon_{\bar{X}} - \cos\lambda\,\varepsilon_{\bar{Y}} \\
\eta &= (\Lambda-\lambda)\cos\varphi - \sin\varphi(\cos\lambda\,\varepsilon_{\bar{X}} + \sin\lambda\,\varepsilon_{\bar{Y}}) + \cos\varphi\,\varepsilon_{\bar{Z}} \\
\psi &= (\Lambda-\lambda)\sin\varphi + \cos\varphi(\cos\lambda\,\varepsilon_{\bar{X}} + \sin\lambda\,\varepsilon_{\bar{Y}}) + \sin\varphi\,\varepsilon_{\bar{Z}}
\end{aligned}\right\}, \tag{6.55}$$

where the equations for η and ψ depend on each other.

We also generalize the equations for the *azimuth* and the *zenith angle* given in the local astronomic and the local ellipsoidal system. From (6.53) we have

$$\mathbf{A}\mathbf{x} = \mathbf{R}(\varepsilon_{\bar{X}},\varepsilon_{\bar{Y}},\varepsilon_{\bar{Z}})\bar{\mathbf{A}}\bar{\mathbf{x}}.$$

Inserting (2.20) and (4.29) yields, after linearization of the trigonometrical functions of A, z at α, ζ:

$$\begin{aligned}
A - \alpha = {} & (\Lambda-\lambda)\sin\varphi + \big((\Phi-\varphi)\sin\alpha - \cos\varphi(\Lambda-\lambda)\cos\alpha\big)\cot\zeta \\
& + \cos\varphi(\cos\lambda\,\varepsilon_{\bar{X}} + \sin\lambda\,\varepsilon_{\bar{Y}}) + \sin\varphi\,\varepsilon_{\bar{Z}}
\end{aligned}, \tag{6.56a}$$

$$\begin{aligned}
z - \zeta = {} & -\big((\Phi-\varphi)\cos\alpha + \cos\varphi(\Lambda-\lambda)\sin\alpha\big) \\
& -(\cos\alpha\sin\lambda - \sin\alpha\sin\varphi\cos\lambda)\varepsilon_{\bar{X}} \\
& +(\cos\alpha\cos\lambda + \sin\alpha\sin\varphi\sin\lambda)\varepsilon_{\bar{Y}} \\
& -\cos\varphi\sin\alpha\,\varepsilon_{\bar{Z}}
\end{aligned}. \tag{6.56b}$$

With the global rotations

$$\varepsilon_{\bar{X}} = \varepsilon_{\bar{Y}} = \varepsilon_{\bar{Z}} = 0\,,$$

we obtain condition equations for the parallelism of the axes, which was presupposed when introducing the deflections of the vertical, cf. [6.1.2]:

$$\left.\begin{aligned} \xi &= \Phi - \varphi, \quad \eta = (\Lambda - \lambda)\cos\varphi \\ \psi &= (\Lambda - \lambda)\sin\varphi \end{aligned}\right\}. \tag{6.57}$$

After inserting (6.57) into (6.56), the condition equations for the azimuth and the zenith angle read

$$A - \alpha = \eta\tan\varphi + (\xi\sin\alpha - \eta\cos\alpha)\cot\zeta \tag{6.58}$$

and

$$z - \zeta = -(\xi\cos\alpha + \eta\sin\alpha)\,. \tag{6.59}$$

Equation (6.58) is known as *Laplace's* equation of orientation, while (6.59) furnishes the component ε of the deflection of the vertical in the azimuth α (6.18), VANIČEK and WELLS (1974).

A geometric interpretation of the condition equations (6.58) and (6.59) reveals that they prevent rotations about the vertical and the horizontal axis of a theodolite. In addition, a rotation about the line of sight must be forestalled to guarantee the parallelism of the global and the ellipsoidal system. This can be accomplished if, in addition to (6.58) and (6.59), another zenith angle equation is introduced at the fundamental point, possibly with an azimuth which differs by 90°. Due to the problems of vertical refraction, classical networks generally employed only the Laplace equation for orientation. A three-dimensional network then would need at least three *Laplace azimuths* at points well distributed over the network.

Two-dimensional positioning utilizes (6.58) for the reduction of observed azimuths and horizontal directions onto the ellipsoid, cf. [6.3.2], and (6.59) enters into trigonometric height determination, cf. [6.4.2].

6.3 Horizontal Positioning

In classical geodetic networks, horizontal positioning has been separated from height determination. This is due to the fact that ellipsoidal height differences

derived from geometric leveling or zenith angles are affected by greater uncertainties, which enter through the reductions of the gravity field and vertical refraction, but especially because users require heights defined in the gravity field.

With the ellipsoid as a reference surface, two-dimensional positioning requires ellipsoidal trigonometry [6.3.1] and reductions of the observed positional quantities onto the ellipsoid [6.3.2]. Ellipsoidal "observation" equations allow the calculation of coordinates, after proper orientation [6.3.3]. Ellipsoidal geodesy is found in textbooks such as GROSSMANN (1976), BOMFORD (1980), and HECK (1995).

6.3.1 Ellipsoidal Trigonometry

In order to carry out computations on the ellipsoidal surface, points on the ellipsoid are connected by surface curves. The arc of the normal section and the geodesic are employed primarily.

The *normal section* is defined by the curve of intersection of the vertical plane with the ellipsoid. Azimuths and distances, after being reduced to the ellipsoid, refer to normal sections. Since the surface normals of two points on the ellipsoid are in general skewed to each other, the reciprocal normal sections from P_1 to P_2 and from P_2 to P_1 do not coincide (Fig. 6.13). The differences in azimuth (less than 0.1″ for $S = 100$ km) and in distance (less than 1 μm for $S = 100$ km) are small and can be taken into account easily (BOWRING 1971).

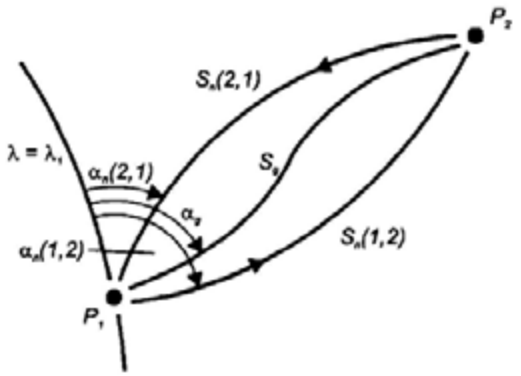

Fig. 6.13. Normal sections and geodesic

Normally, because of its favorable properties, the *geodesic* is used for ellipsoidal calculations. It is uniquely defined as the shortest connection between two points and is generally bounded by the two normal sections. This

definition is equal to the condition that the geodetic curvature (curvature of the normal projection of a surface curve onto the tangential plane) equals zero.

As known from differential geometry, the geodetic curvature k_g is represented by the triple scalar product

$$k_g = (\mathbf{r}' \times \mathbf{r}'') \cdot \mathbf{n} . \tag{6.60}$$

Here, $\mathbf{r}' = d\mathbf{r}/dS$ is the tangent vector and $\mathbf{r}'' = d^2\mathbf{r}/dS^2$ is the curvature vector. Also, S = arc length of the geodesic, and $\mathbf{n}$ designates the normal vector to the surface. With $k_g = 0$, we obtain a second-order vectorial *differential equation* for the *geodesic*:

$$(\mathbf{r}' \times \mathbf{r}'') \cdot \mathbf{n} = 0 ; \tag{6.61}$$

the local projection of the geodesic onto the ellipsoid is a straight line. We introduce the φ,λ-system of ellipsoidal coordinates (Fig. 6.14) and express the geodesic by $\lambda = \lambda(\varphi)$. Corresponding evaluation of (6.61) yields the *scalar* differential equations

$$\left.\begin{aligned} p^2 \frac{d^2\lambda}{d\varphi^2} + 2p \frac{dp}{d\varphi}\frac{d\lambda}{d\varphi} &= 0 \\ M \frac{dM}{d\varphi} - p \frac{dp}{d\varphi}\left(\frac{d\lambda}{d\varphi}\right)^2 &= 0 \end{aligned}\right\}, \tag{6.62}$$

with $p = N\cos\varphi$ = radius of the circle of latitude (4.6) and the principal radii of curvature M and N (4.13), (4.15). From Fig. 6.14, we take the relations

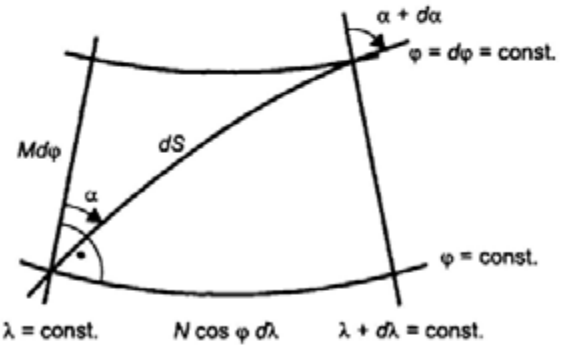

Fig. 6.14. Ellipsoidal (geodetic) surface coordinates

$$\frac{d\varphi}{dS}=\frac{\cos\alpha}{M},\quad \frac{d\lambda}{dS}=\frac{\sin\alpha}{N\cos\varphi}, \tag{6.63}$$

which are valid for any surface curve. We form $d\lambda/d\varphi$ and the second derivative and insert them into (6.62). Integration yields *Clairaut's* equation

$$N\cos\varphi\sin\alpha=\text{const}. \tag{6.64}$$

The constant corresponds to the radius of the parallel circle at which the geodesic has a 90° azimuth. By differentiation with respect to S, and taking (6.63) into account, (6.64) is transformed into

$$\frac{d\alpha}{dS}=\frac{\sin\alpha\tan\varphi}{N}. \tag{6.65}$$

Equations (6.63) and (6.64) resp. (6.65) form a system of *first-order* differential equations for the geodesic. The solution of this system leads to elliptic integrals which cannot be solved elementarily, cf. [6.3.3].

Two-dimensional positioning on the ellipsoid implies the solution of *ellipsoidal triangles*, bounded by geodesics. As the curvature of surface curves changes according to (4.18), the solution of a triangle not only requires three geometric elements (angles, distances) but also the orientation parameters latitude and azimuth.

At point distances less than 100 km (classical terrestrial networks) the ellipsoid may be approximated by the Gaussian osculating sphere (4.23), with a latitude calculated as an arithmetic mean of the latitudes of the triangle vertices. Closed *spherical formulas* then can be used for the solution of triangles (HECK 1995, p.366), e.g., the spherical law of sines

$$\frac{\sin\alpha}{\sin\beta}=\frac{\sin(a/R)}{\sin(b/R)}, \tag{6.66}$$

with the spherical angles α, β and sides a, b, and R = radius of the Gaussian sphere. Errors due to the spherical approximation remain less than 0.002″ for the angles and less than 1 mm for the distances. We finally mention the *spherical excess* which plays a role in spherical trigonometry. It is defined as the surplus over 180° of the angle sum of a spherical triangle. The excess is proportional to the area F of the triangle:

$$\varepsilon = \frac{F}{R^2}. \tag{6.67}$$

For an equilateral triangle with $S = 50$ km, the excess amounts to 5.48″.

6.3.2 Reductions to the Ellipsoid

In order to carry out a transfer of ellipsoidal coordinates on the ellipsoid, observed azimuths and distances have to be reduced to the ellipsoidal quantities α and S, which refer to the geodesic.

The reduction of the *astronomic azimuth* A is composed of three parts. Laplace's equation (6.58) takes the effect of the *deflection of the vertical* into account. The corresponding reduction to the normal section reads

$$\alpha - A = -\left(\eta \tan\varphi + \left(\xi \sin\alpha - \eta \cos\alpha\right)\cot\zeta\right). \tag{6.68}$$

The first term in (6.68) is the azimuthal component of the deflection of the vertical. It does not depend on the azimuth and corresponds to a twist in the observed directions; horizontal angles are not affected. The second term can be viewed as an "error" in setting up the theodolite, by orientating it along the plumb line direction instead of the ellipsoidal normal. While the first term reaches the order of magnitude of the vertical deflections and more, a strong reduction takes place in the second term due to $\cot\zeta$. Hence, this direction dependent term is of the order of a few 0.1″ in flat areas only but may reach some arcsec in the mountains.

If the target point is not situated on the ellipsoid but at a height h_2, a further reduction has to be applied. Namely, the vertical plane formed by the ellipsoidal normal at P_1 and the target point P_2, in general, does not contain the ellipsoidal

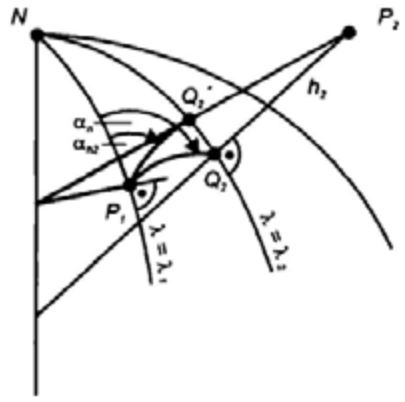

Fig. 6.15. Skew-normal reduction of the azimuth

normal through P_2 (Fig. 6.15). Therefore, the ensuing normal section does not pass through the footpoint Q_2, but through Q_2', which requires a reduction by the angle $Q_2'P_1Q_2$. This *skew-normal* reduction can be derived from the partial derivative $\partial A/\partial h_2$, formed for the adjustment in the φ,λ,h-system, cf. [6.2.1]; it reads

$$\alpha_n - \alpha_{h_2} = \frac{e^2}{2b}\cos^2\varphi \sin 2\alpha\, h_2\,, \tag{6.69}$$

where e is the first eccentricity and b the semiminor axis of the ellipsoid, cf. [4.1.1]. For $\varphi = 0°$ and $\alpha = 45°$, the reduction attains only 0.11″ at h_2 = 1000 m.

Finally, the azimuth has to be reduced from the *normal section* to the *geodesic*:

$$\alpha_g - \alpha_n = -\frac{e^2}{12a^2}\cos^2\varphi \sin 2\alpha\, S^2\,. \tag{6.70}$$

At $\varphi = 0°$ and $\alpha = 45$, this reduction reaches only 0.028″ for S = 100 km.

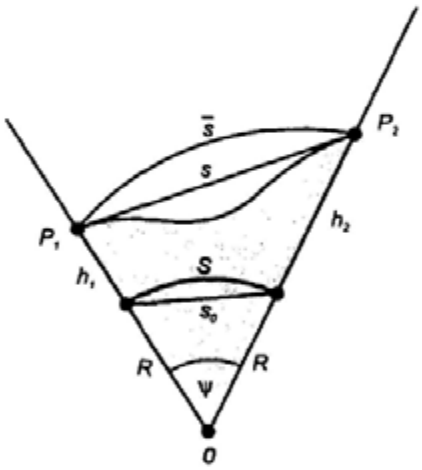

Fig. 6.16. Reduction of the spatial distance on the ellipsoid

The reduction of the chord *distance* s to the ellipsoid is a purely geometric problem, as distances do not depend on the gravity field. We assume that the effects of atmospheric refraction have been reduced beforehand, cf. [5.5.2]. From Fig. 6.16 we read

$$s^2 = (R+h_1)^2 + (R+h_2)^2 - 2(R+h_1)(R+h_2)\cos\psi$$
$$s_0 = 2R\sin\frac{\psi}{2}, \quad S = R\psi$$

which gives closed formulas for the reduction to the normal section

$$s_0 = \sqrt{\frac{s^2 - (h_2-h_1)^2}{(1+h_1/R)/(1+h_2/R)}}, \quad S = 2R\arcsin\frac{s_0}{2R}, \tag{6.71a}$$

where R is taken from Euler's formula (4.18). After series expansion, the different contributions to the reduction become apparent:

$$S - s = -\frac{h_1+h_2}{2R}s - \frac{(h_2-h_1)^2}{2s} + \frac{s_0^3}{24R^2}. \tag{6.71b}$$

The first term in (6.71b) corresponds to a reduction from the mean height to the ellipsoid. It reaches the meter-order of magnitude in the mountains at distances of several km. The second term takes the inclination of the distance into account. It generally remains below the meter-order of magnitude in the lowland but may attain large values in the high mountains. The magnitude of these reduction terms does not allow substitution of the ellipsoidal heights by orthometric or normal heights, otherwise relative errors of 10^{-5} have to be expected. The last term in (6.71b) provides the transition from the ellipsoidal chord to the normal section and reaches the cm-order only at larger distances.

The reduction from the *normal section* to the *geodesic* is given by

$$S_g - S_n = -\frac{e^4}{360\,a^4}\cos^4\varphi\sin^2 2\alpha\, S^5. \tag{6.72}$$

The magnitude reaches the meter-order only at distances of several 1000 km and can be neglected in classical network computations.

6.3.3 Computations on the Ellipsoid

The importance of ellipsoidal calculations has decreased, since the results of three-dimensional positioning in Cartesian coordinates can easily be transformed into ellipsoidal coordinates, see (4.28). Azimuths and distances derived from Cartesian coordinates, see (6.39), can be reduced to the ellipsoid according to [6.3.2]. Nevertheless, computations on the ellipsoid are still of significance in navigation, and they have been the basis for the calculation of classical horizontal control networks, which are still in use today.

The *geodetic datum* of two-dimensional systems has been established by the deflection of the vertical and the geoid height at a fundamental point, cf. [6.2.2], and the parameters of the reference ellipsoid. Equation (6.57) then allows transformation of observed astronomical latitude and longitude into the corresponding ellipsoidal quantities, and (6.46) provides the height relation between the geoid and the ellipsoid. Having reduced the horizontal directions and the distances onto the ellipsoid, only one rotation about the ellipsoidal normal in the fundamental point is possible. This rotation is fixed by applying the Laplace equation on the astronomic azimuth observed at the fundamental point. Equations (6.57) and (6.58) thus provide the parallelism of the axes of the ellipsoidal system with respect to the global geocentric system.

The accuracy of the parallelism of axes depends on the accuracy of the astronomical observations entering into (6.57) and (6.58), and hence is about one to two arcsec or better. The origin of the classical systems may deviate by some 100 m from the geocenter. This is due to the fact that one arcsec in astronomical positioning corresponds to 30 m in horizontal position, but is especially due to the use of only *relative* deflections of the vertical and geoid heights, cf. [7.1.2].

Having fixed the ellipsoidal coordinates and one geodetic azimuth at the fundamental point, ellipsoidal coordinate transfer can be carried out with the ellipsoidal "observations" referring to the geodesic. Here, it is assumed that the ellipsoidal network is errorless; for adjustment strategies see [7.1.2].

We distinguish between

- The *direct problem*, i.e., to compute the ellipsoidal coordinates φ_2, λ_2 of the point P_2, as well as the azimuth α_2, given the coordinates φ_1, λ_1 of point P_1, the azimuth α_1, and the distance S,
- The *inverse problem*, i.e., to compute the azimuths α_1, α_2 and the distance S, given the coordinates φ_1, λ_1 and φ_2, λ_2 of P_1 and P_2.

The direct and the inverse problem correspond to the solution of the ellipsoidal polar triangle P_1NP_2 (Fig. 6.17), EHLERT (1993). With the geodesic introduced as a surface curve connecting P_1 and P_2, elliptic integrals appear in the solutions, cf. [6.3.1], hence no closed solutions are available.

Numerous solutions of the direct and the inverse problem have been developed. They are based either on series expansions or on numerical integration (KNEISSL 1958/1959, SCHNÄDELBACH 1974).

A Taylor series expansion of latitude, longitude, and azimuth as a function of the arc length was given early on by *Legendre* (1806):

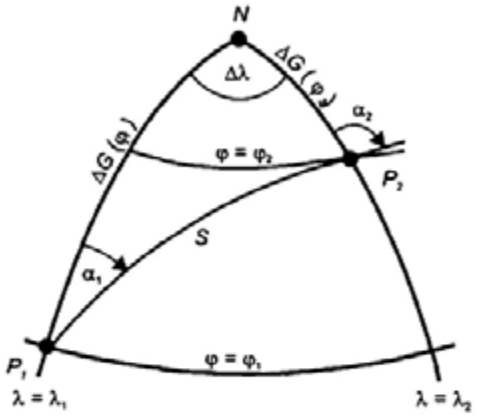

Fig. 6.17. Ellipsoidal polar triangle

$$\left.\begin{aligned}
\varphi_2-\varphi_1 &= \left(\frac{d\varphi}{dS}\right)_1 S+\frac{1}{2}\left(\frac{d^2\varphi}{dS^2}\right)_1 S^2+\cdots\\
\lambda_2-\lambda_1 &= \left(\frac{d\lambda}{dS}\right)_1 S+\frac{1}{2}\left(\frac{d^2\lambda}{dS^2}\right)_1 S^2+\cdots\\
\alpha_2-\alpha_1 &= \left(\frac{d\alpha}{dS}\right)_1 S+\frac{1}{2}\left(\frac{d^2\alpha}{dS^2}\right)_1 S^2+\cdots
\end{aligned}\right\}, \tag{6.73}$$

where the first-order derivatives are provided by (6.63) and (6.65). The higher-order derivatives are calculated according to

$$\frac{d^2\varphi}{dS^2}=\frac{\partial}{\partial\varphi}\left(\frac{d\varphi}{dS}\right)\frac{d\varphi}{dS}+\frac{\partial}{\partial\alpha}\left(\frac{d\varphi}{dS}\right)\frac{d\alpha}{dS}, \tag{6.74}$$

where the equation of the geodesic enters through $d\alpha/dS$.

Since the Legendre series are expanded with respect to S, they converge slowly. An expansion to the fifth (φ,λ) resp. fourth-order (α) is necessary at mid-latitudes in order to provide an accuracy of $\pm$ 0.0001″ and $\pm$ 0.001″ resp., at distances of 100 km. Developments up to the tenth-order are available (KRACK 1982), and modifications of (6.73) improve the convergence and allow an efficient solution for lengths of several 100 km and more.

Series expansions suitable for very long geodesics have been developed by *Bessel* (1826) and improved by *Helmert* (1880). For this method, the ellipsoidal polar triangle is projected onto a concentric sphere with radius a (Fig. 6.18). The latitude φ is transformed to the reduced latitude β (4.10). Due to Clairaut's equation (6.64), which now reads

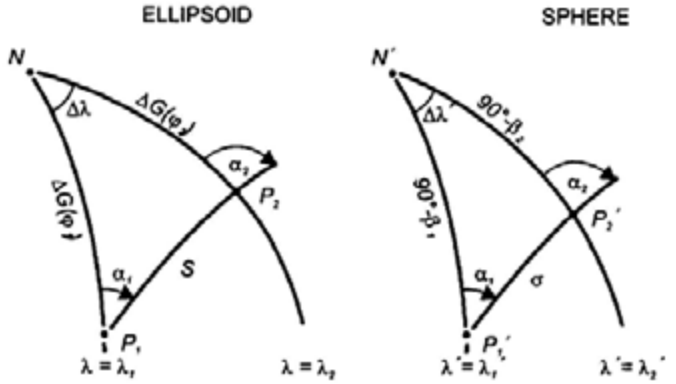

Fig. 6.18. Transfer of ellipsoidal coordinates: Bessel-Helmert solution

$$\cos\beta \sin\alpha = \text{const.},$$

the ellipsoidal azimuths are preserved if the azimuth α_1 is transferred to the sphere. The relation between the ellipsoidal distance S and the spherical distance σ, as well as those between the ellipsoidal and the spherical longitude differences $\Delta\lambda$ and $\Delta\lambda'$, are given by differential formulas which correspond to (6.63):

$$\frac{d\beta}{d\sigma} = \cos\alpha, \quad \frac{d\lambda'}{d\sigma} = \frac{\sin\alpha}{\cos\beta}. \tag{6.75}$$

By combination with (6.63), the following relations are obtained:

$$dS = a\sqrt{1-e^2\cos^2\beta}\, d\sigma, \quad d\lambda = \sqrt{1-e^2\cos^2\beta}\, d\lambda'. \tag{6.76}$$

The elliptic integrals resulting from (6.76) are solved either by expanding the square roots in series and subsequent integration term by term or by numerical methods. As the series expansions are controlled by the (small) numerical eccentricity, they converge rapidly. After projection onto the sphere, the coordinate transfer is carried out by formulas of spherical trigonometry, and the results are then transformed back to the ellipsoid by inverse relations. Computations around the globe are possible with mm-accuracy (VINCENTY 1975, KLOTZ 1993).

Numerical methods are based either on a polynomial approximation of the integrals and subsequent integration (methods of Newton, Gauss, Simpson and others), SCHMIDT (1999), or an numerical integration. In the latter case, the length of the geodesic is subdivided into small increments, which are calculated using the differential formulas (6.63) and (6.64), Fig. 6.19. Clairaut's equation serves for keeping the increments on the direction of the geodesic. Summing the

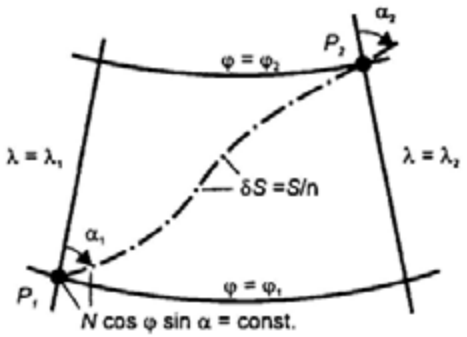

Fig. 6.19. Transfer of ellipsoidal coordinates: numerical solution

line elements provides a first approximation. By iteration with smaller increments and comparison of the results, a given error limit can be obtained. With increments of 100 m length, sub-cm accuracy can be achieved with geodesics of 10 000 km length (DORRER 1966, KIVIOJA 1971).

Inversion of the direct-problem solutions provides formulas for the *inverse problem* and is available for all methods. The adjustment of ellipsoidal networks would require *differential relations* $d\alpha/d\varphi$, $d\alpha/d\lambda$ and $dS/d\varphi$, $dS/d\lambda$. These relations can be derived from the corresponding differentials of a three-dimensional model reduced to the ellipsoid or by differentiating the solutions of the inverse problem (KNEISSL 1958, p.615, WOLF 1963b).

6.4 Height Determination

Precise height determination is based on the relative methods of geometric leveling, triangulation using zenith angles, and GPS heighting. Geometric leveling after applying small reductions provides heights defined in the gravity field [6.4.1]. Zenith angles deliver ellipsoidal heights if the influence of the gravity field is taken into account [6.4.2]. GPS heighting directly results in ellipsoidal heights, which have to be reduced to gravity field related quantities [6.4.3].

6.4.1 Heights from Geometric Leveling

The raw results of geometric leveling $\delta n \approx dn$ are transformed into potential differences by taking surface gravity g along the leveling line into account (5.113). If connected to the zero height surface (geoid, quasigeoid) geopotential numbers (3.104) are obtained:

$$C = W_0 - W_P = \int_0^P g \, dn \,. \tag{6.77}$$

In principle, the evaluation of (6.77) requires a *gravity* value at each leveling point, i.e., at distances of 100 m or less for precise leveling. This requirement can be diminished if we postulate the same relative accuracy for the influence of leveling and gravity on the geopotential differences:

$$\frac{dg}{g} = \frac{d(\Delta n)}{\Delta n} \,. \tag{6.78}$$

Assuming a leveling accuracy of 0.1 mm, gravity would only be needed with an accuracy of $\pm$ 100 μms^{-2} for Δn = 10 m, and $\pm$ 10 μms^{-2} for Δn = 100 m. Consequently, gravity values can be interpolated from gravity measurements carried out at station distances of 5 to 20 km in flat areas, and at 1 to 2 km in the mountains. Preferably, gravity stations should be established at sites where the gravity changes depart from linearity (variations in slope or direction of the leveling line, gravity anomalies). An average gravity value taken over a larger distance then can be used for transforming the leveled height difference into potential units.

Precise leveling in fundamental networks is carried out in closed loops, cf. [7.2]. The calculation of heights is performed by adjusting *potential differences*, with the condition, cf. [3.2.3],:

$$\oint dW = 0 \,. \tag{6.79}$$

Subsequent transformation yields metric heights, cf. [3.4.3].

An alternative approach, used classically, is to first convert the raw leveling results (with $\oint dn \neq 0$) into differences of the respective height system and then adjust *height differences*.

Dynamic height differences are obtained by differencing (3.105):

$$\Delta H_{1,2}^{dyn} = H_2^{dyn} - H_1^{dyn} = \Delta n_{1,2} + E_{1,2}^{dyn} \,, \tag{6.80a}$$

with the dynamic height reduction

$$E_{1,2}^{\mathrm{dyn}} = \int_1^2 \frac{g - \gamma_0^{45}}{\gamma_0^{45}}\, dn\,. \tag{6.80b}$$

For *orthometric heights*, we expand (3.106) by dynamic heights:

$$\Delta H_{1,2} = H_2 - H_1 = \Delta H_{1,2}^{\mathrm{dyn}} + \left(H_2 - H_2^{\mathrm{dyn}}\right) - \left(H_1 - H_1^{\mathrm{dyn}}\right).$$

This leads to

$$\Delta H_{1,2} = \Delta n_{1,2} + E_{1,2}\,, \tag{6.81a}$$

with the *orthometric height reduction*

$$E_{1,2} = \int_1^2 \frac{g - \gamma_0^{45}}{\gamma_0^{45}}\, dn + \frac{\bar{g}_1 - \gamma_0^{45}}{\gamma_0^{45}} H_1 - \frac{\bar{g}_2 - \gamma_0^{45}}{\gamma_0^{45}} H_2\,. \tag{6.81b}$$

An analogue equation is valid for the transformation of leveled height differences into *normal height* differences, where $\bar{g}$ is replaced by $\bar{\gamma}$ and H by H^N (3.107). The *normal height reduction* reads:

$$E_{1,2}^{N} = \int_1^2 \frac{g - \gamma_0^{45}}{\gamma_0^{45}}\, dn + \frac{\bar{\gamma}_1 - \gamma_0^{45}}{\gamma_0^{45}} H_1^N - \frac{\bar{\gamma}_2 - \gamma_0^{45}}{\gamma_0^{45}} H_2^N\,. \tag{6.81c}$$

The dynamic height reduction only depends on the path. It attains values between a few mm (flat terrain) and some cm to dm (mountains). Hence, it has to be taken into account even in local surveys if the vertical reference system is based on dynamic heights. The orthometric and the normal height reduction include the dynamic reduction, and, in addition, contain two terms with the mean gravity values at the end points of the leveling line. The different effects substantially cancel each other, with the consequence that these reductions are below one mm in flat areas and only reach a few cm in the mountains.

Mean normal gravity $\bar{\gamma}$ can be calculated by (4.67) with the spherical approximation

$$\bar{\gamma} = \gamma_0 \left(1 - \frac{H^N}{R}\right). \tag{6.82}$$

Mean gravity $\bar{g}$, on the other hand, requires the knowledge of g along the plumb line between the geoid and the earth's surface. At any point P' with height H', we have

$$g' = g - \int_{H'}^{H} \frac{\partial g}{\partial H}\, dH\,, \tag{6.83a}$$

where g is the surface gravity at P. The actual vertical gravity gradient is given by (3.71), where we may introduce (4.60) for the free-air part and 2670 $\mathrm{kg/m^3}$ as a mean crustal density; this yields

$$g' = g + 0.848\times10^{-6}\left(H - H'\right)\mathrm{ms^{-2}}\,. \tag{6.83b}$$

After inserting into (3.106) and integration between $H' = 0$ and $H' = H/2$, we obtain

$$\overline{g} = g + 0.424\times10^{-6} H\ \mathrm{ms^{-2}}\ . \tag{6.84}$$

Orthometric heights based on this estimate are also called *Helmert*-heights.

As shown in [6.5.3], the second term on the right side of (6.84) can be interpreted as a reduction of the surface gravity to actual gravity at $H/2$, with the Bouguer plate as a model of the topography. The effect of model errors remains small in flat terrain, but improved models that take actual topography and density into account are needed in the mountains (SÜNKEL 1988).

6.4.2 Trigonometrical Heights

Zenith angles can be used for a trigonometrical height transfer if refraction effects have been reduced sufficiently, cf. [5.5.1], Fig. 6.20. The ellipsoidal zenith angle is obtained from the observed quantity z' by

$$\zeta = z' + \delta + \varepsilon = z + \varepsilon\,, \tag{6.85}$$

where δ is the angle of refraction (5.11) and ε the vertical deflection component in the azimuth of the line of sight (6.18). Using spherical trigonometry, the *ellipsoidal height difference* is given by (KNEISSL 1956, p.358):

$$\Delta h_{1,2} = h_2 - h_1 = S\left(1 + \frac{h_m}{R}\right)\cot\zeta_1 + \frac{S^2}{2R\sin^2\zeta_1}\,. \tag{6.86}$$

S is the length of the ellipsoidal normal section, R the radius of curvature (4.18), and $h_m = \left(h_1 + h_2\right)/2$.

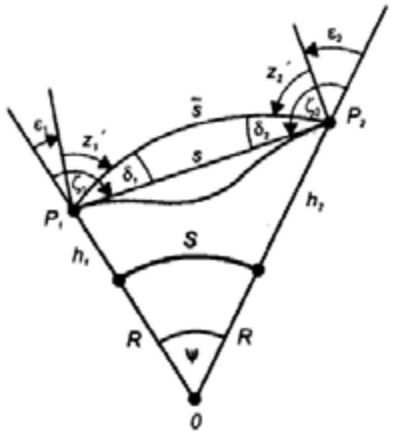

Fig. 6.20. Trigonometrical height transfer

The use of *reciprocal* zenith angles offers significant advantages. With the central angle ψ

$$\psi = \frac{S}{R} = \zeta_1 + \zeta_2 - \pi \tag{6.87}$$

taken from Fig. 6.20, we apply the law of tangents on the triangle P_1OP_2. In connection with (6.85), the height difference is obtained:

$$\Delta h_{1,2} = S\left(1 + \frac{h_m}{R} + \frac{S^2}{12R^2}\right)\tan\frac{1}{2}\left(\left(z_2' + \delta_2 + \varepsilon_2\right) - \left(z_1' + \delta_1 + \varepsilon_1\right)\right). \tag{6.88}$$

Here, only differences in δ and ε appear. Symmetric refraction conditions may be expected with *simultaneous* observations, cf. [5.5.1], thus refraction effects will mostly cancel with the use of simultaneous reciprocal-zenith-angle measurements (KUNTZ and SCHMITT 1995). They also offer a possibility to determine the *coefficient of refraction*. Combining (5.11), (6.85), and (6.87), and neglecting the deflections of the vertical, yields

$$k = 1 - \frac{R}{S}\left(z_1' + z_2' - \pi\right). \tag{6.89}$$

An average value of $k = 0.13 \pm 0.04$ was obtained by Gauss for the arc measurements in the kingdom of Hannover. This value was confirmed by other surveys for lines of sight with a large ground clearance. Close to the ground, k may vary between −1 and +1. Network adjustment models may be extended by introducing individual refraction coefficients for each station or for

each line (HRADILEK 1984), and observed meteorological parameters may also contribute to the determination of actual values for k, cf. [5.1.2], [5.5.1]. In spite of these refinements, refraction irregularities strongly limit the application of trigonometrical heighting. A cm-order of accuracy can be obtained over distances of a few km, but errors of the dm-order of magnitude have to be expected with larger distances.

Trigonometric leveling significantly diminishes the errors of a trigonometrical height transfer, by reducing the lines of sight to 100 to 300 m (RÜEGER and BRUNNER 1982). Height differences are determined by measuring zenith angles and slope distances with a total station, cf. [5.5.2]. Either simultaneous reciprocal-observations are carried out using two reflector-equipped total stations or the method of leveling "from the middle" is applied, in analogy to geometric leveling, cf. [5.5.3]. Refraction effects are substantially reduced using this strategy. The reductions are largely due to the short distances and the fact that the lines of sight run approximately parallel to the earth's surface. In this way, a favorable error propagation over larger distances is obtained (accuracies of ± 1 to 2 mm per km). The efficiency of the method can be increased by motorized procedures (BECKER 1987). By using short lines of sight, trigonometric leveling resembles the procedure employed in geometric leveling. Hence, the results represent a reasonable approximation to leveled height differences.

Trigonometric height determination with long lines played an important role in the establishment of classical horizontal networks by triangulation, as it simultaneously provided heights for reduction onto the ellipsoid and for the construction of topographical maps. Today, it is restricted to special applications, e.g., to the height determination of inaccessible sites. Trigonometric leveling, on the other hand, has been employed successfully for surveying vertical control networks of large extension (WHALEN 1985).

6.4.3 Heights from GPS

The Global Positioning System (GPS), cf. [5.2.5], provides global Cartesian coordinates and, more accurately, coordinate differences, which can easily be transformed to ellipsoidal coordinates, see (4.28), DODSON (1995). Ellipsoidal height differences can be achieved with cm-accuracy over distances up to some 100 km or more, applying differential methods and long (e.g., 24 hours) observation times. For short distances, even sub-cm accuracy can be obtained (GÖRRES and CAMPBELL 1998). Consequently, GPS heighting may support or substitute time-consuming geometric leveling, at least for distances larger than about 10 km. This strategy requires that the reduction of ellipsoidal heights to normal or orthometric heights can be performed with a similar accuracy (TORGE 1990). According to (6.46), quasigeoid or geoid differences provide the necessary reductions:

$$\Delta H^N = \Delta h - \Delta\zeta, \quad \Delta H = \Delta h - \Delta N\,. \tag{6.90}$$

Today, global quasigeoid or geoid models have relative accuracies of a few decimeters, and regional models may reach the cm to decimeter accuracy, cf. [6.6], [6.7]. The use of these models for the reduction of GPS heights presupposes that the model describes the same surface as used as zero height surface for the height system, cf. [3.4.3]. This demand can be fulfilled by fitting the model to quasigeoid or geoid heights at control points where GPS and leveled heights are available. The fitting also reduces long and medium-wave model errors.

Following the method of least squares collocation, cf. [6.8.2], the discrepancies found at the control points can be modeled as follows (MILBERT 1995, DENKER et al. 2000):

$$h_{gps} - H^N - \zeta_{mod} = t + s + n\,, \tag{6.91a}$$

where t describes a trend component, s is a stochastic signal part, and n represents the random noise of all types of observations involved (GPS, leveling, geopotential model). A simple trend function may consist of a three-parameter datum shift according to (6.41):

$$t = \cos\varphi\cos\lambda\,\Delta X + \cos\varphi\sin\lambda\,\Delta Y + \sin\varphi\,\Delta Z\,. \tag{6.91b}$$

Equivalently, the function may describe a change in the ellipsoidal coordinates of some initial point, which corresponds to a vertical shift and tilts in the NS and the EW-direction. The signal part is derived from an empirical covariance function of the de-trended residuals and modeled e.g., by an exponential function, cf. [6.1.3].

Using trend reduction only, the r.m.s. discrepancies between regional and local quasigeoid models and GPS/leveling control points have been reduced to the dm-order of magnitude over a few 1000 km and to a few centimeter over several 100 km (TORGE et al. 1989). By including also a signal part, cm-accuracy may be obtained over distances up to 1000 km, which corresponds to the accuracy of classical leveling networks (DENKER 1998).

For *local* (several 10 km) applications, gravity field related heights may be estimated by purely mathematical interpolation between GPS/leveling control points, employing, e.g., low-order surface polynomials or splines (ILLNER and JÄGER 1995). If a dense net of control points is available, and if the gravity field is sufficiently smooth, cm-accuracy can be achieved (COLLIER and CROFT 1997). The accuracy strongly decreases in rough topography, and a topographic reduction is necessary then, cf. [6.5.3].

With the further improvement of quasigeoid/geoid models, "GPS leveling" will become even more important.

6.5 Fundamentals of Gravity Field Modeling

Gravity field modeling is part of the geodetic boundary-value problem [6.5.1]. Topography plays an important role in the solution of this problem [6.5.2]. Gravity reductions serve for reducing observed gravity field data onto the geoid and also provide different kind of gravity anomalies for field interpolation and geophysical interpretation [6.5.3]. While the orientation of the gravimetrically derived geoid is uniquely defined, the scale has to be determined by distance measurements [6.5.4].

6.5.1 The Geodetic Boundary-Value Problem

The geodetic boundary-value problem comprises the determination of the surface of the earth and of its external gravity field from observations on or close to the earth's surface (SANSÒ and RUMMEL 1997). The surface to be determined is either the geoid (*Stokes'* problem) or the physical surface of the earth (*Molodenski's* problem), SANSÒ (1995).

Based on Green's third identity and the generalized Laplace equation (3.49), the problem may be formulated by a non-linear integral equation of the second kind in the gravity potential W (MOLODENSKI 1958, MOLODENSKI et al. 1962):

$$\begin{aligned} &-2\pi W + \iint_S \left(W \frac{\partial}{\partial n_s}\left(\frac{1}{l}\right) - \frac{1}{l}\frac{\partial W}{\partial n_s} \right) dS \\ &+2\pi\omega^2\left(X^2+Y^2\right) + 2\omega^2 \iiint_v \frac{dv}{l} = 0 \end{aligned} \tag{6.92}$$

Here n_s is the outer surface normal to the surface S, v is the volume of the earth and ω its rotational velocity, and l denotes the distance between the source point and the point of calculation. If W were known on S, then the geometry of the surface would remain as the only unknown quantity. After the determination of S, an upward continuation of W would deliver the external gravity field.

The problem is *linearized* by approximating the earth's surface by the telluroid (physical surface) or the ellipsoid (geoid) and by approximating the actual potential W by the normal potential U, cf. [6.1.1]. As the centrifugal part is well-known, (6.92) then transforms into an *integral equation* for T

$$-2\pi T + \iint_{\Sigma} \left(T \frac{\partial}{\partial n_{\Sigma}} \left(\frac{1}{l} \right) - \frac{1}{l} \frac{\partial T}{\partial n_{\Sigma}} \right) d\Sigma = 0 . \tag{6.93}$$

The integration is performed over the known telluroid Σ. As the surface normal n_{Σ} deviates from the direction of the plumb line, $\partial T / \partial n_{\Sigma}$ not only depends on the gravity anomaly but also on the deflection of the vertical and the slope of the terrain, cf. [6.7.2]. If applied to the geoid as a boundary surface, this dependence reduces to the gravity anomaly.

Instead of the integral equation (6.93), the geodetic boundary-value problem can be formulated by *Laplace*'s differential equation (6.2):

$$\Delta T = 0 . \tag{6.94}$$

The residual gravity field parameters observed on the earth's surface, or reduced to the geoid, then enter into boundary conditions for the solution of (6.94). The primary "observables" are the height anomalies resp. the geoid heights, and the gravity anomalies. Deflections of the vertical and gravity gradient components play a role only in local calculations.

A Taylor development of U in the telluroid point Q gives

$$U_P = U_Q + \left(\frac{\partial U}{\partial \bar{n}} \right)_Q \zeta_P + \cdots , \tag{6.95a}$$

with $\bar{n}$ = normal to $U = U_Q$ and with normal gravity

$$\gamma_Q = -\left(\frac{\partial U}{\partial \bar{n}} \right)_Q . \tag{6.95b}$$

Inserting (6.95) into (6.1) yields the *height anomaly*

$$\zeta_P = \frac{T_P - \left(W_P - U_Q \right)}{\gamma_Q} . \tag{6.96a}$$

With the condition (6.6), we obtain

$$\zeta_P = \frac{T_P}{\gamma_Q} . \tag{6.96b}$$

Equation (6.96) is called *Bruns'* theorem. If applied to the geoid it delivers the *geoid height*

$$N = \frac{T - (W_0 - U_0)}{\gamma_0}. \tag{6.97a}$$

Under the condition $U_0 = W_0$, it reads

$$N = \frac{T}{\gamma_0}. \tag{6.97b}$$

T now refers to the geoid, and γ_0 is normal gravity on the ellipsoid (4.41).

The *deflection of the vertical* is the horizontal derivative of ζ resp. N (Fig. 6.21). Taking (6.96) and (6.97) into account, the components in the direction of the meridian and the prime vertical, cf. [6.1.2], are given by

$$\xi = -\frac{1}{\gamma(M+h)}\frac{\partial T}{\partial \varphi}, \quad \eta = -\frac{1}{\gamma(N+h)\cos\varphi}\frac{\partial T}{\partial \lambda}, \tag{6.98a}$$

where the ellipsoidal arc elements are provided by (4.20). The negative sign follows from the sign conventions for the quasigeoid (geoid) and the vertical deflection, see (6.40).

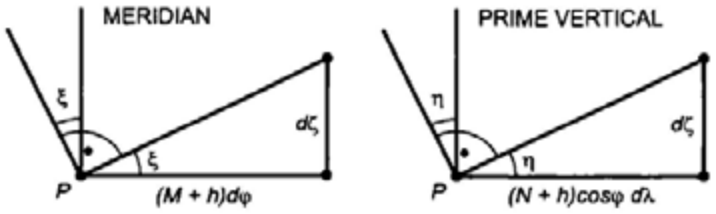

Fig. 6.21. Deflection of the vertical components and height anomaly

In spherical approximation we obtain

$$\xi = -\frac{1}{\gamma r}\frac{\partial T}{\partial \varphi}, \quad \eta = -\frac{1}{\gamma r \cos\varphi}\frac{\partial T}{\partial \lambda}. \tag{6.98b}$$

The *gravity disturbance* (6.11) is related to T by

$$\delta g_P = g_P - \gamma_P = -\left(\frac{\partial W}{\partial n}\right)_P - \left(-\frac{\partial U}{\partial \bar{n}}\right)_P = -\left(\frac{\partial T}{\partial n}\right)_P, \tag{6.99}$$

where again we have neglected the deflection of the vertical. We develop γ_P at the telluroid point Q:

$$\gamma_P = \gamma_Q + \left(\frac{\partial \gamma}{\partial \bar{n}}\right)_Q \zeta_P + \cdots. \tag{6.100}$$

Inserting into (6.99) and taking (6.96b) into account yields the *gravity anomaly*

$$\Delta g_P = g_P - \gamma_Q = -\left(\frac{\partial T}{\partial n}\right)_P + \frac{1}{\gamma_Q}\left(\frac{\partial \gamma}{\partial \bar{n}}\right)_Q T_P. \tag{6.101a}$$

With the spherical approximation, cf. [4.2.2],

$$\frac{\partial \gamma}{\partial \bar{n}} = \frac{\partial \gamma}{\partial r} = -2\frac{\gamma}{r},$$

we obtain

$$\Delta g = -\frac{\partial T}{\partial r} - \frac{2}{r}T. \tag{6.101b}$$

Equations (6.97), (6.98), and (6.101) represent boundary conditions for the solution of the Laplace equation. Because of the importance of (6.101), this first-order partial differential equation in T is known as the fundamental equation of physical geodesy.

High-precision gravity-field modeling (e.g., geoid determination with cm-accuracy) requires some refinements in the formulation and solution of the geodetic boundary-value problem (MORITZ 1974, HECK 1991). This includes the transition to an ellipsoidal approximation by developing the potential in ellipsoidal harmonics or by applying ellipsoidal corrections to the spherical approximation (JEKELI 1988b, WANG 1999). The mass of the atmosphere has to be taken into account by a corresponding reduction, cf. [4.3], and the topography has to be smoothed by a terrain correction, cf. [6.5.3].

The geodetic boundary-value problem resembles the third boundary-value problem of potential theory, namely to determine a harmonic function given a linear combination of the function and its normal derivative on a bounding surface. It differs from the classical problem, as the bounding surface is supposed to be unknown: free boundary-value problem. At the physical surface of the

earth, gravity data do not provide potential derivatives along the surface normal but rather refer to the plumb line: free and oblique boundary-value problem (GRAFAREND and NIEMEIER 1971). The horizontal components of the surface position vector cannot be determined with sufficient accuracy from gravimetric data, cf. [6.2.1], consequently the geometric part of the problem generally is restricted to the determination of heights: scalar free gravimetric boundary-value problem (HECK 1997).

With the rapid progress in satellite positioning, the geometry of the earth's surface can be assumed to be known with increasing accuracy; the only remaining unknown then is the external gravity potential. Hence, a fixed boundary-value problem can be formulated, which employs gravity disturbances as boundary values (KOCH and POPE 1972, BJERHAMMAR and SVENSSON 1983). This corresponds to the second (*Neumann*) boundary-value problem of potential theory, which is to determine a harmonic function from its derivative on the bounding surface. Finally, a mixed altimetric-gravimetric boundary-value problem may be set up, taking into account that altimetric geoid heights and gravity anomalies are the main data sets available on a global scale (SANSÒ 1981, MARTINEC 1998).

6.5.2 Gravitation of Topography

The short wavelength part of the gravitational field is dominated by the effect of the topographical masses. By reducing this effect, the gravity field is smoothed significantly, which simplifies gravity field interpolation and transformation. For the determination of the geoid, the topography has to be removed in order to establish the geoid as a boundary surface (FORSBERG and TSCHERNING 1997).

The effect of the topographic masses on gravity field parameters is calculated by the law of gravitation. The evaluation of (3.10) and corresponding integrals for other parameters poses problems, as topography is rather irregular in geometry (heights) and, to a lesser extent, also in density. Therefore, the topographic masses are subdivided into elementary bodies for which closed solutions of the mass integrals exist. Rectangular *prisms* of constant density are especially appropriate, as the heights of the topography nowadays are provided in gridded form by digital elevation models. Vertical *cylindrical columns* with constant density and height have been used extensively in the past.

In a system of three-dimensional Cartesian coordinates, the gravitational potential of the topography is expressed by

$$V_{\text{top}} = G\rho \iiint_v \frac{dv}{l} = G\rho \int_{x_1}^{x_2} \int_{y_1}^{y_2} \int_{z_1}^{z_2} \frac{1}{l}\, dx\, dy\, dz\,, \tag{6.102}$$

with $l = \sqrt{x^2 + y^2 + z^2}$. The topographic effects on the deflection of the vertical, the gravity disturbance, and the gravity anomaly follow from differentiation, according to (6.98), (6.99), and (6.101). The integration over a *rectangular*

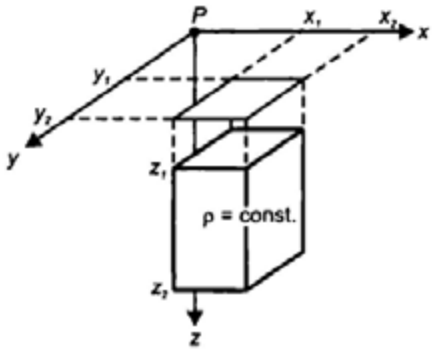

Fig. 6.22. Gravitation of topography: rectangular prism method

prism delivers closed formulas for the potential and its derivatives (FORSBERG 1984, NAGY et al. 2000). As an example, for a point located at the origin of the *x*,*y*,*z*-system, the *vertical* component of the *gravitation* is given by (NAGY 1966), Fig. 6.22:

$$b_z = G\rho \left\| x \ln(y+l) + y \ln(x+l) - z \arctan \frac{xy}{zl} \right|_{x_1}^{x_2} \Bigg|_{y_1}^{y_2} \Bigg|_{z_1}^{z_2} . \qquad (6.103)$$

The total effect of topography results from the sum over the gravitation of the individual elementary bodies:

$$\delta g_{top} = \Sigma b_z . \qquad (6.104).$$

For heights given in a regular grid, Fast Fourier Transform (FFT) techniques provide a powerful tool for the efficient calculation of topographic effects (FORSBERG 1985, SIDERIS 1985, SCHWARZ et al. 1990).

Digital elevation models (DEM), also called digital terrain models, are available on global and regional scale. They are primarily based on digitized topographic and bathymetric maps. Space techniques contribute increasingly to the improvement of DEM's. Satellite radar altimetry serves for the height determination of the Greenland and Antarctica ice sheets and provides bathymetric information, due to the correlation between the ocean surface and the ocean bottom (SMITH and SANDWELL 1994). Space and airborne interferometric synthetic aperture radar (INSAR) has become an efficient method for the development of high resolution DEM's (ZEBKER and GOLDSTEIN 1986, NIELSEN et al. 1998).

Among the global DEM's are the ETOPO5 (5′×5′ gridded land and seafloor elevations) and the GLOBE (global land one-kilometer base elevation) models provided by the NOAA National Geophysical Data Center. GLOBE is given in a 30″×30″ grid; the accuracy depends on the data

quality and varies between ± 20 m and a few 100 m (HASTINGS et al. 2000). The NASA/NIMA Shuttle Radar Topography Mission (SRTM, February 2000) collected a global (between ± 60° latitude) INSAR data set, which will be used for a DEM with 30 m mean resolution, accurate to ± 10 to 20 m. Regional DEM's have been developed in many countries with resolutions down to one arcsec (SMITH and ROMAN 2000).

For large-region applications, a mean *density* value of 2670 kgm^{-3} (corresponding to the density of granite) generally is introduced for the topographic masses. More refined density models have been used for local studies, where the density values are estimated from geological information, rock samples, and gravity profiles exploiting the density-dependent relation between gravity and height (*Nettleton* method, e.g., TORGE 1989).

Spherical harmonic models of the topography have been derived from global DEM's (PAVLIS and RAPP 1990). They serve for the development of topographic-isostatic models, cf. [8.2.2], which may be used for the prediction of mean gravity anomalies in unsurveyed areas, cf. [6.5.3].

6.5.3 Gravity Reductions to the Geoid

In order to determine the geoid as a boundary surface in the gravity field, the topographic masses have to be removed, and the observed gravity values have to be reduced to the geoid. This is done by *gravity reductions*, which provide gravity anomalies on the geoid.

Depending on how the topographic masses are displaced, different types of gravity anomalies are obtained. Uncertainties of the topographic model propagate into the calculation of the geoid. This has to be taken into account in the calculation of orthometric heights (3.106), where the same density model has to be employed.

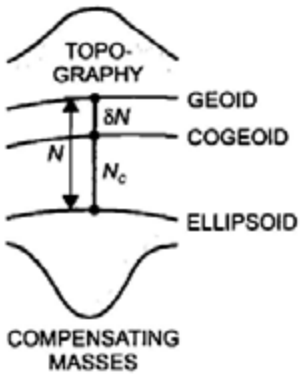

Fig. 6.23. Geoid and cogeoid

The displacement of the topographical masses changes the gravitational field of the earth, including the potential of the geoid. The level surface which possesses the geoid potential after the displacement is called *cogeoid*: *indirect effect* of the gravity reductions (WICHIENCHAROEN 1982, MARTINEC 1998). The following steps may be distinguished in the calculation of the geoid (Fig. 6.23):

- Reduction of the *direct* effect of the topography on gravity and adding of the *direct* effect of the dislocated masses if necessary, both to be calculated by the law of gravitation, cf. [6.5.2],
- Calculation of the *primary indirect* effect on the potential, caused by the removal of the topography and the dislocation of the topographic masses. The calculation is performed according to some rule of compensation:

$$\delta V = V_{top} - V_C , \tag{6.105}$$

  with V_{top} = potential of the topography and V_C = potential of the compensating masses,
- Calculation of the *vertical distance* between the geoid and the cogeoid according to (6.97b):

$$\delta N = \frac{\delta V}{\gamma} , \tag{6.106}$$

- Reduction of the gravity values from the geoid to the cogeoid: *secondary indirect* effect. Here, a free-air reduction (6.101) is sufficient:

$$\delta g_C = 2\frac{\gamma}{r}\delta N , \tag{6.107}$$

- Calculation of the heights N_C of the *cogeoid* above the ellipsoid, cf. [6.6], [6.7],
- Calculation of the *geoid* heights according to

$$N = N_C + \delta N . \tag{6.108}$$

In principle, every kind of gravity reduction could serve for the calculation of the geoid according to this scheme. Naturally, the indirect effect should be small in order to avoid laborious and error susceptible computations. Other criteria for the selection of gravity reductions include the smoothness of the resulting gravity anomalies, which facilitates interpolation, and their geophysical significance, which would allow interpretation. Under these aspects, we may distinguish between the effects of (homogeneous) topography,

density anomalies within the topography and the earth's crust, and isostatic compensation masses, cf. [8.2.2].

The *free-air anomaly* is generally used for the calculation of the geoid, with the assumption that no masses exist above the geoid. The *free-air reduction*

$$\delta g_F = -\frac{\partial g}{\partial H} H \tag{6.109}$$

(H = orthometric height) provides the reduction of the surface gravity to the geoid, and the *simple* free-air anomaly on the geoid is given by

$$\Delta g_F = g + \delta g_F - \gamma_0 . \tag{6.110}$$

According to (6.109), the correct reduction to the geoid requires the knowledge of the actual vertical gravity gradient. Splitting the gradient into a normal and an anomalous part gives

$$\frac{\partial g}{\partial H} = \frac{\partial \gamma}{\partial H} + \frac{\partial (\Delta g)}{\partial H} . \tag{6.111}$$

The actual and the normal part may differ by 10% or more. The normal gravity gradient can be calculated by (4.61). The calculation of the anomalous part corresponds to the downward continuation of a harmonic function. It can be formulated by Poisson's integral, which is a solution of the first (Dirichlet) boundary-value problem of potential theory, and solved by an integration over the surface gravity anomalies, cf. [6.7.2]. If the gravity anomaly depends linearly on elevation, the anomalous gradient corresponds to the terrain correction (MORITZ 1980, p.421), see below. Due to the assumptions made in (6.110), it equals the direct effect of the topographic and the dislocated masses on gravity (SIDERIS 1990). A discrete solution of this problem has been given by BJERHAMMAR (1969, 1985), which takes into account that gravity data are given only at discrete points. This solution satisfies all given data and generates missing data, and it is harmonic down to an internal sphere (Bjerhammar sphere), cf. [3.3.2].

The free-air anomaly on the *geoid* should be clearly distinguished from the free-air anomaly defined on the *surface* of the earth (6.15) where the normal gravity gradient is used for reduction.

The *terrain correction* removes irregularities of the topography. It creates a plate (spherical or planar) of constant thickness and density (Bouguer plate) by filling mass deficits below P and removing excess masses above the plate (Fig. 6.24). For planar approximation (Bouguer plate extending to infinity), both measures increase gravity at P; the terrain correction then is always positive. It can be calculated from digital elevation models, cf. [6.5.2], and attains values of 1 to 10 μms^{-2} in flat areas, reaching several 100 μms^{-2} in the mountains. From (6.102) we obtain

$$\delta g_T = G\rho \int_{-\infty}^{+\infty}\int_{-\infty}^{+\infty}\int_{z=H_P}^{z=H} \frac{z-H_P}{l^3}\,dx\,dy\,dz\,. \tag{6.112a}$$

For small surface slopes, the distance

$$l = \sqrt{(x-x_P)^2 + (y-y_P)^2 + (z-z_P)^2}$$

may be approximated by

$$l_0 = \sqrt{(x-x_P)^2 + (y-y_P)^2}\,.$$

The linear approximation of the terrain correction then reads

$$\delta g_T = \frac{1}{2} G\rho \int_{-\infty}^{+\infty}\int_{-\infty}^{+\infty} \frac{(H-H_P)^2}{l_0^3}\,dx\,dy\,, \tag{6.112b}$$

where H resp. H_P are the orthometric heights of the terrain and the point of calculation (FORSBERG and TSCHERNING 1997).

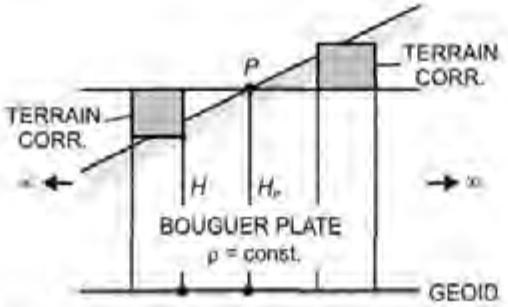

Fig. 6.24. Bouguer plate and terrain correction

By including the terrain correction into (6.110), we obtain the *terrain-corrected* free-air anomaly, called *Faye-anomaly*. The shift of the topographic masses now corresponds to a compensation of the Bouguer plate on the geoid (Helmert's *compensation* method). Here, the *surface density*

$$\mu = \frac{dm}{ds} = \rho\frac{dv}{ds} = \rho H \tag{6.113}$$

replaces the volume density ρ and takes the height of topography into account.

As the mass displacement is slight, the indirect effect of the free-air and the compensation reduction remains small. It reaches at most a few meters in the absolute sense and is of the cm to dm-order for geoid differences. As the height-dependent effect of the topography has not been removed, free-air anomalies are strongly correlated with height. Therefore, point free-air anomalies are not suited for interpolation and cannot be geophysically interpreted. For limited areas, the height-dependence can be described by linear regression, which corresponds to the application of the Bouguer plate reduction (see below). Interpolation and calculation of mean gravity anomalies is then facilitated (GROTEN and REINHART 1968).

By removing the effect of topography explicitly through a *topographic reduction* δg_{top}, we obtain the *Bouguer gravity anomaly* Δg_B. After the removal of the masses the surface gravity again is reduced to the geoid by the free-air reduction and compared with the normal gravity γ_0 (Fig. 6.24):

$$\Delta g_B = g - \delta g_{top} + \delta g_F - \gamma_0 . \tag{6.114}$$

The topographic reduction is calculated from digital elevation models, cf. [6.5.2].

In most cases, the topographic reduction is decomposed into the Bouguer plate reduction δg_P and the terrain correction δg_T. The *Bouguer plate reduction* accounts for the gravitation of an infinitely extended horizontal plate with constant density. Its thickness is given by the height of the computation point. The gravitational effect of the Bouguer plate is derived from the attraction of a circular cylinder on a point located on the cylinder axis (GARLAND 1979, MILITZER and WEBER 1984). By extending the cylinder radius to infinity, one obtains

$$\delta g_P = 2\pi G \rho H = 0.000\,419\,\rho H \ \mu\text{ms}^{-2}, \tag{6.115}$$

where ρ is taken in kg/m^3 and H in m. The *terrain correction* reduces the topography to the Bouguer plate (see above). The *Bouguer anomaly* then reads

$$\Delta g_B = g - \delta g_P + \delta g_T + \delta g_F - \gamma_0 . \tag{6.116}$$

For large-region applications (e.g., national gravimetric surveys), a spherical Bouguer plate and a corresponding terrain correction is used frequently, with a calculation extending 170 km from the computation point and conventional density being 2670 kg/m^3.

Due to the removal of the height-dependent part of topography, Bouguer anomalies display smooth long-wave variations only. Hence, they are well suited for interpolation. Revealing density anomalies below the geoid, the Bouguer anomalies are of considerable significance in geophysics and geology, cf. [8.2.4]. On the other hand, since the topographic masses are

completely removed and not restored (i.e. shifted to infinity), the indirect effect is very large (several 100 m). Hence, Bouguer anomalies are not used for geoid computations.

The Bouguer plate model allows a simple calculation of the *mean gravity* $\bar{g}$ along the plumb line required for the computation of the orthometric height H (3.106), (6.81). If we assume a linear change of g along the vertical, $\bar{g}$ will be found at the height $H/2$. Hence it can be derived from surface gravity by removing a Bouguer plate of thickness $H/2$, a free-air reduction from H to $H/2$, and a subsequent restoration of the Bouguer plate above $H/2$. Removing and restoring the Bouguer plate has the same (negative) effect on gravity; so we obtain

$$\bar{g} = g - \delta g_P(H) + \delta g_F(H/2). \tag{6.117}$$

Evaluation with (6.115) and (6.109), and introducing the density value 2670 $\mathrm{kg/m^3}$, leads to (6.84).

Equation (6.117) also provides an important interpretation of the difference between the heights of the geoid and the quasigeoid resp. the normal and the orthometric height. With the mean normal gravity

$$\bar{\gamma} = \gamma_0 - \delta g_F(H/2), \tag{6.118}$$

the *mean gravity anomaly* (6.9) is identified as the Bouguer anomaly (terrain correction neglected)

$$\bar{g} - \bar{\gamma} = g - \delta g_P(H) + \delta g_F(H) - \gamma_0 = \Delta g_B \ . \tag{6.119}$$

This fact permits a simple transformation from the quasigeoid to the geoid, cf. [6.7.2].

Isostatic anomalies are formed by not only removing the effect of topography but by also restoring compensation masses in the earth's crust below the geoid, according to some isostatic model. In this way, the crust is regularized, obtaining constant thickness and density, cf. [8.2.2]. The gravitational effect of the compensating masses is taken into account by an *isostatic reduction* δg_I to be calculated from the isostatic model according to [6.5.2]. The isostatic anomaly then is given by

$$\Delta g_I = g - \delta_{top} + \delta g_I + \delta g_F - \gamma_0 . \tag{6.120}$$

The largest part of the earth's topography is isostatically compensated. Hence, isostatic anomalies are small and vary smoothly about zero, with the exception of uncompensated areas. They may be

successfully employed for gravity prediction, and they are of great value for geophysical and geodynamic interpretation, cf. [8.2.4]. The compensating masses are arranged more remote from topography than in the free-air reduction (see above). Therefore, the indirect effect is larger and may reach 10 meters. Because of this, isostatic anomalies are rarely used for geoid calculations.

6.5.4 Orientation and Scale of Gravity Field Models

The following *assumptions* were made for the spherical harmonic expansion of the disturbing potential and the transformation to the quasigeoid resp. geoid, cf. [6.1.1], [6.5.1]:

- The level ellipsoid and the earth have the same mass:

$$M_{\text{Ell}} = M \,. \tag{6.121}$$

  Hence, no zero-degree term T_0 appeared in the expansion (6.4),
- The center of the ellipsoid and the earth's center of mass (origin of the global coordinate system) coincide; no first-degree term entered into (6.4), cf. also [3.3.4],
- The normal potential U and the actual potential W are related by

$$U_Q = W_P \,, \tag{6.122a}$$

  which corresponds to the condition

$$U_0 = W_0 \tag{6.122b}$$

  between the potential of the level ellipsoid and the geoid.

A first-degree term in the spherical harmonic expansion would not affect the gravity anomaly, as the corresponding expansion (6.135) contains the factor $(l-1)$. Hence, the ellipsoid may be positioned in the geocenter without changing the gravity field: the gravimetric method yields "absolute" results.

Because of residual uncertainties in the determination of the mass and the potential, small differences between the values for the geoid and the ellipsoid have to be admitted:

$$\delta M = M - M_{\text{Ell}}, \quad \delta W = W_0 - U_0 \,. \tag{6.123}$$

The spherical harmonic expansion of T then must be extended by

$$T_0 = \frac{G\,\delta M}{R}, \tag{6.124}$$

and Bruns' formula must take T_0 and the potential difference into account:

$$N_0 = \frac{G\,\delta M}{\gamma R} - \frac{\delta W}{\gamma}. \tag{6.125}$$

For spherical approximation, the constant N_0 corresponds to a change in scale of the geoid. The expansion of the gravity anomaly (6.135), according to (6.101), has to be extended by (HEISKANEN and MORITZ 1967, p. 100 ff)

$$\Delta g_0 = -\frac{T_0}{R} + \frac{2}{R}\delta W = -\frac{G\,\delta M}{R^2} + \frac{2}{R}\delta W. \tag{6.126}$$

With the usual assumption of equality of mass and potential, the gravimetric solution of the boundary-value problem delivers results which refer to a best-fitting ellipsoid, where the equatorial radius ("scale") remains unknown by N_0.

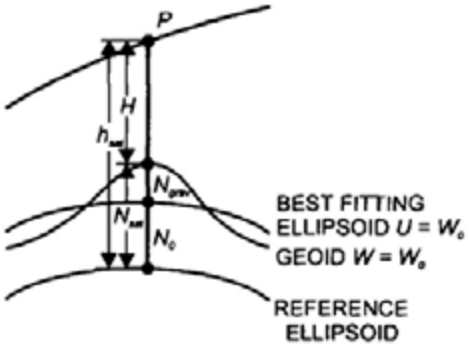

Fig. 6.25. Gravimetric geoid and geodetic reference ellipsoid

The *zero-degree undulation* N_0 can be determined by comparing gravimetrically computed geoid heights with geoid values derived by differencing distances that refer either to the geoid or to the ellipsoid. The primary data sets used are from satellite altimetry on the oceans and GPS heights on the continents (RAPP and BALASUBRAMANIA 1992, JEKELI 1998), Fig. 6.25). The geoid height from these satellite techniques is given by

$$N_{sat} = h_{sat} - H, \tag{6.127}$$

where h_{sat} stands for the ellipsoidal height of the altimeter or the GPS height, and H is the height of the altimeter above the geoid (result of the altimeter measurements) or the orthometric height derived from leveling. The zero-degree term is obtained by

$$N_0 = N_{sat} - N_{grav}. \tag{6.128}$$

It can be used to derive the semimajor axis of the best-fitting ellipsoid to which the gravimetric geoid heights refer:

$$a_{grav} = a_{sat} + N_0. \tag{6.129}$$

Generally, the ellipsoid adopted as part of a geodetic reference system, cf. [4.3], is kept unchanged. The gravimetrically determined geoid heights are then corrected in order to refer to that reference ellipsoid (e.g., the GRS80 ellipsoid):

$$N_{ref} = N_{sat} = N_{grav} + N_0. \tag{6.130}$$

Classically, best-fitting ellipsoids have been determined by comparing horizontal distances measured on the geoid with the ellipsoidal distances obtained by calculation, cf. [7.1.2]. A separation between δM and δW in principle would be possible using (6.126), together with (6.125), using the condition $\Delta g_0 = 0$ (6.19). However, deficiencies in the global gravity coverage still prevent use of this method. On the other hand, the geocentric gravitational constant GM is known today with high accuracy from space probes and high-flying satellites (GROTEN 2000). The determination of N_0 thus provides the potential of the geoid. From Topex/Poseidon altimeter data, the equatorial radius of an ellipsoid that best fits the zero-tide geoid, cf. [3.4.1], has been estimated to 6 378 136.49 ± 0.1 m (RAPP 1995c).

6.6 Global Gravity Field Modeling

Global gravity field modeling is required for large-scale problems including the determination of satellite orbits, inertial navigation, and development of geophysical and geodynamic models. The geoid is required for establishing a global vertical reference system and for deriving sea surface topography. Finally, global models provide the long wavelength part of the gravity field for local gravity field approximation, cf. [6.7].

Global gravity models are based on spherical harmonic expansions [6.6.1]. The low frequency part of these series expansions stems from the analysis of satellite orbits [6.6.2]. Expansions of higher degree are achieved by combining

the low-degree models with the results of terrestrial gravimetry and satellite altimetry [6.6.3], BOUMAN (1997), NEREM et al. (1995), RAPP (1998).

6.6.1 Spherical Harmonic Expansions

Equations (6.3) to (6.5) provide the development of the disturbing potential T into spherical harmonics. A gravity field model thus is represented by the *spherical harmonic coefficients.* The functional relations between T and other relevant gravity field parameters, cf. [6.5.1], also allow spherical harmonic expansions for the height anomaly, the geoid height, and the gravity anomaly. These expansions generally employ fully normalized spherical harmonics, cf. [3.3.2].

By inserting (6.4) into Bruns' theorem (6.96b), we obtain the spherical harmonic expansion for the *height anomaly*

$$\zeta(r,\vartheta,\lambda)=\frac{GM}{r\gamma}\sum_{l=2}^{\infty}\left(\frac{a}{r}\right)^{l}\sum_{m=0}^{l}\left(\Delta\bar{C}_{lm}\cos m\lambda+\Delta\bar{S}_{lm}\sin m\lambda\right)\bar{P}_{lm}(\cos\vartheta)\,. \quad (6.131)$$

Here, the fully normalized coefficients and spherical harmonics are indicated by bars. Equation (6.97b) delivers the corresponding expansion for the *geoid height*, which can be also be derived from (6.131), taking (6.9) into account:

$$N(r,\vartheta,\lambda)=\zeta(r,\vartheta,\lambda)+\frac{\Delta g_B}{\bar{\gamma}}H\,. \quad (6.132)$$

Differentiation of (6.4) with respect to r gives the spherical harmonic expansion for the *gravity disturbance* (6.99):

$$\delta g=-\frac{\partial T}{\partial r}=\frac{1}{r}\sum_{l=2}^{\infty}(l+1)\left(\frac{a}{r}\right)^{l+1}T_l(\vartheta,\lambda)\,. \quad (6.133)$$

Inserting (6.4) and (6.133) into (6.101b) yields the expansion of the *gravity anomaly*

$$\Delta g(r,\vartheta,\lambda)=\frac{1}{r}\sum_{l=2}^{\infty}(l-1)\left(\frac{a}{r}\right)^{l+1}T_l(\vartheta,\lambda)\,. \quad (6.134)$$

Substituting T_l from (6.5) gives

$$\Delta g(r,\vartheta,\lambda) = \frac{GM}{r^2}\sum_{l=2}^{\infty}(l-1)\left(\frac{a}{r}\right)^l \sum_{m=0}^{l}\left(\Delta\bar{C}_{lm}\cos m\lambda + \Delta\bar{S}_{lm}\sin m\lambda\right)\bar{P}_{lm}(\cos\vartheta) \quad (6.135)$$

By comparing the abbreviated form

$$\Delta g(r,\vartheta,\lambda) = \sum_{l=2}^{\infty}\left(\frac{a}{r}\right)^{l+1}\Delta g_l(\vartheta,\lambda) \quad (6.136)$$

with (6.134), we obtain the relation between the surface spherical-harmonics of T and Δg:

$$\Delta g_l(\vartheta,\lambda) = \frac{l-1}{r}T_l(\vartheta,\lambda). \quad (6.137)$$

Corresponding equations can be derived for the deflection of the vertical and for higher derivatives of T (WENZEL 1985). Due to the scarcity of terrestrial data of these types, these expansions are of limited importance. Second-order derivatives of T obtained from satellite gravity gradiometry, on the other hand, will be of great importance for future gravity field modeling (RUMMEL et al. 1993).

Equations (6.131) to (6.135) permit the harmonic coefficients to be determined from "observations", by *least-squares adjustment*, cf. [6.6.2], [6.6.3]. The coefficients can also be determined by *quadrature* over the observations. Taking the orthogonality relations and the properties of the fully normalized harmonics into account, the inversion of (6.131) and (6.135) yields (JEKELI 1998):

$$\begin{Bmatrix}\Delta\bar{C}_{lm}\\ \Delta\bar{S}_{lm}\end{Bmatrix} = \frac{1}{4\pi GM}\iint_{\sigma} r\gamma\left(\frac{r}{a}\right)^l N\bar{P}_{lm}(\cos\vartheta)\begin{Bmatrix}\cos m\lambda\\ \sin m\lambda\end{Bmatrix}d\sigma \quad (6.138a)$$

and

$$\begin{Bmatrix}\Delta\bar{C}_{lm}\\ \Delta\bar{S}_{lm}\end{Bmatrix} = \frac{1}{4\pi GM}\iint_{\sigma}\frac{r^2}{l-1}\left(\frac{r}{a}\right)^l \Delta g\,\bar{P}_{lm}(\cos\vartheta)\begin{Bmatrix}\cos m\lambda\\ \sin m\lambda\end{Bmatrix}d\sigma\,. \quad (6.138b)$$

The integration is extended over the unit sphere σ. In contrast to least squares adjustment, the quadrature approach only allows exploitation of one type of data for the determination of the harmonic coefficients.

Global data sets do not cover the earth homogeneously, and they have a limited spatial resolution. Consequently, *mean* geoid heights and mean gravity anomalies over surface compartments are introduced in gravity field modeling, where the surface blocks generally are bounded by meridians and parallels. The mean values are calculated according to

$$\bar{N} = \frac{1}{\Delta\sigma}\iint_{\Delta\sigma} N \, d\sigma, \quad \Delta\bar{g} = \frac{1}{\Delta\sigma}\iint_{\Delta\sigma} \Delta g \, d\sigma . \tag{6.139}$$

The block size $\Delta\sigma$ depends on the data distribution, cf. [6.6.3]. The maximum gravity field resolution which can be achieved is $\sqrt{\Delta\sigma}$. This corresponds to a maximum degree of the spherical harmonic expansion l_{max} = 180°/resolution°, cf. [3.3.3]. The introduction of mean values causes a local smoothing of the gravity field, which also leads to smoothed harmonic coefficients. This fact has to be taken into account by damping factors (≤ 1), which depend on the degree and the dimension of the compartment (KATSAMBALOS 1979).

The truncation of the spherical harmonic expansion at l_{max} produces an *omission error* due to the neglected part of the gravity field. This error can be estimated from the degree variances of the gravity field parameters. Degree variance models have been derived for gravity anomalies, see (6.27). They are based on the covariance function of the gravity anomalies (6.25), but can also be calculated from Laplace's surface harmonics Δg_l (6.26). In spherical approximation ($r = a = R$), (6.137) gives

$$\Delta g_l = \frac{GM}{R^2}(l-1)\sum_{m=0}^{l}\left(\Delta\bar{C}_{lm}\cos m\lambda + \Delta\bar{S}_{lm}\sin m\lambda\right)\bar{P}_{lm}(\cos\vartheta). \tag{6.140}$$

Inserting (6.140) into (6.26) and evaluating yields the anomaly degree-variances as a function of the harmonic coefficients:

$$\sigma_l^2(\Delta g) = \left(\frac{GM}{R^2}\right)^2 (l-1)^2 \sum_{m=0}^{l}\left(\Delta\bar{C}_{lm}^2 + \Delta\bar{S}_{lm}^2\right). \tag{6.141}$$

This relation can especially be used to calculate the low-degree variances from the harmonic coefficients obtained from satellite orbit analysis.

The functional relations between the gravity field parameters, cf. [6.5.1], also permit the calculation of degree variances for geoid heights, deflections of the vertical, and higher-order derivatives (TSCHERNING and RAPP 1974, TSCHERNING 1976). With $\gamma = GM/r^2$, a comparison between (6.131) and (6.135) gives the geoid degree variance

$$\sigma_l^2(N) = \left(\frac{R}{\gamma(l-1)}\right)^2 \sigma_l^2(\Delta g). \tag{6.142}$$

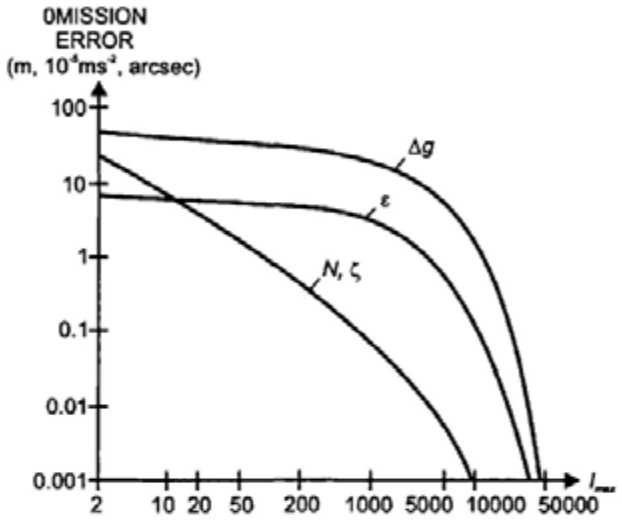

Fig. 6.26. Omission error for geoid heights (height anomalies), vertical deflections, and gravity anomalies (degree variance model TSCHERNING and RAPP 1974)

The omission error for geoid heights, gravity anomalies, and deflections of the vertical is shown in Fig. 6.26. For the presently usual truncation at degree 360, it amounts to ± 0.23 m, ± 253 μms^{-2}, and ± 3.8″. An expansion to l = 7200, corresponding to a spatial resolution of 2.8 km, would reduce these errors to ± 0.002 m, ± 27 μms^{-2}, and ± 0.4″.

6.6.2 Low-degree Gravity Field Models

Low-degree gravity field models are required for precise satellite orbit calculation, positioning of tracking stations, and long-wave geoid representation. They are primarily based on *satellite tracking data*, which are analyzed with respect to the deviations of the actual orbit from a precalculated reference orbit, cf. [5.2.2]. *"Satellite-only"* models use tracking data exclusively. In some cases, they have been utilized for the precise orbit determination of a specific satellite, especially by taking into account observations to that satellite ("tailored" models).

The "perturbing" gravitational potential (5.34) changes the Keplerian orbit elements with time (5.35). As the gravitational potential is modeled by a spherical harmonic expansion, the harmonic coefficients enter as unknowns into the observation equations of satellite geodesy, cf. [6.2.1]. In order to resolve the

gravitational field to a certain degree, satellites in different altitudes and with different inclinations are required, in addition to a good global distribution of the tracking stations and a sufficiently long observation time. The attenuation of the gravity field with height and the decrease of the harmonic coefficients at higher degrees, together with deficiencies in the geometry of the satellite orbits and the ground stations, limits the resolution of "satellite-only" models. With the satellites presently available (altitudes of 800 km and more), developments up to degree 70 have been carried out. Satellite-to-satellite tracking and satellite gravity gradiometry at orbital altitudes of about 300 km will extend this range up to degree 150 to 200, cf. [5.2.8], RUMMEL 1979.

We now regard the influence of the gravitational field on the satellite orbit. We distinguish between secular (linear), long-periodic (few days to months), and short-periodic (periods less than one day or one satellite revolution) perturbations (KAULA 1966, SEEBER 1993). The relationship between the perturbations of the orbital elements and the harmonic coefficients is obtained by transforming the spherical coordinates of the expansion (3.89) into the Keplerian elements, forming the derivatives of the perturbing potential with respect to the elements, and inserting them into (5.35).

Determination of the secular and long-periodic perturbations requires the integration over long arcs (several days). Here, short-periodic perturbations with periods of one or several revolutions are already eliminated. Furthermore, the influence of the tracking station coordinates becomes smaller with longer integration intervals, so that the stations may be even introduced as known. For the low-degree *zonal* coefficients, the integration over one satellite revolution yields the following variations for the orbital elements of main interest:

$$\left.\begin{aligned}
\Delta\Omega &= -3\pi\left(\frac{a_e}{\bar{p}}\right)^2 \cos i\, J_2 + \cdots \\
\Delta\omega &= 6\pi\left(\frac{a_e}{\bar{p}}\right)^2 \left(1-\frac{5}{4}\sin^2 i\right) J_2 + \cdots \\
\Delta e &= -3\pi\left(1-e^2\right)\left(\frac{a_e}{\bar{p}}\right)^3 \left(1-\frac{5}{4}\sin^2 i\right) \sin i \cos\omega\, J_3 + \cdots \\
\Delta i &= 3\pi\left(\frac{a_e}{\bar{p}}\right)^2 \left(1-\frac{5}{4}\sin^2 i\right) \cos i \cos\omega\, e J_3 + \cdots
\end{aligned}\right\}, \qquad (6.143)$$

with $\bar{p} = a\left(1-e^2\right)$ and a_e = semimajor axis of the earth ellipsoid.

J_2 and higher even-zonal-coefficients cause *secular* perturbations in Ω and ω. For $i < 90°$, Ω decreases in time (westward regression of the nodal line). The

change in ω corresponds to a rotation of the orbital ellipse in the orbital plane (Fig. 5.5). This rotation produces *long-periodic* perturbations in the quantities e and i, as they depend on ω. The even zonals thus can be determined primarily from the perturbations in Ω and ω, while the odd zonals are obtained from i and e. If the perturbations are added to the orbital elements of the initial epoch, one obtains the orbital elements at a specific epoch as a function of the zonal harmonics. Substitution into (6.33) provides a system of observation equations for the determination of the zonal harmonic coefficients. As mentioned earlier, the coefficients depend particularly on the inclination but also on the semimajor axis and the eccentricity.

The *tesseral* harmonics are responsible for small-amplitude (a few 100 m) short-periodic perturbations, especially in the elements i, Ω, ω. They can be determined only from dense observations over short arcs. Weather-independent microwave measurements are particularly suitable for this purpose.

Several tesseral terms of higher degree and order can be determined by *resonance* effects, arising after days to weeks. These effects occur if the ratio of the mean angular velocity of the satellite to the rotational velocity of the earth is an integer number, which produces an enhancement of perturbation in a repeat orbit.

Recent "satellite-only" models employ several million records of tracking data. Laser distance and microwave range and range-rate measurements form the bulk of the data, but optical directions still are included and assist in stabilizing the solutions. Spaceborne positioning systems, including GPS, increasingly contribute to the data set. The observations to more than 30 satellites are generally used, with altitudes varying between 800 and 20 000 km and inclinations between 40° and 110°.

While limitations in computational facilities previously forced zonal, tesseral and resonant terms to be computed separately, the harmonic coefficients can now be rigorously determined by a common least squares adjustment, together with the coordinates of the tracking stations, ocean tidal parameters, polar motion and earth rotation. Sometimes the horizontal station velocities and the variations of the low-degree coefficients with time are also included in the adjustment (BOUMAN 1997).

Weighting of data and modeling of systematic effects poses a special problem for these complex adjustments. As the accuracy estimates generally are too optimistic, the calculated standard deviations often are "scaled", e.g., by a factor of 5 (SCHWINTZER et al. 1997).

In most cases, "satellite-only" models are improved and stabilized by *combining* them with satellite altimetry and surface gravity data. Mean values for $1°\times1°$ blocks are introduced as "observations" and calculated either from point or smaller block values, cf. [6.6.3]. The observation equations for satellite

altimetry are given by (5.49), after inserting (6.131) for the altimetric geoid heights and taking a low-degree spherical harmonic model of sea surface topography into account. The observation equation for the gravity anomalies is given by (6.135). The normal equations of these data sets are added to the normal equations of the satellite-only model (RAPP 1997). Tab. 6.1 gives the values for the low degree-and-order harmonic coefficients, as derived from a recent combination solution.

Tab. 6.1. Fully normalized harmonic coefficients ($\times 10^6$), GRIM4-C4 model (SCHWINTZER et al. 1997)

l	m	$\bar{C}_{lm}$	$\bar{S}_{lm}$
2	0	-484.1656	
	2	2.4393	-1.4000
3	0	0.9573	
	1	2.0301	0.2484
	2	0.9050	-0.6194
	3	0.7213	1.4143
4	0	0.5402	
	1	-0.5353	-0.4735
	2	0.3509	0.6626
	3	0.9910	-0.2011
	4	-0.1883	0.3088
5	0	0.0687	
6	0	-0.1506	
7	0	0.0906	
8	0	0.0505	
9	0	0.0282	
10	0	0.0517	

The relative *accuracy* of the harmonic coefficients derived from low-degree spherical harmonic expansions decreases with increasing degree, from about 10^{-7} at $l = 2$ to about 1% at $l = 10$ and approaches 100% at $l = 30$ to 40 (satellite-only models) resp. at $l = 65$ to 70 (combination models). The long-wave part of the marine geoid is accurate to about ± 0.8 m (satellite-only) and ± 0.25 m (combination). Orbit determination for dedicated satellites (TOPEX/POSEIDON, ERS-1) is possible with an accuracy of a few cm with these models.

The first gravity field information from space came from Sputnik I (1957), with the dynamic form factor J_2 (polar flattening); and from Vanguard I (1958), with the coefficient J_3 (unequal flattening at the north and south pole). The Smithsonian Astrophysical Observatory (SAO) Standard Earth I provided a model complete to degree and order 8 (LUNDQUIST and VEIS 1966). Among the recent low-degree solutions are the NASA Goddard Space Flight Center (GSFC) earth model GEM T3 (satellite-only and combination with GEOS-3, Seasat, and GEOSAT altimetry

and 1°×1° surface gravity anomalies, complete to degree and order 50, resolved also for the coordinates of about 400 tracking stations and ocean tides, polar motion and earth rotation parameters, LERCH et al. 1994); the joint (GSFC, University of Texas, Ohio State University, CNES France) gravity model JGM-2S (satellite-only, complete to degree and order 70, NEREM et al. 1994); and the JGM-3 (70,70, including Doris and GPS-tracking, TAPLEY et al. 1996), which was developed primarily for the TOPEX/POSEIDON mission. The GRIM4 models (Geoforschungszentrum Potsdam and Groupe de Recherches de Géodésie Spatiale, Toulouse) include a satellite-only (60,60) and a combination (72,72) solution and also solve for a large number of additional parameters (SCHWINTZER et al. 1997), see also BOUMAN (1997), RAPP (1998).

6.6.3 High-degree Gravity Field Models

Parameters of high-degree gravity-field models are restricted to the harmonic coefficients and do not include other unknowns: *geopotential models*. Degree and order of the spherical harmonic expansion depend on the spatial resolution of the gravity field data available and on their global distribution. Of particular interest is the high-resolution quasigeoid resp. geoid needed for the establishment of a global vertical datum, cf. [3.4.3], as a reference for satellite altimetry in the determination of sea surface topography, cf. [3.4.2], and for the transformation of GPS-heights to normal or orthometric heights, cf. [6.4.3].

The models combine low-degree gravity-field models with surface gravity anomalies and altimetric geoid heights. Hence, they utilize:

- The harmonic coefficients of a "satellite-only" model (sometimes a combination model is used), with the full error covariance matrix,
- Mean free-air anomalies from terrestrial gravimetry on land and sea,
- Mean geoid heights from satellite altimetry. Some solutions use mean gravity anomalies derived from the geoid heights, with a transformation based either on an integral formula, cf. [6.7.1], or on least squares collocation, cf. [6.8.2].

Mean *free-air anomalies* are calculated from point anomalies collected e.g., at the Bureau Gravimetrique International or the U.S. National Imagery and Mapping Agency (NIMA). Least squares prediction is employed for interpolation to gridded values, where Bouguer anomalies are used as intermediate gravity field quantities, cf. [6.5.3], RAPP (1997). 1°×1° mean values based on measurements are available for a large part of the world (about 80%). On the continents, 30′×30′ mean anomalies have also been derived for large regions, but great gaps exist on the oceans and in antarctica. The accuracy of the mean anomalies amounts to about ± 50 to ± 200 μms^{-2} (KIM and RAPP 1990, KENYON 1998).

Mean *altimetric geoid heights* are derived from individual measurements to the sea surface, after least squares adjustment of the crossover discrepancies and reduction of the sea surface topography by an oceanographic model. Data sets of high accuracy and resolution are available

from the GEOSAT and ERS-1 geodetic missions, which cover the oceans between ± 72° resp. 82° latitude with an equatorial track spacing of 4 resp. 8 km. Mean geoid heights, and by inversion 30'×30' mean gravity anomalies, have been calculated from mean values derived for smaller block sizes, cf. [6.7.1], where the accuracy of the altimetric gravity anomalies is about ± 20 μms^{-2} and more homogeneous than surface gravity.

By combining the mean anomalies from surface gravimetry and altimetry, only a few percent of the earth's surface remain uncovered. These gaps are filled either by some low-degree model values and/or isostatic anomalies calculated from topographic-isostatic models (PAVLIS and RAPP 1990).

High-degree geopotential models are calculated either by least squares adjustment or by quadrature methods (RAPP 1997).

A *least squares adjustment*, in principle, would utilize all available data in order to determine the full set of potential coefficients (130 321 coefficients at l,m = 360,360; 3.24 million coefficients at 1800,1800), together with the error variance/covariance matrix. Currently, computational limitations still prevent a rigorous adjustment of these quantities. Consequently, non-optimum solutions have been developed, which, for instance, presuppose a complete data coverage on a grid and homogeneous and uncorrelated errors. Special arrangements of the normal equation matrix (block-diagonal technique) then allow an efficient computation by iterative procedures (COLOMBO 1981, WENZEL 1985, PAVLIS et al. 1996).

The *quadrature* approach employs the integration over the gravity anomalies according to (6.138). As a global and homogeneous data set is required, altimetric geoid heights have to be transformed into gravity anomalies and data gaps have to be filled by model values. After the calculation of the harmonic coefficients from the gravity anomalies, they are combined by adjustment with the coefficients of a low-degree gravity model (COLOMBO 1981, RAPP and PAVLIS 1990).

The long-wave structures of the *free-air anomalies* and the *geoid*, as derived from a recent geopotential model, are shown in Figs. 6.27 and 6.28. The free air anomalies vary rather irregularly about zero, but a correlation with extended mountain chains (Cordilleras, Himalaya) can be recognized. The principal features of the geoid include the maxima near New Guinea (+80 m), in the North Atlantic, the southwestern Indian Ocean, and in the Andes, as well as the minima at Sri Lanka (-105 m), in Antarctica, to the west of California, and near Puerto Rico.

Early spherical harmonic expansions are due to *Jeffreys* (1941-1943), *Zhongolovich* (1952), and *Uotila* (1962). Sparse surface gravity data coverage limited these expansions to the low-degree harmonics. *Kaula* (1959) introduced a constraint from satellite orbit analysis in order to develop a

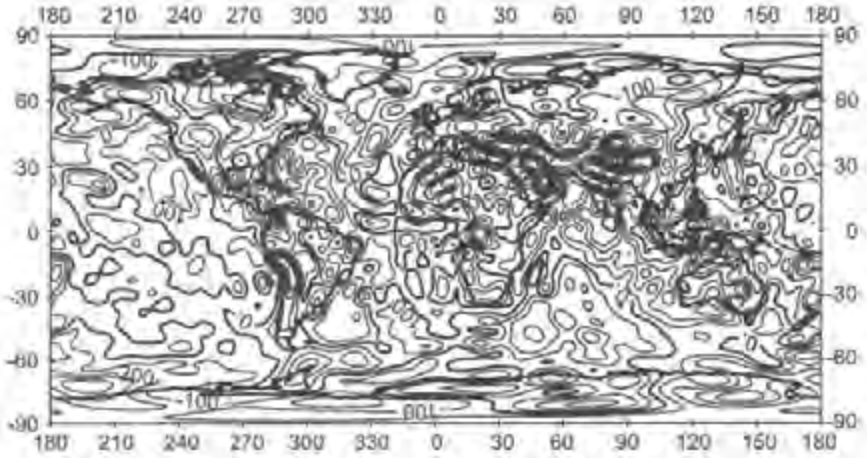

Fig. 6.27. EGM96 gravity anomalies, spherical harmonic expansion truncated at degree and order 36, contour line interval 100 μms^{-2} (LEMOINE et al. 1998)

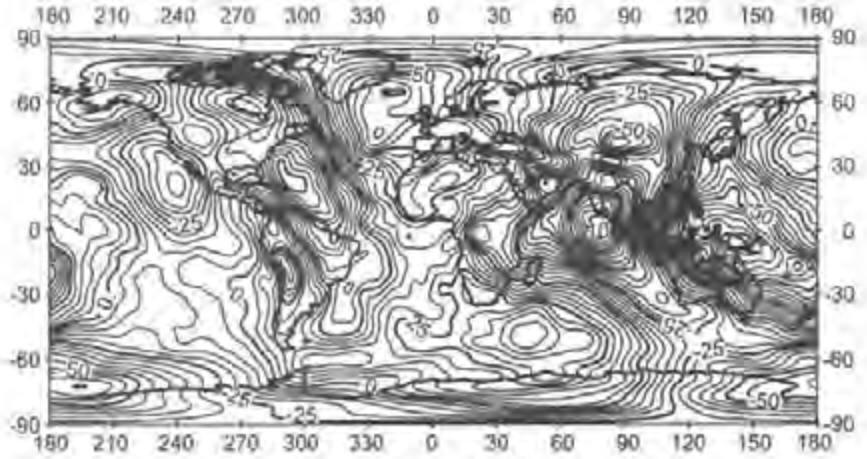

Fig. 6.28. EGM96 geoid heights, spherical harmonic expansion truncated at degree and order 36, contour line interval 5 m (LEMOINE et al. 1998)

8.8 geoid model (RAPP 1998). Among the recently developed geopotential models are the Ohio State University (OSU) model OSU91 (combination of the GEM-T2 36,36 model with 1°×1° and 30°×30° gravity anomalies from surface gravimetry and altimetry, quadrature method, RAPP et al. 1991) and the Geoforschungszentrum Potsdam (GFZ) model GFZ96 (combination of the GRIM-4 60,60 and 72,72 models with terrestrial anomalies and ERS-1 geoid heights, least squares iteration, GRUBER et al. 1997), both complete to degree and order 360.

Most complete sets of satellite tracking data (including altimetry in the form of tracking), gravity anomalies, and recent satellite altimetry (GEOSAT, ERS-1 in the polar regions) have been utilized in the NASA/GSFC and NIMA joint geopotential (360,360) model EGM96 (LEMOINE

et al. 1997, 1998). The model is composed of a 70,70 combination model (least squares adjustment resolving for tidal parameters and a 20,20 model of sea surface topography, as well as for station coordinates) and 30′×30′ mean anomalies. Up to degree and order 359, a block-diagonal solution was performed, and the degree 360 coefficients were calculated by quadrature. Geoid accuracy estimates are between ± 0.5 m (oceans) and ± 1 m (land).

A 1800,1800 ultra-high spherical harmonic model GPM98 was developed by WENZEL (1999) by combining EGM96 with 5′×5′ mean gravity anomalies collected from surface gravity and altimetry for about 75% of the earth's surface (the remaining areas being filled by larger block size values), where integral formulas were applied for the calculation of the coefficients. In areas well covered by high-resolution data, this solution provides a relative geoid accuracy of a few cm and gravity anomalies accurate to several 10 μms^{-2} .

Tailored geopotential models have been developed in order to better approximate the gravity field in a certain region (WEBER and ZOMORRODIAN 1988, KEARSLEY and FORSBERG 1990). Here, a global high-resolution spherical harmonic expansion is used as a starting model, and higher degree coefficients are modified and extended so as to better reproduce high resolution gravity anomalies in the region. Among these models are a 360,360 solution for Europe (BAŠIĆ et al. 1989), a 500,500 solution for Canada (LI and SIDERIS 1994), and a 720,720 solution for China (LU et al. 2000).

6.7 Local Gravity Field Modeling

Local gravity field approximation is especially useful for the determination of geoid or quasigeoid heights with high accuracy, as needed for the reduction of GPS heights, cf. [6.4.3]. Integral formulas allow a pointwise calculation of gravity field quantities, and thus provide the possibility of an arbitrarily high gravity field resolution which depends only on data coverage and quality (SANSO and RUMMEL 1997).

Utilizing gravity anomalies as the primary data set, classical solutions aim at the determination of geoid heights and geoidal deflections of the vertical [6.7.1]. Reduction to the geoid is avoided in the calculation of the corresponding surface quantities, where the quasigeoid plays a special role [6.7.2]. Once the gravity field is known on the geoid or on the physical surface of the earth, an upward continuation provides gravity field quantities in space [6.7.3]. Astronomically determined deflections of the vertical furnish differences of geoid or quasigeoid heights and may locally support or substitute gravimetric solutions [6.7.4].

An alternative approach to the integral formulas is least squares collocation which will be discussed under the more general aspect of "integrated geodesy" in [6.8.2].

6.7.1 Gravimetric Geoid Heights and Deflections of the Vertical

The series expansion (6.4) for the disturbing potential T can also be represented by a surface integral. By inserting (6.137) into (6.3), this expansion reads

$$T(r,\vartheta,\lambda)=\sum_{l=2}^{\infty}\frac{r}{l-1}\left(\frac{a}{r}\right)^{l+1}\Delta g_l(\vartheta,\lambda). \tag{6.144}$$

As known from potential theory, the surface spherical harmonics Δg_l are derived by inversion of (6.136), as a surface integral of the gravity anomalies over the unit sphere σ:

$$\Delta g_l=\frac{2l+1}{4\pi}\iint_{\sigma}\Delta g\, P_l(\cos\psi)\,d\sigma, \tag{6.145}$$

where $P_l(\cos\psi)$ are the Legendre polynomials. Inserting into (6.144) yields the *disturbing potential* on the *geoid* in spherical approximation:

$$T(\vartheta,\lambda)=\frac{R}{4\pi}\iint_{\sigma}S(\psi)\Delta g\,d\sigma, \tag{6.146}$$

where the integral kernel

$$S(\psi)=\sum_{l=2}^{\infty}\frac{2l+1}{l-1}P_l(\cos\psi) \tag{6.147a}$$

can be expressed in closed form:

$$S(\psi)=\frac{1}{\sin\frac{\psi}{2}}+1-5\cos\psi-6\sin\frac{\psi}{2}-3\cos\psi\ln\left(\sin\frac{\psi}{2}+\sin^2\frac{\psi}{2}\right). \tag{6.147b}$$

This integral formula has been derived by STOKES (1849); it is called *Stokes' formula*. If an accuracy of the cm-order of magnitude is required, *ellipsoidal* corrections have to be applied (SÜNKEL 1997).

By inserting (6.146) into Bruns' theorem (6.97b), we obtain the *geoid height*

$$N=\frac{R}{4\pi\gamma_m}\iint_{\sigma}S(\psi)\Delta g\,d\sigma, \tag{6.148}$$

where γ_m is a mean gravity value over the earth. Stokes' formula can also be derived as a solution of the integral equation (6.93), if applied to the geoid.

Stokes' function $S(\psi)$ acts as a weighting function on the gravity anomalies. It depends on the spherical distance ψ between the point of computation and the surface element $d\sigma$ with the gravity anomaly Δg. $S(\psi)$ decreases with ψ until a first zero at $\psi = 39°$, and then oscillates with large values until $\psi = 180°$ (Fig. 6.29). The *neighborhood* of the computation point requires particular attention, as $S(\psi)$ becomes infinite at $\psi = 0°$. The contribution of the innermost zone can be estimated in planar approximation (e.g., with a radius s_i = 5 km), by expanding Δg in a Taylor series and performing integration term by term. To a first approximation, the effect of the *inner zone* on the geoid height depends on the gravity anomaly in the computation point:

$$N_i = \frac{s_i}{\gamma_m} \Delta g_P + \cdots . \tag{6.149}$$

The components of the *deflection of the vertical* are obtained by differentiating T in north-south and east-west direction (6.98). This can be realized by expressing ψ in (6.146) in spherical coordinates of the computation point and the source point (the corresponding formulas of spherical trigonometry are taken from the spherical polar triangle, see Fig. 2.14), differentiation, and resubstitution of ψ. We obtain

$$\begin{Bmatrix} \xi \\ \eta \end{Bmatrix}_0 = \frac{1}{4\pi\gamma_m} \iint_\sigma \frac{dS(\psi)}{d\psi} \Delta g \begin{Bmatrix} \cos\alpha \\ \sin\alpha \end{Bmatrix} d\sigma , \tag{6.150}$$

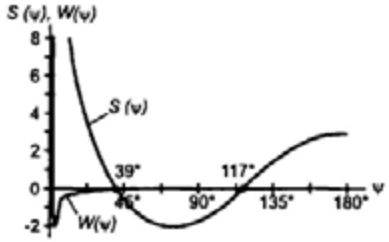

Fig. 6.29. Original and modified Stokes' function

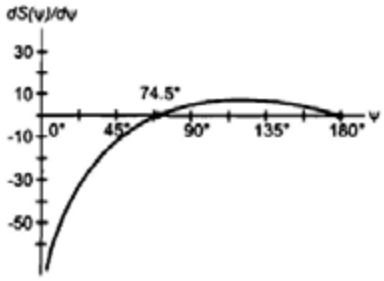

Fig. 6.30. Vening-Meinesz function

where α is the azimuth of the great circle from the computation point to the source point. Equation (6.150) was derived by VENING-MEINESZ (1928).

The *Vening-Meinesz function*

$$\frac{dS}{d\psi} = -\frac{\cos(\psi/2)}{2\sin^2(\psi/2)} + 8\sin\psi - 6\cos(\psi/2) - 3\frac{1-\sin(\psi/2)}{\sin\psi} + 3\sin\psi \ln\left[\sin(\psi/2) + \sin^2(\psi/2)\right] \quad . \quad (6.151)$$

is infinite at $\psi = 0°$ and then decreases rapidly, attaining only small values after $\psi = 50°$ to $60°$ (Fig. 6.30). The contribution of the *innermost zone* depends primarily on the horizontal gradient of the gravity anomalies:

$$\begin{Bmatrix} \xi \\ \eta \end{Bmatrix}_i = -\frac{s_i}{2\gamma_m} \begin{Bmatrix} \partial(\Delta g)/\partial x \\ \partial(\Delta g)/\partial y \end{Bmatrix}_P + \cdots . \quad (6.152)$$

Stokes' and Vening-Meinesz' formulas allow a *pointwise* calculation of the geoid height and the deflection of the vertical, by integrating the gravity anomalies given on the surface of the geoid, cf. [6.5.3]. The properties of Stokes' function require high resolution gravity data all over the earth, while the effect of remote zones is small in the calculation of vertical deflections and can be estimated by low-degree global gravity field models. The inner zone may contribute some cm to the geoid height, this is well accounted for at gravity station distances of 1 to 5 km, depending mainly on the roughness of topography. The effect of the inner zone on the deflection of the vertical can reach several arcsec, especially in the mountains. A dense gravity survey and/or the calculation of the effect of topography is needed in order to achieve an accuracy better than one arcsec.

In practice, the integrals (6.148) and (6.150) are solved by a summation of finite surface elements. For this purpose, either a set of gridded point anomalies is formed from the observed data, using e.g., least squares prediction or spline interpolation, or mean values over surface blocks delineated by meridians and parallels are calculated. The latter case also requires the integration of the Stokes or Vening-Meinesz function over the block. After gridding, a very efficient solution is obtained in the spectral domain using Fast Fourier Transform (FFT) techniques. The convolution required in (6.148) and (6.150) becomes a simple multiplication, and the results are easily retransformed to the space domain by the inverse FFT (SCHWARZ et al. 1990, HAAGMANS et al. 1993, SÜNKEL 1997).

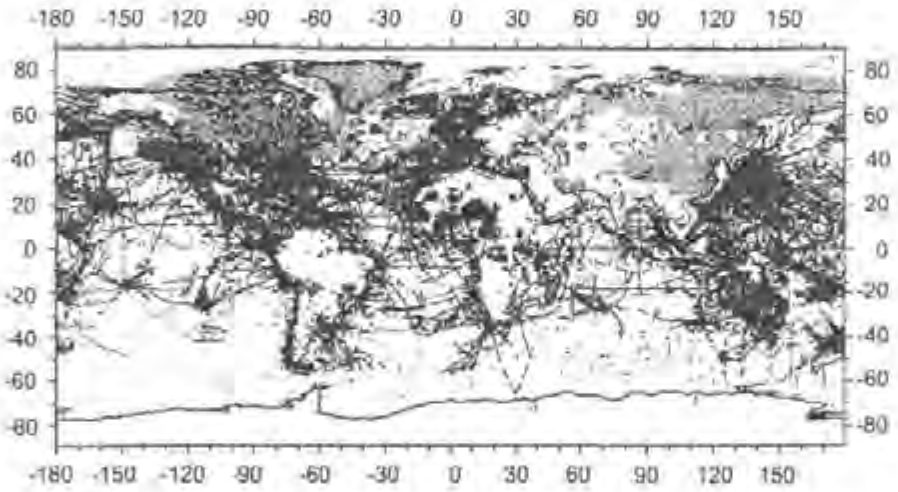

Fig. 6.31. Global distribution of terrestrial gravity data, from IAG (1997)

Point gravity anomalies (or mean gravity anomalies for some countries) are collected and kept at a few global *gravity data bases* (U.S. National Imagery and Mapping Agency NIMA: about 30 mill. point values, Bureau Gravimetrique International: about 13 mill. data freely available, Fig. 6.31). The accuracy of point anomalies derived from land, sea and airborne gravimetry varies between ± 5 and ± 50 μms^{-2}, cf. [5.4.4]. In order to avoid long-wave systematic errors in gravity field modeling, the anomalies have to refer to the same gravity (IGSN71), horizontal (ITRF, GRS80) and vertical reference systems, where the global vertical datum poses a special problem, cf. [3.4.3], HECK (1990).

The data gaps still existing in large parts of the oceans can be filled by the results of *satellite altimetry*, cf. [5.2.7]. For this purpose, the altimetrically derived geoid heights are transformed to gravity anomalies either by least squares collocation, cf. [6.8.2], or by a surface integral resulting from the inversion of Stokes' formula (6.148), taking (6.101b) into account (LELGEMANN 1976):

$$\Delta g_P = -\frac{\gamma_m}{R} N_P - \frac{\gamma_m}{16\pi R} \iint_\sigma \frac{N - N_P}{\sin^3(\psi/2)} d\sigma . \qquad (6.153)$$

Here, N and N_P are the altimetric geoid heights at a particular surface element $d\sigma$ and at the computation point P, respectively. Due to the properties of the integral kernel, the influence of the more remote zones on Δg decreases rapidly. Hence, by combining the altimetric geoid heights with a global geopotential model, the integration can be restricted to a radius of a few degrees.

Altimetric gravity anomalies have been calculated for block sizes down to 5′×5′ and 2′×2′ from high resolution altimetry as provided by the geodetic missions of Geosat and ERS-1 (SANDWELL and SMITH 1997, ANDERSEN and KNUDSEN 1998).

Purely gravimetric or gravimetric/altimetric calculations of geoid heights and deflections of the vertical suffer from the data gaps at the polar caps, in some continental areas, and at coastal zones. They are also hampered by long-wave systematic data errors and by inhomogeneous spatial resolution and accuracy of the gravity data. Free-air anomalies on land, in addition, are rather irregular due to the gravitation of topography.

Global geopotential models, on the other hand, provide the long-wave part of the gravity field, cf. [6.6.3], and dense gravity data with station distances down to 1 to 3 km are available in many regions, usually together with high-resolution digital elevation models, cf. [6.5.2]. This leads to solutions that *combine* the global model with the gravity data in a limited region, where data smoothing techniques are used by considering the terrain effect.

Combination solutions apply the *remove-restore technique* (FORSBERG and TSCHERNING 1981, DENKER et al. 1986), which includes the following steps:

- Reduction of the gravity anomalies Δg by the anomaly part of the global model Δg_M,
- Smoothing of the anomalies by some kind of terrain reduction Δg_T (see below),
- Gridding of the residual gravity anomalies

$$\Delta g_{res} = \Delta g - \Delta g_M - \Delta g_T , \tag{6.154}$$

- Application of Stokes' formula (6.148) on the residual gravity anomalies, resulting in residual geoid heights N_{res},
- Restoration of the effects of the global model and the terrain to the residual geoid heights:

$$N = N_{res} + N_M + N_T . \tag{6.155}$$

The remove-restore technique can also be applied on the deflections of the vertical or any other gravity field quantity. It has been used successfully also with least squares collocation, but for large-scale geoid modeling, integral formulas together with FFT is the only practicable technique to date.

Since the residual gravity anomalies no longer contain the long and short-wave parts of the gravity field, they are considerably smaller and smoother than the original data, and they possess (approximately) homogeneity and isotropy properties, cf. [6.1.3]. With global models complete to

degree and order 360, the integration area can be restricted to the region with dense data coverage and a narrow edge zone around it.

As only a small radius of integration is required for the remove-restore technique, a *planar approximation of Stokes'* formula is permitted. Stokes' function then reduces to

$$S(\psi) \approx \frac{1}{\sin(\psi/2)} \approx \frac{2}{\psi} \approx 2\frac{R}{l_0}, \tag{6.156a}$$

with $l_0 = \sqrt{(x - x_p)^2 + (y - y_p)^2}$ and x_p, y_p = plane coordinates of the computation point. The spherical surface element is replaced by the planar element

$$dS = R^2 \, d\sigma. \tag{6.156b}$$

Inserting (6.156a) and (6.156b) into (6.148) yields *Stokes' formula* in *planar approximation*

$$N = \frac{1}{2\pi\gamma_m} \iint_S \frac{\Delta g}{l_0} \, dS, \tag{6.156c}$$

which is very convenient to evaluate by FFT techniques; the integration can be restricted to spherical distances of a few degrees.

Different strategies can be pursued for the application of *terrain reductions* (FORSBERG and TSCHERNING 1997).

When *Helmert's condensation method* is employed, terrain-corrected Bouguer anomalies are used for gridding, cf. [6.5.3]. After restoring the Bouguer plate term ("condensation"), Faye anomalies reduced by the effect of the global model serve for the calculation of residual geoid heights.

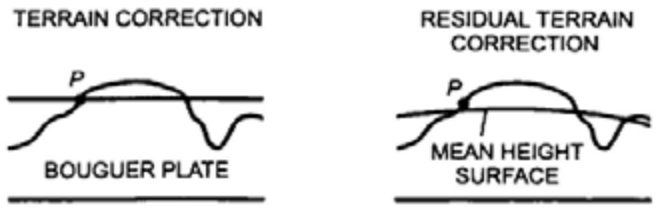

Fig. 6.32. Bouguer plate with terrain correction and residual terrain correction

With the *residual terrain correction*, only the high-frequency part of topography is taken into account in the remove-restore process, as the long-wave part has been subtracted already with the global model (FORSBERG and TSCHERNING 1981). It is calculated from a residual terrain model (RTM) which refers to a reference topography, as provided by a global topographic model (spherical harmonic expansion of the same degree and order as the geopotential model, RUMMEL et al. 1988) or the moving average over mean heights of 15′×15′ or 30′×30′ blocks. This procedure produces a balanced set of positive and negative anomalies (Fig. 6.32). The prism method is used generally for the calculation of the residual terrain correction, cf. [6.5.2].

If applied to Stokes' formula, the remove-restore technique implies that the complete spectrum of the geoid heights is computed from the gravity anomalies in the integration area, augmented by the values of the global model outside this region. In the case of long-wave discrepancies between the terrestrial gravity data and the global model, this leads to an distortion of the long wavelengths of the geoid. This problem is avoided by *least squares spectral combination* (SJÖBERG 1979, WENZEL 1982). Here, the long-wave spectral components of the global model and of the gravity anomalies are combined within the area of integration, using a least squares adjustment with spectral weights

$$w_l = \frac{\sigma_l^2(\varepsilon_M)}{\sigma_l^2(\varepsilon_M) + \sigma_l^2(\varepsilon\,\Delta g)}. \qquad (6.157a)$$

Fig. 6.33. Gravimetric Geoid99 of the U.S.A., contour line interval 2 m (SMITH and ROMAN 2001), courtesy D.A. Smith, National Geodetic Survey/NOAA

The error degree variances $\sigma_l^2(\varepsilon_M)$ of the potential coefficients of the global model are estimated in analogy to (6.142), and the error degree variances of the terrestrial anomalies $\sigma_l^2(\varepsilon_{\Delta g})$ are derived from an error covariance function (WEBER 1984), in analogy to (6.25). Here, Stokes' function is extended by the spectral weights to form an optimum integral kernel

$$W(\psi)=\sum_{l=2}^{\bar{n}}\frac{2l+1}{l-1}w_l P_l(\cos\psi). \tag{6.157b}$$

This function is no longer infinite at $\psi = 0°$, and it converges to zero more rapidly than the original Stokes' function, see Fig. 6.33.

Early gravimetric geoid calculations with Stokes' formula are due to *Hirvonen* (1934) and *Tanni* (1948). Based on isostatic anomalies, the "Columbus Geoid" was calculated at the Ohio State University (HEISKANEN 1957). A combination of a low-degree satellite model (Goddard GEM-6, degree and order 16) with 1°×1° free-air gravity anomalies (integration radius 10°) was presented by MARSH and VINCENT (1974). Among the recent regional solutions is the gravimetric geoid for the U.S.A.. It is based on a 2′×2′ grid of Faye anomalies, constructed from Bouguer anomalies, and employs the EGM96 model as a global reference, cf. [6.6.3], Fig. 6.33. This geocentric geoid, accurate to about 0.2 m, also has been fitted to the North American vertical datum, cf. [7.2], SMITH and MILBERT (1999). Least squares spectral combination has been applied in the calculation of a European quasigeoid, cf. [6.7.2].

6.7.2 Gravimetric Height Anomalies and Surface Deflections of the Vertical

The geodetic boundary-value problem for the *physical* surface of the earth has been formulated by *M.S Molodenski,* through the integral equation (6.92), MOLODENSKI et al. (1962). By introducing the telluroid Σ as an approximation to the earth's surface, an integral equation for the disturbing potential was obtained (6.93). In contrast to the derivative $\partial T/\partial n$ (n = normal to the level surface), the derivative $\partial T/\partial n_\Sigma$ (n_Σ = normal to the telluroid) now not only depends on the gravity anomaly but also on the deflection of the vertical and the inclination of the terrain. Inserting $\partial T/\partial n_\Sigma$ into (6.93) yields (HEISKANEN and MORITZ 1967, p.299)

$$\left.\begin{aligned} &T-\frac{1}{2\pi}\iint_\Sigma\left(\frac{\partial}{\partial n_\Sigma}\left(\frac{1}{l}\right)-\frac{1}{\gamma}\frac{\partial\gamma}{\partial h}\frac{\cos\beta}{l}\right)T\,d\Sigma \\ &=\frac{1}{2\pi}\iint_\Sigma\frac{1}{l}\left(\Delta g-\gamma\left(\xi\tan\beta_x+\eta\tan\beta_y\right)\cos\beta\,d\Sigma\right)\end{aligned}\right\}, \tag{6.158}$$

with β_x, β_y = angle of terrain inclination in NS and EW-direction, β = angle of maximum inclination, and ξ,η = vertical deflection components.

A simpler integral equation can be derived by expressing T as the potential of an infinitely thin *surface layer* condensed on the telluroid. With the surface density μ (6.113), the law of gravitation (3.10) yields

$$T = G\iint_{\Sigma} \frac{\mu}{l}\, d\Sigma . \tag{6.159}$$

As the potential of a surface layer is harmonic outside the surface, Laplace's equation is fulfilled, and we may introduce (6.159) and its normal derivative into (6.101). This strategy results in an integral equation which only depends on Δg and on the terrain inclination. It can be solved by successive approximation, leading to a series expansion for T (MORITZ 1971). With Bruns' formula (6.96), the corresponding development for the height anomaly ζ is obtained. In spherical approximation (σ = unit sphere, R = earth's radius), and limiting the series to its first two terms, the *height anomaly* is given by

$$\zeta = \frac{R}{4\pi\gamma}\iint_{\sigma} \left(\Delta g + G_1\right) S(\psi)\, d\sigma + \cdots , \tag{6.160a}$$

where $S(\psi)$ is Stokes' function (6.147). The main term corresponds to Stokes' formula as applied to the surface gravity anomalies (6.14). The first correction term, in close approximation, is

$$G_1 = \frac{R^2}{2\pi}\iint_{\sigma} \frac{H^N - H_P^N}{l_0^3}\Delta g\, d\sigma, \quad l_0 = 2R\sin\frac{\psi}{2} . \tag{6.160b}$$

It depends on the terrain inclination (H^N = normal height) and on gravity anomalies. Assuming a linear correlation of the gravity anomalies with height, G_1 can be approximated by the gravimetric terrain correction (6.112), MORITZ (1968b), SIDERIS (1990). Hence, Faye anomalies, cf. [6.5.3], are well suited for the computation of height anomalies.

Since the integral kernel in (6.160b) decreases rapidly with increasing spherical distance ψ, the integration can be restricted to a limited area. Higher-order terms in (6.160) contain the tangent of the terrain inclination and can be neglected generally. In order to ensure convergence of Molodenski's series expansion, extreme inclinations and singularities (steep slopes) need to be removed by some smoothing procedure. The Molodenski correction terms reach the dm-order of magnitude in the high mountains and remain at the cm-order in the lowlands. If the remove-restore technique, cf. [6.7.1], is applied, the corrections reduce by about one-order of magnitude and the series convergence is significantly improved.

Molodenski's problem has been thoroughly investigated by MORITZ (1971) and others, and the existence and uniqueness of the solution was proved by HÖRMANDER (1976) and SANSÒ (1988).

A very efficient method for calculating the height anomaly is provided by the "*gradient solution*" (MORITZ 1980). Here, the surface gravity anomalies are first reduced to sea level (geoid or quasigeoid); then Stokes' integral is applied, leading to height anomalies on sea level. An upward continuation finally gives the surface height anomaly:

$$\zeta = \frac{R}{4\pi\gamma}\iint_{\sigma}\left(\Delta g - \frac{\partial(\Delta g)}{\partial H}H\right)S(\psi)\,d\sigma + \frac{\partial\zeta}{\partial H}H\,. \qquad (6.161a)$$

The radial derivative of Δg is given by

$$\frac{\partial(\Delta g)}{\partial H} = \frac{R^2}{2\pi}\iint_{\sigma}\frac{\Delta g - \Delta g_P}{l_0^3}\,d\sigma \qquad (6.161b)$$

and again can be approximated by the terrain correction (see above). The vertical gradient of ζ results from (6.96) and (6.101):

$$\frac{\partial\zeta}{\partial H} = \frac{\partial}{\partial H}\left(\frac{T}{\gamma}\right) = \frac{1}{\gamma}\left(\frac{\partial T}{\partial H} - \frac{1}{\gamma}\frac{\partial\gamma}{\partial H}T\right) = -\frac{\Delta g}{\gamma}\,, \qquad (6.161c)$$

where Δg is the surface gravity anomaly. If the surface anomalies are reduced to the level of the computation point P, H in (6.161a) has to be substituted by $H - H_P$. The last term in (6.161a) then vanishes, as H outside the integral means H_P:

$$\zeta = \frac{R}{4\pi\gamma}\iint_{\sigma}\left(\Delta g - \frac{\partial(\Delta g)}{\partial H}(H - H_P)\right)S(\psi)\,d\sigma\,. \qquad (6.161d)$$

These solutions are particularly well suited for FFT techniques (FORSBERG and TSCHERNING 1997).

The *surface deflection of the vertical* (see Molodenski's definition in [6.1.2]) is derived from (6.160) by differentiation according to (6.98):

$$\begin{Bmatrix}\xi^N\\ \eta^N\end{Bmatrix} = \frac{1}{4\pi\gamma}\iint_{\sigma}(\Delta g + G_1)\frac{dS(\psi)}{d\psi}\begin{Bmatrix}\cos\alpha\\ \sin\alpha\end{Bmatrix}d\sigma - \frac{\Delta g}{\gamma}\begin{Bmatrix}\tan\beta_x\\ \tan\beta_y\end{Bmatrix}. \qquad (6.162)$$

The principal term is Vening-Meinesz' formula (6.150), and the Molodenski correction terms again take the effect of the terrain into account, reaching a few arcsec.

Molodenski's problem is characterized by the fact that no assumptions on the density distribution within the earth are necessary, in contrast to the geoid determination using Stokes' formula. By the relation (6.9) between the geoid and the quasigeoid, a simple method is available to derive geoid heights from height anomalies:

$$N = \zeta + \frac{\Delta g_B}{\bar{\gamma}} H \,.$$

Data reductions onto the geoid and calculations of indirect effects are avoided by this strategy, and density hypotheses enter only through the Bouguer anomaly Δg_B. On a large scale, the Bouguer anomalies are negative on the continents, cf. [8.2.4], hence the quasigeoid generally is above the geoid. The differences between the geoid and the quasigeoid are of the cm to dm-order of magnitude in flat and hilly regions but may assume one meter and more in the mountains. As the quasigeoid is highly correlated with the height, the quasigeoid mirrors the topography.

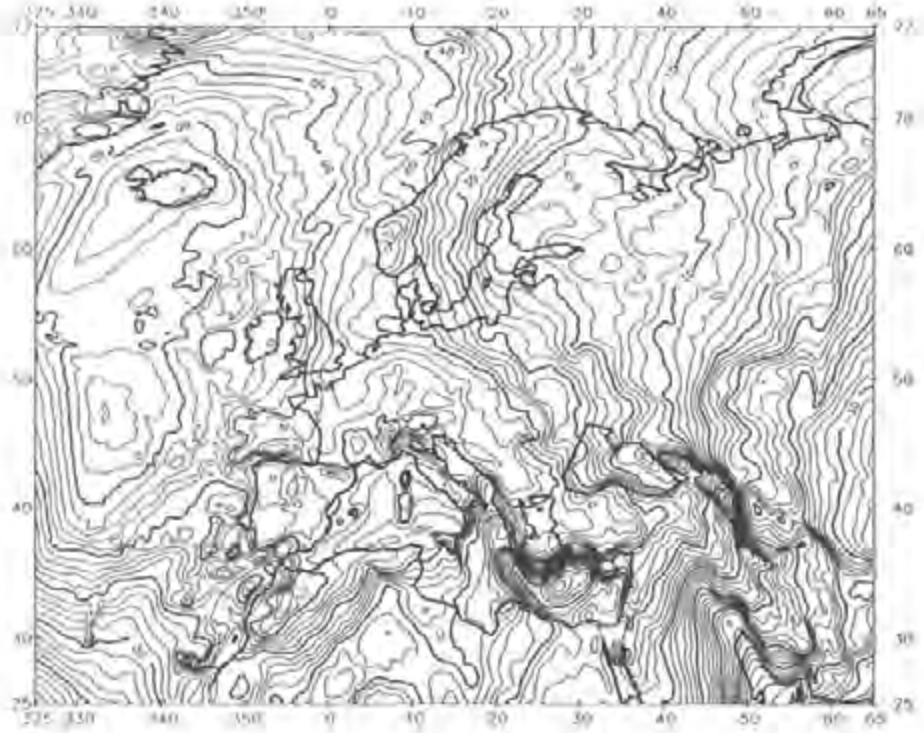

Fig. 6.34. European gravimetric quasigeoid EGG97 (DENKER and TORGE 1998): contour line interval 2 m

One example for a large-region quasigeoid determination is the European Gravimetric Quasigeoid EGG97 (DENKER and TORGE 1998). It is based on a high-resolution data set of point and mean gravity anomalies derived from surface gravimetry and satellite altimetry in the marine areas. The remove-restore technique was applied using the EGM96 geopotential model and a 15′x15′ moving average reference topography. Gridded 1′×1.5′ residual gravity anomalies were transformed to height anomalies by least squares spectral combination, cf. [6.7.1]. The main part of EGG97 (Fig. 6.34) stems from the global model, but the contributions from terrestrial gravity data and topography still amount to ± 0.4 m (maximum 4 m) and ± 0.03 m (maximum 0.8 m), respectively. The error estimates (± a few cm/100 km to ± 0.1 m/1000 km) were confirmed by comparisons with GPS/leveling control points, e.g., on the European NS-GPS-traverse between Munich and Tromsö (TORGE et al. 1989).

6.7.3 The External Gravity Field

The gravity field outside the earth is modeled by *upward continuation* from the boundary surface, either globally or locally.

Global modeling employs the spherical harmonic expansion of the disturbing potential (6.4) and the corresponding expansions for the height anomaly (6.131) and the gravity anomaly (6.135). These expansions converge outside a sphere enclosing the earth, cf. [3.3.2]. They are especially useful for the orbit determination of satellites, but the present limited spatial resolution makes them less suited for low altitudes, e.g., for airborne applications.

For *local modeling*, we start with the *free-air anomaly* Δg, where according to (6.134) the function

$$r\,\Delta g = \sum_{l=2}^{\infty} (l-1)\left(\frac{a}{r}\right)^{l+1} T_l(\vartheta,\lambda) \tag{6.163}$$

is harmonic in space. The calculation of gravity anomalies in space from boundary values thus corresponds to the first boundary-value problem (*Dirichlet* problem) of potential theory. The solution is given by *Poisson's* integral. In spherical approximation we have

$$\Delta g_P = \frac{R^2\left(r_P^2 - R^2\right)}{4\pi r_P} \iint_{\sigma} \frac{\Delta g}{l^3}\, d\sigma\,, \tag{6.164}$$

where Δg_P refers to the point P in space and Δg are the surface anomalies on the spherical boundary surface. The integral kernel decreases rapidly with ψ, which allows restriction of the integration area on a limited zone around the computation point.

By inserting (6.164) into (6.101b) we obtain

$$\Delta g = -\frac{\partial T}{\partial r} - \frac{2}{r} T , \tag{6.165}$$

which now represents a differential equation in *space*. The solution leads to a spatial extension of Stokes' formula for the *disturbing potential*, which was derived by *Pizetti*:

$$T(r,\vartheta,\lambda) = \frac{R}{4\pi} \iint_{\sigma} S(r,\psi) \Delta g \, d\sigma , \tag{6.166a}$$

where

$$S(r,\psi) = \frac{2R}{l} + \frac{R}{r} - \frac{3Rl}{r^2} - \frac{R^2}{r^2} \cos\psi \left(5 + 3 \ln \frac{r - R\cos\psi + l}{2r} \right), \tag{6.166b}$$

with

$$l = \sqrt{r^2 + R^2 - 2Rr\cos\psi} , \tag{6.166c}$$

is the extended Stokes' function.

Bruns' theorem finally gives the separation between the geopotential surface $W = W_P$ and the spheropotential surface $U = U_Q = W_P$ (*height anomaly* in space):

$$\zeta(r,\vartheta,\lambda) = \frac{R}{4\pi\gamma} \iint_{\sigma} S(r,\psi) \Delta g \, d\sigma . \tag{6.167}$$

Corresponding relations can be derived for the gravity disturbance and the deflection of the vertical, using (6.98) and (6.99).

6.7.4 Astrogeodetic Geoid and Quasigeoid Determination

Geoid and quasigeoid height *differences* can be obtained from deflections of the vertical, determined according to (6.17) from astronomic and geodetic latitudes and longitudes.

In *astronomic leveling*, the deflections of the vertical are integrated along the path, either on the geoid or on the earth's surface (Fig. 6.35). On the *geoid*, we have

$$dN = -\varepsilon_0 \, ds \,, \tag{6.168a}$$

where ε_0 is the vertical deflection component in the azimuth of the path (6.18), reduced to the geoid according to Pizetti's definition, cf. [6.1.2]. Integration between P_1 and P_2 yields the geoid height difference

$$\Delta N_{1,2} = N_2 - N_1 = -\int_1^2 \varepsilon_0 \, ds \,. \tag{6.168b}$$

The negative sign follows from the sign conventions for the geoid height (6.8) and the deflection of the vertical (6.17).

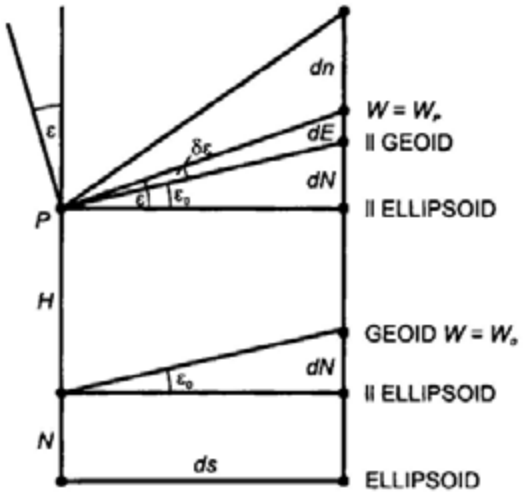

Fig. 6.35. Astronomic leveling

The *geoidal* deflection of the vertical is obtained by *reducing* the observed astronomic latitude and longitude onto the geoid:

$$\Phi_0 = \Phi + \delta\Phi, \quad \Lambda_0 = \Lambda + \delta\Lambda \,, \tag{6.169}$$

where Φ_0 and Λ_0 are the astronomic coordinates on the geoid (Fig. 6.36). The reductions follow from the integration of the plumb line curvature κ_x, κ_y, between the earth's surface and the geoid (3.74):

$$\delta\Phi = -\int_0^H \kappa_x \, dH, \quad \delta\Lambda = -\int_0^H \kappa_y \, dH \,, \tag{6.170a}$$

H = orthometric height. Inserting (3.67) and (3.70) yields

$$\delta\Phi = -\frac{1}{R}\int_0^H \frac{1}{g}\frac{\partial g}{\partial \Phi}\,dH, \quad \delta\Lambda = -\frac{1}{R\cos\Phi}\int_0^H \frac{1}{g}\frac{\partial g}{\partial \Lambda}\,dH\,, \tag{6.170b}$$

R = mean radius of the earth. With (6.17), the NS and EW-components of the vertical deflection are given by

$$\xi_0 = \xi + \delta\Phi, \quad \eta_0 = \eta + \cos\Phi\,\delta\Lambda\,, \tag{6.171a}$$

and the azimuthal component reads

$$\varepsilon_0 = \xi_0\cos\alpha + \eta_0\sin\alpha\,. \tag{6.171b}$$

In order to evaluate (6.170), the gravity and the horizontal gravity gradient along the plumb line are required. Digital terrain models allow estimation of these quantities with an accuracy between 0.1″ and 1″, but errors may be larger in the high mountains. The angle of plumb line curvature itself attains values of a few 0.1″ in the lowlands and may reach 10″ and more at high mountain stations.

Instead of integrating the deflections of the vertical on the geoid, the *surface* vertical deflections (definitions from Helmert or from Molodenski) may be used. *Helmert* deflections of the vertical are given by

$$\varepsilon = \varepsilon_0 - \delta\varepsilon\,, \tag{6.172}$$

where the components of $\delta\varepsilon$ are obtained from (6.170b). Inserting into (6.168b) yields

$$\Delta N_{1,2} = N_2 - N_1 = -\int_1^2 \varepsilon\,ds - \int_1^2 \delta\varepsilon\,ds\,. \tag{6.173a}$$

As seen from Fig. 6.36, the second term on the right side equals the orthometric height reduction E known from geometric leveling (6.81b); the angle of plumb line curvature is the horizontal derivative of E. We thus have

$$\Delta N_{1,2} = -\int_1^2 \varepsilon\,ds - E_{1,2}\,. \tag{6.173b}$$

For *height anomalies*, the difference follows from the differential (MORITZ 1983)

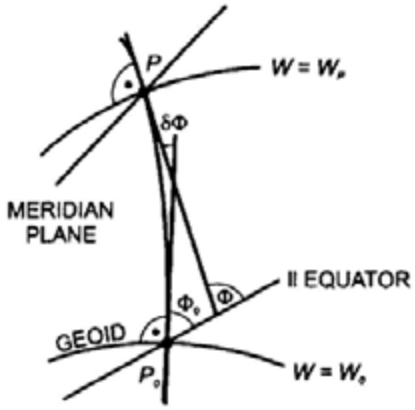

Fig. 6.36. Plumb line curvature in the meridian plane

$$d\zeta = \frac{d\zeta}{ds}\,ds + \frac{d\zeta}{dh}\,dh\,. \tag{6.174}$$

The first term describes the effect of *Molodenski's* vertical deflection. The second term enters because the physical surface of the earth is not a level surface. Using (6.161c) and integration along the path yields Molodenski's astronomic leveling of height anomalies

$$\Delta\zeta_{1,2} = \zeta_2 - \zeta_1 = -\int_1^2 \varepsilon^N ds - \int_1^2 \frac{\Delta g}{\gamma}\,dh\,. \tag{6.175}$$

The relation between geoid and quasigeoid height differences follows from (6.9) and (6.81):

$$\Delta\zeta_{1,2} = \Delta N_{1,2} + E_{1,2} - E^N_{1,2} \tag{6.176a}$$

or when taking (6.173b) into account

$$\Delta\zeta_{1,2} = -\int_1^2 \varepsilon\, ds - E^N_{1,2}\,, \tag{6.176b}$$

where $E^N_{1,2}$ is the normal height reduction.

As the small corrections in (6.173), (6.175), and (6.176) can be derived easily from surface gravity and a digital terrain model, the integration of surface vertical deflections is of advantage compared to the tedious reductions onto the geoid required in (6.168).

The line integrals of astronomic leveling presuppose that the deflections of the vertical are given continuously along the path. In reality, vertical deflections are available only at larger distances (several 10 km or more), which is due to the time-consuming astronomic observations. This poses the problem of *interpolation* between the vertical deflection points (in the following we do not distinguish between the vertical deflections on the geoid and on the earth's surface). Interpolation can be carried out by purely mathematical methods or supported by additional information on the gravity field behavior.

In the simplest case of *mathematical interpolation*, a linear change of the deflections of the vertical between the stations P_1 and P_2 is assumed. The integration then yields

$$\Delta N_{1,2} = -\frac{\varepsilon_1 + \varepsilon_2}{2} s\,, \tag{6.177}$$

where s is the distance between P_1 and P_2.

The linear interpolation model is adequate in flat areas and where the distances between the vertical deflection points are not too large (some km to some 10 km). An area with sufficient control point coverage can be evaluated either by forming triangles and adjusting the geoid height misclosures or by a surface polynomial approximation to the geoid (VANIČEK and MERRY 1973). The polynomial coefficients are determined from the corresponding series expansions of the vertical deflection components, which result from (6.98) and Bruns' formula

$$\xi = -\frac{1}{R}\frac{\partial N}{\partial \varphi}, \quad \eta = -\frac{1}{R\cos\varphi}\frac{\partial N}{\partial \lambda}, \tag{6.178}$$

where the condition of integrability of a potential field, cf. [3.1.5] must be heeded:

$$\frac{\partial \xi}{\cos\varphi\, \partial \lambda} = \frac{\partial \eta}{\partial \varphi}. \tag{6.179}$$

Least squares prediction, cf. [6.1.3], offers another efficient interpolation method (HEITZ 1969), while least squares collocation, cf. [6.8.2], even allows direct estimation of geoid heights from the vertical deflections, thus providing an alternative to the integral formulas.

Additional *gravity field information* between the vertical deflection points can be supplied by terrain models, gravity anomalies, and zenith angles.

A digital *terrain model* (possibly also taking density variations into account) can be used to calculate the effect of topography on the deflections of the vertical. For more extended calculation areas, the effect of isostatically

compensating masses should also be considered, cf. [6.5.2]. By subtracting these effects from the observations, the vertical deflection field is smoothed, and mathematical interpolation methods may be applied. The interpolated residual deflections of the vertical are augmented by the effects of topography and isostasy, leading to a densified network of vertical deflection points. This remove-restore method has proved to be efficient especially in mountainous areas; an interpolation accuracy of 1 to 2 arcsec can be achieved.

If a dense field of gravity stations around the vertical deflection points is available, it can be utilized for a *gravimetric* interpolation. Here, gravimetric deflections of the vertical are computed according to (6.150) by integrating the gravity anomalies over a limited area (e.g., three times the distance between the vertical deflection points). This gravimetric part is then removed from the observations, and a systematic difference between the astrogeodetic and the gravimetric vertical deflections has to be taken into account (different reference systems, effect of the zones neglected in the calculation of the gravimetric vertical deflections). The residual deflections of the vertical thus obtained are smooth and easy to interpolate. This method has been extended to *astrogravimetric leveling*, with a gravimetric "correction" to quasigeoid differences obtained from linear interpolation of surface deflections of the vertical (MOLODENSKI et al. 1962). Gravimetric interpolation allows calculation of geoid or quasigeoid height differences with cm to dm accuracy, even at larger spacing of the vertical deflection points.

Reciprocal *zenith angles* deliver differences of the vertical deflection components ε in the line of sight. According to (6.85), the observed zenith angles z and the ellipsoidal quantities ζ are related by (Fig. 6.20)

$$\zeta_1 = z_1 + \varepsilon_1, \quad \zeta_2 = z_2 + \varepsilon_2 .$$

Inserting the above relations into (6.87), and taking sign conventions into account, yields

$$\varepsilon_2 - \varepsilon_1 = z_1 + z_2 - \frac{S}{R} - \pi , \tag{6.180}$$

where S = spherical distance between P_1 and P_2. Starting at a vertical deflection point, these differences can be used for the interpolation of deflections of the vertical. The method has found limited application in mountainous areas, where an interpolation accuracy of about one arcsec has been achieved (GLEINSVIK 1960).

The advantage of the astrogeodetic method of geoid determination consists in its independence from data outside the area of calculation, in contrast to the

gravimetric method where a global coverage with gravity data is needed. In addition, the demands on the accuracy of the point heights are less stringent as with the formation of gravity anomalies. On the other hand, the establishment of a vertical deflection point requires substantially more time than a gravity measurement. A station spacing of 10 to 20 km is available only in few regions, and even distances of up to 30 to 50 km are limited to well surveyed countries. Large parts of the continents are covered only sparely, with concentration on profiles along first-order triangulation chains, cf. [7.1.1]. Thus, the *accuracy* of astronomic leveling depends entirely on the quality of interpolation. In densely surveyed areas, an accuracy of ± a few cm to 0.1 m over some 100 km can be achieved (BÄUMKER 1984, ELMIGER and GURTNER 1983). The accuracy can be increased by topographic-isostatic reductions, including geological information on rock densities. By fitting the results to GPS/leveling control points, the geoid heights are referred to the national vertical datum and systematic effects are reduced, which increases the accuracy to ± 0.01 to 0.02 m over several 100 km (GROTE 1996).

The superior efficiency of gravimetric methods has greatly reduced the application of astronomic leveling. It is now restricted to areas or profiles which are not well covered by gravity data or where the coverage is not representative, as in the mountains where gravity stations are typically concentrated along the roads.

Astronomic leveling was introduced by HELMERT (1884) and first applied in the Harz mountains, Germany. From the 1950's to the 1970's, astrogeodetic geoid determinations were carried out in a number of countries, using astronomic observations on the first-order triangulation points (HEITZ 1969). Deflections of the vertical, and the resulting geoid, referred to the national geodetic datum and served for the reduction of horizontal angles and chord distances onto the national reference ellipsoid, cf. [6.3.2], [7.1.2]. Large-scale solutions included the "*Bomford*" geoid for Europe (LEVALLOIS and MONGE 1975) and the continent-wide geoid determination by FISCHER et al. (1968), with an average accuracy of a few meters. High precision astrogeodetic geoid models have been developped in Switzerland and Austria, based on a densified net of vertical deflection points and high-resolution digital terrain models and employing remove-restore techniques (ERKER 1987, MARTI 1997).

6.8 Combined Methods for Positioning and Gravity Field Determination

Combined evaluation methods permit simultaneous determination of positions and the gravity field. These quantities are eventually combined with systematic model parameters within *one* mathematical model. By introducing geometrical *and* gravity field observations, the information content of the data is more completely exhausted. On the other hand, the large amount of data and

unknown parameters raises serious problems with respect to proper weighting of the observations, modeling of systematic effects, and data processing. Hence, the application of the combination methods is still restricted to a limited number of parameters and observations.

A functional combination model is based on the observation equations for all relevant data and uses least squares adjustment for the determination of earth models and optimum earth parameters [6.8.1]. In least squares collocation, a stochastic model for gravity field estimation is added, which leads to a very general method of combination [6.8.2].

6.8.1 Earth Models and Optimum Earth Parameters

"Earth models" are determined by rigorous least squares adjustment from satellite tracking data, either alone or in combination with satellite altimetry and surface gravity. They contain the coordinates of the tracking stations and station velocities, the parameters of a low-degree gravity field model, as well as ocean tidal and earth rotation parameters, cf. [6.6.2].

Using the latest supercomputers, present earth models include about 5000 geopotential coefficients and about 10000 parameters in total. The coordinates of the tracking stations are determined with cm-accuracy, and station velocities are accurate to a few mm/a. The long-wave part of the geoid (wavelength > 550 km) is accurate to about ± 0.9 m on the continents and ± 0.3 m on the oceans.

Combination solutions also provide *actual* values of a *model earth*, as represented by a level ellipsoid with optimum approximation to the geoid and the external gravity field, cf. [4.2.1]. These actual values must not be confused with the parameters of a geodetic reference system, recommended as a standard for a longer time interval, cf. [4.3]. The best estimates (1999) for the defining parameters of a level ellipsoid are as follows (GROTEN 2000):

- The *geocentric gravitational constant*

$$GM = (398\,600.442 \pm 0.001) \times 10^9 \ m^3 s^{-2}$$

  including the mass of the atmosphere. This value is derived from orbit analyses of satellites and space probes. A variation of GM with time has not been found,
- The *equatorial radius* of the earth

$$a = 6\,378\,136.6 \pm 0.1\,m\,.$$

The radius is determined by an optimal fit between ellipsoidal heights and orthometric heights, as obtained for satellite tracking stations on the continents, and from satellite altimetry on the oceans, applying the minimum condition

$$\iint_{\sigma} N^2 \, d\sigma = \min . \tag{6.181}$$

on the geoid heights. According to [6.5.4], the *geoid potential* W_0 could also be introduced as a defining parameter if GM and a are known:

$$W_0 = 62\,636\,856.0 \pm 0.5 \ \mathrm{m^2 s^{-2}} .$$

a and W_0 are given in the zero-tide system, which contains the indirect tidal distortion, cf. [3.4.1]. The equatorial radius and the geoid potential can be assumed constant with time.

- The second-degree zonal harmonic coefficient (*dynamical form factor*)

$$J_2 = (1082.6267 \pm 0.0001) \times 10^{-6}$$

in the tide-free system and

$$J_2 = (1082.6359 \pm 0.0001) \times 10^{-6}$$

in the zero-tide system. J_2 is obtained from global gravity models, cf. [6.6]. A long-term temporal change of J_2 was found from the analysis of satellite orbits over long time intervals:

$$\dot{J}_2 = dJ_2/dt = -(2.6 \pm 0.3) \times 10^{-9} / \mathrm{cy} .$$

- The mean angular velocity of the *earth's rotation*

$$\omega = 7.292\,115 \times 10^{-5} \ \mathrm{rad\ s^{-1}}$$

is provided by the International Earth Rotation Service, cf. [2.2.2]. It experiences a long-term variation

$$\dot{\omega} = d\omega/dt = (-4.5 \pm 0.1) \times 10^{-22} \ \mathrm{rad\ s^{-2}} ,$$

which may be decomposed into a component due to tidal dissipation (-6.1×10^{-22} rad s^{-2}) and a non-tidal part ($+1.6\times10^{-22}$ rad s^{-2}) probably reflecting the postglacial rebound of the earth's crust and mantle.

Among the quantities derived from the defining parameters we have

- The reciprocal *flattening*

$$1/f = 298.25642 \pm 0.000\,01$$

and

- The *normal gravity* at the equator

$$\gamma_a = 9.780\,327 \pm 0.000\,001\ \mathrm{ms}^{-2}.$$

The *minimum conditions* for the deflections of the vertical

$$\iint_\sigma \left(\xi^2 + \eta^2\right) d\sigma = \min \tag{6.182}$$

and the gravity anomalies

$$\iint_\sigma \Delta g^2\, d\sigma = \min, \tag{6.183}$$

in principle, could also serve to derive the parameters of a best approximating ellipsoid (HEISKANEN and MORITZ 1967, p.216). While (6.182) has been used for the determination of local reference ellipsoids in classical national geodetic surveys, cf. [7.1.2], (6.183) has not been exploited due to lacking global gravity coverage.

6.8.2 Least Squares Collocation

Least squares collocation combines the calculation of station coordinates and other deterministic unknowns (harmonic coefficients, earth ellipsoid and earth orientation parameters, calibration and drift coefficients, etc.) with the estimation of gravity field quantities of unsurveyed points, utilizing many types of observables (KRARUP 1969, MORITZ 1973). The general form of the *observation equation* reads

$$\mathbf{l} = \mathbf{A}\mathbf{x} + \mathbf{s} + \mathbf{n}, \tag{6.184}$$

where **l** is the linearized vector of observations. It is composed of the deterministic part **Ax** (**x** = parameter vector, **A** = design matrix containing the differential relations between observations and parameters) and two random parts. The signal vector **s** contains the residual gravity field quantities at any point, either observed or to be predicted. It may include, in contrast to least squares prediction, any kind of gravity field quantities such as residual harmonic coefficients, geoid or quasigeoid heights, gravity anomalies, deflections of the vertical, etc. The noise vector **n** represents the observational errors. Each of the random quantities is supposed to have a mean value of zero. The statistical behavior is described by the covariance matrix **C** of the signals and the covariance matrix **D** of the noise, where mutual independence of signal and noise is assumed, cf. [6.1.3].

After linearization with a geodetic earth model, all geodetic observations can be expressed in the form (6.184). The observation equations for leveled heights, gravity, astronomic latitudes, longitudes, and azimuths, satellite tracking data, VLBI observations, zenith angles, and spatial distances are found in the corresponding sections of [6]. While all observations depend on position (described by the geodetic coordinates in connection with the parameters of the ellipsoid), a dependence on the gravity field does not exist with VLBI observations and spatial distances. A complete set of observation equations is given by GRAFAREND (1978).

Least squares collocation is an overdetermined problem with respect to the parameters (number of observations exceeds the number of parameters) and an underdetermined problem with respect to the gravity field signal (more signals have to be predicted than have been observed). It is solved by applying a least squares minimum condition on the weighted quadratic sum of the signal part and the noise, thus combining least squares adjustment with least squares prediction (MORITZ 1980). The solution for the *parameter vector* is given by

$$\mathbf{x} = \left(\mathbf{A}^{\mathrm{T}}\bar{\mathbf{C}}^{-1}\mathbf{A}\right)^{-1}\mathbf{A}^{\mathrm{T}}\bar{\mathbf{C}}^{-1}\mathbf{l}\,, \tag{6.185}$$

with $\bar{\mathbf{C}} = \mathbf{C} + \mathbf{D}$. The component of the *signal vector* predicted in an unsurveyed point results in

$$\hat{\mathbf{s}}_P = \mathbf{C}_P^{\mathrm{T}}\bar{\mathbf{C}}^{-1}\left(\mathbf{l} - \mathbf{A}\mathbf{x}\right), \tag{6.186}$$

where the covariance vectors and matrices are explained in [6.1.3] but now may include heterogeneous signals.

The simultaneous determination of station coordinates and gravity field quantities has been designated as *"integrated"* or *"operational"* geodesy (EEG and KRARUP 1973, HEIN 1986). The main problem in it's practical application is the solution of a system of equations with a dimension equal to the number of

observations for the inversion of the covariance matrix $\bar{\mathbf{C}}$. By separation into subsystems with low correlation (e.g., horizontal positioning on the one hand, and height respectively gravity field determination on the other), the dimension of the system of equations can be reduced significantly. This strategy leads to least squares adjustment for the deterministic part, and offers an efficient and flexible solution for gravity field determination, which is used extensively in various applications.

If applied to *gravity field estimation,* the elements of the signal covariance matrix $\mathbf{C}$ are required, describing the correlation between heterogeneous residual gravity field quantities. Since all these quantities belong to the same gravity field, the covariances have to be derived from a basic covariance function through covariance propagation. The *covariance function* of the *disturbing potential* T is selected for this purpose, as all residual gravity field quantities are related to T in a simple manner. This covariance function is defined in analogy to the covariance function of the gravity anomalies (6.21). It is considered to be the mean value of the products of T in the points P and P' for a constant spherical distance ψ and assumes homogeneity and isotropy. The function is given by:

$$K(\psi) = \operatorname{cov}(T, T', \psi) = M\{T \cdot T'\}_{\psi}. \tag{6.187}$$

Covariance propagation is well known from the theory of errors and is applied here to gravity field signals. As demonstrated by (6.96) to (6.101), the residual gravity field quantities (either observed or to be predicted) can be expressed as a linear functional of T. For an *observation* l_i we thus have

$$l_i = L_i^{P'} T(P'), \tag{6.188}$$

where L_i is the functional to be applied to T in order to transform T into the observed quantity. The covariance between T and l_i is obtained by applying L_i on the covariance function $K(\psi) = K(P, P')$, which can be expressed as a function of the coordinates of P and P' in space:

$$C_{Pi} = M\{T \cdot l_i\} = L_i^{P'} K(\psi). \tag{6.189}$$

For different types of observation at P and P', the covariance results from a subsequent application of the functionals L valid for the transformation of T into the respective observation:

$$C_{ij} = M\{l_i \cdot l_j\} = L_i^{P} L_j^{P'} K(\psi). \tag{6.190}$$

The same rules have to be followed if heterogeneous signals shall be estimated.

A statistical description of the earth's gravity field is available by anomaly degree variance models, cf. [6.1.3]. The relation of these models to the basic covariance function can be derived by applying the mean value operator (6.187) on the spherical harmonic expansion of the disturbing potential (6.4). This yields

$$K(\psi)=\sum_{l=2}^{\infty}\sigma_l^2(T)\left(\frac{R^2}{rr'}\right)^{l+1}P_l(\cos\psi), \tag{6.191a}$$

where the potential degree variances are defined in analogy to (6.26):

$$\sigma_l^2(T)=M\{T_l^2\}. \tag{6.191b}$$

Equation (6.142) provides the relation between the degree variances of the disturbing potential and the gravity anomalies:

$$\sigma_l^2(T)=\left(\frac{R}{l-1}\right)^2\sigma_l^2(\Delta g), \tag{6.192}$$

where we have taken Bruns' formula $N=T/\gamma$ into account. Inserting (6.192) into (6.191) yields

$$K(\psi)=R^2\sum_{l=2}^{\infty}\frac{1}{(l-1)^2}\sigma_l^2(\Delta g)\left(\frac{R^2}{rr'}\right)^{l+1}P_l(\cos\psi), \tag{6.193}$$

which enables the calculation of the basic covariance function from an anomaly degree variance model. For local applications, the covariance function has to be fit to the gravity field behavior in the area of calculation, cf. [6.1.3].

The advantage of least squares collocation is the flexibility in estimating any kind of gravity field quantity from different types of gravity field observations, at surveyed and unsurveyed points. The data can be processed as discrete values and need not be continuous, as required for the application of integral formulas, cf. [6.7]. Neither gridding of the data nor reduction to some reference level is required. For homogeneous and continuously distributed data, least squares collocation transforms into the integral formulas (MORITZ 1976). On the other hand, the amount of data that can be handled is still limited by computing facilities. Applications have therefore been restricted to limited areas and data sets. By introducing some restrictions on the data, computing time can be

reduced and larger data sets evaluated: fast collocation (BOTTONI and BARZAGHI 1993, GROTE 1996).

Least squares collocation has been applied especially for local and regional geoid determination (RAPP 1978, ARABELOS 1980, TSCHERNING and FORSBERG 1986, DENKER 1988), but also for the estimation of gravity anomalies from altimetric geoid heights and for downward continuation problems. Remove-restore techniques are used generally, cf. [6.7.1], which reduces the data collection area.

7 Geodetic and Gravimetric Networks

Geodetic and gravimetric networks consist of monumented control points that provide the reference frames for positioning and gravity-field determination at all scales. Global networks allow realization of the reference systems defined by international conventions. Regional networks form the fundamental basis for national or supranational (continental) geodetic and gravimetric surveys, which are the basis of geo-information systems and map series. Local networks are typically established for engineering and exploration projects and for geodynamic investigations.

In the sequel we concentrate on regional networks, which are increasingly integrated into global reference-frames established for positioning, navigation, cf. [2.5.3], and gravity, cf. [5.4.3]. Horizontal and vertical control networks have been established separately, following the classical treatment of positioning and heighting; these networks still are the basis of national geodetic systems [7.1], [7.2]. Geodetic space methods allow establishment of three-dimensional networks within the geocentric reference system and are now superseding the classical control networks [7.3]. Gravity networks serve the needs of geodesy and geophysics, with the reference provided either by a global network or by absolute gravimetry [7.4].

If reobserved after a certain time span, geodetic and gravimetric networks can be utilized for the investigation of long-term changes of position and gravity with time. Specially designed networks have been set up on global, regional, and local scale in order to monitor geodynamic processes of different origins, cf. [8.3.3].

The establishment of geodetic networks is treated in textbooks on geodesy and geodetic surveying (BOMFORD 1980, KAHMEN and FAIG 1988, HECK 1995, LEICK 1995); for gravity networks see TORGE (1989, 1998).

7.1 Horizontal Control Networks

National horizontal control networks were established from the 18th century until the 1960's, with the networks' design, observation, and computation changing with the available techniques [7.1.1]. Computations were carried out on a reference ellipsoid fitted to the survey area. Since the 1960's, spatial geodetic methods have allowed orientation of the classical networks with respect to the global reference system [7.1.2].

7.1.1 Design and Observation

Horizontal control networks are realized by *trigonometric* (triangulation) *points*, which in principle should be distributed evenly over the country. One distinguishes between different *orders* of trigonometric points, from first order or primary (station separation 30 to 60 km) to second order (about 10 km) to fourth or even fifth order (down to one to two km) stations. The maximum distance between first-order points was determined by the terrestrial measurement methods, which required intervisibility between the network stations. Consequently, first and some second-order stations were established on the top of hills and mountains; observation towers (wooden or steel constructions with heights of 30 m and more) were erected especially in flat areas. The stations have been permanently marked by underground and surface monuments (stone plates, stone or concrete pillars, bolts in hard bedrock). Eccentric marks have been set up in order to aid in the recovery and verification of the center mark.

Classical first and second-order horizontal control networks have been observed by the methods of triangulation, trilateration, and traversing.

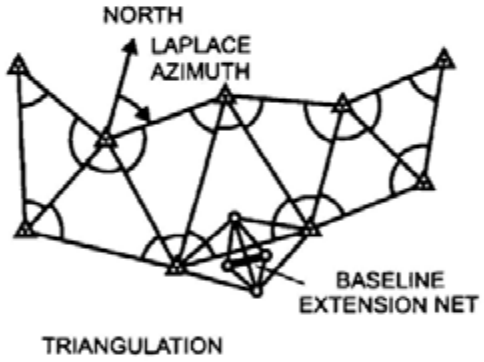

Fig. 7.1. Triangulation with baseline extension net and Laplace azimuth (principle)

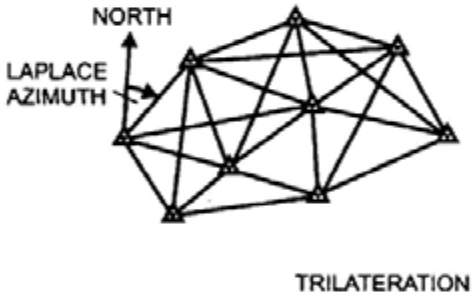

Fig. 7.2. Trilateration with Laplace azimuth (principle)

In *triangulation*, all angles of the triangles formed by the trigonometric points are observed with a theodolite (Fig.7.1). The instrument is set up on the observation pillar or tower; at large distances the targets are made visible by light signals. Either directions (successive observation of all target points) or angles (separate measurement of the two directions comprising one angle) are observed in several sets (i.e., in both positions of the telescope), distributed over the horizontal circle of the theodolite. The scale of a triangulation network is obtained from the length of at least one triangulation side, either derived from a

short *base line* through a base line extension net or measured directly by a distance meter, cf. [5.5.2]. Astronomic observations provide the orientation of the network, cf. [7.1.2], whereas an astronomic azimuth is needed for the horizontal orientation according to Laplace's equation (6.58): *Laplace station.* In extended networks, base lines and Laplace stations often were established at distances of a few 100 km in order to control the error propagation through the network with respect to scale and orientation (effects of lateral refraction).

Trilateration employs electromagnetic distance meters in order to measure the lengths of all triangle sides of a network, including diagonals (Fig.7.2). At least one Laplace azimuth is needed for the orientation of the net. Electromagnetic distance measurements put less demands on the stability of observation towers as compared to angular measurements, and the use of laser light and microwaves makes the method more independent from weather conditions.

Traverses combine distance and angular measurements, where the traverse stations are arranged along a profile (Fig.7.3). Again, a Laplace azimuth is required in order to orientate the traverse. Traversing represents a very effective and flexible method for establishing horizontal control networks, with no more need to establish stations on hilltops. It has been employed primarily for the densification of higher order networks, with the coordinates of the existing control points providing orientation.

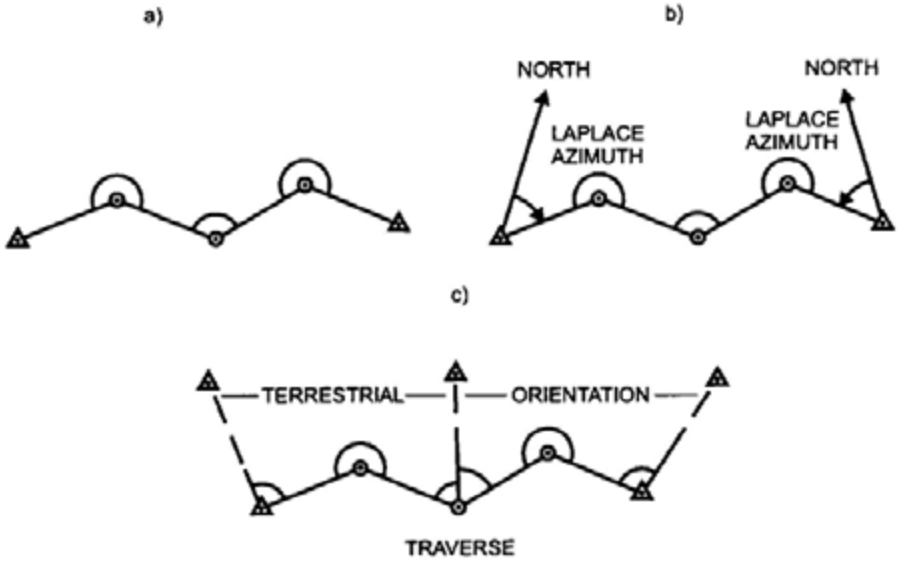

Fig. 7.3. Traverse connecting two control points (principle): a) without additional orientation, b) with orientation by Laplace azimuths, c) with orientation by directions to control points

Horizontal control networks can also be formed by *combining* the methods of triangulation, trilateration, and traversing. Such networks are very stable in design, and allow establishment of first and second-order control simultaneously. *Optimization* methods have been developed for the design and survey of trigonometric networks. Starting from the demands on accuracy and reliability, these methods provide information on the optimum point configuration and the distribution of the measurements in the network given the limitations of available equipment and the maximum allowable cost of the survey (BOSSLER et al. 1973, GRAFAREND and SANSÒ 1985).

Triangulation as part of a national geodetic survey started in France (1733-1750: Carte géométrique de la France, under the direction of *Cassini de Thury*) and in Great Britain (since about 1780 triangulation by the Ordnance Survey, under *W. Roy* and others). It continued to be the method for establishing horizontal control networks in the 19th and 20th century until the introduction of electromagnetic distance measurements. Triangulation often started with chains (in many cases established along meridians and parallels) composed of triangles or quadrilaterals with diagonals tied together every few 100 km. The meshes of this framework then were filled by first or second-order areal triangulation. The triangulations of Bavaria (1808-1828, *J.G. Soldner*) and of Prussia (since 1875, *O. Schreiber*) brought significant improvements in measurement and calculation techniques, which also influenced other national geodetic surveys. Large-scale networks (chains and filling nets) were developed in the U.S.A. (since about 1830, *J.F. Hayford, W. Bowie*) and in the former Soviet Union (since the 1930's, *T.N. Krassovski*), cf. [7.1.2]. *Trilateration* was applied from the 1950's to the 1970's for strengthening, extending, and densifying triangulation networks. Airborne microwave methods were employed for the rapid survey of regions with difficult access and for bridging water areas (a few m to 10 m accuracy over some 100 km). *Traversing* has been used mainly for network densification since the 1960's, but first-order geodimeter traverses also strengthened continental networks (U.S.A.) or even established them (Australia). From the 1960's to the 1980's, *satellite methods* were utilized to control the quality of horizontal control networks and especially to determine the orientation of the ellipsoidal systems with respect to the global geocentric system (Doppler positioning).

7.1.2 Computation and Orientation

Classical first and some second-order horizontal control networks have been calculated on a reference ellipsoid within the system of ellipsoidal coordinates, cf. [4.1]. Lower order networks are primarily calculated in planar Cartesian coordinates, after conformal mapping of the ellipsoid onto the plane (LEE 1974, GROSSMANN 1976, KUNTZ 1990, HOOIJGBERG 1997).

The observed horizontal angles, directions, and spatial distances were *reduced* to the ellipsoid first, cf. [6.3.2]; the gravity-field-related reductions (deflections of the vertical, geoid height) were not considered during earlier surveys. The network *adjustment* was carried out either by the method of conditions or by variation of the coordinates, with redundancy resulting from triangle misclosures, diagonals in trilateration quadrilaterals, and additional base lines

and Laplace azimuths. For the method of conditions, the geometry of the network was adjusted first. The *coordinates transfer* from an initial point (see below) was then carried out using the solutions of the direct problem on the ellipsoid; while for the method of variation of the coordinates, ellipsoidal "observation equations" were derived from the solution of the inverse problem, cf. [6.3.3]. Among the deficiencies of this classical *"development method"* are the neglecting of the deflections of the vertical, the inadequate reduction of distances on the ellipsoid, and especially the step by step calculation of larger networks, with junction constraints when connecting a new network section to an existing one. This led to network distortions of different type, with regionally varying errors in scale ($\pm 10^{-5}$) and orientation (± a few arcsec). Relative coordinate errors with respect to the initial point increased from a few decimeters over about 100 km to about one meter over several 100 km and reached 10 meters and more at the edges of extensively extended networks.

The *geodetic datum* of a horizontal control network comprises the parameters of the reference ellipsoid and of the network's orientation with respect to the earth's body, cf. [6.3.3].

Conventional ellipsoids, as computed by the adjustment of several arc measurements, were introduced during earlier geodetic surveys, cf. [1.3.3]. Some more recent surveys refer to locally *best-fitting ellipsoids*, as derived from a minimum condition on the vertical deflections, according to (6.182):

$$\Sigma\left(\xi^2 + \eta^2\right) = \min., \tag{7.1}$$

using the equations (6.51). Topographic-isostatically reduced deflections of the vertical have been used for larger networks in order to eliminate short and medium-wave effects. The ellipsoid parameters of a geodetic reference system, cf. [4.3], have been used recently. Tab. 7.1 gives the parameters of some

Tab. 7.1. Parameters of reference ellipsoids (rounded values), NIMA (2000)

Name, year	semimajor axis a (m)	reciprocal flattening $1/f$
Airy 1830	6 377 563	299.3
Everest 1830	6 377 276	300.8
Bessel 1841	6 377 397	299.15
Clarke 1866	6 378 206	294.98
Clarke 1880	6 378 249	293.47
Hayford 1909 = Int.Ell.1924	6 378 388	297.0
Krassovski 1940	6 378 245	298.3
GRS 67	6 378 160	298.247
GRS 80	6 378 137	298.257

reference ellipsoids that have been used for national geodetic surveys (STRASSER 1957, NIMA 2000).

The ellipsoids of Airy (applied in Great Britain), Everest (India etc.), Bessel (Germany, Austria, Japan etc.), Clarke 1866 (U.S.A., Canada etc.), and Clarke 1880 (France etc.) are based on the adjustment of arc measurements distributed over the continents. The Hayford ellipsoid fits best to the vertical deflection field in the U.S.A., it has been introduced in a number of countries. The Krassovski ellipsoid resulted from a fit to the Russian triangulation, with additional data from western Europe and the U.S.A. The ellipsoids of the geodetic reference systems GRS67 (Australia etc.) and GRS 80 represent optimum approximations to the geoid.

The *orientation* of the ellipsoid was realized by defining the ellipsoidal coordinates of a fundamental (initial) point, also called network origin, and by conditions for the parallelism of the axes of the ellipsoidal and the global geocentric systems, cf. [6.3.3].

In earlier surveys, the coordinates of the *fundamental point* were fixed by postulating equality between observed astronomic latitude, longitude, and orthometric height and the corresponding ellipsoidal quantities. This is identical to setting the deflection of the vertical and the geoid height of the fundamental point to zero:

$$\xi_F = \eta_F = N_F = 0\,. \tag{7.2}$$

This strategy provides a good approximation of the ellipsoid to the geoid close to the origin, but may lead to larger deviations at more remote areas (Fig.7.4). If

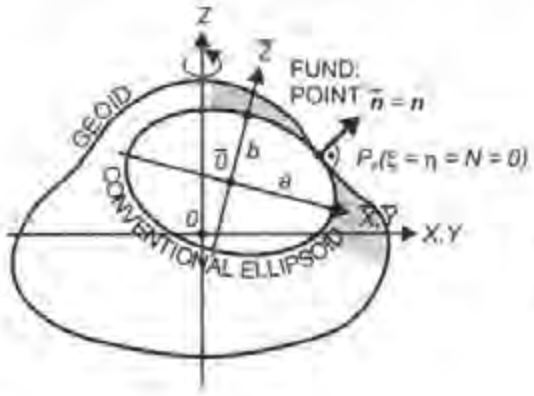

Fig. 7.4. Locally fitting "conventional" ellipsoid

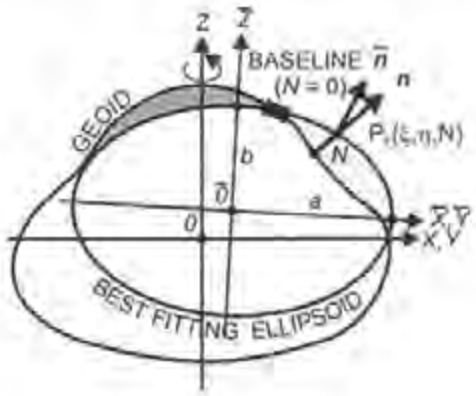

Fig. 7.5. Regionally best fitting ellipsoid

a sufficient number of vertical deflection points were available and well distributed over the area of calculation, the minimum condition (7.1) was used. This condition permits determination of the deflection of the vertical in the fundamental station and, eventually, the parameters of a best-fitting ellipsoid. This procedure led to an *optimum fitting* over the whole area, and kept the deflections of the vertical small. In many cases, the geoid height of the origin point was defined indirectly by reducing the base lines onto the geoid and treating them as ellipsoidal quantities (Fig. 7.5). The minimum condition for the geoid heights (6.181)

$$\Sigma N^2 = \min. \tag{7.3}$$

was occasionally applied using relative geoid heights calculated from astronomic leveling, cf. [6.7.4], and utilizing the last equation of (6.51).The *parallelism* of the axes was achieved by the condition equations (6.57) and (6.58) for the deflection of the vertical and the azimuth (Laplace equation); these were applied to the observations at the fundamental point and eventually at additional Laplace stations. Some recent geodetic datums utilize the ellipsoid parameters of a Geodetic Reference System, cf. [4.3], with optimum approximations to the geoid (mean earth ellipsoid), Fig. 7.6. Tab. 7.2 lists the ellipsoids and the origin points used for some geodetic datums (HOOIJBERG 1997, NIMA 2000).

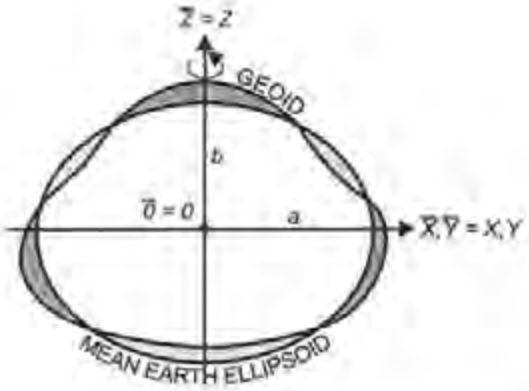

Fig. 7.6. Mean earth ellipsoid

Tab. 7.2. Reference ellipsoids and origin points of some geodetic datums

Geodetic Datum	Reference Ellipsoid	Name of Origin	Origin Latit.	Origin Longit.
Australian Geodetic 1984 (AGD84)	GRS67	Johnston	−25°57'	133°13'
Deutsches Hauptdreiecksnetz (DHDN), Germany	Bessel 1841	Rauenberg/Berlin	52°27'	13°22'
European Datum 1950 (ED50)	Intern.Ellipsoid 1924	Potsdam, Helmertturm	52°23'	13°04'
Indian	Everest 1830	Kalianpur	24°07'	77°39'
North American 1927 (NAD27)	Clarke 1866	Meades Ranch, Kansas	39°13'	261°27'
North American 1983 (NAD83)	GRS80	geocentric		
Ordnance Survey of Great Britain 1936 (OSG36)	Airy 1830	Herstmonceux	50°52'	0°21'
Pulkovo 1942, former Soviet Union	Krassovski 1940	Pulkovo	59°46'	30°20'
South American 1969 (SAD69)	GRS67	Chua, Brazil	−19°46'	311°54'

The horizontal control network of the U.S.A. was constructed by triangulation chains with mesh sizes of about 500 km. Nodal nets at the junctions of the chains were treated as constraints in the adjustment, and areal networks later filled the meshes (BAKER 1974). A conventional ellipsoid (Clarke 1866) was introduced, with the orientation obtained from the minimum condition for vertical deflections (7.1): *North American Datum 1927* (NAD27), see Tab.7.2. This system has been replaced by the North American *Datum of 1983* (NAD83), which combines the horizontal control networks of the U.S.A., Canada, Greenland, Mexico, and Central America by a rigorous adjustment (SCHWARZ 1989, SCHWARZ and WADE 1990), Fig.7.7. The observations include terrestrial data (horizontal directions, azimuths, distances), Doppler stations (large-scale control and reference to the geocenter), and VLBI baselines (scale and orientation). The adjustment (about 1.8 million observations, more than 900 000 unknowns and 266 000 stations) was performed by Helmert-blocking (WOLF 1978) and utilized a height-constrained three-dimensional procedure, cf. [6.2], (VINCENTY 1980, 1982). The two-dimensional results refer to the Geodetic Reference System 1980, with a geocentric position accurate to about ±2 m. The relative station uncertainty is a few cm to a few dm for distances between 10 and 300 km (SNAY 1990). Deflections of the vertical and geoid heights were calculated for all stations by gravimetric methods, cf. [6.7.1].

Since the 1950's, attempts have been made in Europe to establish a unified *European triangulation network* (RETrig). A central European network formed by selected triangulation

Fig. 7.7. Horizontal control network of the U.S.A. (NAD83), with first and second order triangulation, and traverses, courtesy National Geodetic Survey, National Ocean Service, NOAA

chains was calculated first and later augmented by blocks in the southwest, southeast, and north (WHITTEN 1952): *European Datum 1950* (ED50), see Tab.7.2. The International Ellipsoid 1924 served as the reference surface and was orientated by the minimum condition (7.1), which provided vertical deflection components ($\xi = 3.36''$, $\eta = 1.78''$) for the origin Potsdam, Helmertturm. The base lines, reduced to the geoid, indirectly provided the geoid height ($N = 0.4$ m) at the origin (WOLF 1987). For *western* Europe, a rigorous readjustment of all first-order triangulation nets was carried out later, including electromagnetic distance measurements, VLBI, satellite laser ranging, and Doppler observations: *European Datum 1987* (ED87), PODER and HORNIK (1989). The system is more homogeneous than ED50, with improved parallelism of the axes (better than 0.1 arcsec) and scale (0.1×10^{-6}). The International Ellipsoid 1924 was preserved as a reference surface, and the translation was taken from ED50 by adopting the ED50 coordinates for the station Munich, Frauenkirche ($X_0 = -83$ m, $Y_0 = -97$ m, $Z_0 = -117$ m). While ED50 was introduced in several countries, and served as the NATO military system until the 1990's, no practical application was found for ED87. In the former Soviet Union, the triangulation chains were adjusted on the Krassovski 1940 ellipsoid: *Pulkovo Datum 1942*, IZOTOV (1959). Parameters and orientation of the ellipsoid were derived from the minimum condition (7.1), with the geoid height set to zero at the origin Pulkovo. Reductions to the ellipsoid became possible by observed and gravimetrically interpolated deflections of the vertical and quasigeoid heights from astrogravimetric leveling, cf. [6.7.4]. After extension to the *eastern* European countries and inclusion of new measurements, a new adjustment was carried out leading to the astrogeodetic net 1983.

The primary triangulation net of *Germany*, developed since the 1870's, is an example of a local horizontal control network. The northwestern part, between the rivers Elbe and Main, was

covered by triangulation chains and densification nets between 1870 and 1895 as part of the geodetic survey of Prussia. A conventional ellipsoid (Bessel 1841) was introduced for the calculation and orientated by the condition (7.2) at the origin Rauenberg/Berlin, whereby the geoid height was fixed indirectly through the reduction of five base lines, one of them located near Berlin. The Laplace azimuth from Rauenberg to Berlin, Marienkirche provided the network's orientation on the ellipsoid. After the network adjustment, the ellipsoidal coordinates were calculated according to the development method, where the horizontal directions were not reduced for the vertical deflections. The eastern parts of Prussia and the triangulations of the southern German states were later tied to this "*Schreiber's block*" utilizing common points at the networks' margins: *Deutsches Hauptdreiecksnetz* (DHDN), see Tab.7.2. In western Germany, the DHDN has been locally improved since the 1950's by additional horizontal directions and electromagnetic distance measurements, without changing the original datum. While the relative accuracy over some 10 to 100 km is at the dm order of magnitude, distortions up to 1 m have been found between different parts of the network. In eastern Germany, a complete retriangulation was carried out after 1950 and calculated within the common adjustment of the eastern European triangulations (see above): Staatliches Trigonometrisches Netz 1942/1983 (STN42/83), IHDE und LINDSTROT (1995). Due to the different datum definitions, DHDN and STN42/83 differ systematically by about 2″ in latitude and 4″ in longitude. The DHDN90 thus consists of three blocks observed over a time span of more than 100 years with different orientation (SCHMIDT 1995), Fig.7.8. Local transformations between the two systems have been performed for practical applications, and a complete recalculation will be carried out together with the transformation to the three-dimensional system DREF 1991, which is part of the European Reference Frame EUREF, *cf.* [7.3.2].

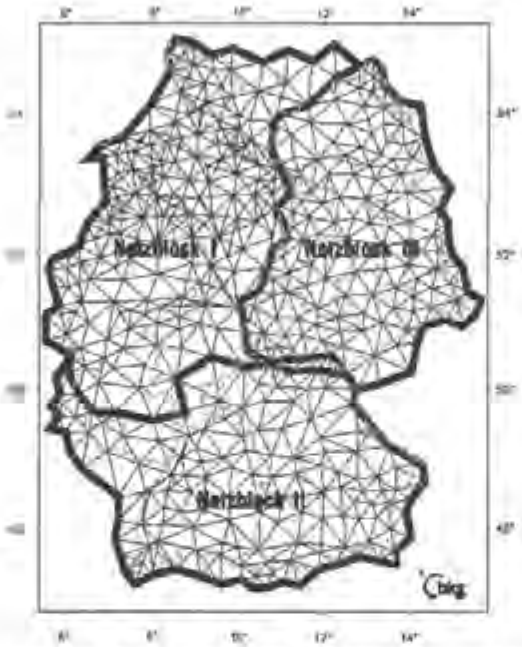

Fig. 7.8. Primary triangulation net of Germany (DHDN90), courtesy Bundesamt für Kartographie und Geodäsie (BKG), Frankfurt a.M., Germany

Satellite positioning was employed early to control the quality of horizontal-control networks and to determine the *datum transformation* parameters with respect to the geocentric system, ASHKENAZI et al. (1988). Equations (6.47) were used to calculate translation, rotation, and scale factor from identical stations coordinated in the global system (especially in the WGS84) and in the local or regional geodetic datum. The results are mean values for the respective geodetic datum, depending strongly on the distribution of the identical points. Tab. 7.3 provides the translations, rotations, and scale factors for some geodetic datums.

Tab. 7.3. Translation, rotation, and scale factors for some geodetic datums (mean values), DMA (1987), NIMA (2000), DHDN and Pulkovo 1942 (STN42/83): IHDE and LINDSTROT (1995)

Geodetic Datum (see Tab. 7.2)	7-Parameter-Transformation							3-Parameter-Transf.		
	Translation (m)			Rotation (arcsec)			Scale Factor	Translation only (m)		
	X_0	Y_0	Z_0	$\varepsilon_{\bar{x}}$	$\varepsilon_{\bar{y}}$	$\varepsilon_{\bar{z}}$	m×10⁶	X_0	$_0$	$_0$
AGD84	-127	-50	153	0.0	0.0	-0.1	1.2	-134	-48	149
DHDN	582	105	414	-1.0	-0.4	3.1	8.3			
ED50	-102	-102	-129	0.4	-0.2	0.4	2.5	-87	-98	-121
Indian	227	803	274	-0.4	-0.6	-0.4	6.6	295	736	257
NAD27	-4	166	183	-0.3	0.3	-0.1	0.4	-8	160	176
OSG36	446	-99	544	-0.9	-0.3	-0.4	-20.9	375	-111	431
Pulkovo 42	24	-123	- 94	0.0	0.2	0.1	1.1	28	-130	- 95
SAD69	-56	-3	-38	0.1	-0.6	-0.2	-0.6	-57	1	-41

Remark: Pulkovo 42 7-Parameter-Transformation values are valid for eastern Germany (STN42/83); 3-Parameter-Transformation values are valid for Russia.

The translation values are at the order of magnitude of the deflections of the vertical. They are larger when conventional ellipsoids have been used and decrease with best-fitting ellipsoids. The rotation angles mirror the accuracy of the astronomic observations and are usually not significant. While the scale errors for older networks reach 10^{-5} and more; they attain only 10^{-6} and less in recent systems, characterizing the progress in length determination. Due to network distortions, local datum-shift values may differ significantly from the mean values, e.g., by 5 to 10 m and more for the translation parameters. If a three-parameter solution (translation only) is carried out, the translation values for older networks experience considerable changes.

The *transformation* from a local geodetic datum to the geocentric system can be done either by a complete readjustment including spatial observations (example: NAD83) or by mean or local (more accurate) transformation parameters. The regional behavior of the translation parameters may also be

modeled by low-order polynomials and provided in the form of datum shift contour charts (DMA 1987). Of special interest is the transformation of ellipsoidal coordinates, which includes the transition from a conventional or best-fitting ellipsoid to a geocentric one. From (6.49) we obtain the changes in the ellipsoidal latitude, longitude, and height (spherical approximation, rotations neglected, ellipsoidal formulas are given by DMA 1987, EHLERT 1991):

$$\begin{aligned}
\Delta\varphi &= -\sin\varphi\cos\lambda \cdot X_0 - \sin\varphi\sin\lambda \cdot Y_0 + \cos\varphi \cdot Z_0 + \sin 2\varphi \cdot \Delta f \\
\cos\varphi\,\Delta\lambda &= -\sin\lambda \cdot X_0 + \cos\lambda \cdot Y_0 \\
\Delta h &= \cos\varphi\cos\lambda \cdot X_0 + \cos\varphi\sin\lambda \cdot Y_0 + \sin\varphi \cdot Z_0 - \Delta a + a\sin^2\varphi \cdot \Delta f
\end{aligned} \tag{7.4a}$$

Here, the sign of the translation vector

$$\mathbf{X}_0 = \begin{pmatrix} X_0 \\ Y_0 \\ Z_0 \end{pmatrix} = \begin{pmatrix} X - \overline{X} \\ Y - \overline{Y} \\ Z - \overline{Z} \end{pmatrix} \tag{7.4b}$$

has been changed (reduction!). All differences are formed in the sense "geocentric – local system", resulting in the transformation

$$\begin{aligned}
&\varphi = \overline{\varphi} + \Delta\varphi,\ \lambda = \overline{\lambda} + \Delta\lambda,\ h = \overline{h} + \Delta h \text{ and} \\
&a = \overline{a} + \Delta a, f = \overline{f} + \Delta f.
\end{aligned} \tag{7.4c}$$

Again, the changes in φ, λ, h can be modeled and given in contour charts, provided a sufficiently large number of identical points have been used. The accuracy of these transformations depends on the area and the number of points available in both systems. A few m accuracy has been achieved for continent-wide networks.

Classical horizontal control networks form the basis for many applications in surveying and mapping. They suffer from network distortions, also they are not geocentric and typically do not use modern geodetic standard-ellipsoids. Within the near future, they will be transformed and integrated into the global geocentric three-dimensional reference frame, cf. [7.3.2].

7.2 Vertical Control Networks

Vertical control networks have been established separately from horizontal control nets. This is due to the demand that heights have to refer to the gravity field rather than the ellipsoidal system used for horizontal positioning.

Vertical control networks are determined by *geometric leveling* and occasionally by hydrostatic leveling, cf. [5.5.3], the control points being designated as *bench marks*. According to the leveling procedure and the accuracy achieved, national geodetic surveys distinguish between different orders of leveling. First-order leveling is carried out in closed loops (loop circumferences of some 100 km) following the rules for precise leveling. The loops are composed of leveling lines connecting the nodal points of the network (Fig.7.9). The lines, in turn, are formed by leveling runs that connect neighboring benchmarks (average spacing 0.5 to 2 km and more). The first-order leveling network is densified by second to fourth-order leveling.

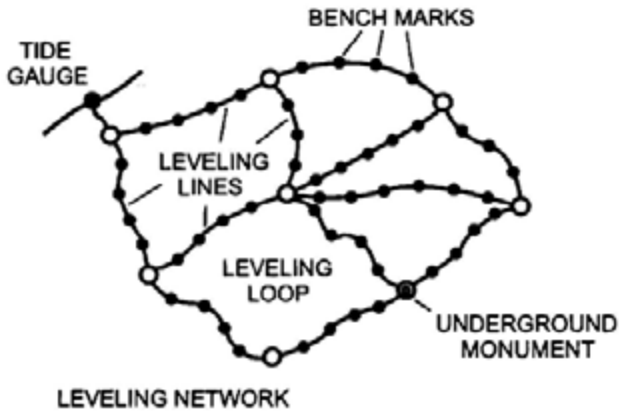

Fig. 7.9. Leveling network (principle)

Leveling lines generally follow main roads, railway lines, and waterways. The benchmarks consist of bolts in buildings, bedrock, or on concrete posts. Long pipes are set up in alluvial regions. Underground monuments are established in geologically stable areas in order to secure the network stability with respect to variations with time. An accuracy of about 1 mm per km is achieved for first-order networks. They should be reobserved at time intervals of some 10 years, as regional and local height changes can reach 1 mm/year and more, especially in areas which experience crustal motion, cf. [8.3.3].

Prior to the adjustment of a leveling network, the observed raw height differences have to be transformed either to geopotential differences or to

differences of normal or orthometric heights by considering surface gravity, cf. [6.4.1]. The adjustment then utilizes the loop misclosure condition of zero and is carried out either by the method of condition equations or, preferably, by the method of parameter variation.

First-order leveling networks were established in many countries between the 1860's and the 1930's when surface gravity along the leveling lines was not available. Hence, gravity reductions were either neglected completely or actual gravity was approximated by normal gravity, leading to *normal* or *spheroidal* orthometric heights. These path-dependent heights may differ from normal or orthometric heights by some mm (flat terrain) to some dm (mountains). With gravity data being generally available now, gravity can be taken into account in calculations of modern leveling networks (WOLF 1974).

The *vertical datum* (zero height surface) is defined by mean sea level (MSL) as derived from tide gauge records. National height systems may differ by some dm to 1 m, and more, between each other. They may also differ from the geoid as a global reference surface, which is due to the effect of sea surface topography, cf. [3.4.3]. Network distortions arise if the vertical datum is constrained to MSL of more than one tide gauge.

Estimates of the vertical datum differences between different height systems are available from satellite positioning and global geoid models and from continental-wide leveling connected to tide gauges (RAPP 1995b, IHDE et al. 1998). For instance, the zero height surface of the North American Vertical Datum of 1988 is about 0.7 m below MSL at Amsterdam, which was used for the European leveling network. In Europe, the national vertical datums have been derived from MSL records in the Mediterranean, the North Sea, and the Baltic Sea. Taking MSL in Amsterdam (used, e.g., in the Netherlands and in Germany) as reference, MSL in Kronstadt (near St.Petersburg, Russia) is about 15 cm higher, and tide gauges along the Mediterranean (Marseille: France, Genoa: Italy, Trieste: Austria) give a MSL that is about 0.4 to 0.5 m lower (SACHER et al. 1999).

In North America, a previous adjustment of first-order leveling provided the *North American Vertical Datum of 1929* (NAVD29), which was constrained to the MSL of 26 tide gauges in the U.S.A. and Canada (BAKER 1974). After replacing destroyed bench marks and extensive releveling, a new adjustment of the leveling data of the U.S.A., Canada, Mexico, and Central America was carried out in geopotential numbers: *North American Vertical Datum of 1988* (NAVD88). Heights are given as orthometric heights according to Helmert (6.84) and refer to MSL of one primary bench mark (Father Point/ Rimouski, Quebec, Canada), ZILKOSKI et al. (1992).

The *United European Leveling Net* (UELN) is formed by first-order leveling lines of the European countries (Fig.7.10). Periodic adjustments have been carried out since 1954, with continuous improvement and extension by including new data. The adjustments are performed in geopotential numbers, and normal heights are available. The average accuracy (UELN95) of the leveling is ±1.1 mm/km, and the standard deviations related to Amsterdam remain less than ±0.1

Fig. 7.10. United European Leveling Net (UELN95), courtesy BKG, Frankfurt a.M., Germany

Fig. 7.11. Primary leveling network of Germany (DHHN92), courtesy BKG, Frankfurt a.M., Germany

m. The vertical datum is taken from MSL of the North Sea as determined in the period 1940 to 1958 at Amsterdam (Normal Amsterdamsch Peil NAP of 1950). The UELN is connected to a large number of tide gauges, which permits determination of sea surface topography around Europe. In the future, UELN will be extended to a kinematic height system by including vertical point velocities (ADAM et al. 2000a).

First-order leveling in *Germany* started around 1865 and first led to a height system calculated from the raw leveling data. Complete resurveys were carried out from 1912 to 1960 and from 1980 to 1985 (western Germany, including gravity measurements). These networks were adjusted as normal-orthometric heights: *Deutsches Haupthöhennetz* (DHHN). The vertical datum was derived by leveling from the Amsterdam normal tide gauge, representing MSL for the period 1683/1684 (WAALEWIJN 1986). The zero height surface (*Normal-Null*, N.N.) was fixed by a standard bench mark, established 37.000 m above N.N. at the former Berlin observatory and, since 1912, by underground marks about 40 km east of Berlin. In eastern Germany, releveling was carried out in the 1970's and adjusted as normal heights. The vertical datum was taken from MSL at the tide gauge in Kronstadt: *Höhennull* (HN). Due to the different definitions of the vertical datum and the heights, systematic height differences between 8 and 16 cm occurred at the boundary between western and eastern Germany. A readjustment was performed in geopotential numbers, where the vertical datum is defined by the geopotential number of the nodal point Wallenhorst taken from the UELN86 adjustment and thus refers to MSL at Amsterdam (Fig.7.11): DHHN92. Normal heights have been introduced as official heights, referring to the reference surface (quasigeoid) *Normalhöhennull* (NHN), WEBER (1995).

Leveling networks are characterized by high accuracy, but systematic errors may accumulate over large distances. Due to the time-consuming measurement procedure, repetition surveys are feasible only after long time intervals. A more rapid establishment of vertical control networks can be achieved by trigonometric leveling, cf. [6.4.2], and a drastic change is to be expected by GPS-heighting in connection with precise geoid or quasigeoid models, cf. [6.4.3]. In this way, vertical control networks will be integrated into three-dimensional control systems, cf. [7.3.2]. Geometric leveling will maintain its importance over short distances, and especially in areas of recent crustal movements, such as regions of land subsidence and zones of earthquake or volcanic activity, cf. [8.3.3].

7.3 Three-dimensional Networks

Geodetic space methods deliver three-dimensional coordinates with cm-accuracy in the global geocentric system on global, regional, and local scale. Global networks realize the terrestrial reference system and provide reference stations for the establishment of continent-wide networks, wherein GPS plays a fundamental role [7.3.1]. Further network densification is carried out nearly exclusively by GPS, with subsequent integration of existing classical control nets [7.3.2].

7.3.1 Global and Continental Networks

The *International Terrestrial Reference Frame* (ITRF) represents the global basis for three-dimensional positioning. It is defined by the geocentric Cartesian coordinates and the horizontal velocities of a global set of space geodetic observing sites, given for a certain epoch, with an accuracy of about ±1 cm and ±1 to 3 mm/year respectively, cf. [2.5.3]. The ITRF results are based on observations obtained by global networks employing different space techniques, which are combined within the frame of the International Earth Rotation Service (IERS), cf. [2.3].

Nowadays, the *Global Positioning System* (GPS) is the primary technique used in all scales for positioning and navigation. The GPS results refer to the *World Geodetic System 1984* (WGS84). The underlying global network is comprised of a limited number of GPS tracking stations, determined with an accuracy of about 5 cm. At this accuracy level, WGS84 also agrees with ITRF, cf. [5.2.5].

The *International GPS Service* (IGS), established by IAG, has been operational since January 1, 1994. It consists of a global network of more than 200 permanently operating GPS stations equipped with geodetic, two-frequency GPS receivers and several data and analysis centers (BEUTLER et al. 1996b).

IGS products include highly accurate (± a few cm) GPS satellite ephemerides, clock corrections, earth rotation parameters provided on a daily basis, and weekly solutions for the station coordinates (sub-cm accuracy in horizontal position, ±1 to 2 cm in height) and velocities. In addition, the raw GPS tracking data (phase and pseudorange observations), station clock, ionospheric, and tropospheric information are available. By using ITRF positions and velocities for a subset of IGS stations, the IGS network is connected to ITRF and contributes significantly to it. On the other hand, IGS stations and products serve for densifying ITRF on continental scale.

The establishment of continent-wide *fundamental networks* with GPS began at the end of the 1980's; an approximate homogeneous station-coverage is generally the goal. Station distances are several 100 km, and at least three stations per country are generally selected as a reference for further densification and for the transformation of existing control networks, cf. [7.1.2], [7.3.2]. The *station sites* are selected according to the requirements of GPS observations (no visibility obstructions between 5° to 15° and 90° elevation, absence of multipath effects, no radio wave interference). Generally the stations are monumented by concrete pillars, providing a forced centering for the GPS antenna and a height reference mark. Eccentric marks are established in order to locally control horizontal-position and height. Existing first-order control points may be used if they fulfill the GPS requirements, otherwise the GPS stations should be connected to the existing control networks by local surveys.

Dedicated *GPS campaigns* are carried out for the determination of the station coordinates, employing relative positioning, cf. [5.2.5]. This strategy requires the inclusion of at least one reference station with coordinates given in the ITRF. Practically all ITRF and IGS stations in the survey region are introduced as reference ("fiducial") stations. Temporary reference stations may be established through baseline connections to IGS stations in order to improve the connection of the network to the ITRF. Depending on the number of stations and available GPS receivers (two-frequency geodetic type), either all stations are observed simultaneously or the network is divided into blocks that are observed sequentially (Fig.7.12). All observations made simultaneously during a given time interval are called a "session" (SNAY 1986). The duration of one session is typically 24 hours, which permits determination of the ambiguity unknowns and a simultaneous solution for the station coordinates and tropospheric correction parameters. The results of *one* session are highly correlated. Consequently, several sessions are generally carried out, leading to a total observation time of some days to one week.

By referencing the network to IGS stations and applying the IGS precise orbital data, the effect of reference station and orbital errors on the station coordinates is only at the few mm level. When different type GPS receivers are employed in one campaign, corrections have to be applied for antenna phase-center

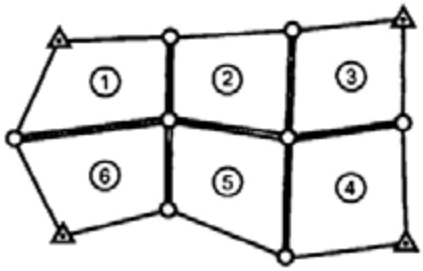

Fig. 7.12. GPS network constructed from individual blocks (principle)

Fig. 7.13. GPS network constructed from baselines to permanent GPS stations (principle)

differences. In addition, phase-center variations have to be taken into account by calibration (SEEBER et al. 1998). Longer observation periods increase the accuracy of the results, due to the changing satellite geometry and the reduction of residual tropospheric, multipath, and antenna effects. This is especially valid for the height component, where small satellite elevations improve the geometry of the solution but introduce larger tropospheric errors. Continent-wide GPS networks can be determined with an accuracy of about ±1 cm.

Permanent ("active") GPS stations have increasingly been established since the 1990's at regional and local scales. They are equipped with geodetic GPS receivers that continuously track all available satellites. Undisturbed visibility to the satellites is achieved by installing the antennas several m to 10 m above the ground on concrete pillars, steel grid masts, etc., or on the top of buildings. Permanent stations provide the raw GPS tracking data, clock corrections, atmospheric information, and daily to weekly solutions for the station coordinates with a precision of a few mm. They serve primarily for the maintenance of the GPS reference system realized by the fundamental network, by controlling variations with time due to plate tectonics and other geodynamic activities. The establishment of GPS control points is facilitated by differential GPS using baselines to the permanent stations and exploiting the data made available for these stations. Thus, a single receiver can be used for precise positioning (Fig. 7.13).

Fundamental GPS networks with permanent stations densify ITRF and IGS on a continental scale and provide the reference for national systems. Following the ITRF strategy, reference epochs are defined for the station coordinates of the fundamental networks, which may differ from the epoch of the ITRF stations introduced and from the time of the observation campaign. Consequently, reductions have to be applied which take the station velocities between the different epochs into account.

A *European Reference Frame* (EUREF) has been built up since the end of the 1980's, as realization of a European Terrestrial Reference System (ETRS). The EUREF stations were determined by successive GPS campaigns that included ITRF and IGS stations and generally covered several countries (SEEGER et al. 1998, ADAM et al. 2000b). The Reference System was defined for the epoch 1989.0 and realized through the European Terrestrial Reference Frame 1989 (ETRF89), which agrees with the definition of ITRF89. In 1999, the ETRF comprised about 200 stations, with distances between 300 and 500 km (Fig.7.14). ETRF89 shall rotate with the stable part of the European tectonic plate, which allows the frame to remain unchanged over a longer time interval. About 90 permanent GPS stations serve for maintaining ETRS and densifying the IGS network. Further applications include investigations of recent geodynamics, sea level monitoring, and contributions to weather prediction, utilizing the tropospheric zenith path delays (BRUYNINX 1999), cf. [5.1.2].

Fig. 7.14. European Reference Frame (EUREF89/97) with permanent GPS stations (status 1999), courtesy BKG, Frankfurt a.M., Germany

A *European Vertical Reference Network* (EUVN) is under construction in order to unify, at a few-cm accuracy level, the different height systems used in the European countries. The network comprises about 200 stations determined in dedicated GPS campaigns (1997) using one-week observation times. It includes EUREF sites, nodal points of the European leveling net UELN, tide gauges, and a number of permanent GPS stations. Three-dimensional coordinates, geopotential numbers, and normal heights will be calculated; hence EUVN will provide fiducial points in order to fit the European quasigeoid to a unified European height system, cf. [6.4.3]. By extension to a kinematic height system, EUVN shall be used for monitoring large-scale, vertical crustal-movements and sea level changes (ADAM et al. 2000a).

In South America, a *Sistema de Referencia Geocentrico para America del Sur* (SIRGAS) was established in 1995 by simultaneous GPS observations (10 days) on some 60 stations well distributed over the sub-continent (HOYER et al. 1998)). Referring to ITRF94, SIRGAS provides the basis for the transformation of the national networks to the global reference system. Within the frame of SIRGAS, another GPS campaign was carried out in 2000 (including Central and North America) on SIRGAS stations, leveling benchmarks, and tide gauges in order to derive a unified vertical height system.

7.3.2 National Networks

National geodetic control-networks have been established by GPS since the 1990's and now supersede the classical horizontal (and possibly vertical) control networks (AUGATH 1997). Although the strategies for establishing and maintaining these three-dimensional reference networks are still under discussion and differ from country to country, the following directions clearly can be identified:

- establishment of a large-scale, three-dimensional network with station distances between 10 and 50 km,
- installation of permanent GPS stations with distances of 50 to 100 km,
- transformation of the existing horizontal control network, eventually using additional GPS control.

A *three-dimensional network* is established by dedicated GPS campaigns using relative positioning, either as a densification of existing continental reference networks or by connection to ITRF and IGS stations, cf. [7.3.1]. Station sites are selected so that they coincide with first and second-order trigonometric points, or are located close to them. GPS observation criteria have to be taken into account, and monuments set below ground are beneficial for the long-term preservation of the network. A separation into a fundamental network with station distances of several 10 km (corresponding to the first-order trigonometric points) and densification nets with distances down to 10 km (second-order triangulation) may be useful for larger countries. Precise leveling benchmarks and tide gauges may be included into these networks in order to incorporate the existing vertical control system. While all stations can be observed simultaneously in smaller networks, a separation into observation blocks with subsequent GPS campaigns will generally be necessary. Each station is occupied at least two times on different days, with session durations between 8 and 24 hours. IGS precise orbital data is used in the network adjustment. Nearby global and continental reference stations are used as "fiducial stations". A "multi-station" adjustment utilizes all data collected during one session, while the "multi-session" adjustment combines the results of several sessions. The national network is transformed to a certain ITRS epoch. Accuracies of ±1 cm and better are achieved for the horizontal components, and ±1 to 2 cm for the heights.

Permanent GPS stations are established at distances of 50 to 100 km or more. The permanent stations are used to maintain the national reference frame with respect to recent crustal movements, but they also serve as reference for all types of GPS surveys which employ differential GPS (DGPS), WANNINGER (1996). The stations are equipped with geodetic GPS receivers; they track all visible GPS satellites at a high data rate (e.g., 1 s). Site selection and delivery of data products (raw tracking data, station coordinates, atmospheric corrections, etc.) follows the rules developed for permanent stations in continental networks, cf. [7.3.1].

By connecting the three-dimensional network stations to first and second-order trigonometric points, the existing horizontal control networks can be *transformed* into the three-dimensional reference frame. Additional GPS control points may be needed if the classical networks contain larger distortions; the selection of the control points depends on the network peculiarities, cf. [7.1.2]. A 7-parameter transformation may suffice for homogeneous networks of high precision, but usually more sophisticated transformation models will be necessary, including polynomial, least squares, or spline approximation (MORITZ 1978). In this way, the local cm-accuracy of classical networks will be kept, and the effect of the network distortions can be reduced to the order of a few cm to dm over distances of some 10 to 100 km.

After the introduction of a three-dimensional reference frame, *GPS-positioning* can be carried out in the relative mode by connection to the reference stations in the survey area. Two or more GPS receivers are required; one (or more) generally serve as a temporary reference with continuous satellite tracking. If a network of permanent GPS stations is operated by a national GPS service, with telemetry data transfer to the users, DGPS can be applied (SEEBER 1993, WANNINGER 2000). Positioning is now possible with one receiver only, depending on the baselines between the new station and the permanent stations. For short (few to 10 km) baselines, a relative cm-accuracy can be achieved in quasi real-time after proper ambiguity solution. For longer baselines, the results are degraded by the distance-dependent errors of GPS, cf. [5.2.5]. By connecting to an array of at least three permanent stations, the known geometry can be used to rapidly determine the ambiguities and to calculate baseline corrections for ionospheric, tropospheric, and orbit effects. Post-processing of DGPS can yield relative sub-cm accuracy. After the completion of the transformation to a three-dimensional reference frame, the classical horizontal networks of lower order will no longer be maintained.

By including first-order leveling benchmarks in the three-dimensional network, the differences between the ellipsoidal heights and the heights of the national height system can be determined (geoid heights, quasigeoid heights). These GPS/leveling control points allow the national height system to be fit to a geoid

or quasigeoid model, and they can be used to derive gravity-field related heights (orthometric heights, normal heights) for all three-dimensional reference stations, cf. [6.4.3]. This will lead to a large-scale *vertical control system* identical with the three-dimensional reference frame and not restricted to the leveling lines. Depending on the accuracy of the geoid-/quasigeoid "reduction" of GPS heights, the application of geometric leveling will be reduced to more local problems where mm-accuracy is required.

Fig. 7.15. German GPS Reference Net 1991(DREF91) with EUREF stations (black circles), courtesy BKG, Frankfurt a.M., Germany

In *Germany*, a three-dimensional network was established in 1991: Deutsches Referenznetz 1991 (DREF91). It consists of 109 stations that are mostly collocated with first or second-order trigonometric points (Fig.7.15). The network comprises the ITRF and EUREF stations and represents the national reference frame embedded in the ETRF, cf. [7.3.1]. Two independent GPS campaigns were carried out (8-hour observation time per session), and the adjusted coordinates (accuracy ±1 cm for the horizontal component and ±1 to 2 cm for the height) were transformed to ETRF89 (LINDSTROT 1999). The network is maintained by about 20 permanent stations operated by BKG and the state survey agencies. DREF densification nets (station distances 15 to 25 km) are under construction by the state survey agencies, which also operate a DGPS service: Satellitenpositionierungsdienst der deutschen Landesvermessung (SAPOS). About 200 permanent GPS stations are planned, which will store the GPS signals and provide them to users in RINEX (receiver independent exchange) format, together with other products. Different accuracy levels are available for real-time and post-processing applications (HANKEMEIER 1996). With SAPOS being fully operational, the lower order trigonometric control networks will not be further maintained. Other examples of national three-dimensional reference networks are found in GUBLER and HORNIK (1999) and GUBLER et al. (1999).

Permanent GPS networks play an increasing role in regions of earthquake activity, cf. [8.3.3]. In *Japan*, a country-wide network of more than 1000 stations is operated by the Geographical Survey Institute, which continuously monitor strain accumulation and tectonic movements.

7.4 Gravity Networks

Gravity networks provide the frame for gravimetric surveys on global, regional, or local scales. They consist of gravity stations where gravity has been determined by absolute or relative methods. On a global scale, the gravity standard is realized by the *International Gravity Standardization Net 1971* (IGSN71), but *absolute gravimeters* now allow independent establishment of the gravity standard, cf. [5.4.3]. A global, absolute-gravity base-station network has been established primarily for the investigation of long-term gravity variations with time, cf. [8.3.4].

National gravimetric surveys are based on a primary or base network, which in most cases is densified by lower order nets. The gravity *base-network* stations should be evenly distributed over the area; station distances of a few 100 km are typical for larger countries. The station sites should be stable with respect to geological, hydrological, and microseismic conditions, and they should be located at permanent locations (observatories etc.). Eccentric stations serve for securing the center station and for controlling local height and mass changes. The stations of the subsequent densification networks may be collocated with horizontal and vertical control points. Horizontal position and height of the network stations should be determined with m and mm to cm-accuracy, respectively.

Absolute gravimeters are increasingly employed for the establishment of base networks, partly in combination with relative gravity-meters. Densification networks are observed primarily with relative instruments. *Relative* gravimeters need to be calibrated, and repeated measurements are necessary in order to determine the instrumental drift. The use of several instruments reduces residual systematic effects, cf. [5.4.2]. Relative gravimetry requires at least two absolute stations in order to derive the gravity "datum" and corrections to the linear calibration coefficient that was determined by the manufacturer or on a calibration line. A network optimization is beneficial for obtaining maximum accuracy and reliability for given restrictions (WENZEL 1977).

The establishment of gravity networks for *geophysical* and *geodynamic* applications follows the same rules, but the distribution of the gravity stations is determined by the geological structures or the geodynamic processes under investigation, cf. [8.3.4].

Gravity networks are generally *adjusted* by the method of parameter variation. Gravity values and - for relative gravimeters - drift and calibration coefficients are the parameters to be determined. Absolute gravity data and relative gravimeter readings, or reading differences, are introduced as observations. The *observation equation* for an *absolute* gravity measurement on the station i reads

$$\bar{z}_i = g_i , \tag{7.5}$$

where $\bar{z}_i$ represents the station mean value corrected for polar motion and earth tides and reduced to ground level, cf. [5.4.1]. For *relative* gravity measurements, the observation equation follows from (5.90) and (5.92). If we restrict ourselves to the linear terms of the drift and the calibration function, the relative gravimeter reading z_i (after approximate calibration and application of the earth tides reduction) on the station i (time t_i) is transformed to gravity by

$$Y_1 z_i - d_1 t_i + N_0 = g_i , \tag{7.6a}$$

which leads to the observation equation

$$z_i = g_i - N_0 - y_1 z_i + d_1 t_i . \tag{7.6b}$$

Here, $d_1 =$ linear drift coefficient, $Y_1 = 1 + y_1 =$ linear calibration coefficient, $y_1 =$ scale correction, $N_0 =$ level unknown. In most applications, reading differences between the stations i and j are introduced as observations, hereby eliminating the level unknowns (TORGE 1993):

$$\Delta z_{ij} = z_j - z_i = g_j - g_i - y_1 \left(z_j - z_i \right) + d_1 \left(t_j - t_i \right). \tag{7.7}$$

The *accuracy* of primary gravity networks, established by absolute gravimeters or by a combination of absolute and relative gravimetry, is about $\pm 0.1\ \mu m s^{-2}$ and may reach $\pm 0.05\ \mu m s^{-2}$.

In *Germany*, gravity base networks and densifying networks were established beginning in the 1930's. The first base-network was observed with relative pendulum instruments; relative gravimeters have contributed since the 1950's. These networks were tied to the Potsdam absolute gravity value, cf. [5.4.3], accuracy increased from some $\pm 1 \mu m s^{-2}$ to $\pm$ a few $0.1 \mu m s^{-2}$. Absolute gravimetry was introduced in 1976/1977 in order to establish a combined absolute/relative base-network in *western* Germany: *Deutsches Schweregrundnetz 1976* (DSGN76), SIGL et al. (1981). This base network was extended to *eastern* Germany and completely remeasured in 1994/1995: DSGN94. The network consists of 30 stations (one center and at least two eccentric points) that were observed with an absolute gravimeter FG5. Repeated observations and relative ties (several gravimeters of type LaCoste and Romberg and Scintrex) served for investigations of accuracy

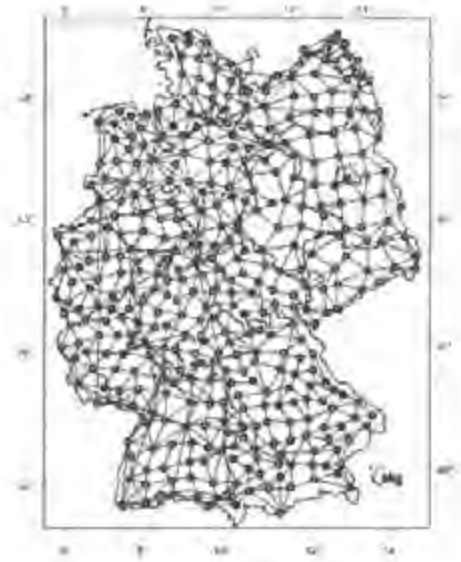

Fig. 7.16. Primary gravity net of Germany (DHSN96), with German gravity base net (DSGN94) stations (black circles), courtesy BKG, Frankfurt a.M., Germany

Fig. 7.17. Gravity network of Uruguay, with absolute stations (black triangles), relative stations, and earth tide station (black circle), after SUBIZA et al. (1998)

($\pm 0.05 \mu m s^{-2}$) and reliability (TORGE et al. 1999a). A first-order densification net (average station distance 30 km) was observed with several relative gravimeters (1978-1982, 1994, accuracy better than $\pm 0.01 \mu m s^{-2}$), Fig.7.16. Further densification down to a few km has been realized or is in progress (WEBER 1998). The gravity network of Uruguay is an example of a combined adjustment of a few absolute stations and relative measurements carried out mainly along leveling lines, Fig.7.17 (SUBIZA et al. 1998).

In the *U.S.A.*, absolute gravity measurements have primarily been carried out within the frame of dedicated projects (investigation of recent vertical crustal-movements, establishment of gravimeter calibration lines, etc.) by NOAA/NGS and other agencies, covering the country by more than 150 stations in 2000. A gravity network established in 1976/1979 by LaCoste and Romberg gravimeters (more than 200 sites) has been constrained to the absolute standard (PETER et al. 1989).

8 Structure and Dynamics of the Earth

Geodesy, within the frame of the geosciences (geophysics, geology, petrology, mineralogy, geochemistry), deals with the determination of the figure and the external gravity field of the earth. The results of geodetic work provide boundary conditions for the development of static and dynamic geophysical earth models. These models, in turn, provide significant information for the planning and implementation of geodetic operations.

Geophysical earth models are based on a radial structure of physical properties, and presuppose hydrostatic equilibrium [8.1]. These assumptions are not valid for the upper layers of the earth, where geodynamic processes play an important role [8.2]. Geodesy contributes to geodynamic research by monitoring the actual variations of the orientation, the physical surface, and the gravity field of the earth [8.3].

From the extensive geophysical literature we mention the classical work of JEFFREYS (1970) and the recent textbooks by BERCKHEMER (1990), STACEY (1992), LOWRIE (1997) and FOWLER (1999). The interrelations between geodesy and geophysics are treated especially in HEISKANEN and VENING-MEINESZ (1958), LAMBECK (1988), and MORITZ (1990). The actual state of geophysical data collection and parameter estimation is given in AHRENS (1995).

8.1 The Geophysical Earth Model

Various observations show that the earth does not posses a *homogeneous* structure:

- The *mass* M of the earth as derived from the geocentric gravitational constant GM, cf. [6.8.1], and the constant of gravitation G, cf. [2.1], amounts to $M = 5.974 \times 10^{24}\,\mathrm{kg}$. With the volume of the earth ellipsoid $1083 \times 10^{18}\,\mathrm{m}^3$, we obtain the *mean density*

$$\rho_m = 5.515 \times 10^3\,\mathrm{kg\,m^{-3}}.$$

  As the density of the earth's crust only amounts to $2.7 \ldots 2.9 \times 10^3\,\mathrm{kg\,m^{-3}}$, density must increase toward the interior of the earth.
- Astronomic observations of the lunisolar precession, cf. [2.4.2], deliver the *dynamic* (mechanical) *ellipticity*

$$H = \frac{C - A}{A}, \tag{8.1}$$

with a value of 1/305.45. With the dynamical form factor provided by satellite geodesy, cf. [6.8.1],

$$J_2 = \frac{C - A}{a^2 M}, \tag{8.2}$$

(C and A being the polar and the mean equatorial moment of inertia, respectively) we obtain the *moment of inertia* with respect to the *rotational* axis

$$C = 0.3307\,\mathrm{a}^2\,\mathrm{M}.$$

If the earth were a homogeneous sphere, we would have $C = 0.4a^2M$. This again indicates a density increase with depth.

- Seismology shows that the earth has a *shell-like* construction, with the shell boundaries being defined by discontinuities of the seismic waves velocities.

With the velocities of the seismic waves being known, and under the assumption of hydrostatic equilibrium, density, gravity, and pressure inside a spherically layered earth model can be calculated as a function of the radial distance from the earth's center of mass.

The assumption of hydrostatic pressure in the earth's interior is justified by the fact that the earth originally existed in a liquid state. In which case, the pressure depended only on the weight of the masses lying above, and it increased toward the center of the earth.

Seismology determines the *velocities* of the primary (compression) and the secondary (shear) seismic waves, v_p and v_s. From these velocities the *seismic parameter*

$$\Phi = \frac{K}{\rho} = v_p^2 - \frac{4}{3}v_s^2 \tag{8.3}$$

is derived, where K is the bulk modulus (compressibility) and ρ is density. K is defined as the ratio between the hydrostatic pressure and the dilation experienced by a body under this pressure. The relationship between changes of *pressure p* and *density* is given by

$$d\rho = \frac{1}{\Phi} dp \,. \tag{8.4}$$

Under hydrostatic equilibrium, the increase of *pressure* with *depth* depends on the weight of the additional vertical mass column. With the radial distance r, the fundamental hydrostatic equation reads

$$dp = -g(r)\rho(r)dr \,, \tag{8.5}$$

where the minus-sign indicates that pressure decreases with increasing radius. Finally, from (8.4) and (8.5) we obtain the relation between *height* and *density* changes (*Adams-Williamson* equation):

$$\frac{d\rho}{dr} = -\frac{g(r)\rho(r)}{\Phi} \,. \tag{8.6}$$

According to (3.52), the radial change of the gravity potential W is given by

$$dW = -g(r)dr \,. \tag{8.7}$$

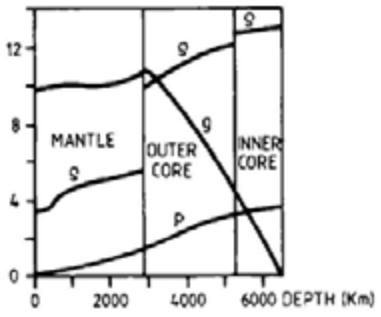

Fig. 8.1. Density ρ (10^3 kg/m^3), gravity g (m/s^2), and pressure p (10^{11} Pa) inside a spherically symmetric earth model, after DZIEWONSKI and ANDERSON (1981)

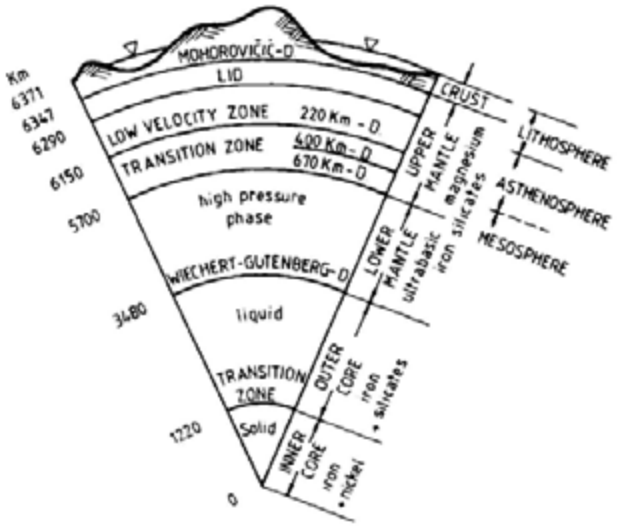

Fig. 8.2. Spherical earth model, with homogeneous shells separated by discontinuity zones (D.), not to scale, after DZIEWONSKI and ANDERSON (1981)

Inserting (8.7) into (8.5) yields

$$dp = \rho(r)dW \,. \tag{8.8}$$

Hence, the surfaces of equal pressure (isobaric surfaces) coincide with equipotential surfaces and, after (8.4), also with surfaces of equal density.

Starting from density and gravity values on the earth surface, density, pressure and gravity inside the earth can be calculated iteratively, using (8.3), (8.4) and (3.22), (3.23). Here we use the total mass and the polar moment of inertia as boundary conditions. Corresponding spherically symmetric *earth models* consist of several layers characterized by chemical and physical properties (composition, pressure, temperature), BULLEN (1975), DZIEWONSKI and ANDERSON (1981). The velocities, or the velocity gradients, of the seismic waves change abruptly at the boundaries of the layers (discontinuity surfaces or zones), as does density (Fig.8.1). Inside one layer, density increases smoothly and reaches about $13000\,\mathrm{kg\,m^{-3}}$ at the earth's center. Gravity remains nearly constant within the earth's mantle and decreases almost linearly to zero in the core. Pressure increases continuously with depth.

The layered structure of the earth is shown in Fig.8.2. The earth's *crust* (average thickness over the continents and the oceans about 24 km) is the uppermost layer and is characterized by a complex structure. It is separated from the *upper mantle* by the *Mohorovičić*-discontinuity. Lateral density variations are pronounced in the crust, but are found also in the upper mantle, cf.[8.2.1]. The crust and the uppermost part of the mantle (also called lid of the low-velocity layer beneath it) behave rigidly and are affected by plate tectonic motions, cf. [8.2.3]. The *lower mantle* starts at a depth of 650 to 670 km and is separated from the core at 2890 km depth, through the *Wiechert-Gutenberg*-discontinuity. The liquid *outer core* extends to 5150 km, followed by the solid *inner core*.

The density distribution of these earth models can also be tested by comparing its *elasticity* parameters with the results obtained from the observation of natural oscillations and (to a limited extent) earth tides, cf. [8.3.5]. The free oscillations especially provide an important constraint on the models.

More refined models have to take the *deviations* from *spherical symmetry* into account, as well as departures from hydrostatic equilibrium. These deviations are clearly indicated by the odd zonal and the tesseral harmonic coefficients of the gravity potential, cf. [3.3.4], and by other geophysical observations. Seismic tomography especially revealed large-scale lateral variations of the P and S-wave velocities in the mantle, correlated with zones of density and temperature anomalies (DZIEWONSKI and WOODHOUSE 1987). A global deviation from

hydrostatic equilibrium is indicated by the flattening of a rotating spheroidal body in equilibrium, composed of density layers that are approximately ellipsoidal. According to *Clairaut*, the following relation holds between the polar moment of inertia C, the mass M, the ellipsoidal quantities a and m (4.50), and the hydrostatic flattening f_h:

$$\frac{C}{a^2 M} = \frac{2}{3}\left(1 - \frac{2}{5}\sqrt{\frac{5m}{2f_h} - 1}\right). \tag{8.9}$$

Inserting the observed values results in *hydrostatic flattening* values of about 1/299.7, which differ significantly from 1/298.25 derived directly from satellite orbit analyses, cf. [6.8.1], DENIS (1989).

The larger actual flattening may be attributed to a "fossil" flattening of the lower mantle, which developed when the earth's rotational velocity was larger and which is not yet compensated. The still incomplete recovery of the ancient ice loads at the polar caps may be another explication.

Refined geophysical earth models that take the ellipsoidal form and the rotation of the earth into account may use the level ellipsoid as a good approximation for the external boundary surface, cf. [4.2.1].

8.2 The Upper Layers of the Earth

Large deviations from the spherically symmetric earth model are found in the earth's crust and upper mantle [8.2.1]. Topographic mass excesses (mountains) and deficiencies (oceans) are, to a large part, compensated by the underlying masses, which leads to isostatic equilibrium [8.2.2]. The theory of plate tectonics introduces (nearly) rigid lithospheric plates that move against each other, causing crustal deformations, especially at the plate boundaries [8.2.3]. Since the gravity field reflects the distribution of the terrestrial masses, it provides an essential constraint in the development of crust and mantle models [8.2.4].

8.2.1 Structure of the Earth's Crust and Upper Mantle

The heterogeneous structure of the uppermost layers of the earth is recognized directly by the distribution and composition of the *topographic* masses. There is a pronounced difference between the mean elevation of the continents (about 0.5 km) and the mean depth of the oceans (about 4.5 km). Ocean depths increase with growing distance from the ocean ridges (mean depth around 2.5 km) due to thermal cooling and contraction of the oceanic lithosphere with sea-floor spreading, cf. [8.2.3]. Consequently, the age of the oceanic crust is at most

200 million years, while the continental crust dates back 4 billion years (CAZENAVE 1995).

The *crust* is composed of a variety of sedimentary, igneous (effusive and intrusive), and metamorphic rocks. Density changes occur primarily between different types of rock, but larger density variations are also found within the same rock material, especially in sediments. Density estimates are based on surface rock samples, borehole probes, and the relationship between density and seismic wave velocities (ST. MUELLER 1974). The *upper mantle* has been investigated by seismic methods especially, and three-dimensional models are now available from seismic tomography (WOODHOUSE and DZIEWONSKI 1984).

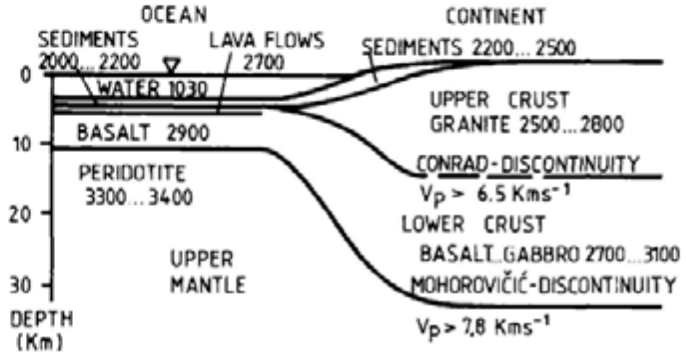

Fig. 8.3. Structure of the earth's crust with rock densities (kg/m^3) and velocities of seismic primary waves, after TORGE (1989)

The *structure* of the earth's *crust* and *upper mantle* may be briefly described as follows (Fig.8.3):

A *sediment* layer with highly varying thickness is found in the uppermost stratum in large parts of the *crust*. Seismic wave velocities and rock densities (average value $2400\,kg\,m^{-3}$ for consolidated sandstone) vary considerably in this zone. In *continental* areas, the next lower layer of the upper crust consists mainly of acidic rocks such as granite (mean density $2700\,kg\,m^{-3}$); primary wave velocities vary between 5.9 and $6.3\,km\,s^{-1}$. The lower crust is composed of basic rocks such as basalt and gabbro (mean density $2700\,kg\,m^{-3}$). Wave velocities exceed $6.5\,km\,s^{-1}$ and gradually increase to more than $7\,km\,s^{-1}$. The boundary between the upper and the lower crust (*Conrad* – discontinuity) is marked only in some parts of the continents, at depths of 10 to 20 km. Beneath the *oceans,* consolidated sediments and basalt lava flows are found in the upper part of the crust above a basaltic layer of 6 to 7 km thickness (TANIMOTO 1995).

A sharp (over a few km) change in seismic velocity ($v_p > 7.8\,km\,s^{-1}$) is found at an average depth of 35 km on the continents and 10 km on the oceans. This

Mohorovičić-discontinuity (Moho) defines the boundary between crust and mantle. Ultrabasic rocks (peridotite, with olivine as the main mineral constituent) are assumed to be located below the Moho, with a density of 3300 to 3400 $kg\,m^{-3}$. The depth of the Moho is closely related to topography. On the *continents*, it may be less than 20 km (Afar hotspot), reaching about 30 to 40 km at shields and platforms. Cenozoic mountain belts (Alps, Rocky Mountains, Himalaya) are characterized by a crustal thickness of 60 to 80 km. On the *oceans*, the crustal thickness is more constant. An extremely thin crust of a few km is found at slow spreading and fracture zones, while a thick crust of about 20 km appears where hotspots (mantle plumes) are located under ridge axes, as in southern Iceland. These variations of crustal thickness are mainly due to isostasy and plate tectonics, cf. [8.2.2], [8.2.3].

A global description of the Moho-depth is provided by a spherical harmonic expansion up to degree and order 20 (SOLLER et al. 1982). More detailed studies on the depth of the Moho are available for the U.S.A. (ALLENBY and SCHNETZLER 1983) and for Europe (MEISSNER et al. 1987), among others. Three-dimensional models are available for the crust (MOONEY et al. 1998) and for the upper mantle.

8.2.2 Isostasy

When considering the topographic masses and ocean waters as deviations from hydrostatic equilibrium, the removal of topography and the filling of the oceans should create an equilibrium figure, with a gravity field coinciding with the normal gravity field, cf. [4.2.2]. However, from the systematic behavior of the residual gravity field quantities, it follows that the visible mass excesses and deficiencies are, to a large part, compensated by a corresponding mass distribution in the interior of the earth (HEISKANEN and VENING-MEINESZ 1958).

During the arc measurement in Peru, cf. [1.3.2], *Bouguer* discovered that the *deflections of the vertical* as computed from the masses of the mountains were larger than the observed values. In the 19th century, the Survey of India (*G. Everest*) revealed significant differences between observed and calculated deflections of the vertical caused by the Himalaya Mountains, the computed values being several times larger than the observed ones. This observation was the basis for the theory of isostasy developed by *Airy* and *Pratt* (see below).

The large-scale behavior of the *Bouguer anomalies*, cf. [6.5.3], is another indication for the compensation of the visible mass anomalies. In mountainous areas, the Bouguer anomalies are generally negative, reaching values as low as $-2000\,\mu m\,s^{-2}$, while positive values (up to $4000\,\mu m\,s^{-2}$) are common over the oceans. A correlation with the mean height or depth (mean over several 100 km) can be demonstrated and approximated by a regression of $-1000\,\mu m\,s^{-2}/1000\,m$ height, and $+1000\,\mu m\,s^{-2}/1000\,m$ depth.

Finally, the *geoid heights* produced by the topographic masses would reach values of up to about 500 m (HELMERT 1884), whereas the observed values remain below 100 m.

The model of *isostasy* is used to explain these observations. It postulates that the topographic masses are compensated in such a way that hydrostatic pressure is achieved at a certain depth of compensation. The compensation depends on the dimension of the topographic load and may be achieved by different mechanisms. Loads of several 10 to 100 km dimensions are supported by the strength of the lithosphere and are not isostatically compensated. Larger loads may lead to an elastic flexure of the lithosphere. Large-scale topographic features of several 100 km dimension, and more, are generally in isostatic equilibrium, at least for the major part of the earth, the exceptions being areas of postglacial isostatic rebound (see below) and the deep-sea trenches, cf. [8.2.3].

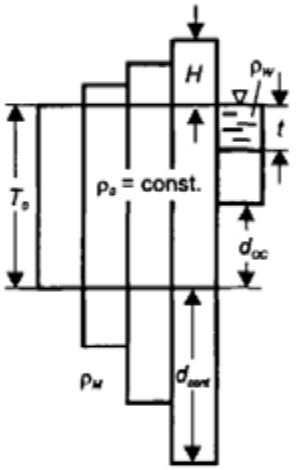

Fig. 8.4. Isostatic model of Airy

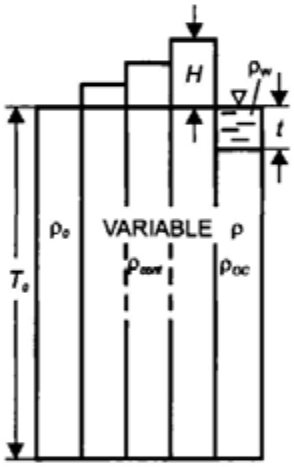

Fig. 8.5. Isostatic model of Pratt

The classical isostasy models of *Airy* and *Pratt* are based on the assumption that isostatic compensation takes place locally in vertical columns only. Utilizing the hydrostatic equation (8.5), the condition of isostasy then reads (with g = const.)

$$\int_{H+T}^{H} \rho \, dz = \text{const.}, \tag{8.10}$$

with z = depth, H = height of topography, T = depth of compensation. The model developed by *G.B. Airy* in 1855 (also designated Airy-Heiskanen model) is based on a crust of constant density ρ_0 and varying thickness, where the "normal" column of height $H = 0$ has the thickness T_0 (Fig.8.4). The continental topography ($H > 0$) forms mountain "roots" (thickness d_{cont}), while

"antiroots" (thickness d_{oc}) are found beneath the oceanic columns. The ocean depth is denoted as t. In this way, the crust penetrates with varying depths into the upper mantle: floating equilibrium. Neglecting the earth's curvature, the following equilibrium conditions hold for the continental and the oceanic columns:

$$\begin{aligned}(\rho_M - \rho_0)d_{cont} &= \rho_0 H \\ (\rho_M - \rho_0)d_{oc} &= (\rho_0 - \rho_w)t,\end{aligned} \tag{8.11}$$

with ρ_0 = density of the crust, ρ_M = density of the upper mantle, ρ_w = sea water density. With the conventional values $\rho_0 = 2670\,\mathrm{kg\,m^{-3}}$, $\rho_M = 3270\,\mathrm{kg\,m^{-3}}$, $\rho_w = 1030\,\mathrm{kg\,m^{-3}}$, the thickness of the root and the antiroot is given by

$$d_{cont} = 4.45H,\ d_{oc} = 2.73t\,. \tag{8.12}$$

The thickness T_0 of the normal column can be estimated from isostatic gravity anomalies calculated on the basis of a certain depth of compensation, cf. [6.5.3]. For $T_0 = 30$ to $40\,\mathrm{km}$, these anomalies generally do not depend on the height of the topography. Hence, the depth of compensation is in good agreement with the depth of the Moho as obtained from seismology, cf. [8.2.1].

The isostatic model of *J.H. Pratt* (1855, also called Pratt-Hayford model) assumes a crustal layer of constant thickness T_0 and allows lateral changes in density in order to obtain isostatic equilibrium (Fig.8.5). With the density ρ_0 for the normal column ($H = 0$), continental columns generate densities smaller than ρ_0, while oceanic columns are denser. The equilibrium conditions for the continents and the oceans are:

$$\begin{aligned}\rho_{cont}(T_0 + H) &= \rho_0 T_0 \\ \rho_w t + \rho_{oc}(T_0 - t) &= \rho_0 T_0,\end{aligned} \tag{8.13}$$

with $\rho = 2670\,\mathrm{kg\,m^{-3}}$ and $\rho_w = 1030\,\mathrm{kg\,m^{-3}}$ the densities of the continental and the oceanic columns are given by

$$\rho_{cont} = 2670\frac{T_0}{T_0 + H},\ \rho_{oc} = \frac{2670T_0 - 1030t}{T_0 - t}\,. \tag{8.14}$$

The depth of compensation can be estimated from the behavior of residual gravity field quantities calculated with depth dependent assumptions. By utilizing topographic-isostatically reduced deflections of the vertical in the U.S.A., *Hayford* obtained minimum values for a compensation depth of 113.7 km. This value is close to the thickness of the continental lithosphere, cf. [8.2.3].

A refined isostatic model was proposed by VENING-MEINESZ (1931). It admits *regional isostatic compensation* by assuming that the upper layer behaves like an elastic plate overlying a weak fluid. A surface load causes a flexure of the plate, with a regional bending over a horizontal distance wider than the load dimension (Fig.8.6). The amount of flexure depends on the distance from the load and can be calculated from the load, the density contrast between the plate and the substratum, and the elastic parameters (Young's modulus, Poisson's ratio) of the plate (ABD-ELMOTAAL 1995).

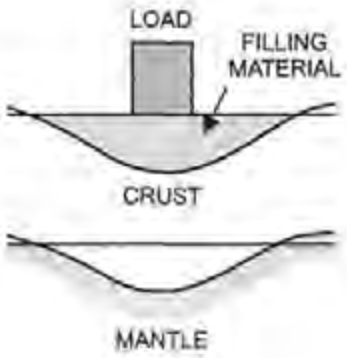

Fig. 8.6. Regional isostatic model of Vening-Meinesz

Globally, the models of Airy respectively Vening-Meinesz describe the dominating isostatic features, but lateral density variations (Pratt model) also contribute to isostasy in some regions. In the compensated parts of the earth, isostatic anomalies vary non-uniformly about zero (maximum values of about $500\,\mu ms^{-2}$), and they clearly indicate areas which are not in isostatic equilibrium. On the other hand, they are not very sensitive with respect to a change of the model or variations of the model parameters, which makes discerning of different models and estimating the absolute depth of the compensation level difficult. Utilizing global models of the topography, cf. [6.5.2], spherical harmonic expansions of the topographic-isostatic potential have been developed (SÜNKEL 1936b). These models can be used for gravity field interpolation and for the analysis of the observed gravity field (RUMMEL et al. 1988).

Incomplete isostatic compensation is found in some mountainous regions and in the areas of strong pleistocene glaciation (Canada, Fennoscandia, Greenland, Antarctica). Mountains may become overcompensated by large erosion, and as a consequence a vertical uplift will occur. The melting of the ice masses after the pleistocene glaciation has caused an isostatic imbalance, which has since been compensated by postglacial rebound. This phenomenon has been especially well investigated in Fennoscandia, where recent uplift rates reach 1 cm/year (KAKKURI 1986). As the rate of uplift depends on the viscosity of the

mantle, corresponding observations contribute to the determination of this geophysical parameter (LAMBECK et al. 1998), cf. [8.3.3].

8.2.3 Plate Tectonics

The theory of plate tectonics synthesizes a multitude of individual observations of geological and geophysical nature. The theory integrates the concepts of *continental drift* (WEGENER 1915) and *sea-floor spreading* (DIETZ 1961, HESS 1962). According to this model, new oceanic crust is formed by uprising basaltic magma at the axes of the mid-oceanic ridges, and it spreads out to both sides of the rift system. The spreading sea-floor is characterized by stripes of interchanging positive and negative magnetic anomalies aligned parallel to the ridges, which indicate the reversal of the earth's magnetic field occurring irregularly at intervals of tens of thousands to tens of million years (VINE and MATTHEWS 1963). Radiometric age determinations of the oceanic rocks show that the age of the ocean floor increases with the distance from the ridge axes and does not exceed 200 million years.

Before that time (Permian and Triassic), the supercontinent Pangaea, postulated by *Wegener*, united all present land masses. Break up started during the Jurassic period, when Pangaea rifted into Laurasia (today North America and Eurasia) and Gondwana (today South America, Africa, India, Antarctica and Australia), with the Tethys Sea between them. This rifting process finally led to the present distribution of the continents and oceans.

The spreading rates of the ocean floor (referring to geological time spans) can be derived from the spacing of the magnetic anomalies and the rock age. They vary between 2 cm/year (e.g., at the Reykjanes Ridge south of Iceland) and 15 cm/year at the East Pacific Rise, MINSTER and JORDAN (1978).

Plate tectonics (McKENZIE and PARKER 1967, MORGAN 1968) postulates seven larger (Pacific, North and South American, Eurasian, African, Indian-Australian, Antarctic) and more than 20 smaller, nearly rigid lithospheric plates which move against each other on the asthenosphere. The *lithosphere* includes the earth's crust and the uppermost part of the mantle; it possesses a thickness of 70 to 100 km under the deep oceans and 100 to 150 km under the continents. The *asthenosphere* is characterized by low viscosity (resistance to flow within a fluid), which allows a viscous flow on geological time scales (LE PICHON et al. 1973). The plate boundaries can be identified by an accumulation of seismic (earthquakes) and volcanic activity, where the boundary zones vary in width between some 10 to some 100 km and more (Fig.8.7).

The movement of the tectonic plates can be described as follows (LE PICHON et al.1973, LOWRIE 1997), Fig.8.8:

Fig. 8.7. Main lithospheric plates and direction of plate movements, AN = Anatolian, AR = Arabian, CA = Caribbean, CO = Cocos, NA = Nazca, PH = Philippines, SO = Somalia plate, after TORGE (1989)

The mid-ocean ridges represent *diverging* (constructive) plate boundaries where new lithospheric material is formed from magma uprising from the asthenosphere and pressed apart. When colliding with a another plate, the cooled, heavier oceanic plate is forced to sink into the upper mantle (subduction) where it is consumed at depths of around 700 km: *converging* (destructive) plate boundary. This process creates deep-sea trenches and island arcs (e.g., at the western and northern Pacific, subduction rate of about 9 cm/year at the Japan trench) or mountain ranges (e.g., the Andes). The collision of two continental plates leads to the formation of mountain chains (e.g., the Himalaya and the Alps). *Transform faults* with relative motion parallel to the strike of the fault are usually found between ridge segments, but also occur where two plates meet with shear movements (e.g., San Andreas Fault, California, shear movements of several cm/year): *conservative* plate boundary. About 85 percent of the earth's surface is covered by the (nearly) rigid plates, while deformations are concentrated on the plate boundary zones. Thermic *convection* (heat transfer by movement of molecules) flows in the mantle are assumed to be the driving mechanism for the plate movements (RUNCORN 1962). Different theories exist on the size and the location of the convection cells (whole-mantle or layered mantle convection).

The *motions* of the lithospheric plates on the spherical earth can be described as a rotation of a spherical cap about an axis through a fixed point (pole of rotation) with a certain angular velocity (GORDON 1995). From these parameters, the *relative* plate motion (direction and magnitude) can be calculated for any location. Geologically-recent (average over the last few million years) plate velocities have been estimated from the spacing of the

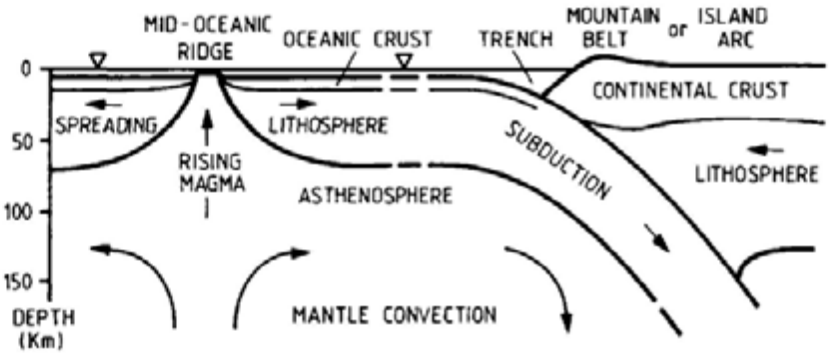

Fig. 8.8. Motion of lithospheric plates at diverging and converging plate boundaries, vertical scale exaggerated, after TORGE (1989)

magnetic anomalies across the mid-ocean ridges and from the azimuths of submarine transform faults and slips from large earthquakes. Recent models such as NUVEL-1 (DE METS et al.1990) and NUVEL-1A (DE METS et al.1994) include the major plates (about 15), keeping either one plate fixed (NUVEL-1: Pacific plate), or referencing the motions to a rotation-free system coupled with the earth: no-net rotation (NUVEL-1A). An *absolute* plate motion can be derived by reference to the hotspots (SOLOMON and SLEEP 1974). Here, hot material is rising from deep mantle plumes that do not participate in the plate tectonic motions. Hotspots are characterized by surface volcanism and high heat flow; examples are Hawaii, Iceland, and Afar (Ethiopia).

It has to be noted that the plate velocities derived from these models represent the average over geological time spans. Furthermore, they suffer from the choice of the plates used, from strong deformations occurring at the converging plate boundaries, and from the existence of intra-plate deformations, as well as from the assumption of non-moving hotspots. Geodetic measurements allow determination of the actual plate motions and identification of local and regional deformations at the plate boundaries and inside the plates, cf. [8.3.3].

8.2.4 Interpretation of the Gravity Field

The observed gravity field reflects the integrated effect of the mass distribution inside the earth and reveals deviations from spherical symmetry and hydrostatic equilibrium, cf. [8.1]. Static and dynamic geophysical earth models must fulfill the constraints imposed by the gravity field. The *inverse problem*, i.e., the determination of the density distribution from the external gravity field, on the other hand, cannot be solved uniquely (SKEELS 1947, MARTINEC 1994). This fact is seen in Stokes' theorem, where the external gravity field of an equipotential surface is completely determined without knowing the distribution of the internal masses, cf. [4.2.1]. Consequently, gravity field interpretation requires additional information through geophysical and geological data, where

seismically derived depths of bounding surfaces and the composition and density of the masses play the major role.

Gravity field interpretation is based on *residual* gravity field quantities obtained by reducing the effect of the normal gravity field, cf. [6.1], and eventually also on the well-known gravitation of the uppermost layers of the earth, cf. [6.5.3]. The primary gravity-field parameters used for interpretation are gravity anomalies and, to a limited extent, deflections of the vertical, as well as geoid heights. The effect of the masses on gravity anomalies and vertical deflections is inversely proportional to the square of the distance, while geoid heights depend on the reciprocal distance to the masses. Consequently, *gravity anomalies* and *deflections of the vertical* are more suited for investigating the density distribution in the upper layers of the earth. Gravity anomalies react primarily to vertically extended masses, while vertical deflections reflect the effect of horizontal layers, hence they especially support local investigations. *Geoid heights* reveal deeper seated mass anomalies, which generally have large dimensions.

The spectral decomposition of the gravity field as provided by the *spherical harmonic expansion*, cf. [6.6.1], is especially appropriate for global and regional interpretation. Degree variance models for the gravity anomalies (6.27) and the geoid heights (6.142) show that about 95 percent of the geoid variance is concentrated in degrees 2 to 10 (corresponding to wavelengths of 20000 to 4000 km), while this long-wave spectral part attains only 9 percent of the gravity anomalies. Medium (degree 2 to 180) and short (degree 181 to 2000) wavelengths, on the other hand, each contribute more than 40 percent to the anomaly variance. Nearly 10 percent of the anomaly variance still stem from wavelengths less than 20 km (degrees > 2000), reflecting small structures in the upper crust (e.g., salt domes). Deflections of the vertical show a spectral distribution similar to that of the gravity anomalies.

Hence, the interpretation of the *geoid* concentrates on the long and medium-wave part of the spectrum. Density and/or temperature anomalies are thought to produce the low degrees of the spherical harmonic expansion, while mantle convection and lithospheric structures are seen in wavelengths of thousands of kilometers (PHILLIPS and LAMBECK 1980, BOWIN 2000). Shorter wavelengths of a few 100 to 1000 km can be correlated with diverging and converging plate boundaries and with hotspots (CAZENAVE 1994). Areas of postglacial rebound or significant crustal thinning are also reflected in this spectral part.

Slow-spreading ridges and hotspots may exhibit relative geoid maxima of several meters. Deep-sea trenches are characterized by narrow zones of geoid depression up to 5 to 20 m, followed by a geoid rise along the island arcs (Fig.8.9). Postglacial land uplift areas show a geoid depression (up to 10 m in Fennoscandia), which is correlated with present uplift rates (BJERHAMMAR 1981), Fig.8.10. The Ivrea body (western Alps) is an example of a local geoid rise (up to 9 m) due to the

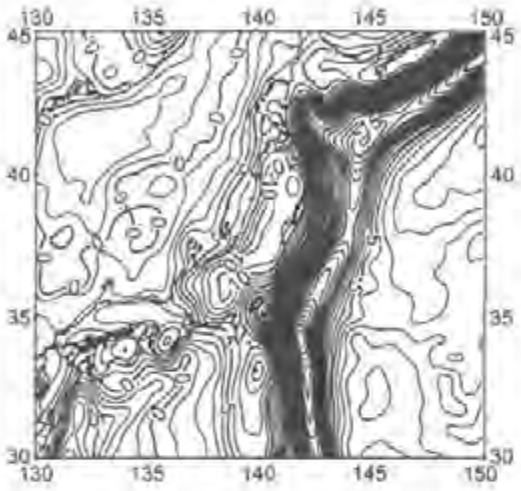

Fig. 8.9. Geoid structures at the Japan subduction zone, EGM96 geoid model, spectral part degree 11 to 360, contour line interval 1 m, after LEMOINE et al. (1998)

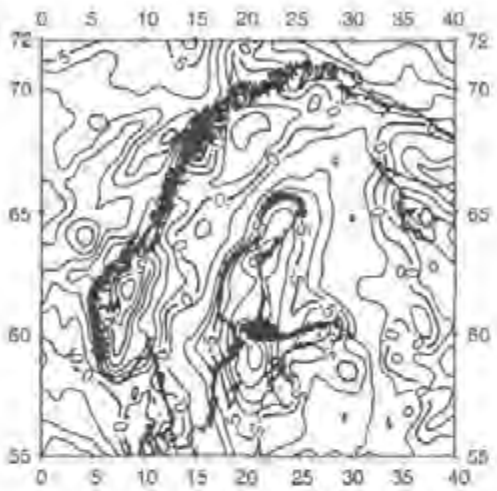

Fig. 8.10. Geoid structure at the Fennocandian land uplift area, EGM96 geoid model, spectral part degree 11 to 360, contour line interval 1 m, after LEMOINE et at. (1998)

shifting of lower crustal/upper mantle material to a shallow level (BURKI 1989).

Modelling of the long-wave geoid structures can be based on equivalent point masses arranged primarily around the bounding surfaces as determined by seismology, cf. [8.1], BOWIN (1994). The solutions strongly depend on the choice of the spectral part to be modeled, the distribution of the masses, and the introduced density differences.

The interpretation of *gravity anomalies* uses either the spherical harmonic expansion (global and large-scale investigations) or local models based on observed or gridded data. Different types of gravity anomalies can be used for regional and local investigations.

Point *free-air anomalies* depend strongly on height and are not suited for interpretation. The long and medium-wave part provided by global models, or corresponding mean anomalies, on the other hand, can be exploited, due to the smoothing of the high frequencies. The free-air anomalies then may be interpreted as isostatic anomalies with a compensation depth of zero. Structures of plate tectonics (e.g., subduction zones) and postglacial rebound can be identified, where proper filtering again may be necessary.

Bouguer anomalies are employed for regional and local investigations, as they are free from the effect of topography, cf. [6.5.3]. They mainly reflect density

anomalies in the crust and upper mantle and can be correlated with tectonic structures such as ocean ridges, deep-sea trenches, continental grabens, young-folded mountains, and with upper mantle structures (KOGAN and MCNUTT 1993). Isostatic compensation is indicated by the large-scale systematic behavior of the Bouguer anomalies, with negative values in the mountains and positive values in the oceans, cf. [8.2.2], Fig.8.11. Bouguer anomalies play an important role in geophysical prospecting (DOBRIN 1976).

Fig. 8.11. Regional Bouguer gravity anomaly map of the United States, composed of wavelengths longer than 250 km, referred to IGSN71 and GRS67, rock density 2670 kg/m^3, contour line interval 200 $\mu m/s^2$, after KANE and GODSON (1985)

More detailed investigations of the deeper regions of the crust are made possible by further reducing the effects of known or assumed mass distributions. *Isostatic anomalies* take the effect of the compensating masses into account; deviations from zero indicate areas of isostatic imbalance and are often correlated with geological features (SIMPSON et al. 1986). The reduction of geologically known structures ("crustal stripping") allows, among others, the estimation of the depth of sedimentary basins and of the crust-mantle boundary (HAMMER 1963, TOMODA and FUJIMOTO 1981).

Gravity anomalies have been used for modeling a variety of crust and mantle structures of local and regional extent. Here, a starting model is iteratively improved by varying the geometry and densities of the masses, taking the constraints from seismic data and geology into account. We mention the

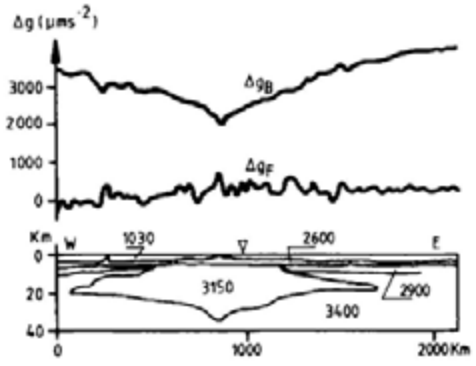

Fig. 8.12. Bouguer and free-air anomalies across the Mid-Atlantic ridge and crustal density model, with oceanic layers (2600 and 2900 kg/m^3), low-density zone (3150 kg/m^3), and upper mantel (3400 kg/m^3), after TALWANI et al. (1965)

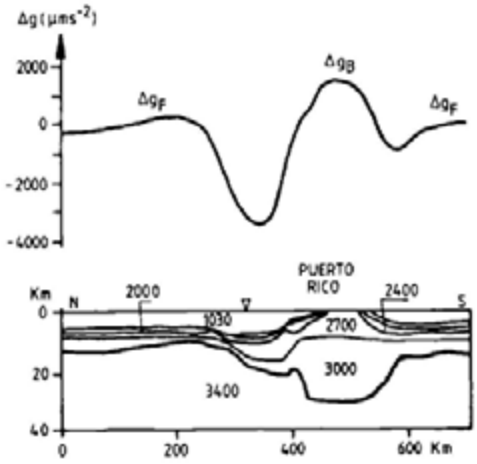

Fig. 8.13. Generalized free-air anomalies (Bouguer anomalies on land) across the the Puerto Rico trench and crustal density model, with unconsolidated (2000 kg/m^3) and consolidated (2400 kg/m^3) sediments, upper (2700 kg/m^3) and lower (3000 kg/m^3) crust, and upper mantle (3400 kg/m^3), after TALWANI et al. (1959)

following from the relationships found between the gravity field and crustal structures (KAULA 1992, NEREM et al. 1995):

- *Oceanic ridges* show negative Bouguer anomalies (up to $-2000\,\mu m s^{-2}$) due to high anomalous mantle material, while free-air anomalies deviate only slightly from zero, Fig.8.12.
- *Deep-sea trenches* are characterized by strong, negative free-air anomalies (up to $-4000\,\mu m s^{-2}$), which are explained in part by thick sedimentary layers and sea floor topography. Further inland, large positive anomalies occur due to cooling of the subtracted material, Fig.8.13.
- *Continental grabens* are correlated with strong negative Bouguer anomalies due to sedimentary layers and/or anomalous mantle material; local highs may occur through crustal thinning.
- *Young, folded-mountains* arising at continental collision zones exhibit negative Bouguer anomalies, indicating isostatic compensation. Isostatic anomalies may differ from zero due to recent tectonic processes and incomplete compensation.
- *Postglacial rebound* areas are characterized by negative free-air anomalies.

8.3 Geodesy and Recent Geodynamics

From repeated measurements, geodetic and gravimetric techniques allow detection of temporal variations of the orientation, surface, and gravity field of the earth. The observed changes are used for modeling the effects on geodetic data and for referring the data to common reference epochs. The variations contain, on the other hand, valuable information on geodynamic processes of global, regional, and local scales. Geodesy thus contributes to research in *geodynamics*, in collaboration with astronomy, oceanography, meteorology, solid earth geophysics, and geology.

In order to obtain significant results for geodynamic modeling, the temporal and spatial resolution of the observations as well as their accuracy must be tuned to the frequencies and amplitudes of the signals to be detected. For this reason, observation stations and platforms must remain stable in position over time, or their changes accurately monitored.

Space-geodetic observations provide changes of the earth rotation due to the redistribution of masses in the atmosphere, the hydrosphere, and the solid earth [8.3.1]. Satellite altimetry, together with tide gauge measurements, represents a powerful tool for the study of sea level variations [8.3.2]. Recent crustal movements are observed by space and terrestrial techniques; they serve as constraints for the modeling of geodynamic processes and as precursor phenomena [8.3.3]. Observed gravity variations contain the integral effect of terrestrial mass redistributions and support and supplement the geodetic observations [8.3.4]. Continuous records of geodetic and gravimetric data are especially useful for earth tide research [8.3.5].

Extensive treatises on the contributions of geodesy to geodynamics research are found in LAMBECK (1988) and MUELLER and ZERBINI (1989).

8.3.1 Changes in Earth Rotation

Temporal changes of the earth rotation vector with respect to the earth's body are described by polar motion and variations of the length of the day (LOD). These changes proceed at different time scales and reach the 0.1" respectively ms order of magnitude. The integral effect of the LOD variations over time leads to larger deviations of the rotational time UT1 from the atomic time TAI (DICKEY 1995), cf. [2.5.2]. VLBI and satellite techniques, including GPS, allow determination of the earth rotation changes with a resolution of a few hours and an accuracy of better than 0.001" respectively 0.01ms (ROTHACHER et al. 1999), cf. [2.3].

The observed rotation changes mirror the combined effects of terrestrial *mass* redistributions, which affect the inertia tensor of the earth, and of the related *motion*, which acts on the respective angular momentum of the layer (e.g., atmosphere, oceans, continental waters, mantle, core). The law of the conservation of the *total* angular momentum of the earth then requires corresponding changes of the rotational vector. The integral effect of the redistribution of masses can be recovered by repeated gravity field observations, cf. [8.3.4].

From the many sources of rotational changes, only a limited number have been clearly identified. The mass redistribution mainly affects polar motion, while LOD variations are dominated by the mass motions (CHAO 1994).

Secular effects have been found in polar motion (redistribution of ice masses and postglacial rebound) and in LOD (tidal friction in the oceans). *Decadal* effects could be due to core/mantle processes but also to long-term atmospheric variations. *Interannual* variations are especially pronounced in LOD; they are produced by changes in the atmospheric angular momentum. The *Chandler wobble* in polar motion is excited from atmospheric mass redistributions, but strong earthquakes may also play a role (CHAO et al. 1996). *Annual, semiannual*, and *seasonal* effects stem mainly from mass shifts in the atmosphere and in the oceans, together with changes in the groundwater layers, in ice/snow coverage, and in the water level of large lakes.

An outstanding example of a large-scale interannual effect is the El Niño phenomenon. It manifests itself by strong disturbances of the atmospheric and oceanic states in the tropical Pacific (atmospheric pressure, wind, ocean temperature, sea level inclination in west-east direction due to ocean warming and shift of water masses), with effects reaching far beyond the Pacific. It recurs after two to seven years with varying intensity; the last strong occurrence happened in 1997/1998. El Niño effects have been clearly identified in LOD (increase of several 0.1 to 1 ms) and in irregular perturbations of polar motion (SALSTEIN et al. 1999).

Diurnal and *subdiurnal* effects, as well as more *irregular* variations in earth rotation, are excited primarily by processes in the atmosphere and hydrosphere and by earthquakes as well. *Tidal* deformations of the solid earth and the oceans cause maximum rotation changes of a few 0.001″ respectively some 0.1 ms; they can be modeled with sufficient accuracy.

By using reasonable models to reduce the effects (tidal effects, atmospheric circulation, ocean circulation, etc.), the residual part of polar motion and LOD can be analyzed, providing information on further geophysical processes and model deficiencies (WILSON 1995), Fig.8.14.

The *nearly diurnal free wobble* (also free-core nutation) is a case of special interest (ZÜRN 1997b). Because the rotational axes of the fluid outer core and the earth's mantle are slightly

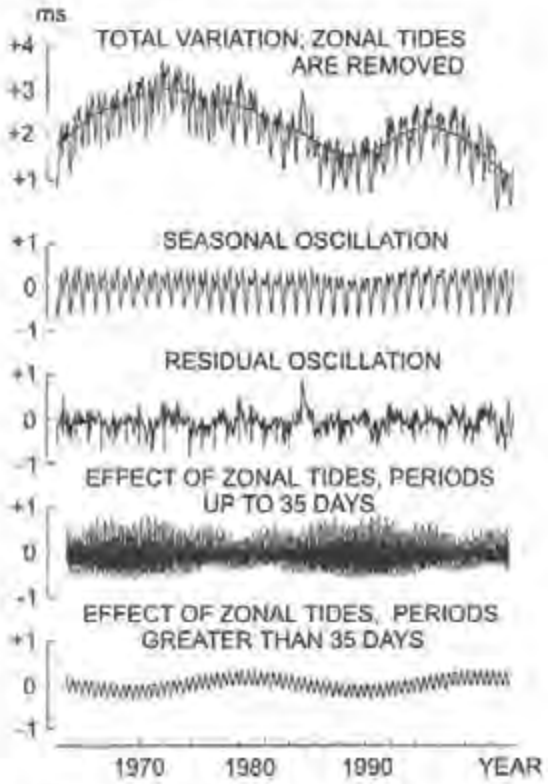

Fig. 8.14. Length of day (LOD) variations, and separation of tidal and seasonal effects, after IERS annual report 1998

misaligned, restoring forces occur at the elliptic core/mantle boundary that try to realign the axes. This leads to a damped wobble of the rotational axis around the figure axis, with nearly diurnal frequency in retrograde (opposite to the earth's rotation) direction and an amplitude of 0.00017". In space, this corresponds to a nutation of the rotational axis around the axis of total angular momentum. The effect has been observed with VLBI (HERRING and DONG 1994) and is also recognized through resonant terms in the tidal analysis of gravity observations, cf. [8.3.5]. The results are utilized for the improvement of the nutation theory, cf. [2.4.2], and for modeling the earth's deep interior.

8.3.2 Sea Level Variations

Variations of sea level with time are relevant in geodesy for the definition and realization of height reference surfaces, especially the geoid, cf. [3.4.3]. The determination and interpretation of sea level changes, on the other hand, is of fundamental importance in order to better understand the ocean-atmosphere interactions and their influence on climate. An acceleration of the global sea level rise would especially indicate climate changes related to global warming. The study of sea level variations thus requires close collaboration between oceanography, meteorology, and geodesy.

Sea level changes occur at a wide range of temporal and spatial scales, with amplitudes at the 0.1 to 1m order of magnitude (LISITZIN 1974). Tide gauge measurements and satellite altimetry allow a *direct* determination of these changes, while oceanographic modeling utilizes meteorological and oceanographic data, cf. [3.4.2]. Observed variations of the earth rotation and of the earth's gravity field contain *indirect* information about the redistribution of the oceanic water masses, cf. [8.3.1], [8.3.4].

Tide gauge records can be evaluated for the determination of the oceanic tides and other short and medium-term phenomena, including the effects of atmospheric pressure changes, storm surges, and meltwater inflow. Averaging over long time intervals reveals long-term water level variations. For the 20th century, an average global rise of 0.1 to 0.2 m/100 years has been found, with large regional and local scatter and decadal variations (WOODWORTH 1997), Fig. 8.15.

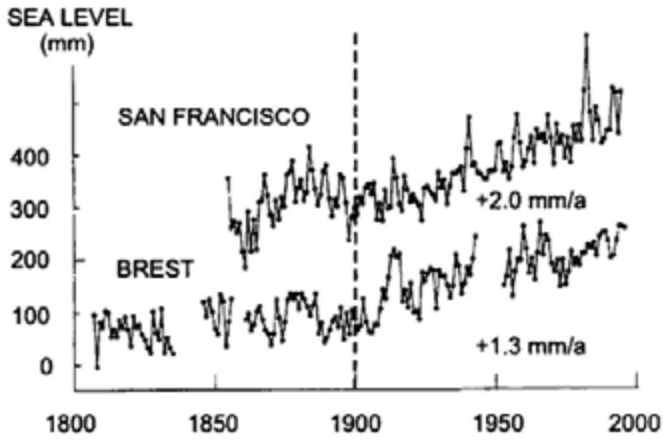

Fig. 8.15. Sea level records for San Francisco and Brest (vertical offset applied),and trend for the 20th century, after WOODWORTH (1997)

It must be emphasized that tide gauge data only provide *relative* water level changes, by a superposition of absolute water level changes and vertical movements of the mareograph. Vertical crustal movements are at the mm/year order of magnitude and may reach several mm/year and more in areas of postglacial land uplift, cf. [8.3.3]; hence a long-term height control with mm-accuracy is required for tide gauges. This is achieved locally by leveling between bench marks and globally by repeated GPS heighting. GPS sampling rates of a half to one year are typical, and connection should be made to the International Terrestrial Reference Frame (ITRF). Repeated absolute gravimetry represents an independent method for the determination of height changes and delivers additional information about the internal mass redistribution, cf. [8.3.4], CARTER et al. (1989).

Satellite altimetry provides a nearly global and quasi-continuous monitoring of the sea level with cm-accuracy. Recent ocean tide models allow reduction of the tidal effects with cm-accuracy (SHUM et al. 1997).The analysis of long-term (several years) observation series improved the ocean tide models (SMITH et al. 2000b) and revealed a number of other phenomena, with variations of 0.1 to 0.3m (NEREM et al. 1997). This includes ocean basin-wide decadal and interannual fluctuations, probably due to the shift of water masses (BOSCH 2001), Fig. 8.16. The annual cycle has a 180° phase shift between the northern and the southern hemisphere caused by thermal expansion and contraction. Interannual and seasonal variations can be correlated with the variability of ocean currents such as the Gulf Stream meandering and eddies and the El Niño phenomenon (sea level rise in the eastern and subsidence in the western Pacific), TAPLEY et al. (1994).

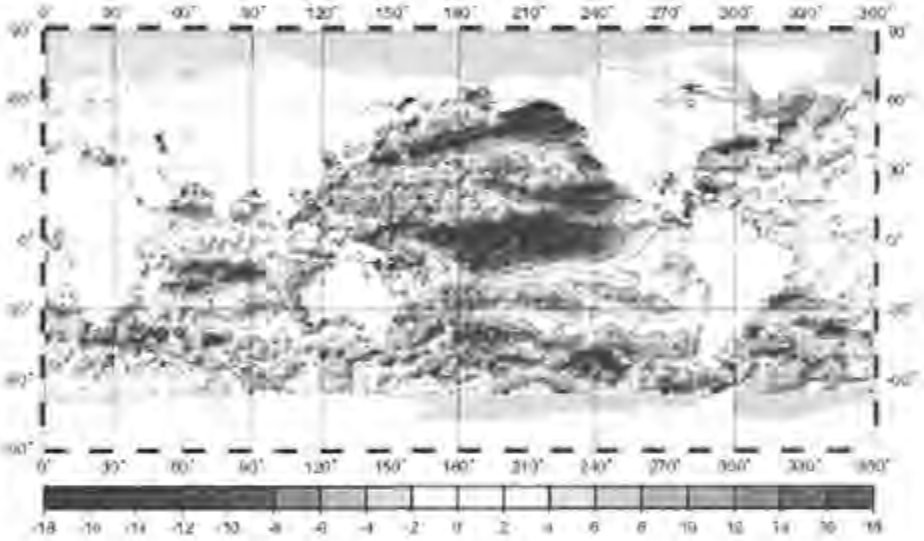

Fig. 8.16. Mean drift rate (mm/year) of sea level change determined between 1992 and 2000 from TOPEX/Poseidon altimetry, from BOSCH (2001)

The *combination* of tide gauge data and satellite altimetry leads to significant improvements. Here, the tide gauge data serve as ground truth and can be used to remove biases in the altimetric results, which may be affected by altimeter drift, systematic orbit errors, and differences between the tracking station's reference systems. By combining the results of different altimetry missions the spatial resolution is improved. Oceanographic and meteorological data such as sea surface temperature, salinity, current velocities, and air pressure may also be integrated.

8.3.3 Recent Crustal Movements

Recent crustal movements (horizontal and vertical) are determined by repeated geodetic measurements carried out at certain epochs, or continuously. The observation sites have to be monumented, and their local stability over time, with respect to changes caused of geological, hydrological, and man-made phenomena, must be controlled. Present-day sub-centimeter accuracies require reductions for the influence of body tides and ocean tide loading (DUCARME and JANSSEN 1990), atmospheric pressure loading (VAN DAM and WAHR 1987), and earth's rotation changes (GIPSON and MA 1998).

On a *global* scale, space-geodetic networks (VLBI, SLR, GPS, DORIS) provide geocentric coordinates for certain epochs and station velocities with mm/year to cm/year accuracy (PLAG et al. 1998), where GPS plays an increasing role (LARSON et al. 1997). The network solutions are combined by the IERS, and the annual station velocities are then part of the International Terrestrial Reference Frame ITRF, cf. [2.5.3]. The horizontal velocities are primarily due to the motions of the tectonic plates (ROBBINS et al. 1993), while the detection and interpretation of vertical motions is still in its infancy (SOUDARIN et al. 1999). For stations located in the interior region of the tectonic plates, the recently observed horizontal velocities generally agree well with the velocities given by geological/geophysical models as mean values over the past 3 to 10 million years, cf. [8.2.3]. Larger discrepancies are found at the plate boundaries, as the local deformations are not taken into account in the models, Fig.8.17.

Fig. 8.17. Recent plate motions as determined from geodetic observations (APKIM 10.0 model) and the geophysical model NNR NUVEL-1A, courtesy Deutsches Geodätisches Forschungsinstitut (DGFI), München

By combining global geodetic data sets, geodetic Actual Plate Kinematic Models (APKIM) have been developed (DREWES et al. 1992). These models assume the plates' interior as being rigid and rotating on the earth's surface. They admit deformation zones at the plate boundaries that result from the forces exerted by the adjacent plates. By interpolation, the actual velocity field is provided in a 1°x1° grid, with the condition that the integrated velocities over the whole earth's surface are zero.

Regional crustal movements are derived from the repeated survey of national or continental control networks and from dedicated networks set up in areas of geodynamic activity.

Triangulation and leveling networks established in large parts of the world between the end of the 19th and the second half of the 20th century are valuable for the detection of long-term crustal movements (KAKKURI 1993b). Systematically repeated surveys of these classical networks have been carried out in high earthquake risk areas such as California and Japan. Higher repetition rates became possible with Laser distance measurements and mobile VLBI and SLR-systems; this led to the detection of medium-term crustal movements (STEIN 1987). GPS receivers are now the primary tool for investigations of recent crustal movements, where measurement campaigns are carried out at different epochs or permanent stations are operated (BEVIS et al. 1997). After strain analysis, the geodetic results can be correlated or combined with geological and geophysical data (HOLT et al. 2000) and thus contribute to the development of global or regional stress maps (ZOBACK 1992).

We mention some examples of large-scale monitoring of plate-boundary and intraplate deformation. Triangulation began in Iceland (diverging plate boundary) in 1938, followed by repeated angular and distance measurements, and GPS epoch observations have been carried out since 1986 (VÖLKSEN 2000). In Japan (converging plate boundary), a continuously operating GPS network with an average station distance of 25 km has been established (TSUJI et al. 1995), and permanent GPS arrays are also in operation in California (shear movements at the San Andreas Fault), BOCK et al. (1997). The strain field in the plate collision zones of southeast Asia (Eurasian, Pacific/Philippine, and Australian plates, WILSON et al. 1998) and the eastern Mediterranean (Eurasian, African, and Arabian plates, KAHLE et al. 2000) have been derived by repeated GPS campaigns.

Large-scale *vertical* crustal movements are found in areas of postglacial rebound, recent mountain building, continental erosion, and sedimentary subsidence. While geometric leveling only allowed repetition rates of several decades, GPS-heighting (epoch measurements or permanent stations) offers the possibility to determine elevation changes with high temporal resolution. Repeated gravity measurements can also be employed, cf. [8.3.4].

Leveling and GPS-heighting refer to different reference surfaces (geoid and ellipsoid, respectively). As the geoid is affected by mass redistributions, the leveling results should be

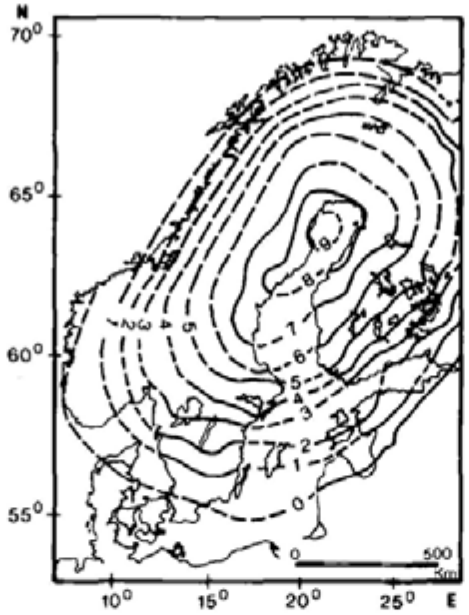

Fig. 8.18. Land uplift (relative to sea level) in mm/year, as determined from repeated geodetic leveling, after KAKKURI (1986)

reduced accordingly, applying the formulas for gravity field modeling on estimated or observed gravity variations with time, cf. [6.6.1], [6.7.1]. Even with large mass shifts, as in Fennoscandia, this reduction remains significantly below 10% of the height changes and can generally be neglected (EKMAN 1993).

Fennoscandia is among the examples of well-surveyed areas of recent vertical movement, where the postglacial land uplift has been investigated by leveling, sea level data, and gravimetry. The apparent land uplift reaches a maximum of 9 mm/year with respect to mean sea level (Fig.8.18) and is associated with a viscous inflow of mass in the upper mantle (EKMAN and MÄKINEN 1996), cf. [8.2.4]. Repeated leveling in the Swiss Alps revealed mountain uplift rates of 1 mm/year and more. These uplifts were caused partly by isostatic rebound after erosion and partly by compression at the European/African plate boundary (GUBLER et al. 1981). From leveling along the German North Sea coast, a land subsidence of 0.5 to 1 mm/year is suspected, with significant local effects at the river estuaries (LEONHARD 1987).

Local investigations in earthquake and volcanic risk areas have generally employed a multitude of techniques (terrestrial distance measurements, leveling, GPS, strain and tilt measurements, gravimetry) in order to detect precursor phenomena and to monitor surface deformations during and after activity phases (RIKITAKE 1982). In *seismotectonically* active zones, the data provide information on the accumulation of strain energy, its release during an earthquake, and the relaxation that follows the quake (LARSON 1995, HUDNUT 1995). Significant deformations have been found in connection with larger earthquakes (BOCK et al. 1993). Preseismic uplift has been explained as the

result of the generation of dilatancies, which occur through the opening of micro-cracks and the subsequent filling with underground water. With *volcanoes*, crustal deformation due to magma injection and outflow is easier to detect, and the detection plays an important role in forecasting volcanic eruptions. Continuous strain and tilt measurements could indicate precursor effects shortly before a phase of activity but may be strongly deteriorated by meteorological and hydrological disturbances (TAKEMOTO 1991). The combination of pointwise measurements (GPS) and interferograms generated from synthetic aperture radar (SAR) images taken at different times (e.g., at the 35 days repeat cycle of the ERS satellites) is a promising tool for obtaining surface information related to vertical ground deformation (MASSONNET et al. 1993).

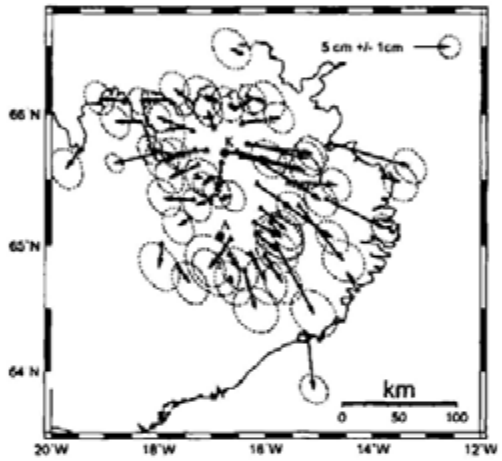

Fig. 8.19. Horizontal crustal deformations 1987 - 1990 in northwestern Iceland, as determined from repeated GPS measurements , with (assumed) non-movable stations in the Krafla fissure swarm, A = Askja volcanoe, K = Krafla volcano, after VÖLKSEN (2000)

The *San Andreas Fault*, California, is among the earthquake areas where co and inter-seismic slip rates are regularly determined by geodetic methods (SAVAGE et al. 1987, GAN et al. 2000). The *Krafla* (northern Iceland) *rifting episode* (1975-1984) and the following period of relaxation has been monitored by terrestrial measurements, GPS, and gravimetry (TRYGGVASSON 1994). The rifting process was triggered by the in and outflow of magma in a shallow magma reservoir, which caused repeated inflation and deflation of the Krafla volcano (BJÖRNSSON 1985). During the rifting episode, large horizontal (several m) and vertical (up to 1m and more) crustal movements have been observed, which decreased to a few cm/year along a narrow zone around the Krafla fissure swarm during the stress relaxation phase that followed. Eventually, the motions approached the average plate-spreading rate of 2 cm/year (JAHN et al. 1994), Fig.8.19. Satellite radar interferometry identified a post-rifting subsidence (several mm to 2 cm/year) above the magma chamber and along the spreading segment, due to cooling contraction and ductile flow of material away from the spreading axis (SIGMUNDSSON et al. 1997). Geodetic monitoring of

volcanoes is described by DVORAK (1995). Among the routinely surveyed active volcanoes are the Kilauea and Mauna Loa, Hawaii (OWEN et al. 2000), Long Valley, California (RUNDLE and WHITCOMB 1986), and Mount Etna, Italy (BONACCORSO et al. 1995).

Man-made vertical crustal movements are related to the exploitation of natural gas, oil, and geothermal fields, the withdrawal of groundwater, mining, and load changes in water reservoirs. They are of more local character and generally result in surface subsidence. Monitoring is carried out by leveling and GPS-heighting, and gravimetry also contributes, cf. [8.3.4].

8.3.4 Gravity Variations with Time

Gravity variations with time result from a multitude of sources, cf. [3.5]. Here we consider only the variations that are caused by the redistribution of terrestrial masses and thus provide information on geodynamic processes, cf. [3.5.3]. Gravimetric tidal effects will be discussed within the frame of earth tides, cf. [8.3.5]. More details are found in TORGE (1989).

Global gravity variations can be determined by comparing the harmonic coefficients of the gravitational field obtained from the analysis of satellite orbits of different epochs, cf. [6.6.2]. Changes of the low degree zonal harmonics (up to degree 5) have been found from laser satellites (Lageos, Starlette, Ajisai) over time intervals of 10 to 20 years (NEREM and KLOSKO 1996). The change of the dynamical form factor $\dot{J}_2 = dJ_2/dt = -2.7\times10^{-11}/a$ is especially pronounced and suspected to result from postglacial rebound. Annual and semiannual variations of the second-degree harmonics are related to mass redistributions in the atmosphere, the oceans, and the continental groundwater (CHENG and TAPLEY 1999). If the harmonics of degree one are included in the evaluation, variations indicate the movement of the geocenter with respect to the terrestrial reference frame realized by the coordinates of the tracking stations, cf. [2.5.2], [3.3.4].

A *terrestrial* network of absolute gravity stations well distributed over the earth's surface and repeatedly observed at time intervals of 10 years or more could also provide long-term global gravity changes (MATHER et al. 1977). This is intended by the *International Absolute Gravity Basestation Network* (IAGBN) proposed by IAG (BOEDECKER and FRITZER 1986). The majority of the 36 scheduled stations have been installed, but only a few observation have been repeated.

Terrestrial absolute and relative gravity measurements are required in order to detect *regional* and *local* gravity changes with time. Corresponding investigations concentrate on areas where recent height changes occur, caused by postglacial uplift, mountain building, earthquake and volcanic activity, and man-made land subsidence, cf. [8.3.3].

In order to detect and analyze the small gravity changes associated with geodynamic phenomena, a high observational accuracy and the adequate *reduction* of tidal effects and local disturbances is required. Present gravimetric earth tide models allow sufficient reduction of the tidal effects for most parts of the continents, cf. [8.3.5]. *Polar motion* only affects absolute gravimetry and can be reduced. This is also valid for the effect of *atmospheric pressure* changes, which can be modeled by a Bouguer plate, modified through the deformation caused by the load of the atmospheric masses (SPRATT 1982), cf. [5.4.1]. For relative gravity measurements, atmospheric pressure effects generally cancel, but they must be taken into account for continuous gravity recording, cf. [8.3.5]. Temporal variations of the *ground water* level and *soil moisture* mainly occur seasonally, with superimposed short-term fluctuations of a few hours to a few days. They may produce maximum gravity changes of 50 to 100 $\mathrm{nms^{-2}}$ (seasonal) and several $100\,\mathrm{nms^{-2}}$ (strong rainfall). For simple hydrological structures, a reduction is possible by applying the Bouguer plate model

$$\delta g_{\text{groundwater}} = 4.2 \cdot P \cdot \delta H \,\mathrm{nms^{-2}}, \tag{8.15}$$

with P = pore volume (%), and δH = change of groundwater level in m. A corresponding relation holds for the soil moisture reduction. The lack of groundwater and soil moisture data, as well as deficiencies of this simple model, generally prevent an adequate reduction of these hydrological effects (MÄKINEN and TATTARI 1988).

Observed *gravity changes* contain the combined effect of internal mass redistributions and a vertical shift of the observer, provided that earth tides, atmospheric pressure, and groundwater/soil moisture effects have been reduced properly. Hence, they can be transformed to *height changes* if a reasonable model for the internal mass redistribution is available (STRANG VAN HEES 1977, BIRO 1983). Assuming a linear relationship between gravity and height changes, the conversion factor may vary between -1.5 and $-3.5\,\mu\mathrm{ms^{-2}/m}$ (JACHENS 1978). The free-air relation of $-3\,\mu\mathrm{ms^{-2}/m}$ is often found locally and corresponds to a vertical shift without mass changes (e.g., dilating sphere). For larger areas, the Bouguer-plate relation of $-2\,\mu\mathrm{ms^{-2}/m}$ is more typical, indicating internal mass displacements according to the Bouguer plate model, cf. [6.5.3]. Simultaneous measurements of gravity and height variations allow the conversion factor to be determined. Gravity data can then be used for the determination of height changes, and the geophysical model for the internal mass redistribution can be verified (TORGE 1986).

Postglacial uplift has been monitored in Fennoscandia for some decades by relative gravimetry in connection with leveling, resulting in a mean conversion factor of $-2\,\mathrm{nms^{-2}/mm}$ (EKMAN and

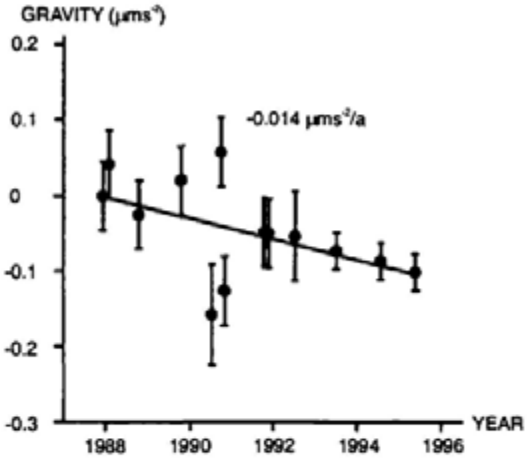

Fig. 8.20. Absolute gravity variations from 1987 to 1995 at Churchill, Manitoba, Canada, after LAMBERT et al. (1996)

MÄKINEN 1996), cf. [8.3.3]. In Canada, repeated absolute gravity measurements yielded gravity changes of -10 to $-20 \text{nms}^{-2}/\text{year}$, in agreement with geophysical rebound models (LAMBERT et al. 1996), Fig. 8.20.

Gravimetric networks established in the Central Andes (subduction of the Nazca plate) and in the Venezuelan Andes (Caribbean/South American plate boundary) are examples of investigations at *tectonic plate boundaries* (BECKER and GROTEN 1998, DREWES et al. 1991). While local effects (subsidence of sedimentary basins, variations related to the rainy and the dry season) have been identified, long-term gravity changes caused by plate tectonic processes are still difficult to extract over time spans of several years.

Gravimetry is extensively employed in areas of *seismotectonic* and *volcanic* activity, as in California (JACHENS et al. 1983) and in Japan (SATOMURA et al. 1986); the results are, in many cases, well correlated with changes in elevation and strain. An absolute gravity network established in Yunnan (collision zone of the Indian and the Eurasian plates) and observed several times between 1990 and 1995 is intended to monitor long-term changes at this region of high earthquake risk (TORGE et al. 1999). The Krafla rifting phenomena in northern Iceland mirrored itself in gravity and height variations with significant correlation, but forerunners are hard to detect (TORGE et al. 1992), Fig. 8.21, cf. [8.3.3]. Occasionally, gravity changes of a few μms^{-2} have been observed before strong *earthquakes*, one example being the 1976 Tangshan/China (M=7.8) earthquake (LI et al. 1989). *Volcano* monitoring, in many cases, includes gravimetry, which has proved to be an efficient tool for detecting magma inflation and deflation and to contribute to eruption forecasting and observation of the phase of activity (RYMER and LOCKE 1995).

Repeated gravity measurements also contribute to the investigation of land subsidence caused by *man-made* activities. This includes the exploitation of geothermal fields (ALLIS and HUNT 1986), of natural gas and oil (VAN GELDEREN et al. 1999), the withdrawal of groundwater, and the

effects of mining (LYNESS 1985).

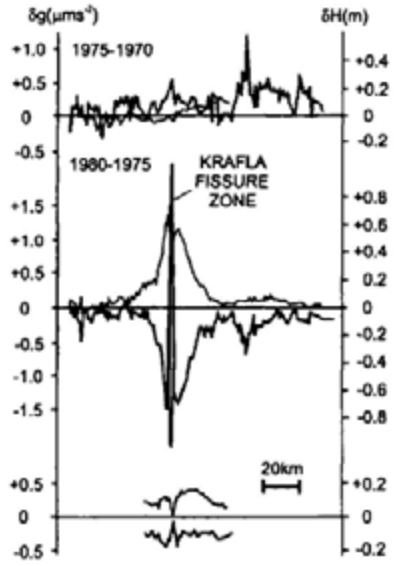

Fig. 8.21. Long-term gravity and height changes along an EW-profile (φ = 65°40') in northern Iceland, related to the Krafla rifting episode, after TORGE et al. (1992)

8.3.5 Earth Tides

Tidal effects on a *rigid* earth can be calculated from the ephemerides of the moon, the sun, and the planets, cf. [3.5.2]. In reality, the *solid* earth reacts to the tidal forces like an elastic body: *Earth tides* (also body tides). The *ocean* tides follow the law of hydrodynamics, with strong disturbances occurring in the adjacent seas and along the coast lines. Tidal phenomena, especially earth tides, are discussed extensively in MELCHIOR (1983), BAKER (1984), and WILHELM et al. (1997).

The tidal response of a *spherically symmetric, non-rotating, oceanless* earth can be described by applying the dimensionless *Love* numbers h, k, l (l also called *Shida* number) to the individual terms of the series expansion of the tidal potential V_t (3.116), WAHR (1995).

The *vertical* deformation of the earth's surface is given by (Fig.8.22)

$$\Delta r_{el} = h \cdot \Delta r_t , \tag{8.16a}$$

where the shift of the level surface follows from (3.52):

$$\Delta r_t = \frac{V_t}{g}. \tag{8.16b}$$

The *horizontal* displacement in NS and EW-direction is obtained by

$$\Delta x_{el} = \frac{l}{g} \cdot \frac{\partial V_t}{\partial \bar{\varphi}}, \Delta y_{el} = \frac{l}{g} \cdot \frac{\partial V_t}{\cos\bar{\varphi}\,\partial\lambda}, \tag{8.17}$$

with $\bar{\varphi},\lambda$ = geocentric latitude and longitude.

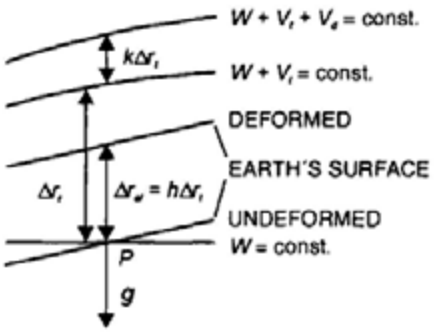

Fig. 8.22. Vertical shift of a level surface and the physical surface of the earth caused by the tides

The tidal-induced mass shift causes an additional *deformation potential* which is proportional to the tidal potential:

$$V_d = k \cdot V_t. \tag{8.18}$$

The *Love numbers* depend on density and elastic properties (compressibility, rigidity) of the earth's body, and they are functions of the radial distance from the earth's center. Restricting ourselves to the dominant (about 98%) term of degree two in the spherical harmonic expansion, we have for a spherical earth model with solid mantle, liquid outer and solid inner core, cf. [8.1]:

$$h = 0.60,\ l = 0.08,\ k = 0.30.$$

The *gravitational potential* on the earth's surface experiences a tidal-induced change which is composed of the direct attraction (3.117), the deformation part (8.18), and the potential change due to the vertical shift of the surface (8.16):

$$V_{el} = V_t + V_d - g \cdot \Delta r_{el} = V_t\left(1 + k - h\right). \tag{8.19}$$

Differentiating with respect to the radial distance r delivers the *vertical* component of the tidal *acceleration*. According to (3.117), (3.118) we have

$$b_r = \frac{\partial V_t}{\partial r} = 2\frac{V_t}{r}. \tag{8.20a}$$

Expressing the deformation potential through a spherical harmonic expansion of degree two (3.89), and with (8.18) we obtain

$$\frac{\partial V_d}{\partial r} = -\frac{3}{r}V_d = -\frac{3}{r}kV_t. \tag{8.20b}$$

Inserting (8.20) into (8.19) and taking (3.118) and (8.16) into account yields the vertical acceleration component

$$b_{r(\mathrm{el})} = \left(1 - \frac{3}{2}k + h\right)b_r, \tag{8.21a}$$

with the *gravimetric* (amplitude) *factor*

$$\delta = 1 - \frac{3}{2}k + h \tag{8.21b}$$

already introduced in (5.97).

The *horizontal* component of the tidal acceleration and its relation to the corresponding component on a rigid earth (3.119) follows from

$$b_{\psi(\mathrm{el})} = -\frac{\partial V_{\mathrm{el}}}{r\partial\psi} = (1 + k - h)b_\psi, \tag{8.22a}$$

with the *tilt* (amplitude) *factor*

$$\gamma = 1 + k - h. \tag{8.22b}$$

With the above model values for the love numbers h and k we obtain

$$\delta = 1.15,\ \gamma = 0.69.$$

Hence, the gravity change observed on an elastic earth is larger than on a rigid one, which is due to the vertical shift of the observer. The tilt factor mirrors the flexibility of the earth's surface with respect to the tidal force.

Rotation and *ellipticity* of the earth cause a slight latitude dependence of the tidal parameters (WAHR 1981). Mantle *anelasticity* results in a frequency dependent amplitude increase and a phase delay of the tidal response (DEHANT 1987); lateral *inhomogeneities* should be visible, with a dependence on position. The *resonance* effect caused by the liquid outer core (nearly diurnal free wobble, cf. [8.3.1]), is reflected in the diurnal tidal band by a frequency dependence of the Love numbers. The deviations from a spherically symmetric earth model remain below 0.1%.

Earth tide observations include the effect of the *ocean tides*, which is composed of the direct attraction and the loading effect of the water masses (JENTZSCH 1997). The ocean tide effects are especially pronounced in the semidiurnal tides and reach several percent at stations located in the continents' interior. Close to the coast, they may assume up to 10% in the gravimetric tidal signal, several 10% in strain, and 100% and more in tilt, with corresponding phase shifts.

The gravitational and the loading part of the *oceanic tidal effect* can be calculated from ocean tide models, cf. [3.4.2]. Here, the ocean load is considered as a surface layer and expanded into spherical harmonics where a development up to degree 10000 is required. The reaction of the earth's surface to the load is described by load Love numbers, which depend on the underlying earth model (FARRELL 1972). A convolution of the ocean tidal model and Green's functions (load Love numbers weighted according to the distance from the load) provides the loading effects in gravity, strain, and tilt for each partial tide.

Tidal perturbations on the earth's surface reach 1 to 2 μms^{-2} in gravity, 0.01″ to 0.02″ in tilt, and 10^{-7} to 10^{-8} in strain, see the estimates for a rigid earth in [3.5.2]. Hence, they are clearly visible in geodetic data series and, after an earth tide analysis, can be evaluated in order to

- derive *tidal reductions* for geodetic (VLBI, SLR, LLR, GPS, precise leveling etc.) and gravimetric measurements,
- verify and improve *global earth models* with respect to deviations from spherical symmetry, after subtraction of the oceanic tidal effects,
- verify *ocean tide models* after subtraction of the body tides,
- investigate local changes in the tidal parameters associated with earthquakes and volcanic activity.

While a relative *accuracy* of about ±1% and ±0.5° generally suffices for tidal reductions, ±0.1% respectively ±0.05° and better is required for model verification and geodynamic investigations.

Gravimetric earth tide observations especially contribute to tidal analysis (WENZEL 1997b). Here, elastic-spring type gravimeters provide the short-periodic partial tides (Fig.8.23), and superconducting instruments also deliver long-periodic tides and the pole tide (Fig.8.24), cf. [5.4.6].

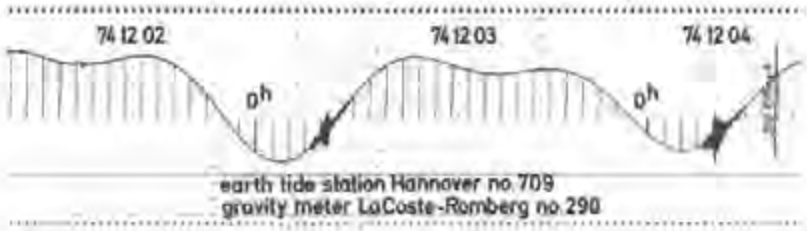

Fig. 8.23. Gravimetric earth tide record, obtained with Lacoste and Romberg gravimeter G298, Institut für Erdmessung (IfE), University of Hannover

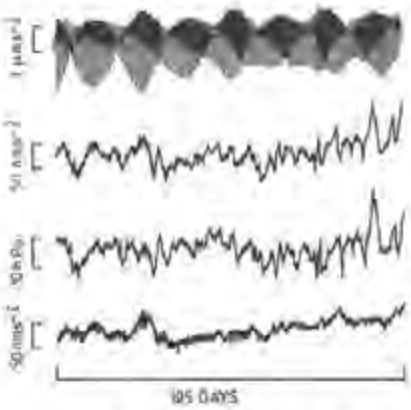

Fig. 8.24. GWR superconducting gravimeter drift, with (top to bottom) raw gravimeter signal, earth tides reduced signal, atmospheric pressure, and gravity residuals after removal of earth tides and atmospheric pressure effects, courtesy GWR-Instruments, Inc., San Diego, CA, U.S.A.

As an example, Tab.8.1 contains the gravimetric tidal parameters for a selected number of partial tides (out of a total number of 57 analyzed wave groups) from a long-term observation with a superconducting gravimeter (DITTFELD 2000), cf. [3.5.2].

The main results of the gravimetric earth tide analysis are (WENZEL 1997b):

- The average *noise level* amounts to a few $0.01 \mathrm{nms}^{-2}$ for the short-periodic tides and may reach $10 \mathrm{nms}^{-2}$ for the annual tide, which characterizes the high observational precision.
- The separation of the small S1 wave mirrors the quality of the *analysis*, as the diurnal tides are strongly contaminated by meteorological effects.

Tab. 8.1. Adjusted Gravimetric Earth Tide Parameters (selection, rounded values), Earth Tide Station No.765, GFZ/Potsdam ($\varphi = 52.38°$ N, $\lambda = 13.07°$ E, $H = 81$ m), Superconducting Gravimeter GWR TT70 No.018, recording time June 1992 to October 1998 (2250 days), after DITTFELD (2000)

Tide Symbol	Period	Amplitude nms^{-2}	Ampl. Factor δ	Phase Lead $\Delta\Phi$
Long-periodic				
Sa	365.26 d	18.4	4.4	-40°
Ssa	182.62 d	29.7	1.13	-2°
Mm	27.55 d	34.0	1.14	0.6°
Mf	13.66 d	64.4	1.14	-3°
Diurnal				
Q1	26.87 h	66.0	1.146	-0.22°
O1	25.82 h	345.6	1.150	-0.13°
P1	24.07 h	160.9	1.150	0.12°
S1	24.00 h	4.2	1.28	2.0°
K1	23.93 h	480.6	1.137	0.2°
ψ_1	23.87 h	4.2	1.26	0.6°
φ_1	23.80 h	7.1	1.18	-0.1°
Semidiurnal				
N2	12.66 h	63.2	1.179	1.99°
M2	12.42 h	332.3	1.186	1.36°
S2	12.00 h	154.6	1.186	0.21°
K2	11.97 h	42.0	1.186	0.45°
Terdiurnal				
M3	8.28 h	3.6	1.073	0.3°

Standard deviation (short and long-periodic tides adjusted): $\pm 9 nms^{-2}$, only short-periodic tides: $\pm 0.8 nms^{-2}$. Air pressure regression coefficient $-2.776 nms^{-2}/hPa$, pole-tide δ-factor 1.13.

- The standard deviations of the adjusted *tidal parameters* are approximately inversely proportional to the amplitude of the waves. The amplitude factor of the principal waves (O1, P1, K1, M2, S2) can be obtained with a relative accuracy of about ±0.01% and the phase lead with ±0.01°, and better. The long-periodic tides (Mm, Mf) are accurate to a few % and a few degrees.
- After reduction of the oceanic tidal effects, the tidal parameters are in close agreement with advanced geophysical *earth models*. A dependence on latitude, lateral heterogeneities, or heat flow has not been clearly recognizable (BAKER et al. 1996, ZÜRN 1997a),

- The *resonance effect* of the liquid outer core can be clearly identified in the diurnal tides (ψ_1, φ_1) and used for model verification.
- *Ocean tide* effects manifest themselves in the semidiurnal waves and provide useful constraints for oceanic tidal models (DUCARME and MELCHIOR 1983),
- *Free oscillations* (vertical component) of the earth with periods between 10 s and 54 min. as excited by strong earthquakes have been analyzed from high resolution records and can be used for the support of global seismic networks.

World-wide *synthetic gravity tide parameters* have been calculated for a 1°x 1° grid, based on the WAHR (1981)/DEHANT (1987) body tide and the SCHWIDERSKI (1980) ocean tide models. With the exception of strongly disturbed coastal zones, the synthetic parameters agree well with the gravimetric earth tide observations and provide the gravimetric tidal reductions with the desired accuracy (see above), TIMMEN and WENZEL (1994b).

The *Global Geodynamics Project* (GGP, 1997 – 2003) comprises about 20 stations equipped with superconducting gravimeters that collect gravity data with a sampling rate of 1 to 10 s and an accuracy of $\pm 1 \mathrm{nms}^{-2}$. The results will be used for improving earth and ocean models, should provide information on geodynamic phenomena, and serve as ground truth for the GRACE mission, cf. [5.2.8], CROSSLEY et al. (1999).

Strain and *tiltmeter* measurements fail to reliably determine the global or regional tidal response of the earth, which is due to strong distortion by local heterogeneities. But these measurements contribute significantly to local investigations, cf. [5.5.4]. Long-term *space-geodetic* observations such as VLBI, SLR, and GPS allow for direct monitoring of tidal displacements of the station sites. Thus they can be used to directly derive the Love numbers h and l, the resonance parameters in the diurnal tidal band, and the ocean loading effects (MATHEWS et al. 1997, SCHUH and HAAS 1998).

References

Abbreviations frequently used:

Allg. Verm. Nachr. = Allgemeine Vermessungsnachrichten, Wichmann-Hüthig, Heidelberg.
Boll. Geof. teor. appl. = Bolletino di Geofisica teorica ed applicata. Osservatorio Geofisico Sperimentale, Trieste.
Bull. Géod. = Bulletin Géodesique. Springer, Berlin-Heidelberg-New York.
DGK = Veröffentlichungen der Deutschen Geodätischen Kommission bei der Bayerischen Akademie der Wissenschaften, München und Frankfurt a.M.
EOS = Transactions American Geophysical Union, Washington, D.C.
J. Geod. = Journal of Geodesy. Springer, Berlin-Heidelberg-New York.
JGR = Journal of Geophysical Research. American Geophysical Union, Washington, D.C.
Man. Geod. = Manuscripta Geodaetica. Springer, Berlin-Heidelberg-New York.
Mitt. BKG = Mitteilungen de Bundesamtes für Kartographie und Geodäsie, Frankfurt a.M.
OSU Rep. = Reports of the Department of Civil and Environment Engineering and Geodetic Science, Geodetic Science and Surveying, The Ohio State University, Columbus, Ohio.
Unisurv G = Univ. of New South Wales, Geodesy Reports, Kensington, N.S.W.
Wiss. Arb. Univ. Hannover = Wissenschaftliche Arbeiten der Fachrichtung Vermessungswesen der Universität Hannover.
ZfV = Zeitschrift für Vermessungswesen. K. Wittwer, Stuttgart.

ABD-ELMOTAAL, H.A. (1995): Theoretical background of the Vening.Meinesz isostatic model. In Sünkel and Marson (1995): 268-277.

ABD-ELMOTAAL, H.A., M. EL-TOKHEY (1995): Does the spherical approximation affect the datum transformation ? In Sünkel and Marson (1995): 472-483.

ADAM, J., W. AUGATH, F. BROUWER et al. (2000a): Status and development of the European height system. In Schwarz (2000b) : 55-60.

ADAM, J., W. AUGATH, C. BOUCHER et al. (2000b): The European Reference System coming of age. In Schwarz (2000b): 47-54.

AGNEW, D.C. (1986): Strainmeters and tiltmeters. Rev. Geophys. 24: 579-624.

AHRENS, T.J., ed. (1995): Global Earth Physics: A Handbook of Physical Constants. AGU ref. shelf 1, Washington, D.C.

ALASIA, F., L. CANNIZZO, G. CERUTTI, I. MARSON (1982): Absolute gravity acceleration measurements: Experiences with a transportable gravimeter. Metrologia 18: 221-229.

ALLENBY, R.J., C.C. SCHNETZLER (1983): United States crustal thickness. Tectonophysics 93: 13-31.

ALLIS, R.G., T.M. HUNT (1986): Analysis of exploitation-induced gravity changes at Wairakei geothermal field. Geophysics 51: 1647-1660.

ANDERLE, R.J. (1986): Doppler satellite measurements and their interpretation. In A.J. Anderson and A. Cazenave, eds. (1986), Space geodesy and geodynamics: 113-167. Academic Press, London etc.

ANDERSEN, N. (1992): The hydrostatic levelling across Fehmarn Belt in 1987. Kort- og Matrikelstyrelsen, Publ. 4. Series, vol. 2, Kobenhavn, Denmark.

ANDERSEN, O.B., P. KNUDSEN (1998): Global marine gravity field from the ERS-1 and Geosat geodetic mission altimetry. JGR 103: 8129-8137.

ANDERSEN, O.B., P.L. WOODWORTH, R.A. FLATHER (1995): Intercomparison of recent ocean tide models. JGR 100: 25261-25282.

ANDERSEN, P.H., S. AKSNES, H. SKONNORD (1998): Precise ERS-2 orbit determination using SLR, PRARE and RA observations. J. Geod. 72: 421-429.

ANDERSON, J.M., E.M. MIKHAIL (1998): Surveying – theory and practice. 7.ed., McGraw-Hill, New York etc.

ANGUS-LEPPAN, P.V. (1984): Refraction in geodetic leveling. In Brunner (1984a): 163-180.

ANZENHOFER, M., T. GRUBER, M. RENTSCH (1996): Global high resolution mean sea surface based on ERS-1 35- and 168-days cycles and Topex data. In Rapp et al. (1996).: 208-217..

ARABELOS. D. (1980): Untersuchungen zur gravimetrischen Geoidbestimmung, dargestellt am Testgebiet Griechenland. Wiss. Arb. Univ. Hannover 98.

ARIAS, E.F., P. CHARLOT, M. FEISSEL, J.-F. LESTRADE (1995): The extragalactic reference system of the International Earth Rotation Service. Astronomy and Astrophysics 303: 604-608.

ASHKENAZI, V., T. MOORE, M.E. NAPIER, C. DE LA FUENTE (1988): Using GPS to control a triangulation network. Survey Review 29: 287-294.

AUGATH, W. (1997): GPS-gestützte Netzverdichtung in der Landesvermessung. DVW Schriftenreihe 28: 154-169, Wittwer, Stuttgart.

BAKER, L.S. (1974): Geodetic networks in the United States. Canadian Surveyor 28: 445-451.

BAKER, T.F. (1984): Tidal deformations of the earth. Sci. Progr., Oxford 69: 197-233.

BAKER, T.F., D.J. CURTIS, H. DODSON (1996): A new test of earth tide models in central Europe. Geophys. Res. Letters 23: 3559-3562.

BANNISTER, A., S. RAYMOND, R. BAKER (1998): Surveying. 7.ed., Longman, Harlow, Essex, England.

BARTHELEMY, J., B. DUCARME, P. MELCHIOR, eds. (1995): New challenges for geodesy in volcanoes monitoring. Cahiers du Centre Européen de Géodynamique et de Séismologie 8, Luxembourg.

BASIC, T., H. DENKER, P. KNUDSEN, D. SOLHEIM, W. TORGE (1990): A new geopotential model tailored to gravity data in Europe. In Rummel and Hipkin (1990): 109-118.

BÄUMKER, M. (1984): Zur dreidimensionalen Ausgleichung von terrestrischen und Satellitenbeobachtungen. Wiss. Arb. Univ. Hannover 130.

BECKER, J.-M. (1987): The experiences with new levelling techniques ML and MTL. In Pelzer and Niemeier (1987): 159-174.

BECKER, M., E. GROTEN (1998): Präzisionsgravimetrische Beobachtungen in den Zentralen Anden 1984-1990. ZfV 123: 37-42.

BECKER, M., G. BERRINO, A.G. CAMACHO et al. (2000): Results of the relative gravimetric measurements at the ICAG97 intercomparison. Bull. d'Inf. Bur.Gravim.Int. 85: 61-71.

BELL, R.E., A.B WATTS (1986): Evaluation of the BGM-3 sea gravity meter onboard R/V Conrad. Geophysics 51: 1480-1493.

BENDER, P.L. (1992): Atmospheric refraction and satellite laser ranging. In De Munck and Spoelstra (1992): 117-125.

BENDER, P.L., D.G. CURRIE, R.H. DICKE et al. (1973): The lunar laser ranging experiment. Science 182: 229-238.

BERCKHEMER, H. (1990): Grundlagen der Geophysik. Wiss. Buchgesellschaft Darmstadt.

BERGER, J., J. LEVINE (1974): The spectrum of earth strain from 10^{-8} to 10^{2} Hz. JGR 79: 1210-1214.

BEUTLER, G., W. GURTNER, I. BAUERSIMA, M. ROTHACHER (1987): Correlation between simultaneous GPS double difference carrier phase observations in the multistation mode. Implementation, considerations and first experiences. Man. Geod. 12: 40-44.

BEUTLER, G., E. BROCKMANN, S. FRANKENHAUSER et al. (1996a): Bernese GPS Software Version 4.0. Doc., Astronomical Institute, Univ. of Bern, Switzerland.

BEUTLER, G., I.I. MUELLER, R.E. NEILAN (1996b): The International GPS Service for Geodynamics (IGS): the story. In Beutler et al. (1996c): 3-13.

BEUTLER, G., G.W. HEIN, W.G. MELBOURNE, G. SEEBER, eds. (1996c): GPS trends in precise terrestrial, airborne, and spaceborne applications. IAG Symp. Proceed. 115, Springer, Berlin-Heidelberg-New York.

BEVIS, M., S. BUSINGER, T.A. HERRING, CH. ROCKEN, A. ANTHES, R.H. WARE (1992): GPS meteorology: Remote sensing of atmospheric water vapor using the Global Positioning System. JGR 97: 15787-15801.

BEVIS, M., Y. BOCK, P. FANG, R. REILINGER, T. HERRING, J. STOWELL, R.J. SMALLEY (1997): Bending old and new approaches to regional GPS geodesy. EOS 78: 61, 64, 66.

BEYER, L.A., R.E. VON HUENE, T.H. MCCULLOH, J.R. LOVETT (1966): Measuring gravity on the seafloor in deep water. JGR 71: 2091-2100.

BIALAS, V. (1982): Erdgestalt, Kosmologie und Weltanschauung. Wittwer, Stuttgart.

BILLS, B.G., S.P. SYNNOTT (1987): Planetary geodesy. Rev. Geophys. 25: 833-839.

BIPM (1991): Le Système International d'Unités (SI). Bureau International des Poids et Mésures, Sèvres, France.

BIRARDI, G. (1976): The establishment of a net of vertical deflection points in Italy by means of a photo-astronomical procedure. Boll. di Geod. e Scienze Affini 35: 113-152.

BIRO, P. (1983): Time variation of height and gravity. Wichmann, Karlsruhe.

BJERHAMMAR, A. (1969): On the boundary value problem of physical geodesy. Tellus 21: 451-516.

BJERHAMMAR, A. (1981): The uplift process in Fennoscandia and the corresponding potential field from satellites. Proceed. 4th Int. Sympl Geodesy and Physics of the Earth, Veröff. Zentralinstitut Physik der Erde 63/III: 554-581.

BJERHAMMAR, A. (1985): A robust approach to global problems in physical geodesy. Bull. Géod. 59: 303-315.

BJERHAMMAR, A., L. SVENSSON (1983): On the geodetic boundary value problem for a fixed boundary surface – a satellite approach. Bull. Géod. 57: 382-393.

BJÖRNSSON, A, (1985): Dynamics of crustal rifting in NE Iceland. JGR 90: 10151-10162.

BKG (1998): Geodätische Vernetzung Europas. Mitt. d. Bundesamtes für Kartographie und Geodäsie, Bd.1, Frankfurt a. M.

BLAKELEY, R.J. (1996): Potential theory in gravity and magnetic applications. Cambridge Univ. Press.

BOCCALETTI, D., G. PUCACCO (1996/1999): Theory of orbits. Springer, Berlin-Heidelberg-New York.

BOCK, Y., D.C. AGNEW, P. FANG et al. (1993): Detection of crustal deformation from the Landers earthquake sequence using continuous geodetic measurements. Nature 361: 337-340.

BOCK, Y., S. WDOWINSKI, P. FANG et al. (1997): Southern California permanent GPS geodetic array: continuous measurements of regional crustal deformation between the 1992 Landers and 1994 Northridge earthquakes. JGR 102: 18013-18033.

BÖDECKER, G., TH. FRITZER (1986): International Absolute Gravity Basestation Network. Veröff. Bayer. Komm. für die Internat. Erdmessung, Astron.-Geod. Arb. 47, München.

BOMFORD, G. (1980): Geodesy. 4.ed., Clarendon Press, Oxford.

BONACCORSO, A., R. VELARDITA, L. VILLARI (1995): Magma uprising and intrusion at Mount Etna (Sicily, Italy): Some insight from ground deformation modelling. In Barthelemy et al. (1995): 231-243.

BONVALOT, S., M. DIAMENT, G. GABALDA (1998): Continuous gravity recording with Scintrex CG-3M meters: a promising tool for monitoring active zones. Geophys. J. Int. 135: 470-494.

BORKOWSKI, K.M. (1989): Accurate algorithms to transform geocentric to geodetic coordinates. Bull. Géod. 63: 50-56.

BOSCH, W. (2001): EOF-Analysen der Meeresspiegelschwankungen im Pazifik. ZfV 126 (in press).

BOSSLER, J.D. E. GRAFAREND, R. KELM (1973): Optimal design of geodetic nets 2. JGR 78: 5887-5897.

BOSSLER, J.D., C.C. GOAD, P.L. BENDER (1980): Using the Global Positioning System (GPS) for geodetic positioning. Bull. Géod. 54: 553-563.

BOTTONI, G.P., R. BARZAGHI (1993): Fast collocation. Bull. Géod. 67: 119-126.

BOUCHER, C. (1987): GPS receiver technology. In Turner (1987), Applied Geodesy: 11-15, Springer, Berlin-Heidelberg-New York.

BOUCHER, C., Z. ALTAMINI, P. SILLARD (1999): The 1997 International Terrestrial Reference Frame (ITRF97). IERS Techn. Note 27, Paris.

BOUMAN, J. (1997): A survey of global gravity models. Delft Inst. for Earth-oriented Space Research (DEOS) Rep. 97.1, TU Delft.

BOWIN, C. (1994): The geoid and deep earth mass anomaly structure. In Vaníček and Christou (1994): 203-219.

BOWIN, C. (2000): Mass anomalies and the structure of the earth. Phys. Chem. Earth (A) 25: 343-353.

BOWIN, C., TH.C. ALDRICH, R.A. FOLINSBEE (1972): VSA Gravity Meter System: Tests and recent developments. JGR 77: 2018-2033.

BOWRING, B.R. (1971): The normal section – forward and inverse formulae at any distance. Survey Review no.161: 131-136.

BOWRING, B.R. (1985): The accuracy of geodetic latitude and height equations. Survey Review 28: 202-206.

BROSCHE, P., H. SCHUH (1999): Neue Entwicklungen in der Astrometrie und ihre Bedeutung für die Geodäsie. ZfV 124: 343-350.

BROSCHE, P., W.R. DICK (1996): GAIA für Gäa ? – Zur geowissenschaftlichen Nutzung eines geplanten Astrometrie-Satelliten. ZfV 121: 577-580.

BROUWER, D., G.M. CLEMENCE (1961): Methods of celestial mechanics. Academic Press, New York.

BROWN, L.D., R. DANIELL, Jr., M.W. FOX, J.A. KLOBUCHAR, P.H. DOHERTY (1991): Evaluation of six ionospheric models as predictors of total electron content. Radio Science 26: 10007-10015.

BROZENA, J.M., M.F. PETERS (1995): State-of-the-art airborne gravimetry. In Sünkel and Marson (1995): 187-197.

BRUNNER, F.K., ed. (1984a): Geodetic refraction. Springer, Berlin-Heidelberg-New York.

BRUNNER, F.K. (1984b): Modelling of atmospheric effects on terrestrial geodetic measurements. In Brunner (1984a): 143-162.

BRUNNER, F.K., ed. (1998): Advances in positioning and reference frames. IAG Symp. Proceed. 118, Springer, Berlin-Heidelberg-New York.

BRUNNER, F.K., CHR. RIZOS, eds. (1990): Developments in four-dimensional geodesy. Lecture Notes in Earth Sciences 29, Springer, Berlin-Heidelberg-New York.

BRUNS, H. (1878): Die Figur der Erde. Publ. Königl. Preuß. Geod. Inst., Berlin.

BRUYNINX, C. (1999): Status and prospects of the permanent EUREF network. In Gubler et al. (1999): 42-46.

BULLEN, K.E. (1975): The earth's density. Chapman and Hall, London.

BÜRKI, B. (1989): Integrale Schwerefeldbestimmung in der Ivrea-Zone und deren geophysikalische Interpretation. Geod. geophys. Arbeiten in der Schweiz 40, Schweiz. Geod. Komm., Zürich.

BURSA, M. (1995): Special Commission SC3 "Fundamental Constants" Report. In Travaux de l'Assoc. Int. de Géod., Tome 30: 370-384, Paris.

CAMPBELL, J., B. WITTE (1978): Grundlagen und geodätische Anwendung der Very Long Baseline Interferometry. ZfV 103: 10-20.

CAMPBELL, J., A. NOTHNAGEL, H. SCHUH (1992): VLBI-Messungen für geodynamische Fragestellungen. ZfV 117: 214-227.

CANNON, M.E., G. LACHAPELLE, eds. (1997): Proceed. Int. Symp. on Kinematic Systems in Geodesy, Geomatics and Navigation, Banff 1997, Univ. of Calgary.

CARTER, W.E., D.S. ROBERTSON, J.R. MACKAY (1985): Geodetic radio interferometric surveying: application and results. JGR 90: 4577-4587.

CARTER, W.E., D.G. AUBREY, T. BAKER et al. (1989): Geodetic fixing of tide gauge bench marks. Woods Hole Oceanographic Institution Report WHOI-89-31/CRC-89-5, Woods Hole, Mass., U.S.A.

CARTWRIGHT, D.E., J. CREASE (1963): A comparison of the geodetic reference levels of England and France by means of the sea surface. Proc. Roy. Soc. London, A 273: 558-580.

CARTWRIGHT, D.E., A.C. EDDEN (1973): Corrected tables of tidal harmonics. Geophys.J. R. Astr. Soc. 33: 253-264.

CARTWRIGHT, D.E., R.J. TAYLER (1971): New computations of the tide-generating potential. Geophys. J. R. Astr. Soc. 23: 45-74.

CAZENAVE, A. (1994): The geoid and oceanic lithosphere. In Vaníček and Christou (1994): 255-283.

CAZENAVE, A. (1995): Geoid, topography and land forms. In Ahrens (1995): 32-39.

CHADWELL, D., F. SPIESS, J. HILDEBRAND, L. YOUNG, G. PURCELL jr., H. DRAGERT (1998): Deep-sea geodesy: monitoring the ocean floor. GPS World 9(9): 44-55.

CHAO, B.F. (1994): The geoid and earth rotation. In Vaníček and Christou (1994): 285-298.

CHAO, B.F., R. GROSS, Y. YAN (1996): Seismic excitation of the polar motion 1977-1993. Pageoph 146: 407-419.

CHEN, J.Y. (1982): Geodetic datum and Doppler positioning. Mitt. Geod. Inst. TU Graz, Folge 39.

CHENEY, R.E. et al. (1995): TOPEX/POSEIDON: Scientific results. JGR 100: 24893-25382.

CHENG, M., B.D. TAPLEY (1999): Seasonal variations in low degree zonal harmonics of the earth's gravity field from satellite laser ranging obsrevations. JGR 104: 2667-2681.

CLARK, T.A., D. GORDON, W.E. HINRICH, C. MA, A. MALLAMA, J.W. RYAN (1987): Determination of relative site motions in the western United States using MKIII Very Long Baseline Interferometry. JGR 92: 12741-12750.

COCHRAN, J.R., D.J. FORNARI, B.J. COAKLEY, R. HERR, M.A. TIVEY (1999): Continuous near-bottom gravity measurements made with a BGM-3 gravimeter in DSV Alvin on the East Pacific Rise crest near 9°31'N and 9°50'N. JGR 104: 10841-10861.

COHEN, S.C., R.W. KING, R. KOLENKIEWICZ, R.D. ROSEN, B.E. SCHUTZ, eds. (1985): Lageos scientific results. JGR 90: 9215-9438.

COLLIER, P.A., M.J. CROFT (1997): Height from GPS in an engineering environment. Survey Review 34: 11-18.

COLOMBO, O. (1981): Numerical methods for harmonic analysis on the sphere. OSU Rep. 310, Columbus, Ohio.

COLOMBO, O.L. (1989): Advanced techniques for high-resolution mapping of the gravitational field. In Sansò and Rummel (1989): 335-372.

COLOMBO, O.L., ed. (1992): From Mars to Greenland: Charting gravity with space and airborne instruments. IAG Symp. Proceed.110, Springer, New York-Berlin-Heidelberg.

COOK, A.H. (1959): The external gravity field of a rotating spheroid to the order of e^3 . Geophys. J. R. Astr. Soc. 2: 199-214.

COORS, S., R. HEER, H. HUSTEDT, V. SCHWIEGER (1998): Zur Leistungsfähigkeit der Empfangssysteme GePos RD24 und Trimble 4000 SSi. ZfV 123: 403-414.

CROSSLEY, D., J. HINDERER, G. CASULA et al. (1999): Network of superconducting gravimeters benefits a number of disciplines. EOS 80: 121, 125-126.

DASSING, R.,W. SCHLÜTER, U. SCHREIBER (1992): Das neue Laserentfernungsmeßsystem der Fundamentalstation Wettzell. ZfV 117: 180-188.

DAVIS, J.L., M.L. COSMO, G. ELGERED (1996): Using the Global Positioning System to study the atmosphere of the earth: overview and prospect. In Beutler et al. (1996c): 233-242.

DE METS, C., R.G. GORDON, D.F. ARGUS, S. STEIN (1990): Current plate motions. Geophys. J. Int. 101: 425-478.

DE METS, C., R.G. GORDON, D.F. ARGUS, S. STEIN (1994): Effect of recent revisions to the geomagnetic reversal time scale on estimates of current plate motions. Geophys. Res. Letters 21: 2191-2194.

DE MUNCK, J.C., T.A.TH. SPOELSTRA, eds. (1992): Proceed. of the Symp. on refraction of transatmospheric signals in geodesy. Neth. Geod. Comm., Publ. on Geodesy, New Series No. 36, Delft.

DEHANT, V. (1987): Tidal parameters for an inelastic earth. Phys. Earth Planet. Inter. 49: 97-116.

DEHLINGER, P. (1978): Marine gravity. Elsevier Scient. Publ., Amsterdam etc.

DEICHL, K. (1975): Zur Messung mit Pendelastrolabien und ihrer Auswertung. ZfV 100: 499-509.

DENIS, C. (1989): The hydrostatic figure of the earth. In Teisseyre (1989): 111-186.

DENKER, H. (1988): Hochauflösende regionale Schwerefeldbestimmung mit gravimetrischen und topographischen Daten. Wiss. Arb. Univ. Hannover 156.

DENKER, H. (1998): Evaluation and improvement of the EGG97 quasigeoid model for Europe by GPS and leveling data. Rep. Finn. Geod. Inst. 98.4: 53-61.

DENKER, H., W. TORGE (1998): The European gravimetric quasigeoid EGG97 – an IAG supported continental enterprise. In Forsberg et al. (1998): 249-254.

DENKER, H., D. LELGEMANN, W. TORGE, G. WEBER, H.G. WENZEL (1986): Strategies and requirements for a new European geoid determination. Proceed. Int. Symp. on the Definition of the Geoid, vol.1: 207-222, Ist. Geogr. Mil., Firenze.

DENKER, H., W. TORGE, G. WENZEL, J. IHDE, U. SCHIRMER (2000): Investigation of different methods for the combination of gravity and GPS/levelling data. In Schwarz (2000b): 137-142.

DEUMLICH, F. (1982): Surveying instruments. De Gruyter, Berlin-New York.

DEUMLICH, F., R. STAIGER (2001): Instrumentenkunde. 9. Aufl., Wichmann/Hüthig, Heidelberg.

DICKEY, J.O. (1995): Earth rotation. In Ahrens (1995): 356-368.

DIETZ, R.S. (1961): Continent and ocean evolution by spreading of the sea floor. Nature 190: 854-857.

DIRAC, P.A.M. (1938): A new basis for cosmology. Proc. Roy. Soc. London, A 165: 199-208.

DITTFELD, H.-J. (2000): Final results of the SG-registration in Potsdam. In Ducarme and Barthelemy (2000): 11-24.

DIVIS, D.A. (1999): Galileo- enthusiasm and money propel Europe's GNSS. GPS World 10 (11): 12-19.

DMA (1987): Department of Defense World Geodetic System 1984. DMA Technical Report TR 8350.2 and Supplement TR 830.2-A,B, Washington, D.C.

DOBRIN, M.B. (1976): Introduction to geophysical prospecting. McGraw-Hill, New York etc.

DODSON, A.H. (1995): The status of GPS for height determination. Survey Review 34: 66-76.

DODSON, A.H., P. FLEMING (1988): The Geomensor CR204: Baseline test results. Survey Review 29: 351-357.

DONG, D., J.O. DICKEY, Y. CHAO, M.K. CHENG (1997): Geocenter variations caused by atmosphere, ocean and surface ground water. Geophys. Res. Letters 24: 1867-1870.

DOODSON, A.I. (1921): The harmonic development of the tide-generating potential. Proc. Roy. Soc. London, A 100: 305-329.

DORRER, E. (1966): Direkte numerische Lösung der geodätischen Hauptaufgaben auf Rotationsflächen. DGK, C 90, München.

DREWES, H., W. TORGE, R.H. RÖDER, C. BADELL, D. BRAVO, O. CHOURIO (1991): Absolute and relative gravimetric surveys of national and geodynamic networks in Venezuela. J. South American Earth Sciences 4: 273-286.

DREWES, H., C. FÖRSTE, C. REIGBER (1992): Ein aktuelles plattenkinematisches Modell aus Laser- und VLBI- Auswertungen. ZfV 117: 205-214.

DUCARME, B., J. BARTHELEMY, eds. (2000): High precision gravity measurements with application to geodynamics and second GGP workshop. Cahiers du Centre Européen de Géodynamique et de Séismologie 17, Luxembourg.

DUCARME, B., B. JANSSEN (1990): Changes of station coordinates with earth tides and ocean loading. In Paquet et al. (1990): 39-45.

DUCARME, B., P. MELCHIOR (1983): A prediction of tidal ocean loading and attraction effects on gravity measurements in continents. Bull. d'Inf. Bur. Gravim. Int. 52: 77-85.

DUCARME, B., P. PAQUET, eds. (1998): Proceedings of the Thirteenth International Symposium on Earth Tides. Obs. Royal de Belgique, Serie Geophysique, Bruxelles.

DVORAK, J.J. (1995): Volcano geodesy: results of 100 years of surveillance. In Barthelemy et al. (1995): 1-119.

DZIEWONSKI, A.M., D.L. ANDERSON (1981): Preliminary reference earth model (PREM). Phys. Earth Planet. Int. 25: 297-356.

DZIEWONSKI, A.M., J.H. WOODHOUSE (1987): Global images of the earth's interior. Science 236: 37-48.

ECKER, E., E. MITTERMAYER (1969): Gravity corrections for the influence of the atmosphere. Boll.Geof. teor. appl. 11: 70-80.

EEG, J., T. KRARUP (1973): Integrated geodesy. Dan. Geod. Inst., int. rep. 7, Copenhagen.

EHLERT, D. (1991): Differentielle Verschiebungen und Drehstreckungen in dreidimensionalen Koordinatensystemen. DGK, B 295, Frankfurt a.M.

EHLERT, D. (1993): Methoden der ellipsoidischen Dreiecksberechnung. DGK, B 292, Frankfurt a.M.

EICHHORN, H. (1974): Astronomy of star positions. Ungar Publ., New York.

EKMAN, M. (1989): Impacts of geodynamic phenomena on systems for height and gravity. Bull. Géod. 63: 281-296..

EKMAN, M. (1993): Postglacial rebound and sea level phenomena, with special reference to Fennoscandia and the Baltic Sea. In Kakkuri (1993a): 7-70.

EKMAN, M., J. MÄKINEN (1996): Recent postglacial rebound, gravity change and mantle flow in Fennoscandia. Geophys. J. Int. 126: 229-234.

ELMIGER, A., W. GURTNER (1983): Astrogeodätische Geoidbestimmung und Lotabweichungsinterpolation in der Schweiz. Inst. für Geodäsie und Photogrammetrie. ETH Zürich, Nr. 74.

ERKER, E. (1987): The Austrian geoid – local geoid determination using modified conservative algorithms. Geod. Arb. Österreichs f.d. Intern. Erdmessung, N.F. IV: 19-46, Graz.

FALK, R. (1995): Erste Erfahrungen mit dem automatischen Gravimeter SCINTREX CG-3M Autograv. ZfV 120: 26-34.

FALLER, J.E., I. MARSON (1988): Ballistic methods of measuring g – the direct free-fall and symmetrical rise- and fall methods compared. Metrologia 25: 49-55.

FALLER, J.E., Y.G. GUO, J. GSCHWIND, T.M. NIEBAUER, R.L. RINKER, J. XUE (1983): The JILA portable absolute gravity apparatus. Bull. d'Inf. Bur. Gravim. Int. 53: 87-97.

FARRELL, W.E. (1972): Deformation of the earth by surface loads. Rev. Geophys. Space Physics 10: 761-797.

FEIST, W., B. DONATH, M. GÖRING, M. KÖHLER, M. SEEBER, L. MONZ (1998): Elta S10 und Elta S20 von Carl Zeiss, Systemtachymeter einer neuen Generation. Verm.wesen und Raumordnung 60: 104-127.

FINETTI, I., C. MORELLI (1973): Geophysical exploration of the Mediterranean Sea. Boll. Geof. teor. appl. 15: 263-344.

FISCHBACH, E., C.L. TALMADGE (1999): The search for non-Newtonian gravity. Springer, New York.

FISCHER, I. (1975): The figure of the earth – changes in concepts. Geophys. Surveys 2: 3-54.

FISCHER, I. (1977): Mean sea level and the marine geoid – an analysis of concept. Marine Geodesy 1: 37-59.

FISCHER, I., M. SLUTSKY et al. (1968): New pieces in the picture puzzle of an astrogeodetic geoid map of the world. Bull.Géod. no. 88: 199-221.

FLACH, D. (1976): The Askania borehole tiltmeter in field operation. Proceed. 7th Int. Symp. on Earth Tides, Sopron 1973: 243-247, Budapest.

FORSBERG, R. (1984): A study of terrain reductions, density anomalies and geophysical inversion methods in gravity modelling. OSU Rep. 355, Columbus, Ohio.

FORSBERG, R. (1985): Gravity field terrain effect computations by FFT. Bull. Géod. 59: 342-360.

FORSBERG, R., J.M. BROZENA (1993): The Greenland airborne gravity project-comparison of airborne and terrestrial gravity data. In Montag and Reigber (1993): 171-175.

FORSBERG, R., C.C. TSCHERNING (1981): The use of height data in gravity field approximation. JGR 86: 7843-7854.

FORSBERG, R., C.C. TSCHERNING (1997): Topographic effects in gravity field modelling for BVP. In F. Sansò and R. Rummel (1997): 241-272.

FORSBERG, R., M. FEISSEL, R. DIETRICH, eds. (1998): Geodesy on the move: Gravity, geoid, geodynamics, and Antarctica. IAG Symp. Proceed. 119, Springer, Berlin-Heidelberg-New York.

FOWLER, C.M.R. (1999): The solid earth. Cambridge Univ. Press.

FRANCIS, O. (1997): Calibration of the CO21 superconducting gravimeter in Membach (Belgium) using 47 days of absolute gravity measurements. In Segawa et al. (1997): 212-219.

FRICKE, W., H SCHWAN, T. LEDERLE, eds. (1988): Fifth Fundamental Catalogue (FK5). Veröff. Astron. Recheninstitut Heidelberg 32, Braun, Karlsruhe.

FROOME, K.D. (1971): Mekometer III: EDM with sub-millimeter resolution. Survey Review 21: 98-118.

Fu, L.-L., J. CHRISTENSEN, C. YAMARONE et al. (1994): TOPEX-POSEIDON mission overview. JGR 99: 24369-24381.

GAN, W., J.L. SVARC, J.C. SAVAGE, W.H. PRESCOTT (2000): Strain accumulation across the Eastern California Shear Zone at latitude 36°30'N. JGR 105: 16229-16236.

GARLAND, G.D. (1979): Introduction to geophysics. Saunders, Philadelphia.

GERARDY, TH. (1977): Die Anfänge von Gauss' geodätischer Tätigkeit. ZfV 102: 1-20.

GERSTBACH, G. (1996): CCD und geodätische Astronomie – Zur Nutzbarkeit von CCD für Lot- und Azimutmessungen. Österr. Z.f.Verm. u. Geoinf. 96: 63-68.

GILLIES, G.T. (1987): The Newtonian Gravitational Constant. Metrologia 24 (suppl.): 1-56.

GIPSON, J.M., C. MA (1998): Site displacement due to variation in earth rotation. JGR 103: 7337-7350.

GLEINSVIK, P. (1960): Studien über die Ermittlung der Geoidform und die Bestimmung von Meereshöhen aus Höhenwinkeln. Mitt. Nr.7, Geod. Inst., ETH Zürich.

GOODKIND, J.M. (1991): The superconducting gravimeters: principle of operation, current performance and future prospects. In Poitevin (1991): 81-90, Luxembourg.

GOPALAPILLAI, S. (1974): Non-global recovery of gravity anomalies from a combination of terrestrial and satellite altimetry data. OSU Rep. 210, Columbus, Ohio.

GORDON, R.G. (1995): Present plate motions and plate boundaries. In Ahrens (1995): 66-87.

GÖRRES, B., J. CAMPBELL (1998): Bestimmung vertikaler Punktbewegungen mit GPS. ZfV 123: 222-230.

GRABOWSKI, J. (1987): Hydrostatic levelling over long distances. In Pelzer and Niemeier (1987): 271-287.

GRAFAREND, E.W. (1972): Three-dimensional geodesy and gravity gradients. OSU Rep. 174, Columbus, Ohio.

GRAFAREND, E.W. (1976): Geodetic applications of stochastic processes. Phys. Earth Planet. Int. 12: 151-179.

GRAFAREND, E.W. (1978): Operational geodesy. In Moritz and Sünkel (1978): 235-284.

GRAFAREND, E.W. (1986): Differential geometry of the gravity field. Man.Geod. 11: 29-37.

GRAFAREND, E.W., W. NIEMEIER (1971): The free nonlinear boundary value problem of physical geodesy. Bull. Géod. no. 101: 243-262.

GRAFAREND, E.W., F. SANSÒ, eds. (1985): Optimization and design of geodetic networks. Springer, Berlin-Heidelberg.

GRAFAREND, E.W., B. SCHAFFRIN (1993): Ausgleichungsrechnung in linearen Modellen. BI Wissenschaftsverlag, Mannheim.

GRONWALD, W. (1963): "Das Einheitliche Europäische Nivellementsnetz" und der "Mittlere Meeresspiegel". ZfV 88: 141-153.

GROSSMANN, W. (1976): Geodätische Rechnungen und Abbildungen in der Landesvermessung. 3.Aufl., Wittwer, Stuttgart.

GROTE, TH. (1996): Regionale Quasigeoidmodellierung aus heterogenen Daten mit cm-Genauigkeit. Wiss. Arb. Univ. Hannover 212.

GROTEN, E. (1979): Geodesy and the earth's gravity field. Dümmler, Bonn.

GROTEN, E. (2000): Parameters of common relevance of astronomy, geodesy, and geodynamics. J. Geod. 74: 134-140.

GROTEN, E., E. REINHART (1968): Gravity prediction in mountaineous areas. Boll. Geof. teor. appl. 10: 28-43.

GRUBER, TH., M. ANZENHOFER, M. RENTSCH, P. SCHWINTZER (1997): Improvements in high resolution gravity field modeling at GFZ. In Segawa et al (1997): 445-452.

GUBLER, E., H. HORNIK, eds. (1999): IAG Section I, Comm. X, Subcomm. for Europe (EUREF), Publ. No. 9, Mitt. BKG 6, Frankfurt a.M.

GUBLER, E., H.G. KAHLE, E. KLINGELE, ST. MUELLER, R. OLIVIER (1981): Recent crustal movements in Switzerland and their geophysical interpretation. Tectonophysics 71: 125-152.

GUBLER, E., J.A. TORRES, H. HORNIK, eds. (1999): IAG, Section I, Comm.X, Subcomm. for Europe (EUREF), Publ. No. 8, Veröff, Bayer. Komm. f.d. Internat. Erdmessung Nr.60, München.

GUMERT, W.R. (1995): Third generation aerogravity system. Proceed. Int. Symp.on Kinematic Systems in Geodesy, Geomatics, and Navigation: 163-169.

HAAGMANS, R., E. DE MIN, M. VAN GELDEREN (1993): Fast evaluation of convolution integrals on the sphere using 1D FFT, and a comparison with existing methods for Stokes' integral. Man. Geod. 18: 227-241.

HAASBROEK, N.D. (1968): Gemma Frisius, Tycho Brahe and Snellius and their triangulation. Publ. Netherl. Geod. Comm., Delft.

HAKE, G., D. GRÜNREICH (1994): Kartographie. 7. Aufl., de Gruyter, Berlin- New York.

HAMMER, S. (1963): Deep gravity interpretation by stripping. Geophysics 28: 369-378.

HAMMER, S. (1979): Relative precision of vertical and horizontal gravity gradients measured by gravimeter. Geophysics 44: 99-101.

HAMMER, S. (1983): Airborne gravity is here. Geophysics 48: 213-223.

HANKEMEIER, P. (1996): The DGPS-Service for the FRG: Concept and status. In Beutler et al (1996c): 75-84.

HANNAH, J. (1989): A long term sea level change scenario and its implications for geodetic networks. Marine Geodesy 13: 91-100.

HARNISCH, M., G. HARNISCH (1993): Helmert's Arbeiten zur physikalischen Geodäsie. In F.R. Helmert, Akademievorträge, Nachr. a.d. Karten- und Verm.wesen 109: 37-77, Inst. f. Angew. Geodäsie, Frankfurt a.M.

HARRISON, J.C. (1976): Cavity and topographic effects in tilt and strain measurements. JGR 81: 319-328.

HARTMANN, T., H.-G. WENZEL (1995): The HW95 tidal potential catalogue. Geophys. Res. Letters 22: 3553-3556.

HASTINGS, D.A., P.K. DUNBAR, A.M. HITTELMAN (2000): Assessing the global land one-km base elevation DEM. In Schwarz (2000b): 101-106.

HECK, B. (1990). An evaluation of some systematic error sources affecting terrestrial gravity anomalies. Bull. Géod. 64: 88-108.

HECK, B. (1991): On the linearized boundary value problem of physical geodesy. OSU Rep. 407, Columbus, Ohio.

HECK, B. (1995): Rechen- und Auswertemodelle der Landesvermessung. 2.Aufl., Wichmann, Heidelberg.

HECK, B. (1997): Formulation and linearization of boundary value problems: From observables to mathematical models. In Sansò and Rummel (1997): 121-160.

HEIN, G.W. (1986): Integrated geodesy – state of the art 1986 reference text. In Sünkel (1986a): 505-548.

HEISKANEN, W.A. (1951): On the world geodetic system. Publ. Isostat. Inst., Int. Ass. Geod., 26, Helsinki.

HEISKANEN, W.A. (1957): The Columbus Geoid. EOS 38: 841-848.

HEISKANEN, W.A., H. MORITZ (1967): Physical geodesy. Freeman and Co., San Francisco and London.

HEISKANEN, W.A., F.A. VENING-MEINESZ (1958): The earth and its gravity field. McGraw-Hill, New York.

HEITZ, S. (1969): An astro-geodetic determination of the geoid for West Germany. Nachr. a.d. Karten- und Verm.wesen II 24, Frankfurt a M.

HEITZ, S. (1973): Ein dreidimensionales Berechnungsmodell für Punktbestimmungen mit Berücksichtigung orthometrischer Höhen. ZfV 98: 479-485.

HEITZ, S. (1988): Coordinates in geodesy. Springer, Berlin-Heidelberg-New York.

HELMERT, F.R. (1880/1884): Die mathematischen und physikalischen Theorien der höheren Geodäsie. Teubner, Leipzig (reprint Minerva GmbH, Frankfurt a.M. 1961).

HERRING, T.A., D. DONG (1994): Measurement of diurnal and semidiurnal rotational variations and tidal parameters of earth. JGR 99: 18051-18071.

HESS, H.H. (1962): History of ocean basins. In A.E. Engel, H.L. James, B.F. Leonard, eds., Petrological studies – Buddington Memorial Volume: 599-620, Geol. Soc. Am., New York , N.Y.

HINDERER, J., D. CROSSLEY, H. XU (1994): A two-year comparison between the French and Canadian superconducting gravimeter data. Geophys. J. Int. 116: 252-266.

HINZE, W.J., ed. (1985): The utility of regional gravity and magnetic anomaly maps. Society of Exploration Geophysicists, Tulsa, Oklahoma.

HIPPARCOS (1995). Astronomy and Astrophysics 304: 34-316.

HIRVONEN, R.A. (1960): New theory of the gravimetric geodesy. Publ. Isostat. Inst., Int. Ass. Geod., 32, Helsinki.

HOFMANN-WELLENHOF, B., H. LICHTENEGGER, J. COLLINS (1997): Global Positioning System: Theory and practice. 5th ed., Springer, Berlin-Heidelberg-New York.

HOLT, W.E., N. CHANNOT-ROOKE, X. LE PICHON, A.J. HAINES, B. SHEN-TU, J. REN (2000): Velocity field in Asia inferred from Quaternary fault slip rates and Global Positioning System observations. JGR 105: 19185-19209.

HOOIJGBERG, M. (1997): Practical geodesy. Springer, Berlin-Heidelberg-New York.

HÖPCKE, W. (1965): Eine Studie über die Korrelation elektromagnetisch gemessener Strecken. Allg. Verm. Nachr. 72: 140-147.

HÖPCKE, W. (1966): On the curvature of electromagnetic waves and its effects on measurement of distance. Survey Review 18: 298-312.

HOPFIELD, H. (1969): Two-quartic tropospheric refractivity profile for correcting satellite data. JGR 74: 4487-4499.

HÖRMANDER, L. (1976): The boundary value problem of physical geodesy. Archive for Rat. Mechanics and Analysis 62: 1-52.

HOTINE, M. (1969): Mathematical geodesy. ESSA Monogr.2, Washington, D.C.

HOYER, M., S. ARCINIEGAS, K. PEREIRA, H. FAGARD, R. MATURANA, R. Torchetti, H. DREWES, M. KUMAR, G. SEEBER (1998): The definition and realization of the reference system in the SIRGAS project. In Brunner (1998): 168-173.

HRADILEK, L. (1984): Threedimensional terrestrial triangulation – applications in surveying engineering. Wittwer, Stuttgart.

HUDNUT, K.W. (1995): Earthquake geodesy and hazard monitoring. Rev. Geophys., Suppl.: 249-255.

HUGGETT, G.R., L.W. SLATER (1975): Precision electromagnetic distance-measuring instrument for determining secular strain and fault movement. Tectonophysics 29: 19-27.

IAG (1971): Geodetic Reference System 1967. Publ. Spec. 3, IAG Central Bureau, Paris.

IAG (1997): Science Services: International Association of Geodesy (IAG) / Federation of Astronomical and Geophysical Services (FAGS). Dep.of Civil and Environmental Engineering and Geodetic Science, The Ohio State Univ, Columbus, Ohio, and IAG Central Bureau, c/o Dep. of Geophysics, Copenhagen, Denmark.

IERS (1995): Missions and goals for 2000. IERS Central Bureau, Paris.

IHDE, J., W. LINDSTROT (1995): Datumstransformation zwischen den Bezugssystemen ETRF/WGS, DHDN und System 42. ZfV 120: 192-196.

IHDE, J., W. SCHLÜTER, J. ADAM, W. GURTNER, B.G.HARSSON, G. WÖPPELMANN (1998): Konzept und Status des European Vertical Reference Network (EUVN). In BKG (1998): 53-67.

ILIFFE, J.C., A.H. DODSON (1987): Refraction effects on precise EDM observations. Survey Review 29: 181-190.

ILK, K.H. (2000): Envisaging a new era of gravity field research. In Rummel et al (2000a): 53-62.

ILLNER; M., R. JÄGER (1995): Integration von GPS-Höhen ins Landesnetz – Konzept und Realisierung im Programmsystem HEIDI. Allg. Verm. Nachr. 102: 1-18.

INGENSAND, H. (1990): Das Wild NA 2000, das erste digitale Nivellier der Welt. Allg. Verm. Nachr. 97: 201-210.

IZOTOV, A.A. (1959): Reference-ellipsoid and the standard geodetic datum adopted in the USSR. Bull. Géod. no.53: 1-6.

JACHENS, R.C. (1978): Temporal gravity changes as applied to studies of crustal deformation. In Proceed. of Conf. VII Stress and Strain Measurements Related to Earthquake Prediction. U.S. Geological Survey Open-File Report 79-370.

JACHENS, R.C., W. THATCHER, C.W. ROBERT, R.S. STEIN (1983): Correlation of changes in gravity, elevation, and strain in southern California. Science 219: 1215-1217.

JAHN, C.-H., G. SEEBER, G.R. FOULGER, P. EINARSSON (1994): GPS epoch measurements spanning the Mid-Atlantic plate boundary in northern Iceland 1987-1990. In Schutz et al. (1994): 109-123.

JANES, H.W., R.B. LANGLEY, S.P. NEWBY (1991): Analysis of tropospheric delay prediction models: comparison with ray- tracing and implications for GPS relative positioning. Bull. Géod. 65: 151-161.

JEFFREYS, SIR HAROLD (1970): The earth – its origin, history and physical constitution. 5.ed., Cambridge Univ. Press.

JEKELI, C. (1988a): The gravity gradiometer survey system (GGSS). EOS 69: 105, 116-117.

JEKELI, C. (1988b): The exact transformation between ellipsoidal and spherical harmonic expansion. Man. Geod. 13: 106-113.

JEKELI, C. (1995): Airborne vector gravimetry using precise, position-aided inertial measurements. Bull. Géod. 69: 1-11.

JEKELI, C. (1998): The world of gravity according to Rapp. In Forsberg et al. (1998): 79-91.

JEKELI, C. (1999): An analysis of vertical deflections derived from high-degree spherical harmonic models. J. Geod. 73: 10-22.

JEKELI, C. (2001): Inertial navigation systems with geodetic applications. De Gruyter, Berlin-New York.

JELSTRUP, J. (1955): Crossing of fjords with precise levelling. Bull. Géod. no. 38: 55-63.

JENTZSCH, G. (1997): Earth tides and ocean tidal loading. In Wilhelm et al. (1997): 145-167.

JGR (1998): Advances in oceanography and sea ice research using ERS observations. JGR special issue 103 (C4).

JOECKEL, R., M. STOBER (1999): Elektronische Entfernungs- und Richtungsmessung. 3.Aufl., Wittwer, Stuttgart.

KÄÄRIÄINEN, J. (1979): Observing the earth tides with a long water-tube tiltmeter. Publ. Finn. Geod. Inst. 88, Helsinki.

KAHLE, H.-G., M. COCARD, Y. PETER, A. GEIGER, R. REILINGER, A. BARKA, G. VEIS (2000): GPS-derived strain rate field within the boundary zones of the Eurasian,African and Arabian plates. JGR 105: 23353-23370.

KAHMEN, H. (1978): Elektronische Meßverfahren in der Geodäsie. 3. Aufl., Wichmann, Karlsruhe.

KAHMEN, H. (1997): Vermessungskunde. 19. Aufl., de Gruyter, Berlin- New York.

KAHMEN, H., W. FAIG (1988): Surveying. De Gruyter, Berlin-New York.

KAKKURI, J. (1966): Versuche mit dem automatischen Doppelinstrument Zeiss Ni2 beim Stromübergangsnivellement. ZfV 91: 160-164.

KAKKURI, J. (1986): Newest results obtained in studying the Fennoscandian land uplift phenomenon. Tectonophysics 130: 327-331.

KAKKURI, J., ed. (1993a): Geodesy and geophysics. Publ. Finn. Geod. Inst. 115, Helsinki.

KAKKURI, J. (1993b): The stress phenomenon in the Fennoscandian shield. In Kakkuri (1993a): 71-86.

KANE, M.F., R.H. GODSON (1985): Features of a pair of long-wavelength (> 250 km) and short wavelength (< 250 km) Bouguer gravity maps of the United States. In Hinze (1985):46-61.

KANNGIESER, E. (1983): Genauigkeitssteigerungen in der Relativgravimetrie. ZfV 108: 180-189.

KANNGIESER, E., K. KUMMER, W. TORGE, H.-G. WENZEL (1983): Das Gravimeter-Eichsystem Hannover. Wiss. Arb. Univ. Hannover 120.

KATSAMBALOS, K.E. (1979): The effect of the smoothing operator on potential coefficient determination. OSU Rep. 287, Columbus, Ohio.

KAULA, W.M. (1959): Statistical and harmonic analyses of gravity. JGR 64: 2401-2421.

KAULA, W.M. (1966): Theory of satellite geodesy. Blaisdell Publ., London.

KAULA, W.M. (1992): Properties of the gravity fields of terrestrial planets. In Colombo (1992): 1-10.

KAULA, W.M. (1993): Higher order statistics of planetary gravities and topographies. Geophys. Res. Letters 20: 2583-2586.

KEARSLEY, A.H.W., R. FORSBERG (1990): Tailored geopotential models – applications and short-comings. Man. Geod. 15: 151-158.

KELLOGG, O.D. (1929): Foundations of potential theory. Springer, Berlin (reprint 1967).

KENYON, S.C. (1998): The development by the National Imagery and Mapping Agency of a global surface gravity anomaly database for the EGM96 geopotential model and future applications. In Forsberg et al. (1998): 99-104.

KIM, J.-H., R.H. RAPP (1990): The development of the July 1989 1°x1° and 30'x30' terrestrial mean free-air anomaly data base. OSU Rep. 403, Columbus, Ohio.

KING, G.C.P., R.G. BILHAM (1973): Strain measurement instrumentation and technique. Phil. Trans. Roy. Soc. London, A 274: 209-217.

KING, G.C.P., R.G. BILHAM (1976): A geophysical wire strainmeter. Bull. Seism. Soc. Am. 66: 2039-2047.

KIVIOJA, L.A. (1971): Computation of geodetic direct and indirect problems by computers acculumating increments from geodetic line elements. Bull. Géod. no. 99: 53-63.

KLEUSBERG, A. (1998): Atmospheric models from GPS. In Teunissen and Kleusberg (1998a): 599-623.

KLINGELÈ, E.E., M. COCARD, H.-G. KAHLE, M. HALLIDAY (1997): GPS as a source for airborne gravity reduction in the airborne gravity survey of Switzerland. JGR 102: 7705-7715.

KLOBUCHAR, J.A. (1991): Ionospheric effects on GPS. GPS World 2 (4): 48-51.

KLOPPING, F. G. SASAGAWA, D. WINESTER et al. (1997): Report on the 1995 Table-Mountains international absolute-gravity-meter intercomparison. In Segawa et al. (1997): 40-46.

KLOTZ, J. (1993): Die Transformation zwischen geographischen Koordinaten und geodätischen Polar- und Parallel-Koordinaten. ZfV 118: 217-227.

KNEISSL, M. (1956): Höhenmessung-Tachymetrie. Jordan-Eggert-Kneissl, Handbuch der Vermessungskunde, Band III, Metzler, Stuttgart.

KNEISSL, M. (1958/1959): Mathematische Geodäsie (Landesvermessung). Jordan-Eggert-Kneissl, Handbuch der Vermessungskunde, Band IV 1/2, Metzler, Stuttgart.

KNUDSEN, P. (1993): Altimetry for geodesy and oceanography. In Kakkuri (1993a): 87-129.

KOCH, K.R. (1989): Der erste europäische Fernerkundungssatellit ERS-1 und seine geodätische Nutzungsmöglichkeit. ZfV 114: 342-345.

KOCH, K.R. (1999): Parameter estimation and hypothesis testing in linear models. 2nd ed., Springer, Berlin-Heidelberg-New York..

KOCH, K.-R., A.J. POPE (1972): Uniqueness and existence of the geodetic boundary value problem using the known surface of the earth. Bull. Géod. no. 106: 467-476.

KOGAN, M.G., M.K. MCNUTT (1993): Gravity field over nothern Eurasia and variations in the strength of the upper mantle. Science 259: 473-479.

KOHL, M., J. LEVINE (1995): Measurement and interpretation of tidal tilts in Southern California. JGR 100: 3929-3942.

KOUBA, J.A. (1983): A review of geodetic and geodynamic satellite Doppler positioning. Rev. Geophys. 21: 41-50.

KOVALEVSKY, J. (1989): Lectures in celestial mechanics. In Sansò and Rummel (1989): 69-114, Springer, Berlin-New York.

KOVALEVSKY, J. (1995): Modern astrometry. Springer, Berlin-Heidelberg-New York.

KOVALEVSKY, J. et al. (1997): The HIPPARCOS catalogue as a realization of the extragalactic reference system. Astronomy and Astrophysics 323: 620-633.

KOVALEVSKY, J., I.I. MUELLER, B. KOLACZEK, eds. (1989): Reference frames in astronomy and geophysics. Kluwer Acad. Publ., Dordrecht-Boston-New York.

KRACK, K. (1982): Rechnergestützte Ableitung der Legendreschen Reihen und Abschätzung ihrer ellipsoidischen Anteile zur Lösung der ersten geodätischen Hauptaufgabe auf Bezugsellipsoiden. ZfV 107: 118-125.

KRARUP, T. (1969): A contribution to the mathematical foundation of physical geodesy. Publ. Danish Geod. Inst. 44, Copenhagen.

KRAUS, K. (1992/1997): Photogrammetry. Vol.1/ Vol.2, Dümmler, Bonn.

KRAUS, K., W. SCHNEIDER (1988/1990): Fernerkundung. Dümmler, Bonn.

KRIEG, L.A. (1981): Mathematical modelling of the behaviour of the LaCoste and Romberg "G" gravity meter for use in gravity network adjustments and data analyses. OSU Rep. 321, Columbus, Ohio.

KUKKAMÄKI, T.J. (1938): Über die nivellitische Refraktion. Publ. Finn. Geod. Inst. 25, Helsinki.

KUKKAMÄKI, T.J. (1949): Tidal correction of the levelling. Publ. Finn. Geod. Inst. 36: 143-152.

KUKKAMÄKI, T.J. (1980): Errors affecting levelling. Proceed. NAD-Symp. Ottawa: 1-10.

KUNTZ, E. (1990): Kartennetzentwurfslehre. 2.Aufl., Wichmann/ Hüthig, Heidelberg.

KUNTZ, E., G. SCHMITT (1995): Präzisionshöhenmessung durch Beobachtung gleichzeitig-gegenseitiger Zenitdistanzen. Allg. Verm. Nachr. 92: 427-434.

KUTTERER, H. (1998): Effiziente Berechnung von Meridianbogenlängen. Allg. Verm. Nachr. 105: 96-98.

LAMBECK, K. (1980): The earth's variable rotation. Cambridge Univ. Press.

LAMBECK, K. (1988): Geophysical geodesy. Clarendon Press, Oxford.

LAMBECK, K., C. SMITHER, P. JOHNSTON (1998): Sea-level change, glacial rebound and mantle viscosity for northern Europe. Geophys. J. Intern. 134: 102-144.

LAMBERT, A., T.S. JAMES, J.O. LIARD, N. COURTIER (1996): The role and capability of absolute gravity measurements in determining the temporal variations in the earth's gravity field. In Rapp et al. (1996): 20-29.

LANGBEIN, J.O., M.F. LINKER, A.F. McGARR (1987): Precision of two-color geodimeter measurements: Results from 15 months of observations. JGR 92: 11644-11656.

LANGLEY, R.B. (1997a): GLONASS: review and update. GPS World 8(7): 46-51.

LANGLEY, R.B. (1997b): GPS receiver system noise. GPS World 8(6): 40-45.

LANGLEY, R.B. (1998): Propagation of the GPS signals. In Teunissen and Kleusberg (1998a): 111-149.

LANGLEY, R.B. (1999): Dilution of precision. GPS World 10(5): 52-59.

LARSON, K., J. LEVINE (1999): Carrier-phase time transfer. IEEE Trans. on Ultrasonics, Ferroelectrics, and Frequency Transfer Control 46: 1001-1012.

LARSON, K.M. (1995): Crustal deformation. Rev. Geophys., Suppl.: 371-377.

LARSON, K.M., J.T. FREYMUELLER, S. PHILIPSEN (1997): Global plate velocities from the Global Positioning System. JGR 102: 9961-9981.

LE PICHON, X., J. FRANCHETEAU, J. BONNIN (1973): Plate tectonics. Developm. In Geotectonics vol. 6, Elsevier, Amsterdam-London-New York

LEDERSTEGER, K. (1956/1969): Astronomische und Physikalische Geodäsie (Erdmessung). Jordan-Eggert-Kneissl, Handbuch der Vermessungskunde, Band V, Metzler, Stuttgart.

LEE, L.P. (1974): The computation of conformal projections. Survey Review 22: 245-256.

LEICK, A. (1995): GPS satellite surveying. 2nd ed., Wiley and Sons, New York etc.

LELGEMANN, D. (1976): On the recovery of gravity anomalies from high precision altimeter data. OSU Rep. 239, Columbus, Ohio.

LEMOINE, F.G., D.E. SMITH, L. KUNZ et al. (1997): The development of the NASA GSFC and NIMA joint geopotential model. In Segawa et al. (1997): 461-469.

LEMOINE, F.G., S.C. KENYON et al. (1998): The development of the Joint NASA GSFC and the National Imagery and Mapping Agency (NIMA) Geopotential Model EGM96. NASA/TP-1998-206861, Goddard Space Flight Center, Greenbelt, Maryland.

LEONHARD, T. (1987): Vertical crustal movements in northern Germany. In Pelzer and Niemeier (1987): 525-538.

LERCH, F.J., R.S. NEREM, B.H. PUTNEY et al. (1994): A geopotential model from satellite tracking, altimeter, and surface gravity data: GEM-T3. JGR 99: 2815-2839.

LEVALLOIS, J.J. (1980): The history of the International Association of Geodesy. Bull. Géod. 54: 249-313.

LEVALLOIS, J.J. (1988): Mésurer la terre – 300 ans de géodésie Francaise. Association Francaise de Topographie, Paris.

LEVALLOIS, J.J., H. MONGE (1978): Le geoid Européen, version 1978. Proc. Int. Symp. on the Geoid in Europe and Mediterranean Area, Ancona 1978: 153-164.

LEVITUS, S. (1982): Climatological atlas of the world ocean. NOAA, Geophys. Fluid Lab., Profess. Paper 13, Dep. of Commerce, Washington, D.C.

LI RUIHAO, SUN HEPING, HU YENCHANG (1989): Investigation of gravity variation associated with crustal deformation of the Tianjin area before and after the Tangshan earthquake. Tectonophysics 167: 341-347.

LI, Y., M. SIDERIS (1994): Minimizationand estimation of geoid undulation errors. Bull. Géod. 68: 201-219.

LINDSTROT, W., ed. (1999): Das Deutsche Referenznetz 1991 (DREF91). Mitt. BKG 9, Frankfurt a.M.

LISITZIN, E. (1974): Sea level changes. Elsevier, Amsterdam etc.

LISTING, J.B. (1873): Über unsere jetzige Kenntnis der Gestalt und Größe der Erde. Nachr.d. Kgl. Gesellsch. d. Wiss. und der Georg-August-Univ., Göttingen: 33-98.

LOWRIE, W. (1997): Fundamentals of geophysics. Cambridge Univ. Press.

LU, Y., H.T. HSU, F.Z. JIANG (2000): The regional geopotential model to degree and order 720 in China. In Schwarz (2000b): 143-148.

LUCHT, H. (1972): Korrelation im Präzisionsnivellement. Wiss. Arb. Univ. Hannover 48.

LUNDQUIST, C.A., G. VEIS (1966): Geodetic parameters for a 1966 Smithsonian Institution Standard Earth. Smithsonian Astrophysical Obs., Spec. Rep. 200.

LYNESS, D. (1985): The gravimetric detection of mining subsidence. Geophysical Prospecting 33: 567-576.

MA, C. et al. (1998): The International Celestial Reference Frame as realized by Very Long Baseline Interferometry. The Astronomical J. 116: 516-546.

MA, C., M. FEISSEL, eds. (1997): Definition and realization of the International Reference System by VLBI astrometry of extragalactic objects. IERS Techn. Note 23, Paris.

MÄKINEN, J., S. TATTARI (1988): Soil moisture and ground water: Two sources of gravity variations. Bull. d'Inf. Bur. Gravim. Int. 62: 103-110.

MARKOWITZ, W. (1973): SI, the international system of units. Geophys. Surveys 1: 217-241.

MARSH, J.G., S. VINCENT (1974): Global detailed geoid computation and model analysis. Geophys. Surveys 1: 481-511.

MARSON, I., J.E. FALLER (1986): g – the acceleration of gravity: its measurement and its importance. J. Phys.E. Sci. Instrum.19: 22-32.

MARTI, U. (1997): Geoid der Schweiz. Geod. geophysik. Arbeiten in der Schweiz 56, Schweiz. Geod. Komm., Zürich.

MARTINEC, Z. (1994): Inversion techniques. In Vaníček and Christou (1994): 125-145.

MARTINEC, Z. (1998): Boundary-value problems for gravimetric determination of a precise geoid. Lecture Notes in Earth Sciences 73, Springer, Berlin-Heidelberg-New York.

MARUSSI, A. (1949): Fondements de géometrie differentielle absolue du champ potential terrestre. Bull. Géod. no. 14: 411-439.

MARUSSI, A. (1985): Intrinsic geodesy. Springer, Berlin-Heidelberg-New York.
MARUSSI, A., H. MORITZ, R.H. RAPP, R.O. VICENTE (1974): Ellipsoidal density models and hydrostatic equilibrium. Phys. Earth Planet. Inter. 9: 4-6.
MASSONNET, D., M. ROSSI, C. CARMONA, F. ADRAGNA, G. PELTZER, K. FIEGL, T. RABAUTE (1993): The displacement field of the Landers earthquake mapped by radar interferometry. Nature 364: 138-142.
MATHER, R.S. (1973): Four dimensional studies in earth space. Bull. Géod. no. 108: 187-209.
MATHER, R.S. (1978): The role of the geoid in four-dimensional geodesy. Marine Geodesy 1: 217-252.
MATHER, R.S., E.G. MASTERS, R. COLEMAN (1977): The role of non-tidal gravity variations in the maintenance of reference systems for secular geodynamics. Unisurv G 26: 1-25.
MATHEWS, P.M., V. DEHANT, J.M. GIPSON (1997): Tidal station displacements. JGR 102: 20469-20447.
McADOO, D.C., D.T. SANDWELL (1988): GEOSAT's exact repeat mission. EOS 69: 1569.
McCARTHY, D.D., ed. (1996): IERS Conventions (1996). IERS Techn. Note 21, Paris.
McDONALD, K. (1999): Opportunity knocks: Will GPS modernization open doors ? GPS World 10(9): 36-46.
McKENZIE, D.P., R.L. PARKER (1967): The North Pacific: an example of tectonics on a sphere. Nature 216: 1276-1280.
MEIER, D., R. LÖSER (1986): Das Mekometer ME 5000 – Ein neuer Präzisionsdistanzmesser. Allg. Verm. Nachr. 93: 82-90.
MEIER-HIRMER, B., R. MEIER-HIRMER (1997): Untersuchungen zur intrinsischen Genauigkeit der Digitalnivelliere NA2000/NA3000 und DiNi20/DiNi10. Verm.wesen und Raumordnung 59: 286-295.
MEISSNER, R., TH. WEVER, E.R. FLÜH (1987): The Moho in Europe- implications for crustal development. Annales Geophysicae 5: 357-364.
MELCHIOR, P. (1983): The tides of the planet earth. Pergamon Press, Oxford etc.
MELCHIOR, P. (1994): A new data bank for tidal gravity measurements (DB92). Phys. Earth Planet. Inter. 82: 125-155.
MENGE, F., G. SEEBER, C. VÖLKSEN, G. WÜBBENA, M. SCHMITZ (1998): Results of absolute field calibration of GPS antenna PCV. Proceed. 11th Intern. Techn. Meeting of the Satellite Division of the Institute of Navigation ION GPS-98: 31-38, Nashville, Tennessee.
MERRIAM, J.B. (1992): Atmospheric pressure and gravity. Geophys. J. Int. 109: 488-500.
MERRY, C.L., P. VANIČEK (1974): The geoid and datum translation components. The Canadian Surveyor 28: 56-62.
MILBERT, D.G. (1995): Improvement of a high resolution geoid model in the United States by GPS heighting on NAVD88 benchmarks. Bull. d'Inf. Bur. Gravim. Int. 77 and Int. Geoid Service Bull. 4, New geoids in the world: 13-36, Milan/Toulouse.
MILITZER, H., F. WEBER (1984): Angewandte Geophysik. Springer, Wien-New York.
MINSTER, J.B., T.H. JORDAN (1978): Present-day plate motions. JGR 83: 5331-5354.

MINSTER, J.-F., C. BROSSIER, PH. ROGEL (1995): Variations of the mean sea level from TOPEX/POSEIDON data. JGR 100: 25153-25162.
MISRA, P.N., R.I ABBOT (1994): SGS 85 – WGS 84 transformation. Man Geod. 19: 300-308.
MITCHUM, G. (1994): Comparison of TOPEX sea surface heights and tide gauge sea level. JGR 99: 24541-24553.
MOLODENSKI, M.S. (1958): Grundbegriffe der geodätischen Gravimetrie. Transl. from Russian (1945), VEB Verlag Technik, Berlin 1958.
MOLODENSKI, M.S., V.F. YEREMEYEV, M.I. YURKINA (1962): Methods for study of the external gravitational field and figure of the earth. Transl. From Russian (1960), Israel. Program for Scient. Transl., Jerusalem.
MONTAG, H., CH. REIGBER, eds. (1993): Geodesy and physics of the earth. IAG Symp. Proceed. 112, Springer, Berlin-Heidelberg-New York.
MOONEY, W.D., M.G. LASKE, T.G. MASTERS (1998): CRUST 5.1: a global crust model at 5°x5°. JGR 103: 727-748.
MORELLI, C., C. GANTAR, T. HONKASALO, R.K. MCCONNELL, J.G. TANNER, B. SZABO, U. UOTILA, C.T. WHALEN (1974): The International Gravity Standardization Net 1971 (IGSN71). I.U.G.G.-I.A.G.-Publ.Spec. 4, Paris.
MORGAN, W.J. (1968): Rises, trenches, great faults, and crustal blocks. JGR 73: 1959-1982.
MORITZ, H. (1962): Interpolation and prediction of gravity and their accuracy. OSU Rep. 24, Columbus, Ohio.
MORITZ, H. (1968a): Mass distributions for the equipotential ellipsoid. Boll. Geof. teor. appl. 10: 59-65.
MORITZ, H. (1968b): On the use of the terrain correction in solving Molodensky's problem. OSU Rep. 108, Columbus, Ohio.
MORITZ, H. (1968c): Kinematical geodesy. DGK, A 59, München.
MORITZ, H. (1970): Least-squares estimation in physical geodesy. DGK, A 69, München (OSU Rep. 130, Columbus, Ohio).
MORITZ, H. (1971): Series solution of Molodensky's problem. DGK, A 70, München.
MORITZ, H. (1973): Least squares collocation. DGK, A 75, München.
MORITZ, H. (1974): Precise gravimetric geodesy. OSU Rep. 219, Columbus, Ohio.
MORITZ, H. (1976): Integral formulas and collocation. Man. Geod. 1: 1-40.
MORITZ, H. (1977): Der Begriff der mathematischen Erdgestalt seit Gauß. Allg. Verm. Nachr. 84: 133-138.
MORITZ, H. (1978): Introduction to interpolation and approximation. In Moritz and Sünkel (1978): 1-45.
MORITZ, H. (1980): Advanced physical geodesy. Wichmann, Karlsruhe.
MORITZ, H. (1983): Local geoid determination in mountain regions. OSU Rep. 352, Columbus, Ohio.
MORITZ, H. (1990): The figure of the earth. Wichmann, Karlsruhe.
MORITZ, H. (2000): Geodetic Reference System 1980. J. Geod. 74: 128-133.
MORITZ, H., B. HOFMANN-WELLENHOF (1993): Geometry, relativity, geodesy. Wichmann, Karlsruhe.
MORITZ, H., I.I. MUELLER (1987): Earth rotation. Ungar Publ., New York.
MORITZ, H., H. SÜNKEL (1978): Approximation methods in geodesy. Wichmann, Karlsruhe.

MUELLER, I.I. (1969): Spherical and practical astronomy. Ungar Publ., New York.
MUELLER, I.I. (1988): Reference coordinate systems, an update. OSU Rep. 394, Columbus, Ohio.
MUELLER, I.I., O. HOLWAY III, R.R. KING jr. (1963): Geodetic experiment by means of a torsion balance. OSU Rep. 30, Columbus, Ohio.
MUELLER, I.I., S. ZERBINI, eds. (1989): The interdisciplinary role of space geodesy. Lecture Notes in Earth Sciences 22, Springer, Berlin etc.
MUELLER, ST., ed. (1974): The structure of the earth's crust based on seismic data. Elsevier,Amsterdam etc.
NAGY, D. (1966): The gravitational attraction of a right angular prism. Geophysics 31: 362-371.
NAGY, D., G. PAPP, J. BENEDEK (2000): The gravitational potential and its derivative for the prism. J. Geod. 74: 552-560.
NASA (1983): The Geodynamics Program: An overview. NASA Techn. Paper 2147, Washington, D.C.
NAT. ACAD. SCIENCES (1978): Geodesy: Trend and prospects. Nat. Acad. of Sciences, Comm. on Geodesy, Washington, D.C.
NEREM, R.S. (1995a): Terrestrial and planetary gravity fields. Rev. of Geophys., Suppl.: 469-476.
NEREM, R.S. (1995b): Measuring global mean sea level variations using TOPEX/POSEIDON altimeter data. JGR 100: 25135-25151.
NEREM, R.S., S.M. KLOSKO (1996): Secular variations of the zonal harmonics and polar motion as geophysical constraints. In Rapp et al. (1996): 152-163.
NEREM, R.S., F.J. LERCH, J.A. MARSHALL et al. (1994): Gravity model development for TOPEX/POSEIDON: Joint gravity models 1 and 2. JGR 99: 24421-24447.
NEREM, R.S., C. JEKELI, W.M. KAULA (1995): Gravity field determination and characteristics: Retrospective and prospective. JGR 100: 15053-15074.
NEREM, R.S., K.E. RACHLIN, B.D. HUGHES (1997): Characterization of global mean sea level variations observed by TOPEX/POSEIDON using empirical orthogonal functions. Surv.Geophys. 18: 293-302.
NEUMEYER, J., H.-J. DITTFELD (1997): Results of three year observation with a superconducting gravimeter at the GeoforschungsZentrum Potsdam. J. Geod. 71: 97-102.
NEUMEYER, J., K. HEHL (1995): State-of-the-art and future sensor technology for airborne gravimetry. In Sünkel and Marson (1995): 151-160.
NIEBAUER, T.M. (1988): Correcting gravity measurements for the effects of local air pressure. JGR 93: 7989-7991.
NIEBAUER, T.M. (1989): The effective measurement height of free-fall absolute gravimeters. Metrologia 26: 115-118.
NIEBAUER, T.M., G.S. SASAGAWA, J.E. FALLER, R. HILT, F. KLOPPING (1995): A new generation of absolute gravimeters. Metrologia 32: 159-180.
NIELL, A.E. (1996): Global mapping functions for the atmospheric delay of radio wavelengths. JGR 101: 3227-3246.
NIELSEN, C.S., R. FORSBERG, S. EKHOLM, J.J. MOHR (1998): SAR interferometry for improved terrain corrections in surface and airborne gravimetry. In Forsberg et al. (1998): 529-534.

NIMA (2000): Department of Defense World Geodetic System 1984. National Imagery and Mapping Agency Technical Report TR 8350.2, 3.ed., Washington, D.C.

NOAA (1966): US Standard Atmosphere Supplements, 1966. Nat. Techn. Inf. Service, US Dept. of Comm., Springfield, Va., U.S.A.

NOAA (1976): US Standard Atmosphere 1976. Nat. Techn. Inf. Service, US Dept. of Comm., Springfield, Va., U.S.A.

OWEN, S., P. SEGALL, M. LISOWSKI, A. MIKLIUS, R. DENLINGER, M. SAKO (2000): Rapid deformation of Kilauea volcano: Global Positioning System measurements between 1990 and 1996. JGR 105: 18983-18998.

PAIK, H.J., J.-S. LEUNG, S.H. MORGAN, J. PARKER (1988): Global gravity survey by an orbiting gravity gradiometer. EOS 69: 1601, 1610-1611.

PAIK, H.J., E.R. CANAVAN, M.V. MOODY (1997): Airborne/Shipborne SGG Survey System. In Cannon and Lachapelle (1997): 565-570.

PAQUET, P., J. FLICK, B. DUCARME, eds. (1990): GPS for geodesy and geodynamics. Cahiers du Centre Européen de Géodynamique et de Séismologie 2, Luxembourg.

PAUL, M.K. (1978): Recurrence relations for the integrals of associated Legendre functions. Bull. Géod. 52: 177-190.

PAVLIS, N.K., R.H. RAPP (1990): The development of an isostatic gravitational model to degree 360 and ist use in global gravity field modeling. Geophys. J. Int. 100: 369-378.

PAVLIS, N.K., J.C. CHAN, F. LERCH (1996): Alternative estimation techniques for global high-degree modeling. In Rapp et al. (1996): 111-120.

PELZER, H., ed. (1980): Geodätische Netze in Landes- und Ingenieurvermessung. Wittwer, Stuttgart.

PELZER, H., W. NIEMEIER, eds. (1987): Determination of heights and height changes. Dümmler, Bonn.

PESCHEL, H. (1974): Das motorisierte Präzisionsnivellement – leistungsfähigstes Verfahren genauer Höhenmessungen. Vermessungstechnik 22: 57-64.

PETER, G., R.E. MOOSE, C.W. WESSELS, J.E. FALLER, T.M. NIEBAUER (1989): High-precision absolute gravity observations in the United States. JGR 94: 5659-5674.

PHILLIPS, R.J., K. LAMBECK (1980): Gravity fields of the terrestrial planets: Long-wavelength anomalies and tectonics. Rev. Geophys. 18: 27-76.

PICK, M., J. PICHA, V. VYSCOCIL (1973): Theory of the earth's gravity field. Elsevier Scient. Publ. Co., Amsterdam-London-New York..

PLAG, H.P., B. AMBROSIUS, T.F. BAKER et al. (1998): Scientific objectives of current and future WEGENER activities. In Zerbini et al. (1998): 177-223.

PODER, K., H. HORNIK, eds. (1989): The European Datum 1987 (ED87). IAG RETRIG Subcomm., Publ. No.18, München.

POITEVIN, C., ed. (1991): Proceed. of the Workshop: Non tidal gravity changes - Intercomparison between absolute and superconducting gravimeters. Cahiers du Centre Europeén de Géodynamique et de Séismologie3, Luxembourg.

POITEVIN, C., ed. (1995): Proceed. of the Second Workshop: Non tidal gravity changes – Intercomparison between absolute and superconducting gravimeters. Cahiers du Centre Européen de Géodynamique et de Séismologie 11, Luxembourg.

RAPP, R.H. (1978): Results of the application of least-squares collocation to selected geodetic problems. In H. Moritz and H. Sünkel (1978): 117-156.

RAPP, R.H. (1983a): The need and prospects for a world vertical datum. In Proceed. IAG Symp. XVIII, IUGG Gen. Ass. Hamburg 1983, vol. 2 : 432-445, Dep. of Geod. Science and Surveying, The Ohio State Univ., Columbus, Ohio.

RAPP, R.H. (1983b): Tidal gravity computations based on recommendations of the Standard Earth Tide Committee. Bull. d'Inf. Marées Terrestres 89: 5814-5819.

RAPP, R.H. (1995a): A world vertical datum proposal. Allg. Verm. Nachr. 102: 297-304.

RAPP, R.H. (1995b): Separation between reference surfaces of selected vertical datums. Bull. Géod. 69: 26-31.

RAPP, R.H. (1995c): Equatorial radius estimates from Topex altimeter data. In: Erwin Groten 60 Festschrift:90-97, Publ. Inst. of Geodesy and Navigation, University FAF Munich.

RAPP, R.H. (1997): Global models for the 1 cm geoid – present status and near term prospects. In Sansò and Rummel (1997): 273-311.

RAPP, R.H. (1998): Past and future developments in geopotential modelling. In Forsberg et al. (1998): 58-78.

RAPP, R.H., N. BALASUBRAMANIA (1992): A conceptual formulation of a world height system. OSU Rep. 421, Columbus, Ohio.

RAPP, R.H., N.K. PAVLIS (1990): The development and analysis of geopotential coefficient models to spherical harmonic degree 360. JGR 95: 21885-21911.

RAPP, R.H., Y. YI (1997): Role of ocean variability and dynamic ocean topography in the recovery of the mean sea surface and gravity anomalies from satellite altimeter data. J. Geod. 71: 617-629.

RAPP, R.H., Y.M. WANG, N. PAVLIS (1991): The Ohio State 1991 geopotential and surface topography harmonic coefficient models. OSU Rep. 410, Columbus, Ohio.

RAPP, R.H., A.A. CAZENAVE, R.S. NEREM, eds. (1996): Global gravity field and its temporal variations. IAG Symp. Proceed. 116, Springer, Berlin-Heidelberg-New York.

RAY, J., ed. (1999): IERS analysis campaign to investigate motions of the geocenter. IERS Techn. Note 25, Paris.

REIGBER, C., M. FEISSEL (1997): IERS missions, present and future. Report on the 1996 IERS workshop. IERS Techn. Note 22, Paris.

REIGBER, CH., H. LÜHR, P. SCHWINTZER (2000): Status of the CHAMP mission. In Rummel et al. (2000a): 63-65.

RICHTER, B. (1987): Das supraleitende Gravimeter. DGK, C 329, Frankfurt a.M.

RICHTER, B. (1995): Cryogenic gravimeters: Status report on calibration, data acquisition and environmental effects. In Poitevin (1995): 125-146, Luxembourg.

RICHTER, B., H. WILMES, I. NOWAK (1995): The Frankfurt calibration system for relative gravimeters. Metrologia 32: 217-223.

RICHTER, BU. (1995): Die Parametrisierung der Erdorientierung. ZfV 120: 109-119.

RIKITAKE, T. (1982): Earthquake forecasting and warning. Center for Acad. Publ. Japan/Tokyo-Reidel Publ. Co., Dordrecht-Boston-London.

RINNER, K. (1977): Über geometrische Aufgaben der Meeresgeodäsie. ZfV 102: 354-366.

RIZOS, C. (1982): The role of the geoid in high precision geodesy and oceanography. DGK, A 96, München.

ROBBINS, J.W., D.E. SMITH, C. MA (1993): Horizontal crustal deformation and large scale plate motions inferred from space geodetic techniques. In Smith and Turcotte (1993): 21-36.

ROBERTSON, D.S., W.E. CARTER, J. CAMPBELL, H. SCHUH (1985): Daily earth rotation determinations from IRIS very long baseline interferometry. Nature 316: 424-427.

ROBERTSSON, L., O. FRANCIS, T. VAN DAM et al. (2001): Results from the fifth international comparison of absolute gravimeters, ICAG'97. Metrologia (in press).

RÖDER, R.H., M. SCHNÜLL, H.-G. WENZEL (1985): Gravimetry with an electrostatic feedback system. Bull. d'Inf. Bureau Gravim. Int. 57: 72-81.

RÖDER, R.H., M. SCHNÜLL, H.-G. WENZEL (1988): SRW feedback for LaCoste-Romberg gravimeters with extended range. Bull. d'Inf. Bureau Gravim. Int. 62: 46-50.

ROTHACHER, M., G. BEUTLER, T.A. HERRING, R. WEBER (1999): Estimation of nutation using the Global Positioning System. JGR 104: 4835-4859..

RÜEGER, J.M. (1997): Electronic distance measurements, an introduction. 4.ed., Springer, Berlin-Heidelberg-New York.

RÜEGER, J.M., F.K. BRUNNER (1982): EDM-height traversing versus geodetic leveling. The Canadian Surveyor 36: 69-88.

RÜEGER, J.M., F.K. BRUNNER (2000): On system calibration and type testing of digital levels. ZfV 125: 120-130.

RUMMEL, R. (1979): Determination of short-wavelength component of the gravity field from satellite-to-satellite tracking or satellite gradiometry – an attempt to an identification of problem areas. Man. Geod. 4: 107-148.

RUMMEL, R.(1986): Satellite gradiometry. In Sünkel (1986a): 317-363.

RUMMEL, R., R.G. HIPKIN, eds. (1990): Gravity, gradiometry, and gravimetry. IAG Symp. Proceed. 103, Springer, New York-Berlin-Heidelberg.

RUMMEL, R., K.H. ILK (1995): Height datum connection – the ocean part. Allg. Verm. Nachr. 102: 321-330.

RUMMEL, R., P. TEUNISSEN (1988): Height datum definition, height datum connection and the role of the geodetic boundary value problem. Bull. Géod. 62: 477-498.

RUMMEL, R., CH. REIGBER, K.H. ILK (1978): The use of satellite-to-satellite tracking for gravity parameter recovery. Proc. ESA Workshop on Space Oceanography, Navigation and Geodynamics (SONG), ESA-SP-137: 151-161.

RUMMEL, R., R.H. RAPP, H. SÜNKEL, C.C. TSCHERNING (1988): Comparison of global topographic-isostatic models to the earth's observed gravity field. OSU Rep. 388, Columbus, Ohio.

RUMMEL, R., F. SANSÒ, M. VAN GELDEREN et al. (1993): Spherical harmonic analysis of satellite gradiometry. Netherl. Geodetic Comm., Publ. on Geodesy, New Series 39, Delft.

RUMMEL, R., H. DREWES, W. BOSCH, H. HORNIK, eds. (2000a): Towards an integrated global geodetic observing system (IGGOS). IAG Symp. Proceed. 120, Springer, Berlin-Heidelberg-New York.

RUMMEL, R., J. MÜLLER, H. OBERNDORFER, N. SNEEUW (2000b): Satellite gravity gradiometry with GOCE. In Rummel et al. (2000a): 66-72.

RUNCORN, S.K. (1962): Convection currents in the earth's mantle. Nature 195: 1248-1249.

RUNDLE, J.B., J.H. WHITCOMB (1986): Modeling gravity and trilateration data in Long Valley, California, 1983-1984. JGR 91: 12675-12682..

RYMER, H., C.A. LOCKE (1995): Microgravity and ground deformation precursors to eruption: a review. In Barthelemy et al. (1995): 21-39.

SAASTOMAINEN, J. (1972/1973): Contributions to the theory of atmospheric refraction. Bull. Géod. 105: 279-298, 106: 383-397, 107: 13-34.

SACHER, M., J. IHDE, H. SEEGER (1999): Preliminary transformation relations between national European height systems and the United European Levelling Network (UELN). In Gubler et al. (1999): 80-86.

SAKUMA. A. (1983): An industrialized absolute gravimeter: Type GA 60. Bull.d'Inf. Bureau Gravim. Int. 53: 114-118.

SALSTEIN, D.A., B. KOLACZEK, D. GAMBIS, eds. (1999): The impact of El Niño and other low-frequency signals on earth rotation and global earth system parameters. IERS Techn. Note 26, Paris.

SANDWELL, D., W. SMITH (1997): Marine gravity anomaly from Geosat and ERS-1 altimetry. JGR 102: 10039-10054.

SANSÒ, F. (1981): Recent advances in the theory of the geodetic boundary value problem. Rev. Geophys. and Space Physics 19: 437-449.

SANSÒ, F. (1988): The Wiener integral and the overdetermined boundary value problems of physical geodesy. Man. Geod. 13: 75-98.

SANSÒ, F. (1995): The long road from measurements to boundary value problem in physical geodesy. Man. Geod. 20: 326-344.

SANSÒ, F., R. RUMMEL, eds. (1989): Theory of satellite geodesy and gravity field determination. Lecture Notes in Earth Sciences 25, Springer, Berlin-New York.

SANSÒ, F., R. RUMMEL, eds. (1997): Geodetic boundary-value problems in view of the one centimeter geoid. Lecture Notes in Earth Sciences 65, Springer, Berlin-Heidelberg-New York.

SATO, T., J.C. HARRISON (1990): Local effects on tidal strain measurements at Esashi, Japan. Geophys. J. Int. 102: 513-526.

SATOMURA, M., I. NAKAGAWA, H. TSUKAMOTO, T. HIGASHI, Y. FUKUDA, K. NAKAMURA (1986): Secular changes of gravity observed in Kinki district, Japan. Bull. d'Inf. Bur. Gravim. Int. 59: 215-223.

SAVAGE, J.C., W.H. PRESCOTT, M. LISOWSKI (1987): Deformation along the San Andreas Fault 1982-1986 as indicated by by frequent geodolite measurements. JGR 92: 4785-4797.

SCHERER, M. (1985): Der Präzisionsdistanzmesser CR204 Geomensor – Funktionsprinzip und erste Felderprobungen. ZfV 110: 135-145..

SCHLEMMER, H. (1984): A new technique to produce precise graduation on invar tape. In H. Pelzer and W. Niemeier, eds. (1984), Precise leveling: 119-125, Dümmler, Bonn.

SCHLEMMER, H. (1996): Grundlagen der Sensorik. Wichmann-Hüthig, Heidelberg.

SCHMID, H. (1974): Worldwide geometric satellite triangulation. JGR 79: 5349-5376.

SCHMIDT, H. (1999): Lösung der geodätischen Hauptaufgaben auf dem Rotationsellipsoid mittels numerischer Integration. ZfV 124: 121-128, 169.

SCHMIDT, R. (1995): Referenz- und Koordinatensysteme in der deutschen Grundlagen-Vermessung. Nachr. a.d. öffentl. Verm.wesen Nordrhein-Westfalen: 23-67.

SCHNÄDELBACH, K. (1974): Entwicklungstendenzen in Rechenverfahren der mathematischen Geodäsie. ZfV 99: 421-430.

SCHNEIDER, M. (1988): Satellitengeodäsie. BI Wissenschaftsverlag, Mannheim-Wien-Zürich.

SCHNEIDER, M. (1992/1993): Himmelsmechanik Bd.I(3.Aufl.1992)/Bd.II(1993). BI Wissenschaftsverlag, Mannheim-Leipzig-Wien-Zürich.

SCHÖDLBAUER, A. (2000): Geodätische Astronomie. De Gruyter, Berlin-New York.

SCHUH, H., R. HAAS (1998): Earth tides in VLBI observations. In Ducarme and Paquet (1998): 101-110.

SCHÜLER, R., G. HARNISCH, H. FISCHER, R. FREY (1971): Absolute Schweremessungen mit Reversionspendeln in Potsdam 1968-1969. Veröff. Zentralinst. Physik der Erde 10, Potsdam.

SCHUTZ, B.E., A. ANDERSON, C. FROIDEVAUX, M. PARKE, eds. (1994): Gravimetry and space techniques applied to geodynamics and ocean dynamics. Geophys. Monograph 82, IUGG vol.17, AGU/IUGG, Washington, D.C.

SCHWARZ, C.R. (1969): The use of short arc orbital constraints in the adjustment of geodetic satellite data. OSU Rep. 118, Columbus, Ohio.

SCHWARZ, C.R. (1989): North American Datum of 1983. NOAA Profess. Paper NOS 2, Nat. Geod. Survey, Rockville, Md.

SCHWARZ, C.R., E.B. WADE (1990): The North American Datum of 1983: Project methodology and execution. Bull. Géod. 64: 28-62.

SCHWARZ, K.-P. (1975): Zur Erdmessung des Eratosthenes. Allg. Verm. Nachr. 82: 1-12.

SCHWARZ, K.-P., ed. (1986): Inertial technology for surveying and geodesy. Proc. Third Intern. Symp, Banff, Canada 1985. The Division of Surveying Eng., The Univ. of Calgary.

SCHWARZ, K.-P. (2000a): An analysis of the current IAG structure and some thoughts on an IAG focus. In Schwarz (2000b): 407-414.

SCHWARZ, K.-P., ed. (2000b): Geodesy beyond 2000: The challenges of the first decade. IAG Symp. Proceed. 121, Springer, Berlin-Heidelberg-New York.

SCHWARZ, K-.P., M.G. SIDERIS, R. FORSBERG (1990): The use of FFT techniques in physical geodesy. Geophys. J. Int. 100: 485-514.

SCHWIDERSKI, E.W. (1980): On charting global ocean tides. Rev. Geophys. 18: 243-268.

SCHWIDERSKY, E.W. (1983): Atlas of ocean tidal charts and maps, part I: The semidiurnal principal lunar tide M2. Marine Geodesy 6: 219-266.

SCHWINTZER, P., C. REIGBER, A. BODE et al. (1997): Long- wavelength global gravity field models: GRIM4-S4, GRIM4-C4. J. Geod. 71: 189-208.

SEEBER, G. (1993): Satellite geodesy. De Gruyter, Berlin-New York.

SEEBER, G., W, TORGE (1985): Zun Einsatz transportabler Zenitkameras für die Lotabweichungsbestimmung. ZfV 110: 439-450.

SEEBER, G., D. EGGE, M. HOYER, H.W. SCHENKE, K.H. SCHMIDT (1982): Einsatzmöglichkeiten von Doppler- Satellitenmessungen. Allg. Verm. Nachr. 89: 373-388.

SEEBER, G., D. EGGE, A. SCHUCHARDT, J SIEBOLD, G. WÜBBENA (1985): Experiences with the TI 4100 NAVSTAR Navigator at the University of Hannover, Proceed. First Int. Symp. on Positioning and GPS, I: 215-226, Rockville, Md.

SEEBER, G., F. MENGE, C. VÖLKSEN, G. WÜBBENA, M. SCHMITZ (1998): Precise GPS positioning improvements by reducing antenna and site dependent effects. In Brunner (1998): 237-244.

SEEBER, H., Y. ALTINER, G. ENGELHARDT, P. FRANKE, H. HABRICH, W. SCHLÜTER (1998): EUREF – 10 Jahre Aufbauarbeit an einem neuen geodätischen Bezugssystem für Europa. BKG Mitt. Band 1 Geodätische Vernetzung Europas: 9-51, Frankfurt a.M.

SEGAWA, J., H. FUJIMOTO, S. OKUBO, eds. (1997): Gravity, geoid and marine geodesy. IAG Symp. Proceed. 117, Springer, Berlin-Heidelberg-New York.

SEIDELMANN, K.P., ed. (1992): Explanatory supplement to the astronautical almanac. Univ. Science Books, Mill Valley, Cal., U.S.A.

SHUM, C.K., P.L.WOODWORTH, O.B. ANDERSEN et al. (1997): Accuracy assessment of recent ocean tidal models. JGR 102: 25173-25194.

SIDERIS, M. (1985): A fast Fourier transform method for computing terrain corrections. Man. Geod. 10: 66-71.

SIDERIS, M.G. (1990): Rigorous gravimetric terain modelling using Molodensky's operator. Man. Geod. 15: 97-106.

SIGL, R. (1985): Introduction to potential theory. Abacus Press, Cambridge.

SIGL, R., W. TORGE, H. BEETZ, K. STUBER (1981): Das Schweregrundnetz 1976 der Bundesrepublik Deutschland (DSGN76). DGK, B 254, München.

SIGMUNDSSON, F., H. VADON, D. MASSONET (1997): Readjustment of the Krafla spreading segment to crustal rifting measured by Satellite Radar Interferometry. Geophys. Res. Letters 24: 1843-1846.

SILVERBERG, E.C. (1978): Mobile satellite ranging. In I.I. Mueller, ed. (1978), Applications of geodesy to geodynamics, OSU Rep. 280: 41-46, Columbus, Ohio.

SIMPSON, R.W., R.C. JACHENS, R.J. BLAKELEY (1986): A new isostatic residual gravity map of the conterminous United States with a discussion on the significance of isostatic residual anomalies. JGR 91: 8348- 8372.

SJÖBERG, L.E. (1979): Integral formulas for heterogeneous data in physical geodesy. Bull. Géod. 53: 297-315.

SJÖBERG, L.E. (1999): An efficient iterative solution to transform rectangular geocentric coordinates to geodetic coordinates. ZfV 124: 295-297. .

SKEELS, D.C. (1947): Ambiguity in gravity interpretation. Geophysics 12: 43-56.

SLATER, L.E. (1983): A long-baseline two-fluid tiltmeter. EOS 64: 208.

SLATER, J.A., S. MALYS (1998): WGS 84 – past, present and future. In Brunner (1998): 1-7.

SMITH, J.R. (1986): From plane to spheroid. Landmark Enterprises, Rancho Cordova, CA, U.S.A.

SMITH, D.A., D.G. MILBERT (1999): The GEOID96 high resolution geoid model for the United States. J. Geod. 73: 219-236.

SMITH, D.A., D.R. ROMAN (2000): Recent advances in the acquisition and use of terrain data for geoid modelling over the United States. In Schwarz (2000b): 107-111.
SMITH, D.A., D.R. ROMAN (2001): GEOID99 and G99SSS: One arc-minute geoid models for the United States. J. Geod. (in press).
SMITH, W.H., D.T. SANDWELL (1994): Bathymetric prediction from dense satellite altimetry and sparce shipboard bathymetry. JGR 99: 21803-21824.
SMITH, D., D. TURCOTTE, eds. (1993): Contributions of space geodesy to geodynamics: Crustal dynamics. AGU, Washington, D.C.
SMITH, D.E., R. KOLENKIEWICZ, P.J. DUNN, M.H. TORRENCE (2000): Earth scale below a part per billion from satellite laser ranging. In Schwarz (2000b): 3-12.
SNAY, R.A. (1986): Network design strategies applicable to GPS surveying using three or four receivers. Bull. Géod. 60: 37-50.
SNAY, R.A. (1990): Accuracy analysis for the NAD83 Geodetic Reference System. Bull. Géod. 64: 1-27.
SNEEUW, N., K.H. ILK (1997): The status of spaceborne gravity field mission concepts: a comparative simulation study. In Segawa et al. (1997): 171-178.
SOLLER, D.R., R.D. RAY, R.D. BROWN (1982): A new global crustal thickness map. Tectonics 1: 125-149.
SOLOMON, S.C., N.H. SLEEP (1974): Some simple physical models for absolute plate motions. JGR 79: 2557-2567.
SOUDARIN, L., J.F. CRETAUX, A. CAZENAVE (1999): Vertical crustal motions from the DORIS space-geodesy system. Geophys. Res. Letters 26: 1207-1210.
SPRATT, R.S. (1982). Modelling the effect of atmospheric pressure variations on gravity. Geophys. J. R. Astr. Soc. 71: 173-186.
STACEY, F.D. (1992): Physics of the earth. Brookfield Press, Brisbane.
STEIN, R.S. (1987): Contemporary plate motion and crustal deformation. Rev. Geophys. 25: 855-863.
STEPHENSON, F.R., L.V. MORRISON (1994): Long-term fluctuations in the earth's rotation: 700 BC to AD 1990. Phil. Trans. Royal Soc. London, A 313: 47-70.
STOKER, J.J. (1969): Differential geometry. Wiley-Interscience, New York.
STOKES, G.G. (1849): On the variation of gravity on the surface of the earth. Trans. Cambridge Phil. Soc. 8: 672-695.
STRANG VAN HEES, G.L. (1977): Zur zeitlichen Änderung von Schwere und Höhe. ZfV 102: 444-450.
STRASSER, G. (1957): Ellipsoidische Parameter der Erdfigur. DGK, A 19, München.
STRYKOWSKI, G. (1998): Geoid and mass density- why and how. In Forsberg et al. (1998): 237-242.
STURGES, W. (1974): Sea level slopes along continental boundaries. JGR 79: 825-830.
SUBIZA, W.H., W. TORGE, L. TIMMEN (1998): The national gravimetric network of Uruguay. In Forsberg et al. (1998): 51-57.
SÜNKEL, H., ed. (1986a): Mathematical and numerical techniques in physical geodesy. Lecture Notes in Earth Sciences 7, Springer, Berlin-Heidelberg-New York.
SÜNKEL, H. (1986b): Global topographic-isostatic models. In Sünkel (1986a): 417-462.
SÜNKEL, H. (1988): Digital height and density model and its use for orthometric height and gravity field determination for Austria. Boll. di Geod. e Scienze Affini 47: 139-144.

SÜNKEL, H. (1997): GBVP-classical solutions and implementation. In Sansò and Rummel (1997): 219-237.

SÜNKEL, H., I. MARSON, eds. (1995): Gravity and geoid. IAG Symp. Proceed. 113, Springer, Berlin-Heidelberg-New York.

TAKEMOTO, S. (1991): Some problems on detection of earthquake precursors by means of continuous monitoring of crustal strains and tilts. JGR 96: 10377-10390.

TALWANI, M., G.H. SUTTON, J.L. WORZEL (1959): A crustal section across the Puerto Rico trench. JGR 64: 1545-1555.

TALWANI, M., X. LE PICHON, M. EWING (1965): Crustal structure of the mid-ocean ridges. 2: Computed model from from gravity and seismic refraction data. JGR 70: 341-352.

TANIMOTO, T. (1995): Crustal structure of the earth. In Ahrens (1995): 214-224.

TAPLEY, B.D., G.H. BORN, M.E. PARKE (1982): The Seasat altimeter data and its accuracy assessment. JGR 87: 3179-3188.

TAPLEY, B.D., D.P. CHAMBERS, C.K. SHUM, R.J. EANES, J.C. RIES, R.H. STEWART (1994): Accuracy assessment of the large-scale dynamic ocean topography from TOPEX/POSEIDON altimetry. JGR 99: 24605-24617.

TAPLEY, B.D., J.C. RIESS, G.W. DAVIS et al. (1995): Precise orbit determination for TOPEX/POSEIDON. JGR 99: 24383-24404.

TAPLEY, B.D., M.M. WATKINS, J.C. RIESS et al. (1996): The Joint Gravity Model 3. JGR 101:28029-28049.

TEISSEYRE, R., ed. (1989): Gravity and low-frequency geodynamics. Elsevier, Amsterdam etc.

TEUNISSEN, P.J.G., A. KLEUSBERG, eds. (1998a): GPS for geodesy. 2nd ed., Springer, Berlin-Heidelberg-New York.

TEUNISSEN, P.J.G., A. KLEUSBERG (1998b): GPS observations and positioning concepts. In Teunissen and Kleusberg (1998a): 187-229.

THAYER, G.D. (1974): An improved equation for the radio refractive index of air. Radio Science 9: 803-807.

TIMMEN, L., H.-G. WENZEL (1994a): Improved gravimetric earth tide parameters for station Hannover. Bull. d'Inf. Marées Terrestres 119: 8834-8846.

TIMMEN, L., H.-G. WENZEL (1994b): Worldwide synthetic gravity tide parameters available on INTERNET. Bull. d'Inf. Bur. Gravim. Int. 73: 32-40.

TIMMEN, L., G. BOEDECKER, U. MEYER (1998): Flugzeuggestützte Vermessung des Erdschwerefeldes. ZfV 123: 378-384.

TODHUNTER, I. (1873): A history of the mathematical theories of attraction and the figure of the earth. Macmillan and Co. (reprint Dover Publ., New York 1962).

TOLKATCHEV, A. (1996): Global Sea Level Observing System (GLOSS). Marine Geodesy 19: 21-62.

TOMODA, Y., H. FUJIMOTO (1981): Gravity anomalies in the western Pacific and geophysical interpretation. J. Phys. Earth 29: 387-419.

TORGE, W. (1977): Untersuchungen zur Höhen- und Geoidbestimmung im dreidimensionalen Testnetz Westharz. ZfV 102: 173-186.

TORGE, W. (1980a): Drei- und zweidimensionale Modellbildung. In Pelzer (1980): 113-130.

TORGE, W. (1980b): Geodätisches Datum und Datumstransformation. In Pelzer (1980): 131-140.

TORGE, W. (1984): Observation strategy and –technique in gravimetry. In B.G. Harsson, ed. (1984), Optimization of geodetic operations: 126-210, Norges Geografiske Oppmäling, Publ.3.

TORGE, W. (1986): Gravimetry for monitoring vertical crustal movements: potential and problems. Tectonophysics 130: 385-393.

TORGE, W. (1989): Gravimetry. De Gruyter, Berlin-New York.

TORGE, W. (1990): Approaching the "cm-geoid" – strategies and results. Mitt. Geod. Inst. TU Graz 67: 1-9.

TORGE, W. (1991): The present state of absolute gravimetry. In Poitevin (1991): 9-22, Luxembourg.

TORGE, W. (1993): Gravimetry and tectonics. In Kakkuri (1993a): 131-172.

TORGE, W. (1996): The International Association of Geodesy (IAG) – More than 130 years of international cooperation. J. Geod.70: 840-845.

TORGE, W. (1997): Von Gauss zu Baeyer und Helmert – Frühe Ideen und Initiativen zu einer europäischen Geodäsie. In H. Junius und K. Kröger (eds.), Europa wächst zusammen: 39-65, Wittwer, Stuttgart.

TORGE, W. (1998): The changing role of gravity reference networks. In Forsberg et al. (1998): 1-10.

TORGE, W., H.-G. WENZEL (1978): Dreidimensionale Ausgleichung des Testnetzes Westharz. DGK, B 234, München.

TORGE, W., G. WEBER, H.-G. WENZEL (1984): 6'x10' free air gravity anomalies of Europe including marine areas. Marine Geophys. Res. 7: 93-111.

TORGE, W., R.H. RÖDER, M. SCHNÜLL, H.-G. WENZEL, J.E. FALLER (1987): First results with the transportable absolute gravity meter JILAG-3. Bull. Géod. 61: 161-176.

TORGE, W., T. BASIC, H. DENKER, J. DOLIFF, H.-G. WENZEL (1989): Long range geoid control through the European GPS traverse. DGK, B 290, München.

TORGE, W., T. GROTE, R.H. RÖDER, M. SCHNÜLL, H.-G. WENZEL (1992): Introduction of absolute gravimetric techniques into a high-precision gravity and vertical control system in northern Iceland.DGK, B 297, München.

TORGE, W., R. FALK, A. FRANKE, E. REINHART, B. RICHTER, M. SOMMER, H. WILMES (1999a): Das Deutsche Schweregrundnetz 1994 (DSGN94). DGK, B 309, München.

TORGE, W., M. SCHNÜLL, L. TIMMEN, JIA MINYU, XING CANFEI, LI HUI (1999b): Absolute and relative gravimetry 1990/1992/1995 in the WesternYunnan Earthquake Prediction Experimental Area. DGK, B 307, München.

TRYGGVASON, E. (1994): Surface deformation at the Krafla volcano, North Iceland, 1982-1992. Bull. of Volcanology 56: 98-107.

TSCHERNING, C.C. (1976): Covariance expressions for second and lower order derivatives of the anomalous potential. OSU Rep. 225, Columbus, Ohio.

TSCHERNING, C.C., R. FORSBERG (1986): Geoid determination in the Nordic countries from gravity and height data. Proceed. Int. Symp. on the Definition of the Geoid, vol. 1: 325-352, Ist. Geogr. Mil. Ital., Firenze.

TSCHERNING, C.C., R.H. RAPP (1974): Closed covariance expressions for gravity anomalies, geoid undulations, and deflections of the vertical implied by anomaly degree variance models. OSU Rep. 208, Columbus, Ohio.

TSCHERNING, C.C., R.H. RAPP, C.C. GOAD (1983): A comparison of methods for computing gravimetric quantities from high degree spherical harmonic expansions. Man. Geod. 8:249-272.

TSUJI, H., Y. HATANAKA, T. SAGIYA, M. HASHIMOTO (1995): Coseismic crustal deformation from the 1994 Hokkaido-Toho-Oki earthquake monitored with a nationwide continuous GPS array in Japan. Geophys. Res. Lett. 22: 1669-1672.

TURNER, S., ed. (1987): Applied geodesy. Springer, Berlin-Heidelberg-New York.

VÄISÄLÄ, Y. (1946): An astronomic method of triangulation. Sitz. Ber. Finn. Akad. der Wiss.schaften 8: 99-107.

VAN DAM, T.M., J.M. WAHR (1987): Displacement of the earth's surface due to atmosperic loading: effects on gravity and baseline measurements. JGR 92: 1281-1286.

VAN GELDEREN, M., R. HAAGMANS, M. BILKER (1999): Gravity changes and natural gas extraction in Groningen. Geophysical Prospecting 47: 979-994.

VAN GYSEN, H., R. COLEMAN (1997): On the satellite crossover problem. J. Geod. 71: 83-96.

VAN RUYMBEKE, M. (1976): Sur un pendule horizontal équipé d'un capteur de déplacement a capacité variable. Bull. Géod. 50: 281-290.

VANIČEK, P., N.T. CHRISTOU (1994): Geoid and its geophysical interpretations. CRC Press, Boca Raton etc.

VANIČEK, P., E.J. KRAKIWSKY (1986): Geodesy: The concepts. 2.rev. ed., Elsevier Science Publ., Amsterdam-New York.

VANIČEK, P., C.L. MERRY (1973): Determination of the geoid from deflections of the vertical using a least squares surface fitting technique. Bull. Géod. no. 109: 261-280.

VANIČEK, P., D.E. WELLS (1974): Positioning of horizontal geodetic datums. The Canadian Surveyor 28: 531-538.

VASCO, D.W., C. TAYLOR (1991): Inversion of airborne gravity gradient data, southwestern Oklahoma. Geophysics 56: 90-101.

VENING-MEINESZ, F.A. (1928): A formula expressing the deflection of the plumb-lines in the gravity anomalies and some formulae for the gravity field and the gravity potential outside the geoid. Proc. Koninkl. Akad. Wetenschaft 31: 315-331, Amsterdam.

VENING-MEINESZ, F.A. (1931): Une nouvelle méthode pour la réduction isostasique régionale de l'intensité de la pesanteur. Bull. Géod. no. 29:33-51.

VENING-MEINESZ, F.A. (1950): New formulas for systems of deflections of the plumb-line and Laplace's theorem.-Changes of deflections of the plumb-line brought about by a change of the reference ellipsoid. Bull. Géod. no. 15: 33-51.

VILLARCEAU, Y. (1868): Nouveau théoremè sur les attractions locales. Compt. Rend. Hebd. des Séances de L'Acad. des Sciences 67: 1275-1281, Paris.

VINCENTY, T. (1975): Direct and inverse solutions of geodesics on the ellipsoid with application of nested equations. Survey Review 23: 88-93.

VINCENTY, T. (1980): Height-controlled three-dimensional adjustment of horizontal networks. Bull. Géod. 54: 37-43.

VINCENTY, T. (1982): Methods of adjusting space systems data and terrestrial measurements. Bull. Géod. 56: 231-241.

VINE, F.J., D.H. MATTHEWS (1963): Magnetic anomalies over ocean ridges. Nature 199: 947-949.

VIRTANEN, H. (2000): On the observed hydrological environmental effects on gravity at the Metsähovi station, Finland. In Ducarme and Barthelemy (2000): 169-175, Luxembourg.

VÖLKSEN, C. (2000): Die Nutzung von GPS für die Deformationsanalyse in regionalen Netzen. Wiss. Arb. Univ. Hannover 237.

WAALEWIJN, A. (1964): Hydrostatic levelling in the Netherlands. Survey Review 17: 212-221, 267-276.

WAALEWIJN, A. (1986): Der Amsterdamer Pegel. Österr. Z. für Verm.wesen und Photogrammetrie 74: 264-270.

WAGNER, C.A., D.C. MCADOO (1986): Time variations in the earth's gravity field detectable with Geopotential Research Mission intersatellite tracking. JGR 91: 8373-8386.

WAHR, J. (1981): Body tides on an elliptical, rotating, elastic and oceanless earth. Geophys. J. R. Astr. Soc. 64: 677-704.

WAHR, J. (1995): Earth tides. In Ahrens (1995): 40-46.

WANG, Y.M (1999): On the ellipsoidal corrections to gravity anomalies using the inverse Stokes integral. J. Geod. 73: 29-34.

WANNINGER, L. (1995): Enhancing differential GPS using regional ionospheric error models. Bull. Géod. 69: 283-291.

WANNINGER, L. (1996): Präzise GPS-Positionierung in regionalen Netzen permanenter Referenzstationen. ZfV 121: 441-454.

WANNINGER, L. (2000): Präzise Positionierung in regionalen GPS-Referenzstationsnetzen. DGK, C 508, München.

WARBURTON, R.J., E.W. BRINTON (1995): Recent developments in GWR instruments' superconducting gravimeters. In Poitevin (1995): 23-56, Luxembourg.

WEBB, F.H., J.F.ZUMBERGE (1997): An introduction to GIPSY/OASIS –II- precision software for the analysis of data from the Global Positioning System. Doc., Jet Propulsion Laboratory, California Institute of Technology, Pasadena, Cal., U.S.A.

WEBER, D. (1995): Berechnung des Deutschen Haupthöhennetzes 1992 abgeschlossen. ZfV 120: 196-200.

WEBER, D. (1998): Die Schweremessungen der Landesvermessung in Deutschland. ZfV 123: 370-378.

WEBER, G. (1984): Hochauflösende mittlere Freiluftanomalien und gravimetrische Lotabweichungen für Europa. Wiss. Arb. Univ. Hannover 135.

WEBER, G., H. ZOMORRODIAN (1988): Regional geopotential improvement for the Iranian geoid determination. Bull Géod. 62: 125-141..

WEGENER, A. (1915): Die Entstehung der Kontinente und Ozeane. 4. Aufl., Vieweg und Sohn, Braunschweig 1962.

WEI, M., K.P. SCHWARZ (1998): Flight test results from a strapdown airborne gravity system. J. Geod. 72: 323-332.

WELLS, W.C. ed. (1984): Spaceborne gravity gradiometers. NASA Conf. Publ. 2305 (Proceed. of a workshop held at NASA GSFC, Greenbelt, Md., 1983.

WELLS, D.E., ed. (1986): Guide to GPS positioning. Canadian GPS Associates, Fredericton, N.B.

WENZEL, H.-G. (1976): Zur Genauigkeit von gravimetrischen Erdgezeitenbeobachtungen. Wiss. Arb. Univ. Hannover 67.

WENZEL, H.-G. (1977): Zur Optimierung von Schwerenetzen. ZfV 102: 452-457.

WENZEL, H.-G. (1982): Geoid computation by least-squares spectral combination using integral kernels. Proceed. Gen. Meeting IAG, Special Issue J. Geod. Soc. of Japan: 438-453, Tokyo.

WENZEL, H.-G. (1985): Hochauflösende Kugelfunktionsmodelle für das Gravitationspotential der Erde. Wiss. Arb. Univ. Hannover 137.

WENZEL, H.-G. (1989): On the definition and numerical computation of free air gravity anomalies. Bull.d'Inf. Bur.Gravim. Int. 64: 23-31..

WENZEL, H.-G. (1996): The nanogal software: Earth tide data processing package ETERNA 3.30. Bull. d'Inf. Marees Terrestres 124: 9425-9439.

WENZEL, H.-G. (1997a): Tide-generating potential for the earth. In Wilhelm et al. (1997): 9-26.

WENZEL, H.-G. (1997b): Analysis of earth tide observations. In Wilhelm et al. (1997): 59-75.

WENZEL, H.-G. (1999): Schwerefeldmodellierung durch ultra-hochauflösende Kugelfunktionsmodelle. ZfV 124: 144-154.

WHALEN, C.T. (1985): Trigonometric motorized leveling at the National Geodetic Survey. In D.B. Zilkoski, ed. (1985), Proceed. Third Intern. Symp. on the North American Vertical Datum (NAVD'85): 65-80. Nat. Geod. Inform. Center, NOAA, Rockville, Md.

WHITTEN, C.A. (1952): Adjustment of European triangulation. Bull. Géod. no.24: 187-203.

WICHIENCHAROEN, C. (1982): The indirect effects on the computation of geoid undulations. OSU Rep. 336, Columbus, Ohio.

WIELEN, R., H. SCHWAN, C. DETTBARN, A. LENHARDT, H. JAHREISS, R. JÄHRLING (1999): Sixth catalogue of fundamental stars (FK6). Veröff. Astron. Rechen-Institut Heidelberg No. 35, Braun, Karlsruhe.

WILHELM, H., W. ZÜRN, H.-G. WENZEL, eds. (1997): Tidal phenomena. Springer, Berlin-Heidelberg-New York.

WILLIAMS, D.C., H. KAHMEN (1984): Two wavelength angular refraction measurements. In Brunner (1984a): 7-31.

WILSON, C.R. (1995): Earth rotation and global change. Rev. Geophys., Suppl.: 225-229.

WILSON, P., J. RAIS, C. Reigber, H. SEEGER et. al. (1998): The GEODYSSEA project: an investigation of the geology of south and south-east Asia. EOS 79: 545, 548-549.

WOLF, H. (1963a): Dreidimensionale Geodäsie. Herkunft, Methodik und Zielsetzung. ZfV 88: 109-116.

WOLF, H. (1963b): Die Grundgleichungen der dreidimensionalen Geodäsie in elementarer Darstellung. ZfV 88: 225-233.

WOLF, H. (1967): Computation of satellite triangulation by spatial fitting of the orbit. DGK, B 153: 75-92.

WOLF, H. (1974): Über die Einführung von Normalhöhen. ZfV 99: 1-5.

WOLF, H. (1978): The Helmert-block method, ist origin and development. Proceed. 2nd Int. Symp. on Problems Related to the Redefinition of North American Geodetic

Networks, Arlington, Va.: 319-326. Nat. Geod. Inform. Branch, NOAA, Rockville, Md.

WOLF, H. (1987): Datums-Bestimmungen im Bereich der deutschen Landesvermessung. ZfV 112: 406-413.

WOLF, H. (1993): Friedrich Robert Helmert – sein Leben und Wirken. ZfV 118: 582-590.

WOLF, H. (1997): Ausgleichungsrechnung nach der Methode der kleinsten Quadrate. 3.Aufl., F.Dümmler, Bonn.

WOODHOUSE, J.H., A.M. DZIEWONSKI (1984): Mapping the upper mantle: three dimensional modelling of earth structure by inversion of seismic waveforms. JGR 89: 5953-5986.

WOODWORTH, P.L. (1997): The Permanent Service for Mean Sea Level and the Global Sea Level Monitoring System. In IAG (1997): 55-58.

WÜBBELMANN, H. (1992): Das hydrodynamische Nivellement am Beispiel eines Pegelnetzes am Fehmarn-Belt. Wiss. Arb. Univ. Hannover 176.

WÜBBENA, G. (1989): The GPS adjustment software package GEONAP- Concepts and models. Proc. Fifth Int. Geod. Symp.on Satellite Positioning: 452-461,Las Cruces, New Mexico, U.S.A.

WYATT, F., D.C. AGNEW, H.O. JOHNSON (1990): Pinyon Flat Observatory: Comparative studies and geophysical investigations. U.S. Geol. Survey, open-file report 90-380: 242-248.

YODER, O.F. (1995): Astrometric and geodetic properties of earth and the solar system. In Ahrens (1995): 1-31.

YUNCK, T.P., W.G. MELBOURNE (1996): Spaceborne GPS for earth science. In Beutler et al. (1996c): 113-122.

ZAHEL, W. (1997): Ocean tides. In Wilhelm et al. (1997): 113-143.

ZARRAO, N. W. MAI, E. SARDON, A. JUNGSTAND (1998): Preliminary evaluation of the Russian GLONASS system as a potential geodetic tool. J. Geod. 72: 356-363.

ZEBKER, H.A., R.M. GOLDSTEIN (1986): Topographic mapping from interferometric synthetic aperture radar observations. JGR 91: 4993-4999.

ZERBINI, S., L. BASTOS, H.-P. PLAG, B. RICHTER, eds. (1998): WEGENER: An interdisciplinary contribution to unraveling the geodynamics of the European and Mediterranean arc. Tectonophysics 294, nos. 3-4.

ZILKOSKI, D.B., J.H. RICHARDS, G.M. YOUNG (1992): Results of the general adjustment of the North American Vertical Datum of 1988. Surveying and Land Information Systems 52: 133-149.

ZILKOSKI, D.B., J.H. RICHARDS, G.M. YOUNG (1995): A summary of the results of the general adjustment of the North American vertical datum of 1988. Allg. Verm. Nachr. 102: 310-321.

ZOBACK, M.L. (1992): First- and second-order patterns of stress in the lithosphere: The world stress map project. JGR 97: 11703-11728.

ZUMBERGE, M.A. (1981): A portable apparatus for absolute measurements of the earth's gravity. Ph.D. thesis, Univ. of Colorado, Dep. of Physics, Boulder, Col.

ZUMBERGE, M.A., E.L. CANUTESON (1995): An ocean bottom absolute gravity meter. In Sünkel and Marson (1995): 7-16.

ZÜRN, W. (1997a): Earth tide observations and interpretation. In Wilhelm et al. (1997): 77-94.

ZÜRN, W. (1997b): The nearly-diurnal free wobble-resonance. In Wilhelm et al. (1997): 95-109.

ZÜRN, W., H. WILHELM (1984): Tides of the earth. In Landolt-Börnstein, New Series V, vol.2: 259-299, Springer, Heidelberg-New-York.

ZÜRN, W., D. EMTER, E. HEIL, J. NEUBERG, W. GRÜNINGER (1986): Comparison of short and long- baseline tidal tilts. In Viera, R., ed.: Proceed. Tenth Intern. Symp. on Earth Tides, Madrid 1985: 61-70, Madrid.

Index

Names of the authors cited in the text are not included in the index